TRANSACTIONS
OF THE ASME
Series C

Journal of HEAT TRANSFER

February 1961

RADIATION • CONDUCTION • CONVECTION • COMPLEX SYSTEMS • PHASE CHANGES AND MIXTURES • TRANSIENT PHENOMENA • THERMOPHYSICAL PROPERTIES • EXPERIMENTAL TECHNIQUES • THERMOMETRY • ANALOG METHODS • ANALYTICAL AND NUMERICAL METHODS • APPLICATIONS • DESIGN TECHNIQUES • HEAT EXCHANGERS • INSULATION • ECONOMIC FACTORS BIOTECHNOLOGY • ASTRONAUTICS

Published Quarterly by
THE AMERICAN SOCIETY OF MECHANICAL ENGINEERS

TRANSACTIONS
OF THE ASME
Series C

EDITORIAL DEPARTMENT

Editor, J. J. JAKLITSCH, JR.
Consulting Editor, LED BLODGETT
Production, JEAN NORTH
Production Asst. CARMEN L. CABRANES
Art Editor, HENRY BALFOUR

HEAT TRANSFER DIVISION

Chairman, W. ROHSENOW
Secretary, S. OSTRACH
Papers Review, T. F. IRVINE, JR.
Consulting Editor, S. P. KEZIOS

OFFICERS OF THE ASME

President, W. H. BYRNE
Secretary, O. B. SCHIER, II
Treasurer, E. J. KATES
Assistant Treasurer, H. J. BAUER

PUBLICATIONS COMMITTEE

Chairman, HENDLEY N. BLACKMON
R. D. MINDLIN
MARTIN GOLAND
VITO L. SALERNO
F. J. HEINZE

Junior Representatives
J. W. FOLLANSBEE
STEWART H. ROSS

REGIONAL ADVISORY BOARD

Region I, H. M. ROGERS, JR.
Region II, ROBERT E. ABBOTT
Region III, A. F. BOCHENEK
Region IV, FRANCIS C. SMITH
Region V, WM. J. TITZEL
Region VI, C. R. EARLE
Region VII, RALPH L. SCORAH
Region VIII, G. CORRY MCDONALD
Region IX, M. S. UMBENHAUER
Region X, CARL J. ECKHARDT

Published quarterly by The American Society of Mechanical Engineers. Publication office at 20th and Northampton Streets, Easton, Pa. The editorial department is located at the headquarters of the Society, 29 West Thirty-Ninth Street, New York 18, N. Y. Cable address, "Mechaneer," New York. Price $3.00 a copy, $10.00 annually, to members, $4.50 a copy, $15.00 annually. Add 50 cents for postage to all countries outside the United States and Canada. Changes of address must be received at Society headquarters seven weeks before they are to be effective on the mailing list. Please send old as well as new address. . . . By-Law: The Society shall not be responsible for statements or opinions advanced in papers or . . . printed in its publications (B13, Par. 4). . . . Second-class mail privilege authorized at Easton, Penna. . . . This publication is authorized to be mailed at the special rates of postage prescribed by Section 132.122 . . . © Copyrighted, 1961, by The American Society of Mechanical Engineers. Reprints from this publication may be made on condition that full credit be given the TRANSACTIONS OF THE ASME, Series C—Journal of Heat Transfer, and the author, and that date of publication be stated.

TRANSACTIONS OF THE ASME
is indexed by the Engineering Index, Inc.

Journal of HEAT TRANSFER

VOL. 83 • SERIES C • NO. 1

February 1961

CONTENTS

1 **A Survey of P-V-T Data for Water in the Critical Region** (60—HT-25)
E. S. Nowak, R. J. Grosh, and P. E. Liley

14 **Smooth Pressure-Volume-Temperature Data for Water in the Critical Region Derived From Experimental Measurements** (60—HT-26)
E. S. Nowak, R. J. Grosh, and P. E. Liley

27 **Experimental Determination of Limit of Supersaturation of Nitrogen Vapor Expanding in a Nozzle** (60—SA-8)
G. L. Goglia and G. J. Van Wylen

33 **Some Temperature and Pressure Measurements in Confined Vortex Fields** (60—SA-4)
J. M. Savino and R. G. Ragsdale

39 **The Influence of Bypass Channels on the Laminar Flow Heat-Transfer and Fluid Friction Characteristics of Shell and Tube Heat Exchangers** (60—SA-7)
Frederick L. Test

48 **An Analytical Study of Laminar Film Condensation: Part 1—Flat Plates** (60—HT-37)
Michael Ming Chen

55 **An Analytical Study of Laminar Film Condensation: Part 2—Single and Multiple Horizontal Tubes** (60—HT-38)
Michael Ming Chen

61 **Transient Natural Convection From Vertical Elements** (60—HT-33)
B. Gebhart

71 **Determination of Boiling Film Coefficient for a Heated Horizontal Tube in Water-Saturated Wick Material** (60—HT-11)
W. D. Allingham and J. A. McEntire

77 **Optimization of a Sandwiched Thermoelectric Device** (60—HT-24)
B. W. Swanson, E. V. Somers, and R. R. Heikes

83 **The Heat-Balance Integral—Further Considerations and Refinements** (60—SA-9)
T. R. Goodman

87 **Effect of Aspect Ratio and Tube Orientation on Free Convection Heat Transfer to Water and Mercury in Enclosed Circular Tubes** (60—SA-21)
F. W. Larsen and J. P. Hartnett

TECHNICAL BRIEFS

94 **A Note on the "Implicit" Method for Finite-Difference Heat-Transfer Calculations**
G. M. Dusinberre

95 **The Influence of Prandtl Number on the Heat Transfer From Rotating Nonisothermal Disks and Cones**
J. P. Hartnett and E. C. Deland

96 **A Fully Integrated Solution of the Problem of Laminar or Turbulent Flow in a Tube With Arbitrary Wall Heat Flux**
R. N. Noyes

98 **The Leveque Solution With a Finite Wall Resistance**
E. M. Rosen and E. J. Scott

101 **Condensation on a Rotating Cone**
E. M. Sparrow and J. P. Hartnett

102 **Refrigerator Heat Leak for Sandwiched Thermoelectric Elements**
B. W. Swanson and E. V. Somers

E. S. NOWAK
Graduate Assistant,
School of Mechanical Engineering,
Purdue University,
Lafayette, Ind.

R. J. GROSH
Professor of Mechanical Engineering,
Purdue University.
Assoc. Mem. ASME

P. E. LILEY
Assistant Professor of
Mechanical Engineering,
Purdue University

A Survey of P-V-T Data for Water in the Critical Region

A comprehensive review is given of P-V-T data available for water at pressures from 2700 to 4000 psia, specific volumes from 0.025 to 0.125 cu ft per lb, and temperatures from about 680 to 800 deg F. Experimental and computed values of various investigations are given. A description of the various methods and formulas used to interpolate the original data is also given. The results indicate there is a lack of smoothed or computed values for the specific volumes of the superheated vapor at sufficiently close intervals in the critical region. This makes it difficult to interpolate accurately and derive such properties as density and coefficients of volume expansion and compressibility. Furthermore, there are significant differences between the data for superheated steam given in the various tables which can be attributed to erroneous methods of interpolating the original experimental data.

Introduction

EXPERIMENTAL and theoretical studies of flow, heat transfer, and power cycles on systems using water in the vicinity of the critical point require accurate and detailed information about certain of its thermodynamic and transport properties. This paper presents a summary of existing information on the volumetric behavior of water in the critical region; i.e., for pressures of 2700 to 4000 psia, specific volumes 0.025 to 0.125 cu ft per lb, and temperatures from around 680 to about 800 F. This information, of course, forms only a part of that needed to insure the success of heat-transfer work and its subsequent correlation in the critical region.

This paper is divided into four sections dealing consecutively with saturation, subcooled liquid, and superheated-vapor data, and finally with the observations and conclusions of various investigators on the critical point. Usually, experimental data, computed values, and the constants in various formulations have been converted into English units.

The starting point of this survey was an investigation of the various steam tables. The book by Dorsey [7][1] was also very useful in the early stages.

[1] Numbers in brackets designate References at end of paper.

Contributed by the Heat Transfer Division of THE AMERICAN SOCIETY OF MECHANICAL ENGINEERS and presented at the ASME-AIChE Heat Transfer Conference, Buffalo, N. Y., August 15–17, 1960. Manuscript received at ASME Headquarters, May 19, 1960. Paper No. 60—HT-25.

Saturation Data

Vapor Pressure. Table 1 shows the extent of accurate measurements on the vapor pressure of saturated water. Egerton and Callendar [10] and Holborn and Baumann [14] employed dynamic methods to measure the vapor pressure while other investigators [41, 48] employed static methods.

In order to interpolate the experimental data accurately and utilize such useful relations as the Clapeyron equation, a number of empirical equations have been proposed for the dependence of saturation pressure on temperature. The more recent of these formulations are given in Table 2.

Osborne, et al. [41], and Smith, et al. [48], evaluated the constants of equations (1) and (2) from their measurements on the vapor pressure of saturated water. Osborne and Meyers [42] derived the constants of equation (3) from the adjusted measurements of Holborn and Baumann,[2] Egerton and Callendar, Osborne, et al., and Smith, et al. The adjusted measurements of Holborn and Baumann were only used for temperatures to 392 F, the implication being that they were in error at the higher temperatures. Equation (4) was proposed by Timroth [55] while equation (5) was proposed by Sugawaro [50].[3] The experimental values used by Timroth were not referenced but the equation he proposed gives almost identical results as equation (3).

[2] These are given in [3] and it is thought that Holborn, Scheel, and Henning adjusted the measurements of Holborn and Baumann [14].

[3] Unfortunately, Sugawaro's paper was not available to the authors and therefore it is not possible to give the basis for equation (5).

Nomenclature

J = mechanical equivalent of heat, 778.29 ft-lb/Btu
P = pressure, psia
R = gas constant for water vapor, 0.595661 cu ft-sq in. deg R
T = absolute temperature, 459.69 + t, deg R
V = volume, cu ft
h = enthalpy, Btu/lb
v = specific volume, cu ft/lb
t = temperature, deg F
$(\partial P/\partial T)_v$ = change in pressure with temperature along an isometric
JSME = Japan Society of Mechanical Engineers
TIC = Third International Conference on Vapor Tables
VDI = Verein Deutscher Ingenieure, Germany
VTI = All-Union Institute of Heat Engineering, Russia

Subscripts

c = property at the critical point
1 = property along liquid water saturation line, known condition
v = property along the water-vapor saturation line
s = property at saturation condition
2 = unknown condition

Table 1 Summary of vapor-pressure measurements

Number	Investigators	Pressure Range psia	Pressure Range kg/cm^2
1	Holborn and Baumann, 1910, Ref. 14.	To 3200	To 225
2	Egerton and Callendar, 1932, Ref. 10.	120 to 3202	8.5 to 225
3	Osborne, et al., 1933, Ref. 41.	14.7 to 3200	1 to 225
4	Smith, et al., 1934, Ref. 48.	69 to 3206	4.8 to 225

Table 2 Empirical equations proposed for saturation pressure

Author(s) and Date	Ref.	Eq. No.	Temperature Range °F	Temperature Range °C	Equation *	Constants
Osborne, Stimson, et. al., 1933	41	1	527 to 705.2	275 to 374	$T \log_{10} p = aT + b + cx^3 + dx^5 + ex^6$ where $x = 1.03571 \times 10^{-6} T^2 - 1$	a = 6.5903158 b = -3605.348 c = 197.17 d = -1094.8 e = 2518.2
Smith, Keyes, et. al., 1934	48	2	212 to 705.4	100 to 374.11	$\log_{10} \frac{p_c}{p} = \frac{x}{t}\left[\frac{a + bx + cx^3 + ex^4}{1 + dx}\right]$ where $x = t_c - t$	P_c = 3206.2 psia t_c = 705.40 °F a = 3.146313 b = 2.30063×10^{-2} c = -1.28866×10^{-9} d = $-7.6636095 \times 10^{-3}$ e = -6.253277×10^{-2}
Osborne and Meyer 1934	42	3	32 to 705.2	0 to 374	$\log_{10} p = A + \frac{B}{T} + \frac{Cx}{T}(10^{Dx^2} - 1) + E(10^{Fx^{5/4}})$ where $x = \frac{T^2 - X}{3.24}$, $y = \frac{705.40 - t}{1.8}$	X = 951.588 A = 6.5938507 B = -3609.2 C = 2.4964×10^{-4} D = 1.1965×10^{-11} E = -0.0044 F = -0.0057148
1952 V.T.I Steam Tables (D. L. Timroth)	55	4	32 to 705.47	0 to 374.15	$\log_{10} p = 2.23142 + y_1 - (3.309 \times 10^{-4} T + 0.03985) y_2$ where $y_1 = 4.16294 \frac{T - 828.29}{T - 65.009}$, $y_2 = \frac{1}{251.694}(x - \frac{\alpha x}{100})\left[3.4969 - \frac{(x - \frac{\ldots 2}{100})}{\ldots}\right]$, $\alpha = \frac{x^2(3.427 - x^2)}{\beta}$, $x = \frac{T - 828.29}{180}$, $\beta = 0.1150 - 0.064x + \frac{0.7500}{(x-1.2)^2 + 1}$	
1955 Steam Tables of J.S.M.E.	1	5	410 to 705.47	210 to 374.15	$\log_e \frac{3209.5}{p_c} = \left[7.21379 + (\alpha + \beta T + \gamma' T^n)\frac{(T - 844.69)^2}{1.8}\right]\left(\frac{1165.16}{T} - 1\right)$ where n = 32	$\alpha = 1.0071 \times 10^{-6}$ $\beta = 1.07299 \times 10^{-8}$ $\gamma' = -6.0374 \times 10^{-32}$

* p = pressure psia t = temperature °F T = absolute temperature °R = t + 459.69

These equations with the exception of equation (1) have been employed in the various steam tables: Equation (2) was used in tables of Keenan and Keyes [23]. Equation (3) was employed in the tables of the TIC [2] (Third International Conference on Vapor Tables), Osborne, et al. [44], Vukalovich [58, 59], Faxen [12], and Dzung and Rohrbach [8]. Those values in the tables of [37] and the VDI [46] (Verein Deutscher Ingenieure) were probably based on the TIC values. Timroth's tabulations [55, 56] were computed from equation (4) while that of the JSME [1] (Japan Society of Mechanical Engineers) was calculated from equation (5). Those in the Callendar tables [4] were derived from the measurements of Egerton and Callendar [10].

Table 3 lists values of saturation pressure of water in the critical region computed from the five equations listed in Table 2 along with experimental measurements. Fig. 1 gives deviations of the experimental and computed values from those obtained from

Table 3 Saturation vapor pressure of water, psia

Saturation Temperature		Calculated Values from Equations of Table #2					Vapor Pressure Measurements		
°C	°F	Eq. 1	Eq. 2	Eq. 3	Eq. 4	Eq. 5	Egerton et al.(10)	Osborne et al.(41)	Smith et al.(48)
360.0	680.0	2708.33	2708.0	2708.4	2708.4	2709.1	2708.46	2708.43	2707.88
361.0	681.8	2741.1	2741.0	2741.2	2741.2				
362.0	683.6	2774.3	2774.2	2774.3	2774.3			2774.41	
363.0	685.4	2807.8	2807.7	2808.0	2808.0				
364.0	687.2	2841.8	2841.6	2841.8	2841.8			2841.88	
365.0	689.0	2876.2	2875.9	2876.1	2876.1	2875.8			
366.0	690.8	2910.8	2910.5	2910.7	2910.7			2910.75	
367.0	692.6	2945.8	2945.5	2945.8	2945.8				
368.0	694.4	2981.4	2980.9	2981.2	2981.2			2981.19	
369.0	696.2	3017.2	3016.8	3017.1	3017.1				
370.0	698.0	3053.5	3052.9	3053.5	3053.5	3053.5	3054.40	3053.40	3052.9
371.0	699.8	3090.3	3089.5	3090.2	3090.2	3090.3		3090.13	
372.0	701.6	3127.5	3126.6	3127.4	3127.4	3127.5	3128.53	3127.24	
373.0	703.4	3165.1	3164.0	3165.1	3165.1	3165.4		3164.97	
374.0	705.2	3203.1	3202.0	3203.4	3203.4	3203.7	3204.49	3203.51	
374.11	705.4		3206.2						3206.18
374.15	705.47				3209.5	3209.5			

* As recorded by Smith, et al (48).

Table 4 Measurements of specific volume along vapor-saturation line

Number	Investigators	Type of Experiment	Temperature Range °F	Temperature Range °C
1	Callendar, 1929, Ref. 5.	Calorimetric	400 to 717	210 to 380
2	Jakob and Fritz, 1935, Ref. 18.	Calorimetric	32 to 690	0 to 365
3	Keyes, Smith and Gerry, 1936, Ref. 27.	Extrapolation	383 to 704.1	195 to 373.4
4	Rek, 1936, Ref. 9.	Direct Volume Measurement	662 to 705.64	350 to 374.24
5	Osborne, Stimson and Ginnings, 1937, Ref. 43.	Calorimetric	212 to 705.2	100 to 374
		Direct Volume Measurement	At 698	At 370
6	Timroth, 1950, Ref. 54.	Extrapolation	662 to 705.47	350 to 374.15

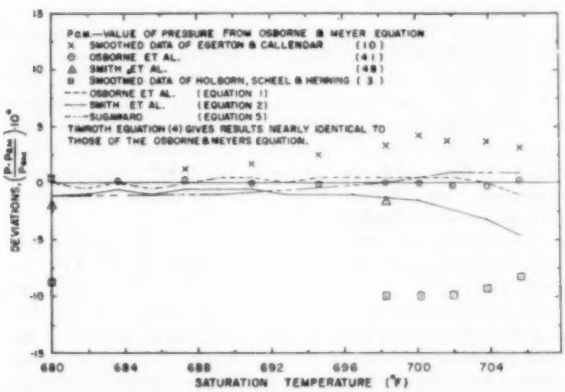

Fig. 1 Deviations of experimental and formulated values of vapor pressure from the Osborne and Meyer equation

equation (3). For temperatures from 680 to 705.2 F all of the experimental values, with the exception of Holborn, Scheel, and Henning's, agree with the Osborne and Meyers formulation to within 5 parts in 10,000. Osborne and Meyers considered the deviations of the experimental values as being serious and noteworthy and recommended more precise measurements to establish the true course of the saturation curve in the immediate vicinity of the critical point. However, these deviations though significant were within the experimental uncertainty. Therefore saturation pressures computed from equation (3) would appear to be the most reliable, since it was derived from three independent sets of measurements for temperatures above 392 F.

Specific Volume of Saturated Water Vapor. The specific volume along the saturation line may be determined from calorimetric and volumetric experiments with the vapor at, or close to, saturation conditions. Volumes also have been derived from the extrapolation of the isometrics, lines of constant volume on a pressure-temperature diagram, for superheated vapor to the saturation line. Table 4 lists the investigations conducted on the specific volume of saturated water vapor; while Table 5 gives the primary data which were obtained by various investigators.

Callendar [5] conducted enthalpy measurements along the vapor-saturation line from which he was able to derive specific volumes. These values are in error and a detailed discussion of his experiments in the critical region is given in the fourth section of this paper. Jakob and Fritz [18] obtained volume data along the vapor-saturation line from their enthalpy of vaporization measurements by utilizing the Clapeyron equation. In the derivation of saturated-vapor volumes they used the Smith and Keyes [49] liquid saturated values. Since then Keyes [28] found that the values of [49] were in error in the critical region, which in turn therefore invalidated the derived values of Jakob and Fritz in the critical region.

Keyes, Smith, and Gerry [27] obtained specific-volume data to within about 2 deg F of the critical point by extrapolating their isometrics to the saturation line. However, Keyes [28] since then

Table 5 Primary data on specific volume of saturated vapor, cu ft per lb

Temperature °F	Callendar (5)	Jakob & Fritz (18)	Keyes et al. (27)	Eck (9)	Osborne et al. (43)	1934 Skeletal Steam Tables (2)	1952 Timroth Tables (55)	1956 V.D.I. Tables (46)
680.0	.1124*	.1118		.1115	.1112	.1115	.1112	.1115
681.2					.109		.109	.109
681.8					.108		.108	.109
682.8					.107		.107	.107
683.6					.105		.105	.106
684.3					.104		.104	.104
685.4					.102		.102	.103
685.9					.102		.101	.102
687.2					.0991		.0992	.0998
687.3			.1001		.0990		.0990	.0993
688.8					.0963		.0964	.0968
689.0	.0957	.0967		.09624	.0961		.0966	.0968
690.0	.0936							
690.3					.0937		.0939	.0943
690.8					.0929		.0929	.0937
691.8					.0910		.0911	.0918
692.6					.0896		.0895	.0905
693.2					.0884		.0881	.0892
694.4					.0863		.0862	.0871
694.7					.0847		.0847	.0865
696.1					.0838		.0828	.0838
696.2					.0827		.0827	.0836
697.5					.0799		.0799	.0807
698.0	.0777*	.0799		.07936	.0790	.08004	.0790	.0798
698.9			.08009		.0770		.0769	.0775
699.8					.0750	.07626	.0750	.0756
700.0	.0731*							
700.3					.0740		.0737	.0743
701.6		.0717		.07112	.0705	.07205	.0705	.0710
701.8					.0698		.0702	.0708
703.0					.0660		.0666	.0666
703.4					.0649*	.06708	.0655	.0657
704.1			.06407					
704.5					.0597		.0615	.0612
705.2	.0607*			.05815	.0556*	.05844	.0578	.0573
705.47					.0477		.0528	.0509
705.64				.04911				

* Differences between these values and those in 1934 skeletal tables exceed 1934 recommended tolerances.

found that the values in [27] were in error in the critical region.

Osborne [40] proposed the following three calorimetric experiments to evaluate the thermodynamic properties along the saturation line:

(*a*) Observe change in pressure and temperature when heat is added to a constant vapor-liquid mass.

(*b*) Measure quantity of saturated water removed when heat is added isothermally to a vapor-liquid mass under saturation conditions.

(*c*) Measure quantity of saturated vapor formed when heat is added isothermally to a vapor-liquid mass under saturation conditions.

By employing the laws of thermodynamics and the Clapeyron equation, it was shown that the enthalpy and specific volume of saturated water and water vapor could be calculated from the results of these three experiments. These experiments were subsequently performed by Osborne, et al. [43], and Table 5 gives their derived values for the specific volume of saturated water vapor. Equation (3) was used to obtain values for the coefficient dP_s/dT.

Osborne, et al. [43], made several direct measurements of the specific volume of superheated vapor within 0.4 deg F of saturation conditions at a temperature of 698 F. By extrapolation, a value of 0.07889 cu ft per lb was obtained. This agreed with the value of 0.0790 cu ft per lb derived from the foregoing calorimetric measurements, indicating that the calorimetric measurements up to 698 F showed no sign of error. Special tests also were carried out to investigate possible mixing of the liquid with the vapor phase which would give lowered values. No mixing effect was observed up to and including 703.4 F, while some effect was observed at 704.3 F. Osborne, et al. [43], concluded from these special tests that their calorimetric results could not be relied upon in the small region within about 2 deg of the critical point.

In 1950, Timroth and Vargaftik [53] described research at the VTI (All-Union Institute of Heating Engineering), Russia. It is thought, therefore, the saturation vapor volumes listed in the 1952 and 1958 Timroth tables [55, 56] were derived from the isometrics measured by Timroth [54]. No basis was given for the saturation-volume data in the 1956 VDI tables [46], but it is probable that the enthalpy of vaporization values of Koch [35] were used to derive specific volumes along the vapor-saturation line. The data adopted at the TIC [2] were probably based on German and American measurements [18, 27, 35].

The data given in Table 5 have been employed in the various steam tables: The formulations of Osborne, et al. [43], were used to compute the values in the tables of Osborne [44], Vukalovich [58, 59], Faxen [12], and Dzung and Rohrbach [8]. The TIC values [2] were used to derive the data in the tables of reference [37], Callendar [4], and Keenan and Keyes [23]. The TIC values also were used to derive the values listed in the JSME tables [1] above 3000 psia. Those in the JSME tables for pressures lower than 3000 psia were computed from the equation of state proposed by Tanishita [52].

The tolerances on pressure and specific volumes along the liquid and vapor-saturation line, which were adopted at the TIC, are given in Table 6. It can be seen from Table 5 that all of the Callendar data and those of Osborne, et al., above 702 F, fall outside the tolerances of Table 6. If the tolerances adopted at the 1934 conference are correct, it would appear that the conclusion reached by Osborne, et al., about the trustworthiness of their measurements near the critical point, are correct.

Fig. 2 shows deviations of the various primary data from specific-volume data in the Timroth (VTI) tables. Up to about 702 F there is excellent agreement between the Timroth and Osborne, et al., values. From 702 to 705.2 there is good agreement between the Eck, VDI, and the Timroth values. It appears, therefore, that up to 702 F, the almost identical values of Timroth and Osborne, et al., are the most reliable, while from 702 to 705.2 F the values of Eck, VDI, and Timroth are the most reliable.

Specific Volume of Saturated Water. Specific volumes along the liquid-saturation line have been derived from calorimetric data

and from values obtained by extrapolating isometrics and isotherms to the saturation line. However, a few volumetric measurements have been made at saturation conditions. Table 7 summarizes the work to date while Table 8 gives the results of these investigations.

Smith and Keyes [49] derived saturation specific-volume values by extrapolating their isotherms to the saturation line. Osborne, et al. [43], and Keyes [28] found, however, that these were in error above 626 F.

Osborne, et al. [43], derived values for the specific volume of saturated water from calorimetric experiments previously described. They also made several volumetric measurements on subcooled water at a temperature of 698 F. The value derived

Table 6 Tolerances[a] adopted at The Third International Conference on Vapor Tables for Saturation Pressures and Specific Volumes

Temperature °F	Saturation Pressure ± psia	Saturation Specific Volumes Liquid ± ft³/lb	Vapor ± ft³/lb
680.0	.7	.000064	.0006
698.0	.7	.00034	.00160
699.8	1.4	.00042	.00160
701.6	1.6	.00054	.00176
703.4	1.6	.00085	.00192
705.2	1.6	.0024	.00192

[a] Issaresco 17 noted discrepancies along the saturation lines between the various properties of different steam tables. After an isentropic checking of these tables along the saturation line he concluded that the tolerances adopted in 1934 for the enthalpy and specific volume along the liquid and vapor saturation lines were too large.

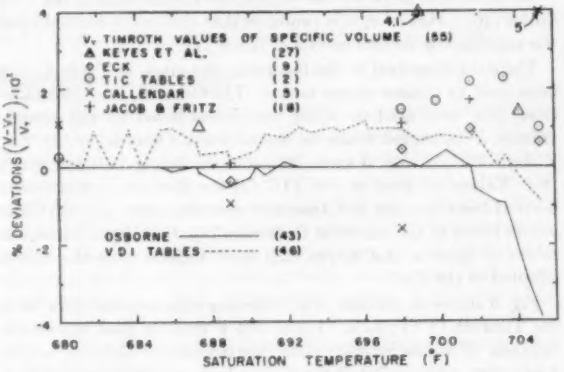

Fig. 2 Deviations of specific volume for saturated vapor from values of Timroth

Table 7 Measurements of specific volume along liquid-saturation line

Number	Investigators	Type of Experiment	Temperature Range °F	Temperature Range °C
1	Smith and Keyes, 1934, Ref. 49	Extrapolation	86 to 680	30 to 360
2	Eck, 1937, Ref. 9	Volumetric	662 to 705.64	350 to 374.24
3	Osborne, Stimson and Ginnings, 1937, Ref. 43	Calorimetric	212 to 705.2	100 to 374
		Volumetric	At 698	At 370
4	Timroth, 1950, Ref. 54	Extrapolation	680 to 705.47	360 to 374.15

Table 8 Primary data on specific volume of saturated liquid cu ft per lb

Temperature °F	Smith and Keyes (49)	Eck (9)	1934 Skeletal Tables (2)	Osborne et al. (43)	1952 Timroth Tables (55)	1956 V.D.I. Tables (46)
680.0	.03054	.03034	.030541	.03034	.03034	.03055
681.2				.03053	.03056	.03080
681.8				.03072	.03069	.03090
682.8				.03080	.03090	.03112
683.6				.03112	.03106	.03128
684.3				.03111	.03124	.03146
685.4				.03132	.03146	.03168
685.9				.03144	.03156	.03180
687.2				.03190	.03189	.0322
687.3				.03183	.0319	.0322
688.8				.0322	.0322	.0325
689.0		.03226		.0323	.0324	.0325
690.3				.0327	.0325	.0328
690.8				.0328	.0328	.0330
691.8				.0332	.0330	.0333
692.6				.0334	.0333	.0335
693.2				.0336	.0335	.0338
694.4				.0340	.0340	.0341
694.7				.0341	.0341	.0343
696.1				.0348	.0348	.0348
696.2				.0348	.0348	.0349
697.5				.0354	.0354	.0354
698.0		.03542	.03574	.0356	.0356	.0357
698.9				.0362	.0360	.0362
699.8			.03679	.0367	.0367	.0368
700.3				.0370	.0370	.0372
701.6		.03760	.03814	.0381	.0381	.0381
701.8				.0381	.0383	.0383
703.0				.0396	.0397	.0397
703.4			.04008	.0402	.0402	.0400
704.5				.0428	.0424	.0418
705.2		.04245	.0447	.0449	.0449	.0445
705.5	.05123			.0497	.0529	.0509
705.64		.04911				

for the specific volume of saturated water from their volumetric measurements was identical to that derived from their calorimetric measurements. They concluded that their calorimetric measurements up to 698 F showed no sign of error.

It is thought by the authors that the saturation-volume data in the Timroth tables (VTI) [55, 56] were derived from the isometrics measured by Timroth.

No basis was given for the saturation-volume data in the VDI tables [46]. However, it is probable that they were derived from the calorimetric measurements of Koch [35].

The data described in the foregoing and given in Table 8 have been used in various steam tables: The Osborne, et al., formulations [43] were used to derive the values listed for the specific volume of saturated water in the tables of Osborne, et al. [44], Vukalovich [58, 59], Faxen [12], and of Dzung and Rohrbach [8]. Values adopted at the TIC [2] are thought to have been derived from German and American measurements [35, 49]. The values listed in the tables of Callendar [4], JSME [1], and in the tables of Keenan and Keyes [23] were derived from the values adopted at the TIC.

Fig. 3 shows deviations of the various experimental data from the Timroth (VTI) data. Up to 704 F there is good agreement between all of the primary data, the deviations all being within 1 per cent. Above 701 F the Eck values are low in comparison with the other values.

It may be concluded that all the values up to 701 F appear to be equally reliable. From 701 to 705.2 F the values of the Timroth and VDI tables are to be favored since it appears that the Eck values are in error above 701 F.

Subcooled-Water Data

The basic method of volume measurement employed, for subcooled water, is essentially that of observing the pressure and temperature of a known amount of water in a closed container. Another method, though not used extensively, derives specific volumes from enthalpy measurements. The method and the equation used to derive data from enthalpy measurements will be given in the third section of this paper.

Table 9 summarizes the work conducted in the subcooled-liquid region. The 1930 Trauts and Steyer data [57] have been criticized by Jakob [19] on the grounds that the apparatus was poorly insulated, error in temperatures exceeded the estimated 1 deg F, and partial evaporation of water had occurred at the walls before the contents reached saturation conditions. A comparison of these data with those of Keyes and Smith [25],[4] made by Jakob, showed that the Trauts and Steyer data were in error by as much as 4 per cent.

The measurements of Tammann and Ruhenbeck were conducted at intervals of 180 deg F and are not of utility, since none of their data fall in the region considered in this study.

The measurements of Smith and Keyes [49], Havlicek and Miskovsky [13], Timroth [54],[5] and Kirillin, et al. [29–32], are considered as the most precise and are given in Table 10. The estimates which have been made on the accuracies of these measurements and those of Nieuwenburg and Blumendal [38] are given in the third section of this paper.

The data of Kennedy [24], which were found to be in error owing to chemical reaction between the container walls and the water samples, have been superseded by data of Holser and Kennedy [15]. However, Holser and Kennedy did not extend

[4] These data formed part of the results given by Smith and Keyes [49].

[5] The authors were unable to obtain Timroth's measurements [54].

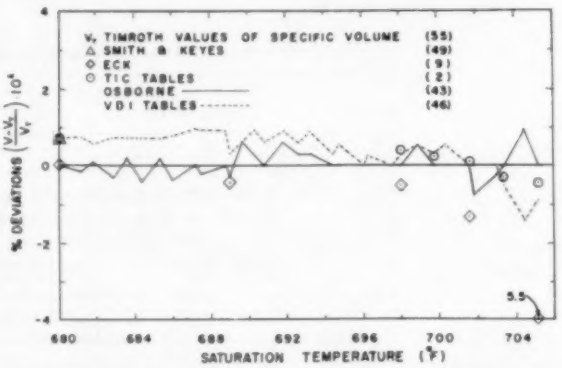

Fig. 3 Deviations of specific volume for saturated water from values of Timroth

Table 9 Summary of pressure-volume-temperature measurements on subcooled water

Number	Investigators	Pressure Range psia	Pressure Range kg/cm²	Temperature Range °F	Temperature Range °C
1	Trauts and Steyer, 1931, Ref. 57.	100 to 4300	50 to 300	32 to 698	0 to 370
2	Tammann and Ruhenbeck 1932, Ref. 51.	14 to 36,500	1 to 2500	78 to 572	20 to 300
3	Nieuwenburg and Blumendal, 1932, Ref. 38.	2300 to 8500	160 to 600	662 to 701.6	350 to 372
4	Smith and Keyes, 1934 Ref. 49.	60 to 5000	4 to 350	86 to 705.2	30 to 374
5	Havlicek and Miskovsky,[6] 1936, Ref. 13.	14 to 5690	1 to 400	482 to 703.4	250 to 373
6	Timroth, 1950, Ref. 54	1570 to 4260	110 to 300	662 to 705.2	350 to 374
7	Kirillin, et al., 1953 to 1958, Refs. 29 to 32.	820 to 7000	57 to 490	570 to 704.8	298.3 to 373.78

[6] Havlicek and Miskovsky derived volumetric data from their enthalpy measurements.

their measurements [16] into the critical region. They [15] stated that this was not practical since their equipment was inferior to the equipment used in the Keyes and Kirillin investigations.

Apparently Keenan [22] and Smith and Keyes [49] have been the only investigators to propose formulations for the pressure-volume-temperature relations of subcooled water. The formulation of Smith and Keyes, however, is not of utility since it does not extend into the region considered in this paper.

The following equation was derived by Keenan [22] from the measurements of Amagat,[6] and Smith and Keyes [49].

$$v = 0.04943 - 0.013169x^{0.147100} - 0.011166(p - 3211)y^{-.8} + \delta \quad (6)$$

where $x = 705.4 - t$, $y = 725 - t$, and δ is a graphical function of temperature and pressure.

The data and equation just described have been used in the various steam tables: The values adopted at the TIC [2] were derived by Keenan from equation (6). The data in the tables of Vukalovich [58, 59], Faxen [12], and of the JSME [1] were derived from the values from equation (6) and those adopted at the TIC [2]. It appears to the authors that the values listed in the 1952 and 1958 Timroth tables [55, 56] were derived from the measurements of Timroth [54] and Smith and Keyes [49]. Values in the VDI tables have been taken from the Timroth tables. The values in the Keenan and Keyes steam tables [23] were derived from the volumetric measurements of Smith and Keyes and the calorimetric measurements of Havlicek and Miskovsky [13].

The values for subcooled water in the tables of Keenan and Keyes are to be preferred over those in the tables of Vukalovich and Faxen. The values in the former tables were derived from two independent sets of measurements [13, 49], while those in the former were only derived from the volumetric measurements of Smith and Keyes [49]. A comparison of the data in the Keenan and Keyes and Timroth tables is given in the next section.

[6] The measurements of Amagat did not extend beyond 400 F.

Superheated Water Vapor

As in the case of the subcooled liquid measurements, the common method which was used in determining the specific volume of superheated vapor was that of observing the pressure and temperature of a known amount of vapor in a closed piezometer or container. Some investigators [13] were successful in deriving specific volume data from enthalpy and specific heat measurements. This method, though not common, merits considerable attention, since many accurate enthalpy and specific heat measurements have been made in the critical region. Furthermore, the volume data which could be derived from enthalpy data would serve as an independent check on volumetric measurements or on interpolated data.

Table 11 lists work to date on superheated vapor in the critical region while the results obtained are given in Table 12. The most extensive of these measurements are those of Nieuwenburg and

Table 10 Experimental P-V-T data for subcooled water

Havlicek & Miskovsky (13)			Kirillin, et al. (29-32)			Smith & Keyes (49)		
Temp. °F	Pressure psia	Sp. Vol. ft³/lb	Temp. °F	Pressure psia	Sp. Vol. ft³/lb	Temp. °F	Pressure psia	Sp. Vol. ft³/lb
680.0	3129.15	.02859	695.87	3009.80	.048864	680.0	2785.47	.0298248
680.0	3200.00	.02842	695.87	3011.24	.04773	680.0	2872.91	.0293631
680.0	3271.38	.02826	695.87	3011.52	.041189	680.0	2877.42	.0293390
680.0	3413.62	.02794	695.87	3142.90	.032487	680.0	3314.82	.0278638
680.0	—	—	695.87	3341.50	.03068	680.0	4190.23	.0262766
698.0	3129.15	.03298	695.87	3533.7	.029853	698.0	3137.49	.0332383
698.0	3200.00	.03229	702.81	3154.7	.03908	698.0	3233.49	.0320368
698.0	3217.38	.03165	702.81	3231.7	.03551	698.0	3311.99	.0313392
698.0	3413.62	.03080	702.81	3390.4	.03281	698.0	3486.62	.0302661
698.0	—	—	702.81	3595.2	.03106	698.0	3661.68	.0295028
698.0	—	—	702.81	3985.7	.02941	698.0	3836.68	.0289057
703.4	3200.00	.03639	703.72	3183.2	.03899	705.2	3226.74	.0381166
703.4	3271.38	.03413	703.72	3221.6	.03684	705.2	3313.24	.0345909
703.4	3413.62	.03239	703.72	3298.7	.03454	705.2	3487.63	.0322386
			703.72	3600.2	.031244	705.2	3662.24	.0309844
			704.80	3195.4	.046998	705.2	3837.24	.0301130
			704.80	3215.9	.038872	705.2	4012.18	.0294415
			704.80	3308.4	.035056			
			704.80	3464.1	.032593			
			704.80	3644.9	.031173			

Table 11 Summary of pressure-volume-temperature measurements on superheated vapor

Number	Investigators	Pressure Range psia	Pressure Range Kg/cm²	Temperature Range °F	Temperature Range °C
1	Nieuwenburg and Blumendal 1932, Ref. 38.	2300 to 8900	160 to 600	662 to 895	350 to 480
2	Keyes, Smith and Gerry 1936, Ref. 27.	190 to 5400	14 to 380	387 to 860	195 to 460
3	Havlicek and Miskovsky 1936, Ref. 13.	14.2 to 5690	1 to 400	482 to 1022	250 to 550
4	Timroth, 1950, Ref. 54.	1570 to 4260	110 to 300	662 to 1022	350 to 550
5	Kirillin, et al., 1953 to 1958, Refs. 29 to 32.	825 to 13500	58 to 950	570 to 1200	298.3 to 650
6	Kiyama, et al., 1955, Ref. 33.	2660 to 12000	187 to 850	716 to 860	380 to 460

Table 12 Experimental P-V-T data for superheated water vapor

Havlicek & Miskovsky (13)			Keyes et al. (27)			Kirillin et al. (29-32)			Kirillin et al. (29-32)		
Press. psia	Vol. ft³/lb	Temp. °F	Press. psia	Vol. ft³/lb	Temp. °F	Press. psia	Vol. ft³/lb	Temp. °F	Press. psia	Vol. ft³/lb	Temp. °F
2986.91	.09598	698.0	2665.69	.12014	680.0	2979.2	.1063	702.81	3580.3	.036924	716.00
						3141.7	.07501	702.81	3617.7	.033177	716.00
2986.91	.1056	703.4	2852.76	.10012	688.1				4148.1	.031092	716.00
						3144.8	.07429	703.72			
2986.91	.1106	707.0	2967.9	.10012	698.0				3360.3	.08629	721.94
3129.15	.09050	707.0	2839.7	.12014	698.0	2995.4	.10681	704.80	3600.9	.04549	721.94
3200.00	.07638	707.0				3145.1	.081894	704.80	3685.3	.03931	721.94
3271.38	.03812	707.0	3097.7	.08009	700.7	3193.2	.06036	704.80	3869.2	.03495	721.94
3413.62	.03420	707.0									
			3242.6	.04806	707.0	2869.6	.1251	705.94	3235.1	.1419	722.71
2986.91	.1173	712.4	3230.8	.06407	707.0	3123.5	.08890	705.94	3530.1	.06173	722.71
3129.15	.1006	712.4				3216.8	.05371	705.94	3612.9	.04516	722.71
3200.00	.09046	712.4	3936.7	.09204	716.0	3224.0	.04325	705.94	3948.3	.03447	722.71
3271.38	.07897	712.4	3444.3	.04806	716.0	3281.3	.03662	705.94			
3413.62	.04013	712.4	3393.8	.06407	716.0	3396.8	.03383	705.94	3053.8	.12839	730.40
			3318.6	.08009	716.0	3616.4	.03160	705.94	3247.1	.10932	730.40
2986.91	.1212	716.0	3175.3	.10012	716.0				3419.3	.091739	730.40
3129.15	.1056	716.0	3008.0	.12014	716.0	3030.4	.1065	707.43	3587.0	.072690	730.40
3200.00	.09715	716.0				3336.0	.03606	707.43	3653.7	.066213	730.40
3271.38	.08759	716.0	3856.3	.04806	734.0	3587.9	.0[illegible]224	707.43	3724.5	.054897	730.40
3413.62	.05909	716.0	3714.4	.06407	734.0				3793.7	.047275	730.40
						3106.1	.097707	708.94	3853.3	.044422	730.40
2986.91	.1249	719.6	3851.5	.08009	752.0	3174.7	.086688	708.94	3985.0	.038447	730.40
3129.15	.1100	719.6	3578.7	.10012	752.0	3183.5	.085439	708.94	3323.2	.1206	752.00
3200.00	.1022	719.6	3333.4	.12014	752.0	3216.1	.079770	708.94	3619.4	.09672	752.00
3271.38	.09380	719.6	4032.1	.06407	752.0	3282.8	.055166	708.94	3910.2	.07370	752.00
3413.62	.07309	719.6				3304.5	.042759	708.94	3610.8	.11117	770.00
			3964.2	.10012	780.0	3396.1	.026024	708.94	3898.6	.091889	770.00
3129.15	.1158	725.0	3645.3	.12014	788.0	3531.5	.023597	708.94			
3200.00	.1085	725.0				3693.8	.032051	708.94			
3271.38	.1008	725.0				3701.6	.031944	708.94			
3413.62	.08608	725.0				4070.6	.030042	708.94			
3129.15	.1242	734.0				3132.0	.10534	716.00			
3200.00	.1172	734.0				3314.9	.080387	716.00			
3271.38	.1104	734.0				3392.3	.065075	716.00			
3413.62	.09609	734.0				3430.7	.053417	716.00			
3271.38	.1234	752.0				3443.5	.044550	716.00			
3413.62	.1126	752.0				3460.6	.034509	716.00			
						3495.3	.04064[illegible]	716.00			

Blumendal [38]. Unfortunately, their measurements were not precise since they estimated that temperatures were only measured to within 1.8 deg F. Furthermore, they stated the pressures were measured only to within 60 psia. The newer measurements of Kiyama, et al. [33], are also not precise, since they state that the pressures under 7000 psia could be in error by as much as 20 psi. On the other hand, the data obtained by Keyes, et al. [27], Havlicek and Miskovsky [13], Timroth [54], and by Kirillin, et al. [29–31], appear to be quite precise.

Keyes, et al. [27], made no specific estimate of the accuracy of their volumetric measurements. However, in reference [49] it is mentioned that temperatures were reproducible to about 0.02 deg F while pressures were accurate to well within 5 parts in 10,000. According to Keyes [28] and Juza [20] the volumetric data derived by Havlicek and Miskovsky [13] were in good accord with the data reported in [27].

Timroth and Vargaftik [53] state that the over-all error in volume measurements in the critical region, which were conducted at the VTI [54], amounted to less than 0.3 per cent. No mention was made on the accuracy with which either pressure or temperature was measured.

Kirillin, et al. [31], made specific estimates of the error in their measurements on pressure, volume, and temperature. They estimated that the maximum error in pressure was some five to ten parts in 10,000, while that in temperature was within 0.09 deg F. They were able to show that the over-all error in their volume measurements was within 0.2 per cent and only exceeded this value near the critical point.

It was previously mentioned that Havlicek and Miskovsky [13] derived volumetric data from their enthalpy measurements. In so doing they started with the following thermodynamic relation,

$$\left(\frac{\partial h}{\partial P}\right)_T = \frac{-T^2}{JP}\left[\frac{\partial Pv/T}{\partial T}\right]_P \tag{7}$$

and by considering changes in state at constant pressure they derived the following equation:

$$\frac{v_2}{RT_2} - \frac{v_1}{RT_1} = \frac{-J}{R}\int_{T_1}^{T_2}\frac{1}{T^2}\left(\frac{\partial h}{\partial P}\right)_T dT \tag{8}$$

The integrand was evaluated from a graphical relationship for their data while the interpolated data of Keyes [26] along the 752 F isotherm was chosen for the known condition (v_1).

The experimental data and equations described have been used in various steam tables: The values in tables of Keenan and Keyes [23] were derived from the volumetric measurements of Keyes, et al. [27], and the calorimetric measurements of Havlicek and Miskovsky [13] in conjunction with equation (8). Equation (9)[7] was used by Keenan and Keyes to evaluate the integrand of equation (8):

$$h = 477 - \frac{859.5\ 10^4}{P} + \frac{14{,}200}{P}\,t + \Delta \tag{9}$$

where Δ was a graphically formulated function of P and t.

The values adopted at the TIC [2] for volumes less than 0.16 cu ft per lb were obtained by interpolating the measurements of Keyes, et al. [27]. An equation of state derived by Keyes, et al. [27],[8] was used to obtain the values adopted at the TIC for volumes greater than 0.16 cu ft per lb.

The values in the 1951 and 1955 Vukalovich tables were largely computed from an equation of state derived from 1934 skeletal table values; however, the values between 705.5 and 770 F were derived by means of a combined analytical and graphical

[7] Based on the measurements of Havlicek and Miskovsky and adjusted upward by 1.8 Btu per lb.

[8] Keyes [28] since then has derived a new equation of form $p = F(v, T)$ from his measurements. However, Keyes stated "that additional volume data in the critical region are indeed required before a satisfactory analytical representation of the pressure-sensitive critical state can be formulated."

Table 13 Superheated data of different steam tables

Author(s)	Pressure (psia)	Temperature °F 698	716	734	752	770	788
Vukalovich (58)	2845	.119					
	2987	.0956	.123				
	3129		.106	.125			
	3271		.0873	.111	.125		
	3414		.0593	.0966	.113		
	3556		.0376	.0822	.102	.115	
	3698		.0348	.0671	.0905	.105	.116
	3840		.0341	.0556	.0796	.0953	.107
	3983		.0324	.0412	.0687	.0859	.0984
Faxen (12)	2828	.1217					
	2901	.1112					
	3046	.08778	.1156				
	3191		.09803	.1184			
	3336		.07609	.1044	.1200		
	3481		.04434	.08938	.1084	.1209	
	3626		.03836	.07496	.09627	.1105	.1213
	3771		.03511	.06055	.08441	.1004	.1118
	3916		.03309	.04998	.07272	.09066	.1027
J.S.M.E. (1)	2845	.1189					
	2987	.0968	.1221				
	3129		.1062	.1248			
	3271		.0873	.1107			
	3414		.0601	.0963	.1134		
	3556		.0412	.0820	.1020	.1152	
	3698		.0360	.0671	.0907	.1051	.1166
	3840		.0338	.0521	.0796	.0955	.1076
	3982		.0324	.0436	.0684	.0862	.0992
Timroth (55)	2845	.1193					
	2987	.0956	.1227				
	3129		.1059	.1246			
	3271		.0873	.1105	.1249		
	3414		.0586	.0963	.1132		
	3556		.03812	.08201	.1017	.1147	
	3698		.03476	.06712	.09018	.1046	.1160
	3840		.03300	.05126	.07897	.09547	.1075
	3983		.03188	.04117	.06808	.08634	.09915
Holser & Kennedy (15)	1626		.03611		.0971		
Skeletal Tables (2)	3556				.10197		

Table 13b

Author(s)	Pressure (psia)	Temperature °F 705.4	710	720	730	740	750	760	770	780	790	800
Keenan and Keyes (23)	3000		.1142									
	3100		.1012	.1140	.1238							
	3200		.0852	.1027	.1138	.1226						
	3206.2	.0503	.0843	.1020	.1132	.1220						
	3300		.0545	.0905	.1037	.1134	.1215					
	3400		.0363	.0773	.0935	.1042	.1129	.1204				
	3500	.0322	.0342	.0557	.0823	.0952	.1047	.1126	.1195			
	3600		.0329	.0410	.0701	.0860	.0965	.1049	.1121	.1185	.1243	
	3700		.0320	.0371	.0557	.0764	.0885	.0975	.1051	.1117	.1177	.1231
	3800		.0313	.0349	.0456	.0664	.0804	.0903	.0983	.1052	.1113	.1169
	3900		.0308	.0317	.0400	.0558	.0721	.0832	.0917	.0989	.1052	.1109
	4000	.0295	.0303	.0328	.0373	.0478	.0638	.0761	.0852	.0927	.0993	.1052

technique. It appears to the authors that in the 705 to 770 F region, reliance was placed upon the measurements of Keyes, Smith, and Gerry [27], and Kirillin, et al. [29].

A combined analytical and graphical technique was used to obtain values listed for the specific volumes in the critical region in the 1952 and 1958 Timroth tables [55, 56]. It is thought that the isometrics of Timroth [54] were used for this purpose. It is interesting to note that two equations of state were given in the 1952 and 1958 Timroth tables. The first equation describes the whole range of parameters covered by the tables with the exception of those near the saturation line and the critical region. The second equation describes the region near the saturation line as well as the supercritical region. Both equations were based on the specific-heat determinations of German [36] and Russian [54] investigators.

The values listed in the 1956 VDI tables [46] were taken from the Timroth tables [55].

The Faxen table values were computed by means of the equation of state suggested by Juza [20]. Juza derived the equation from calorimetric measurements made in Germany [36], England [11], and Czechoslovakia [13], and from volume measurements made in the United States [27]. No mention was made by Faxen for the basis of the values of superheated water vapor in the critical region. Recently, however, Juza [21] proposed an equation of state of the form $p = F(v, T)$ which is valid in the critical region. He found that it was not possible to represent the complete region with a single equation. A comparison of the values derived by him [21] with values derived from appraised measurements in the critical region will be given in a later paper [39].

The equation of state by Tanishita [52] was used to compute values listed for superheated vapor in the 1955 JSME tables [1]. In the critical region values were derived by interpolating graphically the data adopted at the TIC [2].

The data of the various steam tables are given in Table 13 and

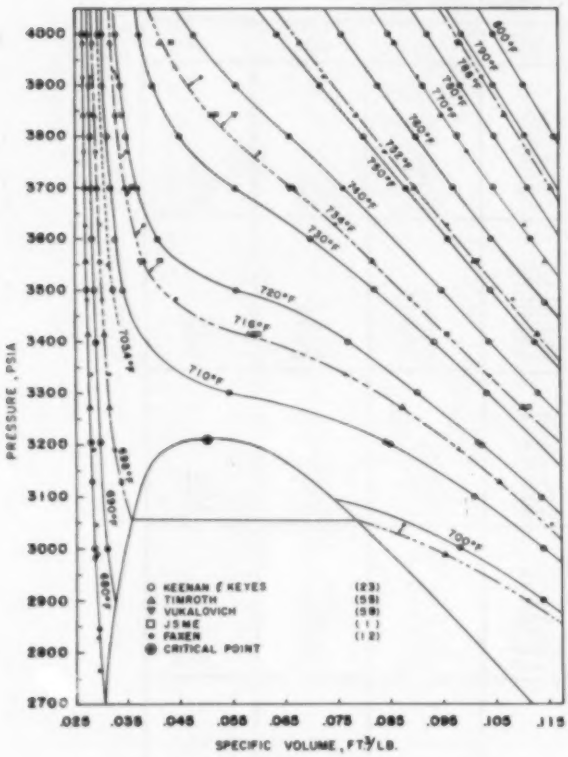

Fig. 4 Pressure-volume diagram for water

a comparison is given in Fig. 4. Lines were drawn through all of the Keenan and Keyes' data and broken lines through the 1952 Timroth values in the subcooled-liquid and superheated-vapor region. The good agreement in the subcooled-liquid region is not surprising, in view of the fact that all values were derived from the Smith and Keyes' measurements [49] or the equation of Keenan [22], which was based on the Smith and Keyes' data.

In the superheated-vapor region there are significant discrepancies between the data of various tables. Along the 734 F isotherm, for example, the deviation between the Faxen and Timroth values of pressure at a specific volume of 0.050 cu ft per lb is about 170 parts in 10,000, while the deviation between the Vukalovich and Timroth values of pressure at 0.056 cu ft per lb is about 130 parts in 10,000. Similarly, at a volume of 0.041 cu ft per lb along the 716 F isotherm the deviation between the JSME and Timroth values amounts to about 160 parts in 10,000. At higher specific volumes the deviations in general tend to be smaller. However, there are some exceptions which may be noted, for example along the 698 F isotherm at a volume of 0.088 cu ft per lb the deviation between the Faxen and Timroth values is about 70 parts in 10,000.

Above 752 F the figure indicates satisfactory agreement between the various data. However, in this region it may be noted that there are no marked changes in the trends of the isotherms.

The foregoing deviations between the derived data in the steam tables are significant, in view of the fact that they exceed the experimental uncertainty in the measured data. Therefore it may be concluded that either the experimental data were interpolated incorrectly or that estimates made of experimental error were not correct.

One important conclusion reached as a result of this survey is that it is virtually impossible to derive accurate values for such important thermodynamic properties as density, coefficient of volume expansion, and compressibility from the existing data in the various steam tables. To remedy this situation pressure-volume-temperature data will be taken at relatively small intervals in the next paper. These proposed values [39] are more accurate than those appearing in the various steam tables, since deviations from the original experimental values are entirely within the experimental uncertainties.

Critical Data

This survey would not be complete if various investigations on the critical point were not reviewed. At the turn of the twentieth century opinions were held by many investigators [45] that the region above the point of meniscus disappearance might be a two-phase region. This probably was the underlying cause for the many investigations conducted on the critical point in the past two decades. In some investigations a transparent closed container was used to observe visually the point of meniscus disappearance. In the other investigations the critical point was investigated by analyzing calorimetric and volumetric data.

Table 14 gives values for the critical constants derived in this century with the exception of that in the first entry. As a matter of historical interest alone, the critical point was first observed by la Tour[9] in 1822 with a bent, sealed tube. A sample of water was contained in one arm of the tube, while air to indicate the pressure was in the other. Mercury, which separated the water from the air, served as a transmitter of pressure. A value of 683.6 F was obtained for the critical temperature. The reasons given for this low value [45] was that a foreign substance was added to retard leaching of the glass, and also the effect of mercury on the vapor pressure was not taken into account.

Holborn and Baumann concluded from their measured isotherms in the critical region that the critical temperature was between 705.3 and 706.3 F.

Several noteworthy experiments on the critical point were carried out subsequently with precision and care. H. L. Callendar[10] measured the pressure-volume-temperature relations of saturated water in the vicinity of the critical point. His experiments showed that the density of saturated water was about twice that of saturated vapor at the temperature where the miniscus disappeared; i.e., at 705.2 F. He further observed that the density of the vapor became equal to the density of the liquid at 717 F and 3650 psia, which is considerably different from the modern day values of 705.5 F (374.15 C) and 3210 psia (225.65 kg/sq cm). He postulated that the region between the point of meniscus disappearance and the point of identical density was, in fact, a continuance of the two-phase region.

Callendar conducted calorimetric experiments (*a*) to corroborate his volumetric experiments, and (*b*) to investigate the effect of air and other impurities on the pressure-volume-temperature relation of water and water vapor in the critical region. He found that during condensation, in the two-phase region above the point of meniscus disappearance, the pressure did not remain constant but increased uniformly. It should be pointed out that these trends are somewhat similar to that for isotherms in the region now accepted as supercritical. However, Callendar attributed the uniform increase of pressure during condensation to air in the water vapor.

Unfortunately, there were differences between the amount of air contained in the water of the volumetric and calorimetric experiments. In the former, he considered the water vapor as being air-free, since it contained air in the proportion of 1 part out of 10^9 by volume. In the latter experiments the air content was

[9] The la Tour experiments are recorded by Preston [45].
[10] Some of Callendar's observations were recorded by Jakob [19].

Table 14 Critical constants for water derived from experimental data

Number	Investigators	Pressure psia	Pressure kg/cm²	Specific Volume ft³/lb	Specific Volume cm³/gram	Temperature °F	Temperature °C
1	La Tour, 1822, Ref. 45.					683.6	362
2	Traube and Tichoner, 1898, Ref. 2.					705.2	374
3	Holborn and Baumann, 1910, Ref. 14.	3200	225			705.3 to 706.3	374.07 to 374.63
4	Schroer, 1927, Ref. 47.					705.6 ± .4	374.20 ± .22
55	Callendar, H. L., * 1929, Ref. 5.	3222	226.5			705.2	374
6	Callendar, H. L.,** 1929, Ref. 5.	3650	257	.0443	2.6	717	380.5
7	Keyes and Smith, 1931, Ref. 25.	3211	225.79	.04543	3.086	705.4 ± 2	374.11 ± 1
8	Egerton and Callendar, 1932, Ref. 10.					705.2 to 706	374 to 374.5
9	Nieuwenburg and Blumendal, 1932, Ref. 38	3214	226	.045 to .048	2.8 to 3.0	705.2	374
10	Smith, et al., 1934, Ref. 48.	3206.2	225.41	.0512	3.1975	705.4 ± .2	374.11 ± .1
11	Eck, 1937, Ref. 9.	3206.8	225.51	.0491	3.066	705.6	374.23
12	Havlicek and Miskovsky, 1938, Ref. 13.	3200 to 3225	225 to 227			706	374.5
13	Osborne, et al., 1937, Ref. 41.	3209.5	225.65	.05	3.1	705.47	374.15
14	Timroth, 1952, Ref. 55.	3209.5	225.65	.0528	3.3	705.47	374.15
15	Kirillin, 1955, Ref. 30.	3209.5	225.65	.0528	3.3	705.47	374.15
16	Kowak and Grosh, 1959, Ref. 39.	3208	225.54	.0525 ±.0005	3.28 ± .03	705.5	374.35

* Meniscus disappeared

appreciably higher, being about 2 parts in 10^4 by volume of air. Callendar did not measure the enthalpy of air-free water for temperatures above 705.2 F, but merely conjectured that during condensation there should be no increase in the pressure. It appears, therefore, that his conjecture was invalid since it was not based on experiment. Callendar, therefore, was not justified in attributing the uniform increase of pressure during condensation to air in the water vapor.

Similar objections to the observations of Callendar were made earlier by Davis and Keenan [6] and requoted in [19, 39]. Davis and Keenan mentioned that the measurements of Callendar were not accurate enough to decide whether the slopes of the isotherms should be flat or slightly curved in the immediate vicinity of the critical point. In view of the foregoing discussion the measurements of Callendar are not of utility to this paper, since his pressure-temperature measurements were not as accurate as estimated [6], and since it is probable that air (impurity) was present to a larger amount in his volumetric and calorimetric experiments than estimated by him.

Experiments subsequently carried out by Havlicek and Miskovsky [13], Egerton and Callendar [10], and Koch [34] showed that only one phase existed above the critical point. Havlicek and Miskovsky [13] concluded, from their measurements of enthalpy and specific heat, that the critical pressure lies between 3200 and 3225 psia. They found that the enthalpy of vaporization was zero for temperatures greater than 706 F.

Keyes and Smith [25] and Smith and Keyes [49] derived critical constants from their P-V-T measurements. No explanation was given for the significantly different values for the critical volume in the Keenan and Keyes' tables [23].

Nieuwenburg and Blumendal [38] derived critical constants from their measured isometrics in the critical region. They were of the opinion that the critical volume derived was slightly unreliable, being somewhat less than the true value.

The method used by Osborne, et al. [43], to derive the critical constants of water was not given. However, it appears that these were evaluated from their saturation pressure [4] and calorimetric [43] measurements.

Timroth [55], Kirillin, et al. [30], and reference [39] derived critical volumes by essentially identical methods. The assumption made is that the isometrics in the critical region are linear over a limited range of pressures, volume, and temperature. Furthermore, the method is based on the fact that the change of saturation pressure with temperature $(dP_s/dT)_{P_c,\ T_c}$ is identical to $(\partial P/\partial T)^{V_c}$. They [30, 39, 55] derived almost identical values for the critical constants of water. Their values are to be recommended, since the method employed to derive them involves the use of volumetric data in conjunction with saturation pressure data.

Conclusions

Saturation pressures computed from Osborne and Meyers' formula are recommended for use, since the formula was derived from a series of accurate and independent measurements. The deviations of the experimental measurements from the computed values of the formula are entirely within 5 parts in 10,000.

There is agreement to within 1.2 per cent between the specific-volume data along the vapor saturation line of Osborne, et al., Eck, VDI, and Timroth (VTI) up to a temperature of 702 F. However, the Osborne, et al., and VTI data are to be preferred up to this temperature, since they are consistent to within 0.5 per cent. From 702 to 705.2 F there is good agreement between the Eck, VDI, and VTI data. These are to be preferred, since in this range the Osborne, et al., data are in error.

There is agreement within 1 per cent between the data of Eck Osborne, et al., VDI, and VTI for the specific volume of saturated water up to a temperature of 701 F. For temperatures between 701 and 705.2 F the VDI and VTI data are to be preferred since in this range the Eck data are in error.

The pressure-volume-temperature values of subcooled water in the Keenan and Keyes' tables are to be favored over those listed in the Vukalovich, Faxen, and JSME tables, since the former were derived from the volumetric measurements of Smith and Keyes and the enthalpy measurements of Havlicek and Miskovsky, while the latter were only derived from Smith and Keyes' data.

In the superheated region, values for pressure, volume, and temperature in the various steam tables were derived graphically from the volumetric measurements of Keyes, et al., Timroth (VTI), and Kirillin and the enthalpy measurements of Havlicek and Miskovsky and of Egerton and Callendar. However, the derived

data in the steam tables are not of utility because (*a*) the deviations in pressures of 100 to 200 parts in 10,000 existing between them are far in excess of the experimental uncertainties, and (*b*) the data are given at large intervals, making it virtually impossible to interpolate and obtain accurate values for such functions as density, coefficient of volume of expansion, and so on.

None of the various equations of state has been completely successful in the critical region. The various theories used in deriving the equations of state have failed to explain accurately the volumetric behavior in the immediate vicinity of the critical point.

Acknowledgments

The authors are grateful for material which was kindly sent by different investigators and organizations and are particularly indebted to the following: E. A. Bruges, A. C. Egerton, Electrical Research Association, E. R. G. Eckert, J. H. Keenan, G. C. Kennedy, F. G. Keyes, V. A. Kirillin, Library of Congress, J. C. McCabe, C. H. Meyers, J. R. Moszynski, B. H. Sage, J. Small, R. C. Spencer, H. F. Stimson, and E. Whalley. They wish to thank A. Bushell, D. Cash, T. Fitzsimmons, R. Hunter, W. Kunimoto, and T. Miyazaki for performing many computations and for preparing the diagrams.

The authors wish to acknowledge the support of the Argonne National Laboratory under Subcontract 31-109-38-704, which made this work possible. We also wish to acknowledge the advice and encouragement given by P. A. Lottes of the Argonne National Laboratory throughout the entire period of this investigation.

References

1 Anonymous, "Revised Steam Tables and Diagrams of the JSME," *The Japan Society of Mechanical Engineers*, second edition, 1955.

2 Anonymous, "Skeletal Tables for Water and Water Vapor Adopted at the Third International Conference on Steam Tables," *Mechanical Engineering*, vol. 57, 1935, pp. 710–713.

3 Anonymous, "Warmetabellen," F. Vieweg und Sohn, Braunschweig, Germany, 1919.

4 G. S. Callendar and A. C. Egerton, "The 1939 Callendar Steam Tables," Arnold Press, London, England, second edition, 1949.

5 H. L. Callendar, "Extended Steam Tables," *Proceedings, Inst. Mech. E.*, vol. 1, 1929, pp. 507–527.

6 H. N. Davis and J. H. Keenan, "Recent Research on the Thermal Properties of Steam," *World Engineering Congress*, Tokyo, Japan, vol. 4, 1929, pp. 239–263.

7 N. E. Dorsey, "Properties of Ordinary Water Substance," first edition, Reinhold Publishing Corp., New York, N. Y., 1940.

8 L. S. Dzung and W. Rohrbach, "Enthalpy, Entropy Diagrams for Water and Water Vapor," Springer Verlag, Berlin, Germany, 1955.

9 H. Eck, "Zustandsgrössen des Wassers im Kristischen Gebiet," *Physikalische Zeitschrift*, vol. 38, 1937, p. 256.

10 A. C. Egerton and G. S. Callendar, "On the Saturation Pressures of Steam (170° to 374°C)," *Philosophical Transactions of Royal Society*, series A, vol. 231, 1932–1933, pp. 147–205.

11 A. C. Egerton and G. S. Callendar, Electrical Research Association Report J/T 115, 1940.

12 O. H. Faxen, "Thermodynamic Tables in the Metric System for Water and Steam," *Nordisk Rotogravyr*, Stockholm, Sweden, 1953.

13 J. Havlicek and L. Miskovsky, *Helvetica Physica Acta*, vol. 9, 1936, pp. 161–207. Translated into English by School of Mechanical Engineering, Purdue University, 1959.

14 L. Holborn and A. Baumann, "Über den Sättigungsdruck des Wasser dampfes ober halb 200°," *Annalen der Physik*, vol. 31, 1910, pp. 945–970.

15 W. T. Holser and G. C. Kennedy, "Properties of Water. Part IV," *American Journal of Science*, vol. 256, 1958, pp. 744–754.

16 W. T. Holser and G. C. Kennedy, Document No. 5756, American Documentation Institute, Library of Congress, Washington, D. C.

17 U. Issarescu, "Isentropic Checking of Vapor Tables at Saturation Boundary Lines and Ways of Improving Them," Thermodynamic and Transport Properties of Gases, Liquids, and Solids, ASME, New York, N. Y., 1959, pp. 157–169.

18 M. Jakob and W. Fritz, "Die Verdampfungswärme des Wassers und das spezifische Volumen von Sattdampf bis zu 202 kg/cm² (365°)," *Physikalische Zeitschrift*, vol. 36, 1935, pp. 651–659.

19 M. Jakob, "Steam Research in Europe and in America," *Engineering*, vol. 132, 1931, pp. 143–146, 518–521, 651–653, 684–686, 707–709, 744–746, and 800–804.

20 J. Juza, "Equation of State for Steam," *Engineering*, vol. 146, 1938, pp. 1–3 and 34–36.

21 J. Juza, "A General Steam Equation in the Range 0 to 800°C and 0 to 2500 Bars," Prague, Czechoslovakia, 1958.

22 J. H. Keenan, "Thermal Properties of Compressed Liquid Water," *Mechanical Engineering*, vol. 53, 1931, pp. 127–131.

23 J. H. Keenan and F. G. Keyes, "Thermodynamic Properties of Steam," first edition, John Wiley & Sons, New York, N. Y., 1953.

24 G. C. Kennedy, "Pressure-Volume-Temperature Relations in Water at Elevated Temperatures and Pressures," *American Journal of Science*, vol. 248, 1950, pp. 540–564.

25 F. G. Keyes and L. B. Smith, "Some Final Values for the Properties of Saturated and Superheated Water," *Mechanical Engineering*, vol. 53, 1931, pp. 132–135.

26 F. G. Keyes, et al., "Reports on Steam Research," *Mechanical Engineering*, vol. 54, 1932, pp. 123–127.

27 F. G. Keyes, L. B. Smith, and H. T. Gerry, "Steam Research Program. Part IV. The Specific Volume of Steam in the Saturated and Superheated Condition . . .," *Proceedings, American Academy of Arts and Sciences*, vol. 70, 1936, pp. 319–364.

28 F. G. Keyes, "The Consistency of the Thermodynamic Data for Water Substance Vapor Phase to 550°. VII," *Journal of Chemical Physics*, vol. 17, 1949, pp. 923–934.

29 V. A. Kirillin and L. I. Rumyanstev, "Experimental Investigations of the Thermodynamic Properties of Water and Water Vapor at High Pressures and Temperatures," *Transactions, Moscow Order of Lenin*, Power Institute, named for V. M. Molotov, VII, State Power Publishing House, Moscow, USSR, 1953.

30 V. A. Kirillin and V. N. Zubarev, "Experimental Investigation of the Specific Volume of Water and Water Vapor at High Pressures," translated into English from *Teploenergetika*, vol. 2, 1955, pp. 19–23.

31 V. A. Kirillin, L. I. Rumyanstev, and V. N. Zubarev, Collected reports of the USSR, Fifth International Conference on Properties of Steam, London, England, 1956.

32 V. A. Kirillin and S. A. Ulybin, *Teploenergetika*, vol. 5, No. 4, 1958, p. 53.

33 R. Kiyama, H. Kinoshita, and S. Kitahara, "State Diagram of Steam," *Review of Physical Chemistry of Japan*, vol. 25, 1955, pp. 21–24.

34 W. Koch, "Die spezifische Wärme des über hitzten Wasserdampfes für Drücke von 120 bis 200 at und von der Sättigungstemperatur bis 450°C," *Forschung auf dem Gebiete des Ingenieurwesens*, vol. 3, 1932, pp. 1–10.

35 W. Koch, "Die Verdampfungswärme des Wassers im Druckbereich von 100 bis 200 kg/cm²," *Forschung auf dem Gebiete des Ingenieurwesens*, vol. 5, 1934, pp. 257–259.

36 W. Koch, "Die spezifische Wärme des Wassers von 0° bis 350°C und vom jeweiligen Sättigungsdruck bis 260 kg/cm²," *Forschung auf dem Gebiete des Ingenieurwesens*, vol. 5, 1934, pp. 138–145.

37 E. F. Leib, "Steam Tables," Combustion Engineering Inc., New York, N. Y., third edition, 1940.

38 C. J. van Nieuwenburg and H. B. Blumendal, "The Isotherms of Water From 350°–480° C and for Pressures up to 600 kg per sq cm," *Recueil des Travaux Chimiques des Pays-Bas*, vol. 51, 1932, pp. 707–714.

39 E. S. Nowak and R. J. Grosh, Argonne National Laboratory, Argonne National Laboratory Report 6064, October, 1959. See also, E. S. Nowak, R. J. Grosh, and P. E. Liley, "Smoothed *P-V-T* Data for Water in the Critical Region Derived From Experimental Measurements," published in this issue, pp. 14–26.

40 N. S. Osborne, "Calorimetry of a Fluid," *Journal of Research of the National Bureau of Standards*, vol. 4, 1930, pp. 609–629.

41 N. S. Osborne, H. F. Stimson, E. F. Fiock, and D. C. Ginnings, "The Pressure of Saturated Water Vapor in the Range 100° to 374°C," *Journal of Research of the National Bureau of Standards*, vol. 10, 1933, pp. 155–188.

42 N. S. Osborne and C. H. Meyers, "A Formula and Tables for the Pressure of Saturated Water Vapor in the Range 0 to 374 C," *Journal of Research of the National Bureau of Standards*, vol. 13, 1934, pp. 1–20.

43 N. S. Osborne, H. F. Stimson, and D. C. Ginnings, "Calorimetric Determination of the Thermodynamic Properties of Saturated Water in Both the Liquid and Gaseous States From 100 to 374°C," *Journal of Research of the National Bureau of Standards*, vol. 18, 1937, p. 389.

44 N. S. Osborne, H. F. Stimson, and D. C. Ginnings, "Thermal Properties of Saturated Water and Steam," *Journal of Research of the National Bureau of Standards*, vol. 23, 1939, pp. 261–270.

45 T. Preston, "The Theory of Heat," The Macmillan Company, London, England, 1904.

46 E. Schmidt, "VDI Steam Tables Including a Mollier Diagram for Temperatures up to 800°C," Springer-Verlag, Berlin, Germany, 1956.

47 E. Schröer, "Untersuchungen über den kristischen Zustand," *Zeitschrift für Physikalische Chemie*, vol. 129, 1927, pp. 79–110.

48 L. B. Smith, F. G. Keyes, and H. T. Gerry, "Steam Research Program. Part II. The Vapor Pressure of Water," *Proceedings, American Academy of Arts and Sciences*, vol. 69, 1934, pp. 137–168.

49 L. B. Smith and F. G. Keyes, "Steam Research Program. Part III. The Volumes of Unit Mass of Liquid Water and Their Correlation as a Function of Pressure and Temperature," *Proceedings, American Academy of Arts and Sciences*, vol. 69, 1934, pp. 285–312.

50 S. Sugawaro, Jokikogaku, Genron, Kioshen Yokendo, 1945, p. 97.

51 G. Tammann and A. Ruhenbeck, "Die spezifischen Volumen des Wassers zwischen 20° und 650°, die des Athyläthers und des Athylalkohols Zwischen 20° und 400° bei Drucken von 1—2500 kg/cm^2," *Annalen der Physik*, series 5, vol. 13, 1932, pp.63–79.

52 I. Tanishita, *Trans. Japan Society of Mechanical Engineers*, vol. 10, 1944.

53 D. L. Timroth and N. B. Vargaftik, "Heat Conductivity, Viscosity, and Thermodynamical Properties of Steam at High Temperatures and Pressures," *Transactions Fourth World Power Conference*, London, England, vol. III, 1950, pp. 1642–1666.

54 D. L. Timroth, "High Pressure Steam in Power Engineering," State Power Publishing House, Moscow, USSR, 1950.

55 D. L. Timroth, "Tables of Thermodynamic Properties of Water and Water Vapor," first edition, Moscow, 1952, Leningrad, translated into English by Land Turbine Engineering Division, Westinghouse Electric Corporation, South Philadelphia Works, 1954.

56 D. L. Timroth, S. L. Rivkin, A. M. Sirota, and N. B. Vargaftik, "Tables of Thermodynamic Properties of Water and Water Vapor," second edition, Gosudarstvennoe Energe-ticheskoe, Izadelstvo, Moscow, USSR, 1958.

57 M. Trautz and H. Steyer, "Die Zustandsgrössen des Wassers im Bereich von 10° bis 500° und von Sättigungsdruck vis 300 at," *Forschung auf dem Gebiete des Ingenieurwesens*, vol. 2, 1931, pp. 45–52.

58 M. P. Vukalovich, "Thermodynamic Properties of Water and Water Vapor," Moscow, 1951, translated into English by Large Steam Turbine Generator Department, General Electric Company, Schenectady, N. Y., 1954.

59 M. P. Vukalovich, "Thermodynamic Properties of Water and Water Vapor," State Scientific Technical Publication, Moscow, USSR, 1955.

Smoothed Pressure-Volume-Temperature Data for Water in the Critical Region Derived From Experimental Measurements

E. S. NOWAK
Graduate Assistant,
School of Mechanical Engineering,
Purdue University, Lafayette, Ind.

R. J. GROSH
Professor of Mechanical Engineering,
Purdue University,
Assoc. Mem. ASME

P. E. LILEY
Assistant Professor of
Mechanical Engineering,
Purdue University

A graphical technique was used to derive pressure-volume-temperature data from previous American, Czechoslovakian, and Russian experimental measurements. The data were derived at close intervals throughout the region encompassed by pressures from 3000 to 4000 psia, specific volumes from 0.030 to 0.120 cu ft per lb, and temperatures from 690 to 752 F. The average deviation of experimental values of pressure from the derived values was less than one part in 10,000 in the region for specific volumes greater than the critical volume (0.0525 cu ft per lb) and was less than ten parts per 10,000 in the region for specific volumes less than the critical volume. These deviations are thought to be insignificant since they are entirely within the uncertainty of recent experimental measurements [8].[1] In a previous paper [13], deviations of some 100 to 200 parts in 10,000 in pressure were shown to exist between the data of various steam tables. Since the data in the steam tables were derived from the same primary data used in this paper, one may conclude that these deviations greatly exceed the experimental uncertainty and must therefore be charged to previous interpolation methods and the previous paucity of data. One of the important results of this study was the establishment of the fact that there was excellent agreement between recent measurements by Kirillin, et al. [7–10], and older measurements by Keyes and Smith [5] and by Havlicek and Miskovsky [2].

Introduction

No equation of state for steam has yet been derived which represents accurate experimental measurements to within their experimental uncertainties throughout the critical region. In 1949, Keyes [6] derived an equation of state for steam having the form $P = F(V, T)$ from his experimental measurements [5]. However, he found that in the range of pressures, specific volumes, and temperatures of interest in this paper, the equation failed to represent his measurements to within the experimental uncertainties. In addition, the values of enthalpy calculated from his equation were not in agreement with the precise enthalpy measurements of Havlicek and Miskovsky as the critical volume was approached. He concluded that to derive an accurate equation of state it is necessary to have additional volumetric measurements for steam in the critical region, as his own measurements were recognised as being taken over too coarse an interval of pressure, volume, and temperature.

In reference [13] a survey was made of experimental and smoothed *P-V-T* (pressure, specific volume, temperature) data available for water in the critical region. It was found that even though extensive measurements were now available, there was a lack of smoothed data in the various steam tables at close intervals of pressure, volume, and temperature. Therefore the purpose of the work reported in this paper was to rectify this situation by deriving accurate *P-V-T* values at sufficiently close intervals in the critical region. Since many researchers[2] and theoreticians were unsuccessful in their attempts to derive an accurate equation of state it was decided to derive *P-V-T* in the critical region by a graphical technique. The graphical technique used to derive these data along with the error analysis is fully explained herein.

[1] Numbers in brackets designate References at end of paper.

[2] After the work of this paper was completed it was noted that Juza's most recent equation [4] was successful in representing experimental measurements in a part of the critical region.

Contributed by the Heat Transfer Division of The American Society of Mechanical Engineers and presented at the ASME-AIChE Heat Transfer Conference, Buffalo, N. Y., August 15–17, 1960. Manuscript received at ASME Headquarters, May 19, 1960. Paper No. 60—HT-26.

Saturation Data

P-V-T values along the saturation line were derived from the measurements considered reliable in reference [13]. Fig. 1 gives a comparison between the derived and experimental values of specific volume along the liquid and vapor saturation line. A tabulation of the derived values is given in Table 1.

The values derived for the specific volume of saturated liquid up to 3100 psia are essentially the arithmetic mean of the values given by Eck [1], Osborne, et al. [16], and those given in the steam tables of Schmidt [17] and Timrot [19]. From 3100 to 3203 psia the derived values correspond to the arithmetic mean of the values given in the Timrot and Schmidt tables. By means of the error analysis in reference [13], it may be concluded that the specific-volume data of Table 1 for saturated water are accurate to at least $^1/_2$ per cent.

The derived values for the specific volume of saturated vapor up to 3127 psia correspond to the arithmetic mean of the almost identical Osborne and Timrot values, while those derived for pressures from 3127 to 3203 psia are the arithmetic mean of the Eck, Timrot, and Schmidt values. Up to 3127 psia the derived values are accurate to at least $^1/_2$ per cent, and from 3127 to 3203 psia the derived values are accurate within 1 per cent.

The temperature values for saturation pressure up to 2900 psia were those obtained from the Osborne and Meyers formula [15]. The values, however, for pressures greater than 2900 psia were obtained by graphically interpolating the measurements given in

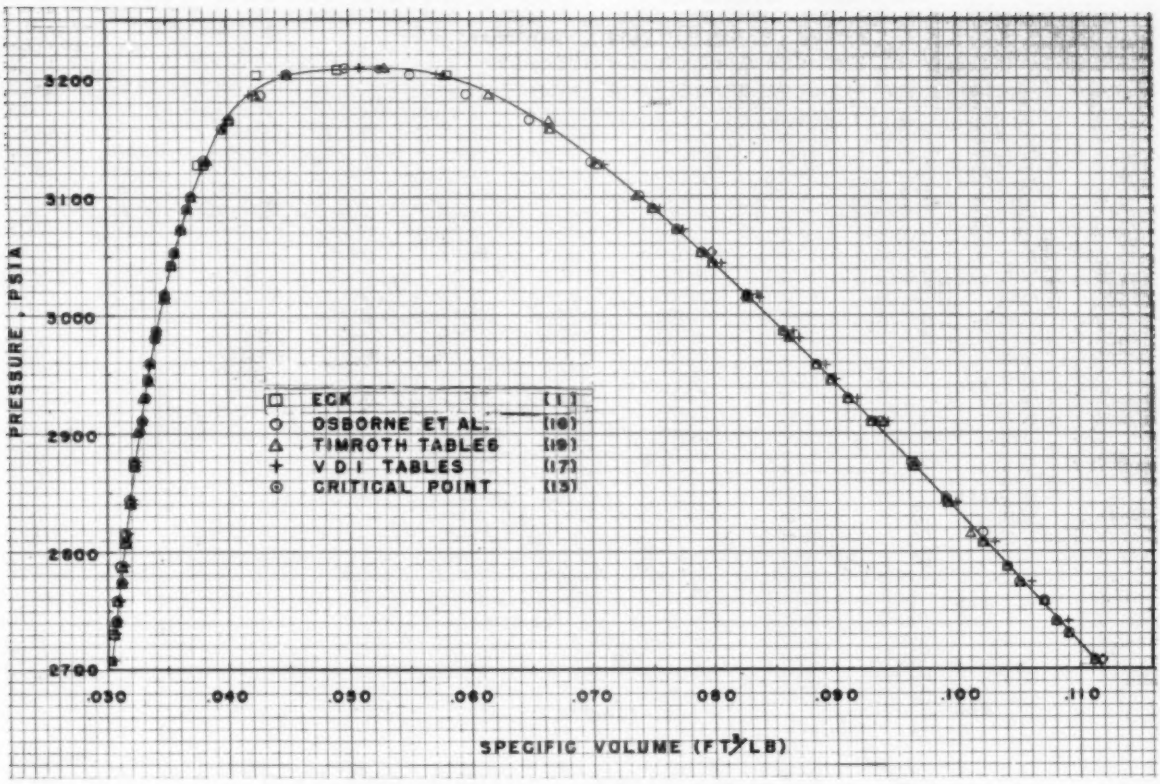

Fig. 1 Pressure-volume diagram for saturated water and water vapor

Table 3 of reference [13] by plotting pressure against temperature. From the analysis given in reference [13] it can be determined that the values of Table 1 for saturation temperature and pressure do not deviate from precise experimental data by more than 5 parts in 10,000 for pressure.

Recommended *P-V-T* Data for Superheated Water Vapor

The *P-V-T* values of this paper were derived from measurements that were considered the most reliable in reference [13]. More specifically, the measurements of Kirillin [7–10], Keyes, et al. [5, 18], and those derived by Havlicek and Miskovsky [2] and by Osborne, et al. [16], were considered as if they were a single consistent body of data. This was done out of necessity since it was found that the data of Keyes and Smith, Havlicek and Miskovsky, and Kirillin, et al., did not, in themselves, form a comprehensive body of data in the critical region, from which accurate *P-V-T* values could be derived.

It was noted in reference [14] that there were marked changes in the slopes of the isotherms in the critical region. In order that the experimental measurements be interpolated accurately it is necessary that they be plotted in such a way that they yield lines of small curvature. The graphical method used in this paper consisted of plotting the product of pressure and volume PV against volume V with temperature as a parameter. Thus, from such a plot, isometrics and finally isotherms were constructed at close intervals throughout the critical region.

Fig. 2 is a small-scale reproduction of a PV-V plot in which the various experimental values were drawn accurately to a few parts in 10,000 with temperature as a parameter. At 716 F one may note the excellent agreement between the values of Keyes, et al. [5], Havlicek and Miskovsky [2], and Kirillin, et al. [7–10], and the corresponding smooth curve. This agreement is particularly noteworthy since the measurements of the Keyes and Havlicek groups were conducted about 25 years ago.

Table 1 Pressure-volume temperature along saturation line

Pressure, psia	Temp, deg F	Specific volume, cu ft per lb — Saturated liquid	Saturated vapor
2700	679.54	0.0303	0.1118
2750	682.23	0.0308	0.1075
2800	684.98	0.0314	0.1030
2850	687.63	0.0320	0.0985
2900	690.25	0.0327	0.0939
2950	692.82	0.0334	0.0893
3000	695.32	0.0344	0.0844
3020	696.32	0.0349	0.0824
3040	697.30	0.0354	0.0804
3060	698.28	0.0359	0.0783
3080	699.26	0.0364	0.0762
3100	700.23	0.0371	0.0740
3120	701.20	0.0378	0.0717
3140	702.17	0.0386	0.0691
3160	703.13	0.0396	0.0663
3180	704.10	0.0411	0.0631
3200	705.05	0.0443	0.0586
3208	705.45	0.0525	0.0525

From Fig. 2, values of PV were read at uniform increments of volume (usually every 0.002 or 0.003 cu ft per lb). These values were then divided by the specific volume to give pressure values which were subsequently used to construct the isotherms[3] shown in Fig. 3. Good agreement is seen to exist between the

[3] Smooth continuous curves were drawn through computed values of pressure.

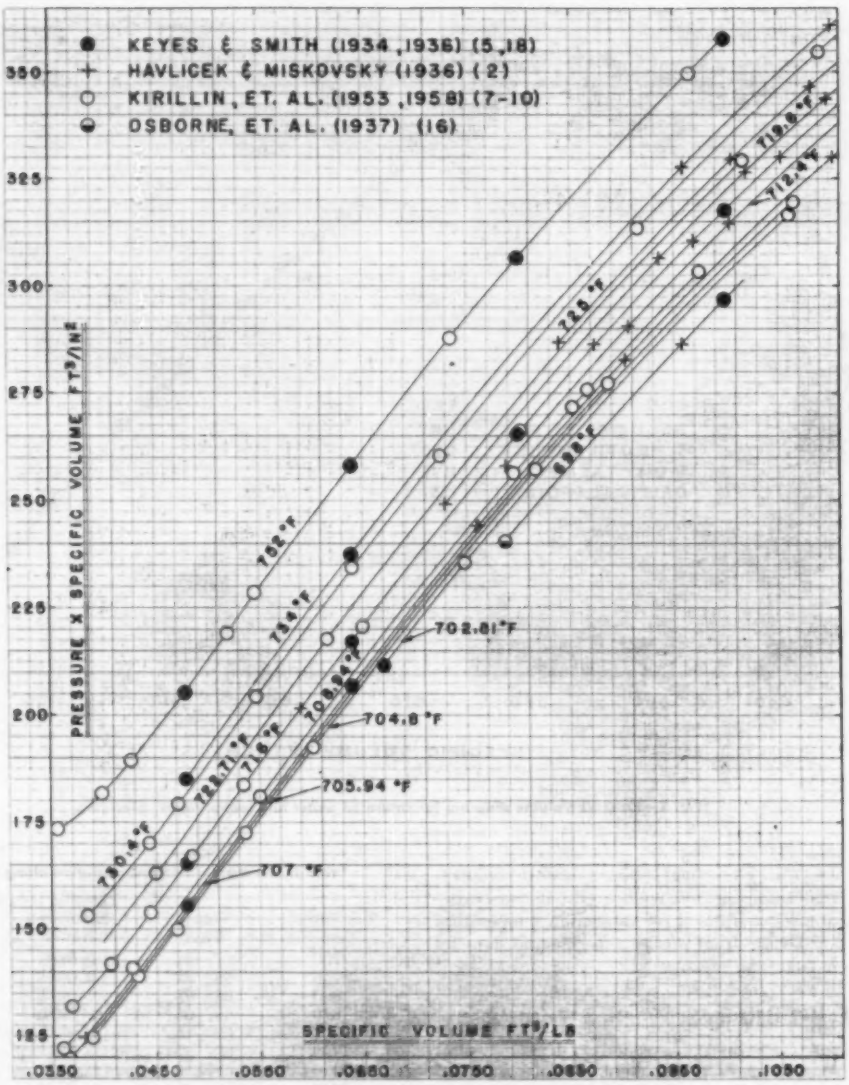

Fig. 2 *PV-V* isotherms in the critical region

smoothed computed pressure values and the experimentally observed values. Fig. 3 shows conclusively that when equal weight is given all the measurements they form a consistent body of data which is more than adequate in tracing out isotherms in the critical region.

The values of pressure computed from the *PV-V* isotherms of Fig. 2 were next plotted against temperature for constant specific volume, and some of these isometrics are shown in Fig. 4 to illustrate the temperature dependence. For the range of pressures and temperatures shown it is interesting to note that, within experimental error, the isometrics between 0.045 and 0.060 cu ft per lb are linear. Fig. 4 also indicates the excellent agreement between the data obtained from the various isotherms of Fig. 2. The only exception to this is the deviation of the data along the 730.4 F isotherm at specific volumes between 0.040 and 0.051 cu ft per lb and at pressures between 3750 and 3950 psia. These deviations which amount to as much as 30 psia in pressure are outside the limits of error and therefore the experimental values must be in error. Since the data along the 730.4 F isotherm were derived solely from the measurements of Kirillin, et al. [7–10], Figs. 2 and 3, it was concluded that his two experimental values along the 730.4 F isotherm in this range were too high by as much as 30 psi.[4]

Values of *P-V-T* read from Fig. 4 were plotted on a pressure-volume diagram. A small-scale reproduction of this diagram is given in Fig. 5 and the results are tabulated in Table 2.[5]

[4] After the work described in the present paper was completed, the authors noted that Kirillin [11] had recently analyzed his measurements. From his analysis he concluded that some of his values for pressure along the 730.4 F isotherm were in error and were somewhat high. Kirillin's new values [11] of *P-V-T* along the 730.4 F isotherm are in good agreement with the isometrics (dotted lines) of Fig. 4.

[5] A large-scale diagram of Figs. 3 and 5 has been deposited as Document No. 6469 with the ADI Auxiliary Publications Project, Photoduplication Service, Library of Congress, Washington 25, D. C. A copy may be secured by citing the Document number and by remitting $5 for photoprints, or $2.25 for 35 mm microfilm. Advance payment is required. Make checks or money orders payable to: Chief, Photoduplication Service, Library of Congress.

Table 2 Pressure-volume-temperature data for subcooled water and superheated water vapor. Specific volume, cu ft per lb.

Temp, °F Press, psia	690	691	692	693	694	695	696	697	698	699
3000	.03149	.03187	.03233	.03283	.03341	.03412			.0928	.0954
3020	.03131	.03167	.03209	.03256	.03308	.03368	.03450		.08883	.09150
3040	.03114	.03148	.03187	.03231	.03279	.03332	.03397	.03494	.08425	.08733
3060	.03098	.03129	.03168	.03209	.03253	.03300	.03361	.03437	.03536	.08280
3080	.03083	.03113	.03150	.03188	.03228	.03274	.03331	.03390	.03476	.03584
3100	.03069	.03097	.03134	.03169	.03206	.03250	.03300	.03351	.03426	.03512
3120	.03056	.03082	.03118	.03152	.03186	.03228	.03275	.03319	.03385	.03457
3140	.03042	.03069	.03103	.03136	.03169	.03207	.03250	.03291	.03351	.03412
3160	.03029	.03056	.03088	.03120	.03153	.03188	.03227	.03265	.03320	.03373
3180	.03017	.03043	.03074	.03105	.03137	.03169	.03205	.03242	.03293	.03340
3200	.03005	.03032	.03061	.03090	.03121	.03152	.03188	.03221	.03268	.03313
3210	.03000	.03025	.03055	.03084	.03114	.03143	.03179	.03212	.03257	.03300
3220		.03020	.03048	.03077	.03107	.03136	.03171	.03203	.03245	.03288
3230		.03014	.03042	.03070	.03099	.03127	.03163	.03194	.03233	.03276
3240		.03009	.03036	.03063	.03093	.03120	.03155	.03187	.03223	.03264
3250		.03004	.03030	.03057	.03086	.03113	.03147	.03179	.03213	.03253
3260			.03024	.03051	.03079	.03106	.03139	.03171	.03203	.03242
3270			.03018	.03045	.03072	.03100	.03132	.03163	.03194	.03231
3280			.03012	.03038	.03066	.03092	.03125	.03156	.03186	.03221
3290			.03007	.03033	.03059	.03085	.03117	.03148	.03177	.03211
3300			.03002	.03027	.03053	.03079	.03111	.03142	.03168	.03202
3310				.03021	.03048	.03073	.03104	.03134	.03161	.03193
3320				.03016	.03041	.03066	.03097	.03127	.03153	.03185
3330				.03010	.03035	.03059	.03090	.03120	.03145	.03177
3340				.03005	.03030	.03054	.03083	.03113	.03138	.03168
3350				.03000	.03024	.03047	.03077	.03107	.03131	.03162
3360					.03018	.03042	.03071	.03100	.03123	.03154
3370					.03012	.03036	.03064	.03093	.03117	.03144
3380					.03007	.03031	.03058	.03087	.03109	.03139
3390					.03002	.03025	.03052	.03081	.03103	.03132
3400						.03020	.03047	.03074	.03097	.03124

Temp, °F Press, psia	700	701	702	703	704	705	706	707	708	709
3000	.09780	.10009	.10188	.10345	.10496	.10661	.10785	.10927	.11065	.11205
3020	.09418	.09635	.09850	.10025	.10205	.10370	.10525	.10665	.10820	.10955
3040	.09025	.09260	.09502	.09698	.09900	.10075	.10246	.10393	.10553	.10694
3060	.08615	.08870	.09140	.09357	.09584	.09765	.09958	.10115	.10286	.10435
3080	.08127	.08455	.08757	.08996	.09247	.09440	.09650	.09828	.10005	.10169
3100	.03639	.07967	.08330	.08608	.08873	.09092	.09335	.09524	.09722	.09892
3120	.03554	.03705	.07790	.08180	.08477	.08735	.09000	.09205	.09420	.09610
3140	.03492	.03603	.03795	.07625	.08023	.08335	.08628	.08865	.09092	.09310
3160	.03442	.03533	.03666	.03900	.07463	.07885	.08225	.08500	.08755	.08983
3180	.03400	.03477	.03582	.03735	.04035	.07255	.07750	.08105	.08390	.08640
3200	.03367	.03431	.03516	.03627	.03787	.04200	.07122	.07612	.07988	.08275
3210	.03352	.03409	.03488	.03567	.03721	.03975	.06530	.07320	.07755	.08075
3220	.03337	.03390	.03464	.03552	.03668	.03867	.04900	.06945	.07500	.07870
3230	.03323	.03374	.03440	.03522	.03623	.03788	.04105	.06385	.07195	.07635
3240	.03310	.03358	.03420	.03495	.03587	.03724	.03948	.05220	.06835	.07375
3250	.03297	.03343	.03401	.03471	.03555	.03675	.03845	.04255	.06260	.07060
3260	.03284	.03330	.03384	.03448	.03528	.03631	.03773	.04037	.05310	.06690
3270	.03273	.03317	.03368	.03427	.03501	.03595	.03720	.03911	.04450	.06155
3280	.03262	.03303	.03353	.03409	.03478	.03564	.03675	.03831	.04160	.05440
3290	.03250	.03292	.03339	.03393	.03456	.03536	.03636	.03772	.04005	.04700
3300	.03240	.03280	.03326	.03378	.03436	.03512	.03602	.03722	.03900	.04265
3310	.03229	.03269	.03314	.03363	.03418	.03488	.03572	.03679	.03827	.04077
3320	.03220	.03258	.03302	.03350	.03401	.03467	.03543	.03641	.03772	.03961
3330	.03211	.03248	.03289	.03337	.03384	.03447	.03518	.03607	.03723	.03882
3340	.03202	.03238	.03278	.03323	.03370	.03428	.03495	.03577	.03682	.03817
3350	.03193	.03228	.03267	.03311	.03356	.03412	.03474	.03549	.03646	.03764
3360	.03186	.03219	.03257	.03299	.03343	.03394	.03454	.03524	.03614	.03723
3370	.03178	.03211	.03247	.03288	.03330	.03379	.03436	.03501	.03584	.03686
3380	.03171	.03202	.03237	.03277	.03317	.03366	.03418	.03480	.03558	.03652
3390	.03163	.03193	.03228	.03267	.03306	.03352	.03402	.03462	.03534	.03621
3400	.03156	.03186	.03218	.03256	.03293	.03338	.03387	.03443	.03511	.03591

Table 2 (Continued)

Temp, °F Press, psia	710	711	712	713	714	715	716	717	718	719
3000										
3020	.11085	.11195								
3040	.10830	.10960	.11075	.11236						
3060	.10582	.10718	.10842	.10992	.11122	.11250				
3080	.10335	.10470	.10595	.10750	.10880	.11008	.11133			
3100	.10068	.10212	.10355	.10504	.10638	.10765	.10896	.11022	.11137	.11258
3120	.09788	.09945	.10100	.10255	.10388	.10525	.10665	.10787	.10915	.11030
3140	.09505	.09665	.09836	.10000	.10135	.10277	.10425	.10550	.10690	.10805
3160	.09192	.09378	.09565	.09733	.09880	.10030	.10185	.10314	.10457	.10577
3180	.08883	.09075	.09260	.09457	.09620	.09780	.09940	.10075	.10223	.10345
3200	.08545	.08757	.08985	.09175	.09345	.09527	.09687	.09833	.09985	.10115
3210	.08366	.08602	.08835	.09025	.09213	.09393	.09557	.09710	.09865	.09996
3220	.08175	.08433	.08665	.08875	.09070	.09258	.09425	.09582	.09737	.09875
3230	.07980	.08250	.08500	.08725	.08922	.09120	.09293	.09455	.09615	.09755
3240	.07758	.08064	.08338	.08570	.08773	.08975	.09160	.09327	.09492	.09635
3250	.07522	.07863	.08158	.08410	.08619	.08825	.09023	.09192	.09363	.09515
3260	.07255	.07645	.07970	.08243	.08463	.08679	.08880	.09065	.09235	.09390
3270	.06955	.07421	.07765	.08065	.08300	.08525	.08736	.08925	.09107	.09270
3280	.06590	.07165	.07542	.07870	.08133	.08373	.08590	.08785	.08975	.09137
3290	.06100	.06870	.07305	.07662	.07957	.08220	.08435	.08640	.08838	.09015
3300	.05500	.06515	.07055	.07440	.07770	.08045	.08278	.08495	.08692	.08880
3310	.04845	.06055	.06772	.07215	.07572	.07870	.08118	.08336	.08550	.08745
3320	.04371	.05525	.06435	.06973	.07360	.07675	.07948	.08175	.08405	.08608
3330	.04190	.04990	.06001	.06700	.07130	.07482	.07773	.08012	.08253	.08471
3340	.04029	.04485	.05545	.06375	.06887	.07277	.07578	.07835	.08097	.08321
3350	.03934	.04264	.05075	.05985	.06616	.07058	.07385	.07667	.07933	.08165
3360	.03864	.04112	.04625	.05575	.06300	.06817	.07185	.07495	.07763	.08005
3370	.03808	.04004	.04340	.05173	.05955	.06548	.06977	.07308	.07589	.07840
3380	.03763	.03921	.04188	.04761	.05590	.06245	.06750	.07115	.07417	.07672
3390	.03720	.03858	.04080	.04420	.05230	.05925	.06505	.06913	.07241	.07506
3400	.03683	.03808	.03994	.04267	.04845	.05606	.06227	.06688	.07050	.07327

Temp, °F Press, psia	720	722	724	726	728	730	732	734	736	738
3000										
3020										
3040										
3060										
3080										
3100										
3120	.11145									
3140	.10926	.11144								
3160	.10705	.10930	.11147							
3180	.10480	.10720	.10936	.11160						
3200	.10250	.10500	.10725	.10946	.11172					
3210	.10135	.10393	.10620	.10843	.11070					
3220	.10022	.10280	.10515	.10735	.10965	.11160				
3230	.09905	.10175	.10405	.10633	.10860	.11065				
3240	.09783	.10062	.10295	.10525	.10760	.10968	.11160			
3250	.09665	.09945	.10183	.10420	.10650	.10865	.11060			
3260	.09545	.09833	.10077	.10313	.10550	.10770	.10960	.11175		
3270	.09428	.09723	.09970	.10203	.10445	.10665	.10860	.11075		
3280	.09305	.09605	.09860	.10100	.10339	.10562	.10759	.10975	.11180	
3290	.09178	.09490	.09750	.09992	.10240	.10466	.10660	.10878	.11075	
3300	.09052	.09370	.09635	.09883	.10135	.10363	.10565	.10775	.10979	.11162
3310	.08923	.09250	.09525	.09775	.10030	.10262	.10469	.10680	.10880	.11070
3320	.08792	.09128	.09413	.09670	.09923	.10162	.10373	.10586	.10784	.10978
3330	.08659	.09009	.09297	.09560	.09817	.10060	.10275	.10492	.10687	.10880
3340	.08525	.08880	.09177	.09450	.09712	.09955	.10175	.10395	.10595	.10787
3350	.08380	.08749	.09059	.09333	.09605	.09853	.10076	.10300	.10508	.10696
3360	.08232	.08614	.08935	.09221	.09500	.09746	.09979	.10209	.10412	.10608
3370	.08084	.08480	.08812	.09104	.09388	.09640	.09880	.10112	.10320	.10518
3380	.07930	.08335	.08685	.08987	.09282	.09533	.09779	.10015	.10223	.10422
3390	.07772	.08192	.08561	.08871	.09171	.09422	.09680	.09915	.10127	.10330
3400	.07607	.08048	.08430	.08748	.09052	.09315	.09580	.09817	.10033	.10237

Table 2 (Continued)

Temp, °F 740	742	744	746	748
Press, psia				
3000				
3020				
3040				
3060				
3080				
3100				
3120				
3140				
3160				
3180				
3200				
3210				
3220				
3230				
3240				
3250				
3260				
3270				
3280				
3290				
3300				
3310				
3320	.11168			
3330	.11067	.11254		
3340	.10971	.11152		
3350	.10872	.11055	.11250	
3360	.10780	.10963	.11150	
3370	.10690	.10873	.11054	.11222
3380	.10600	.10786	.10965	.11135
3390	.10516	.10703	.10877	.11050 .11211
3400	.10427	.10618	.10790	.10963 .11125

Temp, °F 695	696	697	698
Press, psia			
3420 .03009	.03035	.03063	.03084
3440 .03000	.03023	.03050	.03072
3460	.03013	.03039	.03059
3480	.03002	.03027	.03049
3500		.03016	.03037
3520		.03005	.03027
3540			.03017
3560			.03007
3580			
3600			
3620			
3640			
3660			
3680			
3700			
3720			
3740			
3760			
3780			
3800			
3820			
3840			
3860			
3880			
3900			
3920			
3940			
3960			
3980			
4000			

Temp, °F 699	700	701	702	703	704	705	706	707	708
Press, psia									
3420 .03112	.03142	.03171	.03201	.03237	.03272	.03313	.03358	.03410	.03472
3440 .03098	.03128	.03157	.03185	.03218	.03252	.03291	.03333	.03381	.03436
3460 .03084	.03116	.03142	.03171	.03200	.03233	.03269	.03309	.03353	.03403
3480 .03073	.03103	.03129	.03157	.03186	.03216	.03250	.03287	.03329	.03374
3500 .03061	.03091	.03116	.03143	.03172	.03200	.03231	.03267	.03306	.03348
3520 .03049	.03078	.03104	.03130	.03157	.03186	.03214	.03247	.03283	.03324
3540 .03038	.03067	.03092	.03117	.03144	.03171	.03199	.03229	.03263	.03302
3560 .03027	.03056	.03080	.03105	.03132	.03158	.03186	.03212	.03245	.03280
3580 .03017	.03045	.03068	.03093	.03119	.03144	.03172	.03198	.03228	.03261
3600 .03007	.03035	.03058	.03082	.03107	.03132	.03159	.03185	.03212	.03243
3620	.03024	.03047	.03071	.03095	.03119	.03147	.03172	.03198	.03227
3640	.03014	.03037	.03059	.03084	.03107	.03134	.03158	.03184	.03212
3660		.03027	.03049	.03073	.03095	.03122	.03146	.03172	.03198
3680		.03017	.03038	.03062	.03084	.03110	.03133	.03159	.03184
3700		.03007	.03028	.03051	.03073	.03098	.03122	.03146	.03172
3720			.03018	.03041	.03063	.03087	.03110	.03136	.03160
3740			.03008	.03030	.03052	.03076	.03099	.03124	.03148
3760			.03000	.03019	.03042	.03065	.03087	.03114	.03135
3780				.03011	.03032	.03055	.03077	.03102	.03124
3800				.03002	.03022	.03045	.03066	.03092	.03113
3820					.03013	.03036	.03056	.03082	.03102
3840					.03004	.03026	.03046	.03073	.03091
3860						.03016	.03037	.03062	.03081
3880						.03007	.03027	.03052	.03071
3900							.03018	.03042	.03061
3920							.03009	.03032	.03051
3940							.03000	.03023	.03041
3960									
3980									
4000									

Table 2 (Continued)

Temp, °F / Press, psia	709	710	711	712	713	714	715	716	717	718
3420	.03539	.03620	.03725	.03853	.04037	.04330	.04940	.05625	.06191	.06635
3440	.03494	.03567	.03658	.03757	.03899	.04084	.04405	.05015	.05640	.06145
3460	.03458	.03523	.03600	.03684	.03800	.03931	.04145	.04485	.05075	.05640
3480	.03425	.03483	.03549	.03626	.03727	.03832	.03979	.04214	.04555	.05123
3500	.03394	.03448	.03507	.03577	.03663	.03755	.03873	.04037	.04243	.04620
3520	.03366	.03416	.03469	.03533	.03607	.03692	.03793	.03912	.04075	.04310
3540	.03341	.03387	.03435	.03494	.03559	.03637	.03726	.03824	.03950	.04127
3560	.03317	.03362	.03405	.03459	.03519	.03589	.03667	.03753		.03990
3580	.03297	.03338	.03378	.03429	.03483	.03547	.03614	.03694		.03883
3600	.03277	.03316	.03353	.03400	.03451	.03508	.03568	.03641		.03795
3620	.03258	.03295	.03332	.03374	.03422	.03474	.03528	.03597		.03730
3640	.03242	.03275	.03311	.03350	.03394	.03442	.03493	.03555		.03675
3660	.03226	.03257	.03291	.03328	.03369	.03413	.03462	.03518		.03635
3680	.03212	.03239	.03273	.03308	.03346	.03387	.03433	.03485		.03603
3700	.03198	.03224	.03256	.03288	.03324	.03362	.03408	.03455		.03570
3720	.03184	.03208	.03239	.03271	.03305	.03339	.03383	.03427		.03535
3740	.03170	.03194	.03224	.03254	.03286	.03318	.03359	.03401		.03504
3760	.03157	.03181	.03210	.03238	.03268	.03300	.03337	.03377		.03473
3780	.03145	.03168	.03196	.03223	.03252	.03282	.03316	.03355		.03443
3800	.03134	.03156	.03183	.03209	.03236	.03265	.03296	.03333		.03420
3820	.03123	.03145	.03171	.03195	.03222	.03249	.03279	.03314		.03398
3840	.03111	.03134	.03158	.03183	.03207	.03234	.03263	.03294		.03375
3860	.03099	.03124	.03147	.03170	.03193	.03219	.03248	.03278		.03352
3880	.03088	.03113	.03136	.03158	.03181	.03207	.03233	.03261		.03329
3900	.03077	.03104	.03126	.03147	.03169	.03193	.03218	.03244		.03311
3920	.03067	.03093	.03116	.03137	.03158	.03182	.03205	.03232		.03288
3940	.03058	.03083	.03107	.03127	.03147	.03170	.03193	.03216		.03271
3960										
3980										
4000										

Temp, °F / Press, psia	719	720	722	724	726	728	730	732	734	736
3420	.06976	.07277	.07760	.08170	.08515	.08812	.09090	.09380	.09614	.09838
3440	.06578	.06930	.07446	.07885	.08263	.08575	.08865	.09168	.09410	.09643
3460	.06115	.06545	.07130	.07605	.08007	.08333	.08641	.08946	.09200	.09443
3480	.05640	.06097	.06797	.07318	.07742	.08092	.08415	.08721	.08991	.09246
3500	.05163	.05638	.06450	.07022	.07473	.07852	.08185	.08490	.08780	.09045
3520	.04684	.05196	.06060	.06713	.07205	.07604	.07955	.08265	.08570	.08840
3540	.04350	.04773	.05660	.06392	.06925	.07350	.07715	.08041	.08347	.08635
3560	.04165	.04410	.05258	.06030	.06630	.07092	.07481	.07821	.08130	.08420
3580	.04030	.04206	.04871	.05650	.06327	.06830	.07240	.07593	.07915	.08206
3600		.04065	.04522	.05285	.06015	.06561	.07000	.07371	.07705	.08002
3620		.03960	.04285	.04940	.05677	.06275	.06750	.07136	.07490	.07797
3640		.03872	.04129	.04622	.05346	.05978	.06496	.06900	.07272	.07586
3660		.03792	.04025	.04377	.05023	.05679	.06235	.06671	.07055	.07380
3680		.03727	.03933	.04213	.04720	.05375	.05965	.06435	.06835	.07176
3700		.03676	.03855	.04096		.05080	.05686	.06195	.06616	.06967
3720		.03639	.03780	.03996		.04807	.05406	.05954	.06397	.06762
3740		.03612	.03721	.03913		.04535	.05130	.05692	.06163	.06553
3760		.03592	.03675	.03845			.04862	.05432	.05925	.06339
3780		.03550	.03636	.03782			.04603	.05171	.05686	.06126
3800		.03519	.03610	.03721				.04923	.05450	.05912
3820		.03488	.03581					.04700	.05208	.05690
3840		.03462	.03553						.04972	.05467
3860		.03433	.03525						.04755	.05240
3880		.03410	.03500						.04555	.05031
3900		.03387	.03468							.04835
3920		.03361	.03437							.04660
3940		.03335	.03410							.04500
3960										
3980										
4000										

Table 2 (Continued)

Temp, °F / Press, psia	738	740	742	744	746	748	750	752
3420	.11050	.10249	.10442	.10622	.10791	.10955	.11121	.11255
3440	.09868	.10067	.10263	.10450	.10616	.10787	.10959	.11100
3460	.09680	.09885	.10089	.10279	.10448	.10617	.10790	.10942
3480	.09488	.09703	.09913	.10105	.10275	.10455	.10627	.10781
3500	.09290	.09520	.09735	.09935	.10109	.10291	.10465	.10628
3520	.09095	.09334	.09555	.09760	.09943	.10131	.10295	.10472
3540	.08892	.09137	.09365	.09580	.09775	.09970	.10131	.10315
3560	.08680	.08940	.09177	.09403	.09600	.09800	.09971	.10152
3580	.08493	.08750	.08985	.09225	.09430	.09632	.09806	.09993
3600	.08291	.08555	.08797	.09045	.09255	.09465	.09642	.09833
3620	.08088	.08356	.08620	.08870	.09082	.09295	.09482	.09672
3640	.07885	.08162	.08431	.08683	.08909	.09121	.09322	.09512
3660	.07683	.07968	.08241	.08500	.08730	.08946	.09160	.09347
3680	.07488	.07775	.08050	.08313	.08556	.08775	.08998	.09180
3700	.07288	.07581	.07857	.08123	.08378	.08610	.08830	.09021
3720	.07090	.07387	.07676	.07939	.08203	.08440	.08665	.08863
3740	.06896	.07204	.07492	.07760	.08028	.08271	.08500	.08710
3760	.06701	.07020	.07312	.07580	.07853	.08100	.08332	.08555
3780	.06500	.06825	.07128	.07407	.07675	.07929	.08167	.08393
3800	.06303	.06637	.06947	.07229	.07508	.07765	.08007	.08237
3820	.06102	.06450	.06768	.07045	.07338	.07602	.07842	.08073
3840	.05904	.06263	.06585	.06861	.07170	.07435	.07682	.07922
3860	.05697	.06072	.06412	.06683	.07000	.07267	.07521	.07763
3880	.05495	.05883	.06232	.06515	.06822	.07092	.07355	.07605
3900	.05285	.05692	.06055	.06341	.06642	.06925	.07190	.07450
3920	.05084	.05502	.05873	.06176	.06471	.06761	.07025	.07289
3940	.04899	.05305	.05697	.06010	.06306	.06587	.06860	.07123
3960	.04728	.05111	.05517	.05848	.06147	.06425	.06700	.06960
3980	.04571	.04927	.05322	.05696	.06000	.06277	.06545	.06800
4000	.04420	.04750	.05131	.05550	.05860	.06127	.06390	.06640

Table 3 Results of statistical analysis of data of Table 2

Item	$V > 0.0525$ cu ft per lb (volumes above critical)	$V < 0.0525$ cu ft per lb (volumes below critical)
[a] Mean deviation $\bar{y}$ (parts per 10,000)	$\bar{y} = -0.5$	$\bar{y} = -10$
[b] Standard deviation σ (parts per 10,000)	7.1	28
Number of data points, n	32	21
Number of points falling within 3σ of mean	32	20

[a] $\bar{y} = 1/n \sum_{n=1}^{n} y_n$ and $y_n = \left(\frac{P_{OBS} - P_{TAB}}{P_{TAB}}\right) 10^4$

[b] $\sigma = \left(1/n \sum_{n=1}^{n} y_n^2 - \bar{y}^2\right)^{1/2}$

In the difficult region encompassed by specific volume from 0.0300 to 0.0400 cu ft per lb, where large changes in pressure occur for small changes in volume, P-V-T values were derived by starting with a large-scale plot of Fig. 3. That is, the measurements of the Havlicek, Smith, and Kirillin groups were plotted on a P-V diagram. Finally, isometrics and isotherms were constructed as before. The agreement between the measurements of Havlicek, Smith, Keyes, and Kirillin was fair but not as good as that found in the region for specific volumes greater than 0.040 cu ft per lb. More specifically it was found from a large-scale plot of Fig. 4 that the experimental measurements of Smith and Keyes [18] and Havlicek and Miskovsky [2] between 0.0300 and 0.0330 cu ft per lb along the 698 and 705.2 isotherms were in error.

Error Analysis

Fig. 6 gives deviations of the observed pressures from the derived values of Table 2 and of Fig. 5. The results of a statistical analysis, given in Table 3, indicated that the mean deviations for specific volumes greater and less than the critical volume was within 1 and 10 parts per 10,000, respectively. The analysis also showed that the probable error (0.675σ) is within 5 parts per 10,000 for volumes greater than the critical while it is within 30 parts per 10,000 for volumes less than 0.0525 cu ft per lb. These deviations are not significant or serious since the experimental error in the recent measurements of Kirillin [9] is about 20 parts in 10,000, and in the immediate vicinity of the critical point the error was estimated to be higher. It may be concluded therefore that the P-V-T values derived in this paper and given in Table 2 are precise since the error in them is small and entirely within experimental uncertainty.

With the exception of the deviation for specific volumes less than 0.040 cu ft per lb, along the critical isotherm there is remarkably good agreement between our tabulated values and those computed by Juza's most recent equation of state [4]. This equation is based on the calorimetric measurements of Havlicek and Miskovsky [2] and presumably supersedes the equation first derived by Juza [3] some 25 years ago from the same calorimetric measurements. The equation is of the form $P = F(V, T)$ and will not be discussed here since it is still being modified by Juza. However, there is some evidence not shown in Fig. 6 which indicates that the equation is not successful in representing the P-V-T behavior in the superheated-vapor region at specific volumes less than the critical specific volume. For example, along the critical isotherm at a volume of about 0.03 cu ft per lb the deviation between the computed value of Juza and our tabulated value is minus 150 parts in 10,000. For volumes less than 0.0525 cu ft per lb, it may be concluded that Juza's equation of state is not too successful in representing the P-V-T relation of water.

The authors have endeavored to make a reasonable estimate of the accuracy of the values appearing in Fig. 5. One may conclude that the reason for the significant deviations amounting up to about 200 parts in 10,000 between P-V-T values in various steam tables was because of the paucity of data at the time of the formulations and because inaccurate interpolation techniques and equations of state were used.

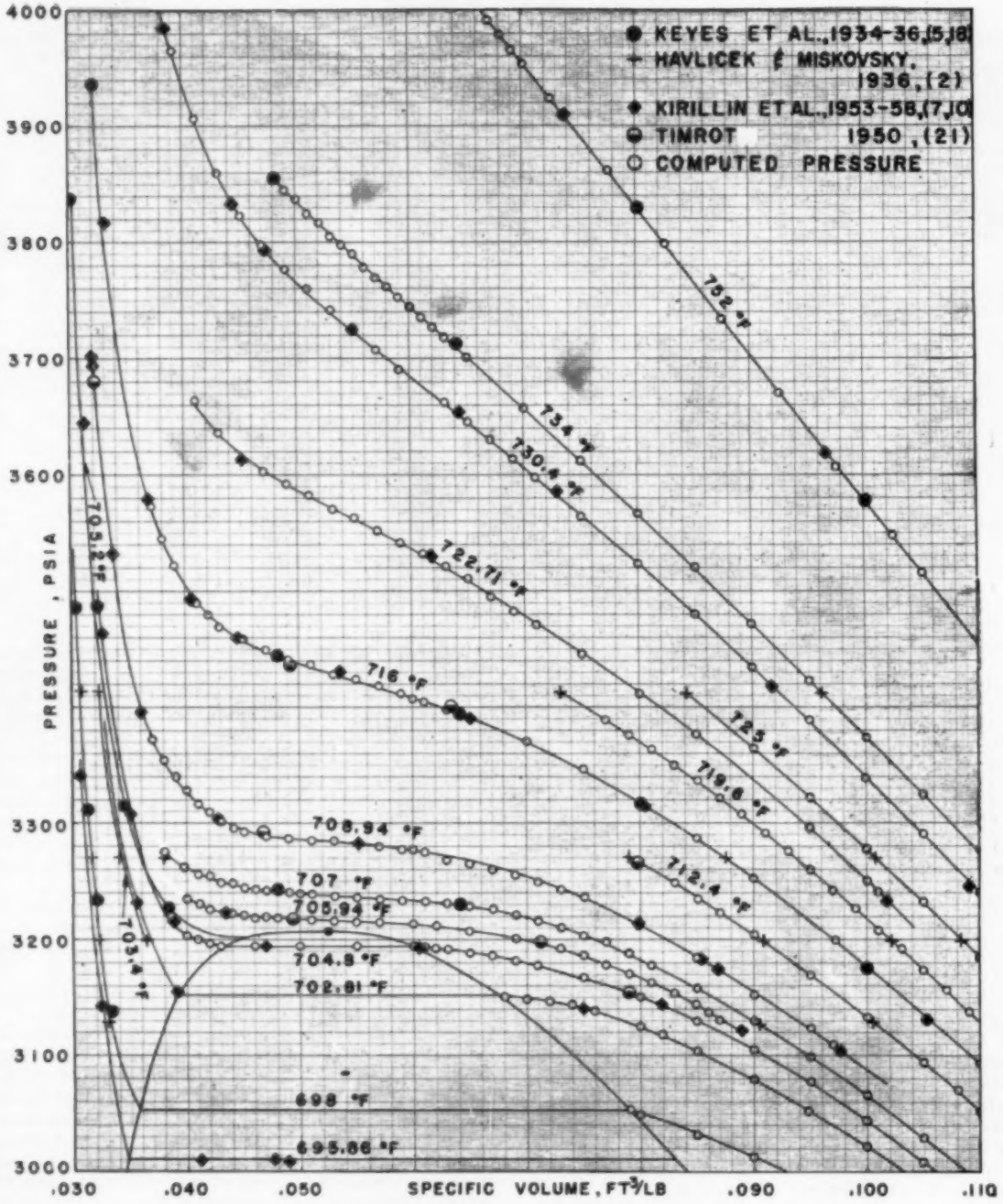

Fig. 3 Isotherms for water vapor in the critical region

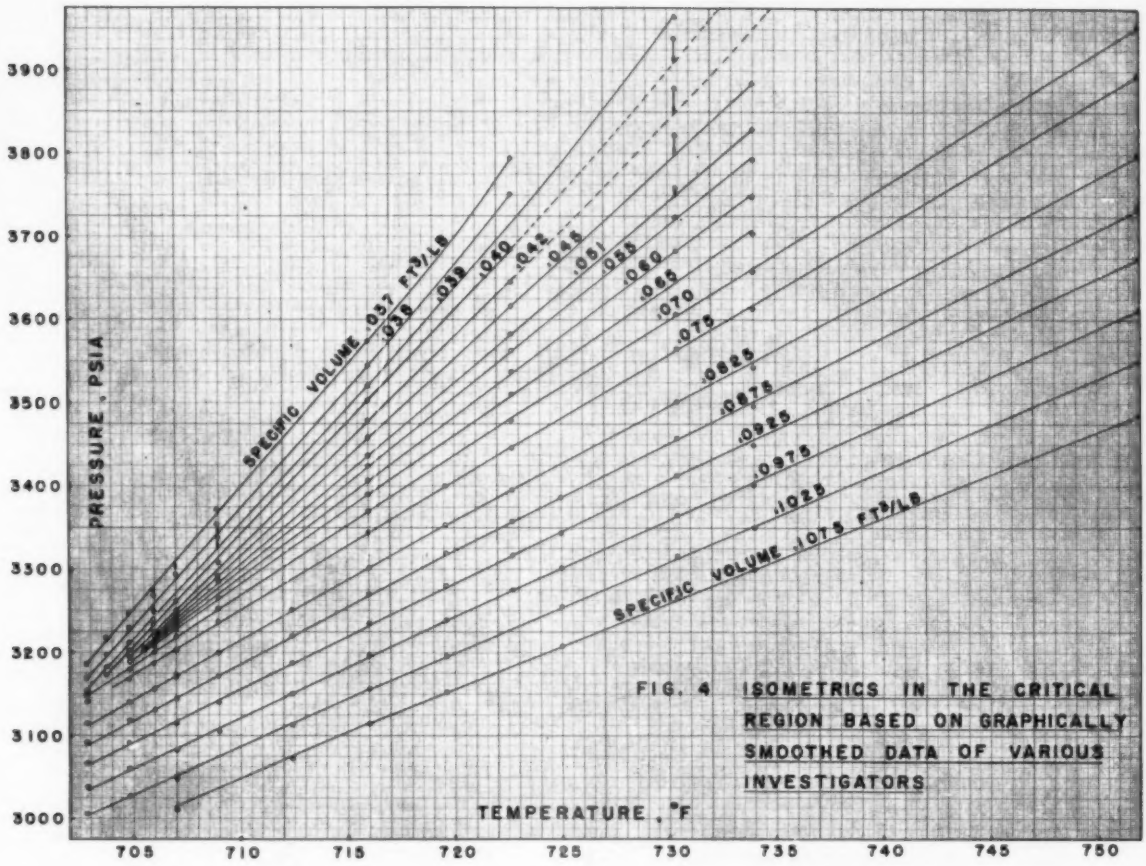

FIG. 4 ISOMETRICS IN THE CRITICAL REGION BASED ON GRAPHICALLY SMOOTHED DATA OF VARIOUS INVESTIGATORS

Fig. 4

Critical Volume of Water

The critical volume of water may be derived by evaluating the slopes of isometrics in the critical region. The method makes use of the phenomenological law that the change of saturation pressure with temperature at the critical point is identical to the change of pressure with temperature along the critical isometric; i.e.,

$$(dP_s/dT)_{P_c, T_c} = (\partial P/\partial T)_{V_c} \tag{1}$$

Nieuwenburg and Blumendal [12] were among the first to use the condition given in equation (1) for locating the critical volume. However, the value so obtained by them was not considered precise [12] as their P-V-T measurements were not accurate. The foregoing condition has been used subsequently by Timrot [19], Kirillin, et al. [9], and also by the authors of this paper.

Timrot showed that the slopes of his measured isometrics in the critical region at the saturation curve were a function of specific volume alone. Incorporating this functional relation into equation (1) he derived a value of 0.0528 cu ft per lb for the critical volume. In so doing he used a value of 21.3 psia/deg R for $(dP_s/dT)_{P_c, T_c}$ which was obtained from the differentiation and evaluation at the critical point of his vapor-pressure equation [19]. He used values of P_c, T_c which were identical to those listed by Osborne, et al. [15].

Kirillin derived a value for the critical volume which was identical to that derived by Timrot. Kirillin's method is not clearly given, but he states: "The critical specific volume of water was determined on the basis of the experimental data and by considering that the critical isometric should be generally tangent to the saturation curve at the critical point."

The authors derived a value for the critical volume of water which is in good agreement with that obtained by Timrot and Kirillin. Use was made of the fact that within experimental error the isometrics shown in Fig. 4 are nearly linear and hence

$$(\partial^2 P/\partial T^2)_{V_c} = 0 \tag{2}$$

The following relation may be obtained for the pressure and temperature along the critical isometric from equations (1) and (2):

$$P = (dP_s/dT)_{P_c, T_c}(T - T_c) + P_c \tag{3}$$

After a careful consideration the following values were used for the constants in equation (3):

$$(dP_s/dT)_{P_c, T_c} = 21.4 \text{ psia/deg R}$$

$$P_c = 3207.9 \text{ psia}$$

$$T_c = 705.5 \text{ F}$$

The value for $(dP_s/dT)_{P_c, T_c}$ is the mean of the value obtained from Timrot's and Osborne and Meyers' vapor equations. The value for T_c is the mean of the values proposed by Smith, et al., Osborne, et al., and Eck while the value for the critical pressure P_c is the mean of the values proposed by Smith, et al., and Os-

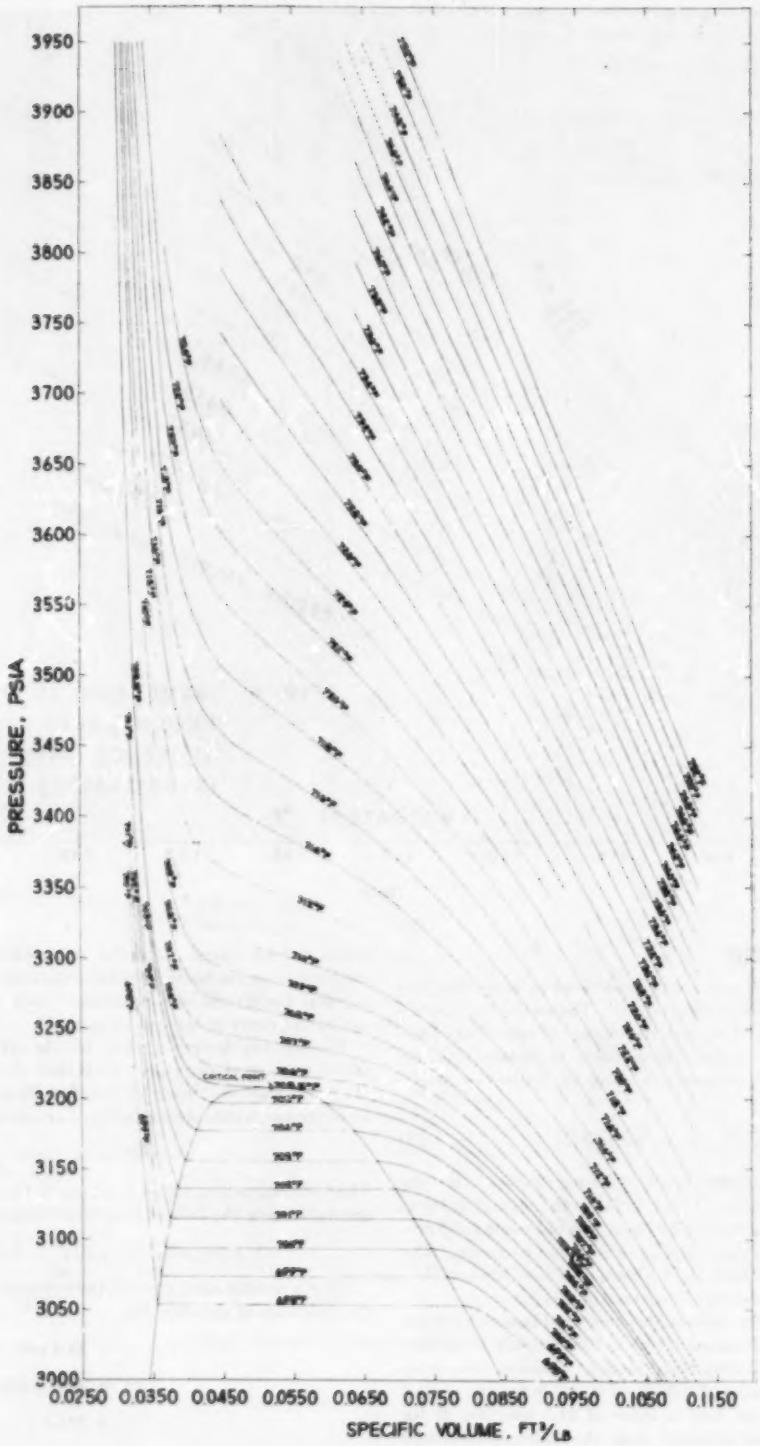

Fig. 5 Smoothed *P-V* isotherms in the critical region for water and water vapor

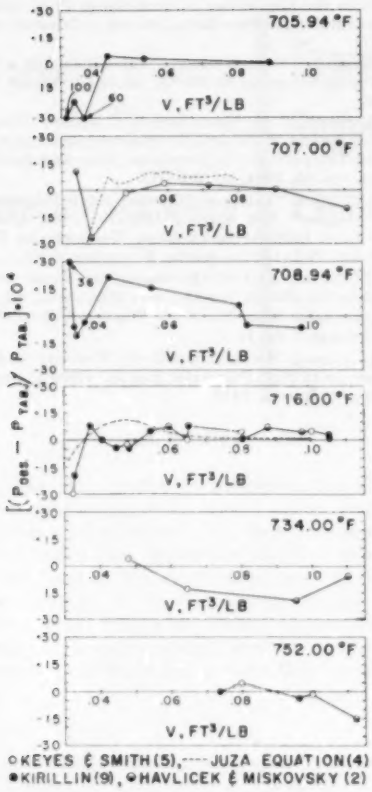

Fig. 6 Deviations of observed pressures from tabulated values

borne, et al. The values of pressures computed using equation (3) for temperatures from 706 to 730 F were used to obtain corresponding values of specific volumes from a large-scale diagram of Fig. 5. From the values of specific volume so obtained it was concluded that the critical volume of water is 0.0525 ± 0.0005 cu ft per lb. It is interesting to note that at a volume of 0.0525 cu ft per lb and at a temperature of 705.5 F, a value of 3208 psia is read for the critical pressure which is in excellent agreement with the value chosen for use in equation (4).

Conclusions

Smoothed *P-V-T* data for water in the critical region were derived from the experimental work of various investigators. A statistical analysis indicated that the average deviations of the *P-V-T* data of Table 2 from experimental values are entirely within some 1 and 10 parts in 10,000 in pressure for specific volumes greater and smaller than the critical volume, respectively. These deviations are not serious in view of the fact that they are entirely within the limits of experimental uncertainty of recent measurements which have been estimated at about 20 parts in 10,000. The values derived in this paper are recommended for use because the errors in the values of existing steam tabulations are outside the experimental uncertainty. Furthermore, the values of this paper are given over close intervals of pressure, volume, and temperature enabling one to obtain accurate values for the density and the coefficient of volume of expansion.

In 1950, Timrot and Vargaftik [20] stated that the older data of Keyes [5, 18] and Havlicek [2] were seriously in error. However, in this paper it is shown that the data of Keyes and Havlicek were in excellent agreement with the measurements of Kirillin. At the conclusion of this investigation Prof. F. G. Keyes communicated to the senior author the Russian article of Timrot [21]. A preliminary checking revealed excellent agreement (within a few parts in 10,000 in pressure) between the derived values of this paper and the actual measurements of Timrot.

In references [13 and 14] it was noted that the values in the various steam tables were based on either the measurements of Keyes [5], or Havlicek [2], or the recent measurements of Kirillin [7–10] and Timrot [20]. Deviations of some 100 to 200 parts in 10,000 in pressure were seen to exist between the data of various steam tables. In view of the results of this paper, the authors conclude that the significantly large deviations existing between the data of various steam tables can be attributed to imperfect analytical and interpolation calculations and the previous paucity of volumetric measurements.

Acknowledgments

The authors wish to acknowledge the material sent in by different organizations, libraries, and individual researchers. In particular they appreciate the material sent in and useful correspondence with Profs. E. R. G. Eckert, J. H. Keenan, F. G. Keyes, and V. A. Kirillin. The authors also acknowledge the support of the Argonne National Laboratory under Sub-Contract 31-109-38-704, which made this work possible. The advice and encouragement given by Dr. P. A. Lottes of the Argonne National Laboratory throughout the entire period of this work is very much appreciated. Finally, the authors wish to thank D. Cash, T. Fitzsimmons, R. Hunter, W. Kunimoto, and T. Miyazaki for performing computations and for preparing the exacting illustrations.

References

1 H. Eck, "Important Properties of Water in the Critical Region," *Physikalische Zeitschrift*, vol. 38, 1937, p. 356.

2 J. Havlicek and L. Miskovsky, "Experiments of the Masaryk Academy in Prague on the Physical Properties of Water and Steam," *Helvetica Physica Acta*, vol. 9, 1936, pp. 161–207, translated into English during the investigation described.

3 J. Juza, "Equation of State for Steam," *Engineering* (London), vol. 146, 1938, pp. 1–3 and 34–36.

4 J. Juza, "A General Steam Equation in the Range 0–800°C, and 0–2500 Bars," Academy of Sciences of Czechoslovakia, June, 1958, available from Prof. J. H. Keenan, Executive Secretary, U. S. A. Commission on Properties of Steam, Cambridge 39, Mass.

5 F. G. Keyes, L. B. Smith, and H. T. Gerry, "The Specific Volume of Steam in the Saturated and Superheated Condition Together With Derived Values of the Enthalpy, Entropy, Heat Capacity, and Joule-Thomson Coefficients," *Proceedings, American Academy of Arts and Sciences*, vol. 70, 1936, pp. 319–364.

6 F. G. Keyes, "The Consistency of the Thermodynamic Data for Water Substance Vapor Phase to 550°," *Journal of Chemical Physics*, vol. 17, 1949, pp. 923–934.

7 V. A. Kirillin and L. I. Rumyanstev, "Experimental Investigations of Water and Water Vapor at High Pressures and Temperatures," *Transactions of the Moscow Order of Lenin Power Institute*, named for V. N. Molotov, vol. 9, State Power Publishing House, 1953; available from Library of Congress, Washington 25, D. C.

8 V. A. Kirillin and V. N. Zubaryev, "Experimental Investigations of the Specific Volumes of Water and Water Vapor at Extremely High Pressures," *Teploenergetika*, vol. 2, no. 11, 1955, pp. 19–23; translated into English by S. L. A. Translation Services.

9 V. A. Kirillin, L. I. Rumyantsev, and V. N. Zubaryev, "Experimental Research for Specific Volumes of Water and Steam of High Parameters," Fifth International Conference on Properties of Steam, London, England, 1956, available from Prof. J. H. Keenan.

10 V. A. Kirillin and S. A. Ulybin, "Experimental Investigation Into Compressibility of Water and Water Vapor in the Range of Critical Temperatures," (in Russian), *Teploenergetika*, vol. 5, no. 4, 1958, pp. 53–54, available from Linda Hall Library, Kansas City, Mo.

11 V. A. Kirillin and S. A. Ulybin, "Precision Analysis and the Combined Table of Experimental Values for Water and Water Vapor Specific Volumes Obtained in the Moscow Power Institute," (in Russian), *Teploenergetika*, vol. 6, no. 9, 1959, pp. 3–7; translated into English during investigation described.

12 C. J. van Nieuwenburg and H. B. Blumendal, "The Isotherms of Water From 350° to 480° C and for Pressures up to 600 kg per sq cm," *Recueil des Travaux Chimiques des Pays-Bas*, vol. 51, 1932, pp. 707–714; this paper is given in English.

13 E. S. Nowak, R. J. Grosh, and P. E. Liley, "A Survey of *P-V-T* Data for Water in the Critical Region," published in this issue, pp. 1–13.

14 E. S. Nowak and R. J. Grosh, "An Investigation of Certain Thermodynamic and Transport Properties of Water and Water Vapor in the Critical Region," Argonne National Laboratory Report 6064, October, 1959, available from the Office of Technical Services, Department of Commerce, Washington 25, D. C. See also E. S. Nowak, "A Preliminary Analytical Investigation of the Thermodynamic and Transport Properties for Water and Water Vapor in the Critical Region," MS thesis in Mechanical Engineering, Purdue University, July, 1959.

15 N. S. Osborne and C. H. Meyers, "A Formula and Tables for the Pressure of Saturated Water Vapor in the Range 0 to 374 C," United States Bureau of Standards, *Journal of Research*, vol. 13, 1934, pp. 1–20.

16 N. S. Osborne, H. F. Stimson, and D. C. Ginnings, "Calorimetric Determination of the Thermodynamic Properties of Saturated Water in Both the Liquid and Gaseous States From 100 to 374°C," United States Bureau of Standards, *Journal of Research*, vol. 18, 1937, pp. 389–447.

17 E. Schmidt, "V. D. I. Steam Tables Including a Mollier Diagram for Temperatures up to 800°C," Springer Verlag, Berlin, Germany, 1956.

18 L. B. Smith, F. G. Keyes, and H. T. Gerry, "The Volumes of Unit Mass of Liquid Water and Their Correlations as a Function of Pressure and Temperature," *Proceedings, American Academy of Arts and Sciences*, vol. 69, 1934, pp. 285–312.

19 D. L. Timrot, "Tables of Thermodynamic Properties of Water and Water Vapor," first edition, Moscow, 1952, translated into English by Land Engineering Division, Westinghouse Electric Corporation, South Philadelphia Works, November, 1954.

20 D. L. Timrot and N. B. Vargaftik, Paper No. E 3/10, *Transactions of the Fourth World Power Conference*, vol. 3, 1950, pp. 1642–1666, available from Mr. F. L. Weaver, Federal Power Commission, Washington 25, D. C.

21 D. L. Timrot, "Heat Conductivity, Viscosity, and Thermodynamic Properties of High Parameter Steam," State Power Publishing House, Moscow, Russia, 1950.

GENNARO L. GOGLIA
Associate Professor of Mechanical Engineering, North Carolina State College, Raleigh, N. C. Mem. ASME

GORDON J. VAN WYLEN
Professor and Chairman, Department of Mechanical Engineering, University of Michigan, Ann Arbor, Mich. Mem. ASME

Experimental Determination of Limit of Supersaturation of Nitrogen Vapor Expanding in a Nozzle

The limit line of supersaturation of slightly superheated nitrogen vapor as it expands in a two-dimensional nozzle has been determined. The results indicate that the degrees of supersaturation vary from 12.3 F at a condensation temperature of 109 R to 3.5 F at 126 R. These results are in agreement with work of other investigations with nitrogen gas initially at room temperature.

Introduction

THE PHENOMENON of supersaturation, that is, the existence of a metastable state, is well known and has been studied by many investigators. The limit of supersaturation, known as the Wilson line, has been established for steam, primarily on the basis of the experimental work of Yellot [1].[1] The primary purpose of the work reported in this paper was to study these phenomena when slightly superheated nitrogen vapor expands in a nozzle, and to establish the limit line of supersaturation for nitrogen vapor under these conditions.

Apparatus

The apparatus used to conduct this investigation consisted of a storage tank assembly, a nozzle-diffuser assembly, a photomanometer, a pitot tube assembly, a Sanborn recorder, and the necessary piping, valving, and insulation.

The storage tank assembly was constructed to be essentially one tank within another. The inner tank was used for the storage of the nitrogen necessary for test runs, and the outer tank, which contained liquid nitrogen, was used to maintain a constant temperature in the inner tank. In order to provide sufficient nitrogen vapor for the test runs, a capacity of four cubic feet was required for the inner tank. Since both tanks were to be subjected to −320 F temperatures and pressures as high as 400 psig, 18-8 stainless-steel type 304 was used in construction. The entire tank assembly was enclosed in a 5-in. jacket of insulation.

The complete nozzle-diffuser assembly, shown in Fig. 1, was made of aluminum to prevent corrosion and subsequent contamination of the nitrogen vapor. The nozzle-diffuser assembly, designed to discharge against a back pressure of one standard atmosphere, had parallel sides and was 1 in. wide with a nozzle exit area of approximately 0.5 sq in. The straight divergent section of the nozzle was machined to a high microfinish surface, and the sides were hand lapped to the side walls. Static pressure taps with a diameter of 0.04 in. were provided at half inch intervals in the divergent section of the nozzle. The nozzle-diffuser assembly was so constructed that the throat height was adjustable from a minimum of 0.0 to a maximum of 0.2 in. The side walls were securely clamped into position to eliminate leakage.

The central body type diffuser assembly was so designed that the diffuser angle was approximately twice the divergent angle of the nozzle. The diffuser had a two-dimensional wedge which could be traversed along the axis of the entire length of the diffuser. The central body type diffuser was selected because the wedge provided a convenient support for the pitot tube in its traverse of the nozzle axis. The wedge angle was made slightly greater than the divergent angle of the diffuser.

The stagnation pressure upstream of the nozzle was maintained constant by a pressure regulating valve placed between the tank and nozzle assemblies. A valve positioner was used in conjunction with the pressure regulator to increase the response of the regulator. A bronze tube Bourdon gage, just ahead of the nozzle, was used to measure the upstream stagnation pressure.

The nozzle static pressures were observed and photographed on a multiple tube photomanometer panel on which 13 different pressures could be indicated at one time. The asymmetry of the static pressure holes (see Fig. 1) in the nozzle block allowed a check to see that the flow was the same on the top and bottom of the nozzle. The stagnation pressure probe consisted of a 3-in. length of 0.042-in. diameter stainless-steel hypodermic tube with an inside diameter of 0.026 in. By use of this probe, which could traverse the nozzle center line, the stagnation pressure on the nozzle center line could be measured at any axial station. The probe was designed in accordance with the dimensions recom-

[1] Numbers in brackets designate References at end of paper.

Contributed by the Heat Transfer Division and presented at the Summer Annual Meeting, Dallas, Texas, June 5–9, 1960, of THE AMERICAN SOCIETY OF MECHANICAL ENGINEERS. Manuscript received at ASME Headquarters, August 19, 1959. Paper No. 60—SA-8.

Nomenclature

- d = axial distance downstream measured from throat
- p = pressure in equilibrium with droplet of radius r at absolute temperature T
- p_c = static pressure at the onset of condensation
- p_d = static pressure at station d
- p_{oz} = stagnation pressure upstream of nozzle
- p_{oy} = stagnation pressure downstream of a normal shock
- p_0' = stagnation pressure as measured by pitot tube
- p_y = static pressure downstream of normal shock
- p_∞ = saturation vapor pressure in equilibrium with a liquid surface of infinite radius
- r = radius of droplet
- R = gas constant
- T = absolute temperature
- T_c = absolute temperature at onset of condensation
- ρ = density of liquid
- σ = surface tension of liquid

mended in the National Advisory Committee of Aeronautics Technical Note No. 2223.

The stagnation temperature of the working fluid entering the nozzle was measured by a copper-constantan thermocouple, mounted in a tee just ahead of the nozzle, in conjunction with a Sanborn recorder. Fig. 2 is a schematic diagram of the apparatus.

Operation

The test runs conducted were for nozzle entrance stagnation pressures of 4.38, 6.09, 7.80, 9.15, 9.84, 10.60, 12.90, and 13.22 atmospheres. For each pressure the degrees of superheat was varied. The nozzle throat settings corresponding to the operating pressures were 0.195, 0.150, 0.125, 0.100, 0.090, 0.090, 0.060, and 0.060 sq in., respectively.

In preparation for a test run the nozzle throat area was first adjusted to one of the settings. The storage tank was charged with liquid nitrogen and a period of time was then allowed for the generation of the pressure necessary for a test run. While equilibrium was being established in the tank, the 1-in. line connecting the tank with the nozzle-diffuser assembly was precooled by forcing liquid nitrogen through it. With this procedure it was possible to maintain approximately 100 deg F of superheat at the inlet to the nozzle. Following the establishment of equilibrium conditions in the tank and the completion of precooling, a test run was made. In general the duration of test runs did not exceed 45 sec. During each test run the following information was recorded: The stagnation temperature and stagnation pressure at nozzle inlet, the static pressure along the nozzle block, and the measured stagnation pressure along the axis of the nozzle.

The liquid nitrogen used was obtained from the liquid nitrogen generating machine operated by the Mechanical Engineering Department of the University of Michigan and the mass spectrometer analysis showed its purity to be 95 per cent. The higher purity nitrogen used was purchased and guaranteed at 99.995 per cent purity.

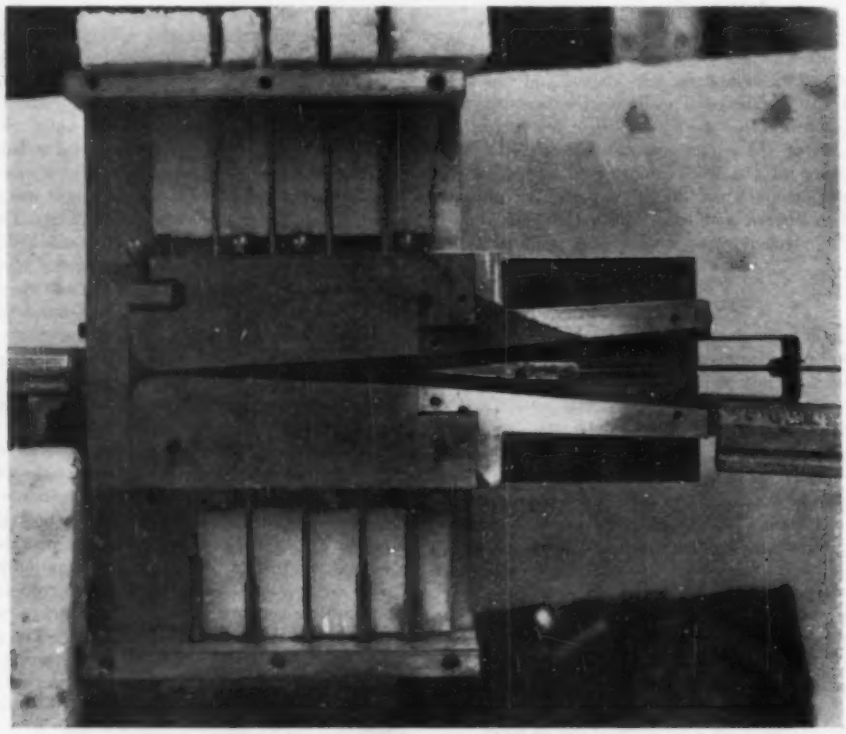

Fig. 1 Photograph of nozzle-diffuser assembly

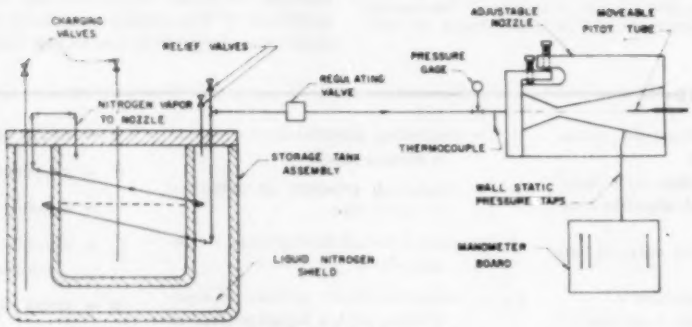

Fig. 2 Sketch of apparatus

Determination of the Onset of Condensation From the Experimental Data

Three different methods were used to locate the onset of condensation, each involving a comparison of the actual expansion with an isentropic expansion. The first was done by plotting p_s/p_0' (the ratio of the measured static pressure to measured stagnation pressure at a given station—see Fig. 3 illustrating the nomenclature) versus p_0'/p_{0x} (the ratio of the measured stagnation pressure to the upstream stagnation pressure) for the actual expansion. For the isentropic expansion p_s/p_{0y} is plotted against p_{0y}/p_{0x} (p_{0y} is the stagnation pressure downstream of a normal shock of the given station and p_y is the static pressure downstream of a normal shock given station). The actual and isentropic curves essentially coincide before condensation begins, and the point where the actual curve deviates from the isentropic curve marks the point where condensation begins. Fig. 4, which shows these plots for run 100-5, is a typical curve. It is evident that the departure from the isentrope is gradual and it is therefore difficult to precisely locate the onset of condensation by this method.

The second method is quite similar and involves a comparison of the measured static pressure at given stations with the static pressure which would be achieved just downstream of a normal shock at that station with isentropic flow upstream. It was noted, as indicated in Fig. 5, that the measured stagnation pressure was essentially equal to the isentropic stagnation pressure at that station. The isentropic static pressure at each station was

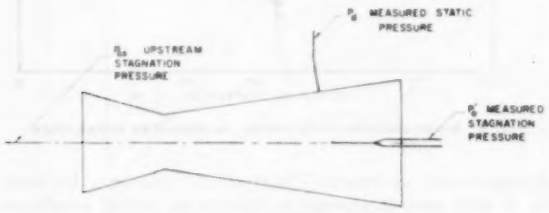

Fig. 3 Nomenclature sketch

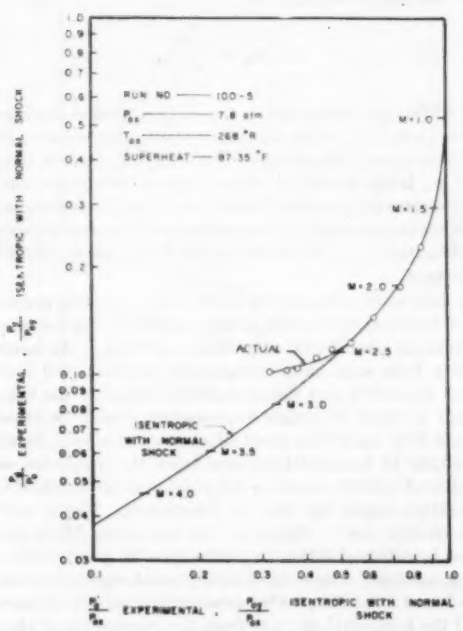

Fig. 4 Comparison of actual expansion with isentropic

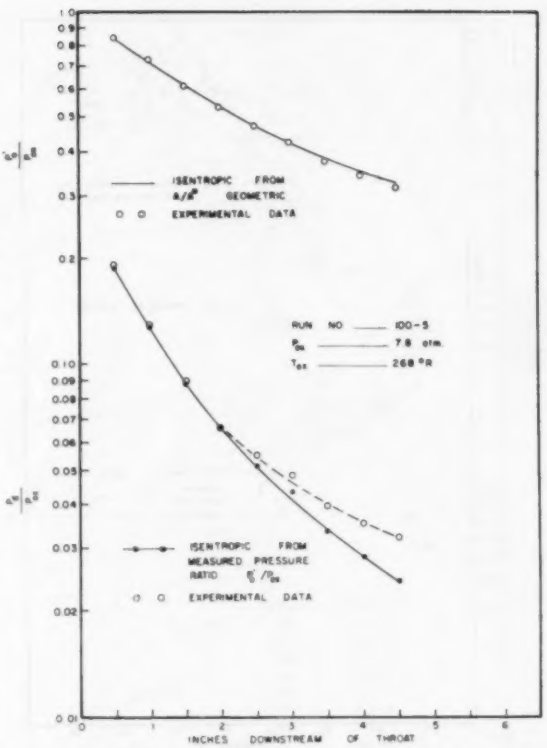

Fig. 5 Comparison of experimentally measured pressure ratios along nozzle with isentropic

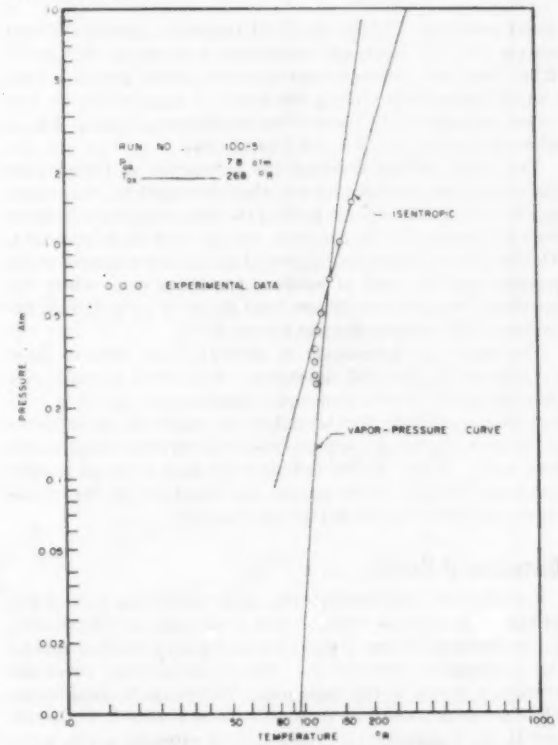

Fig. 6 Measured static pressure versus computed temperature

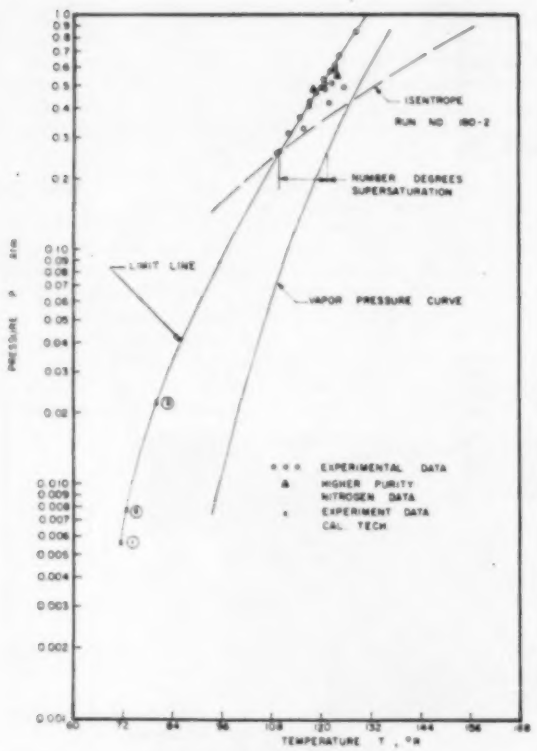

Fig. 7 Supersaturation limit line curve

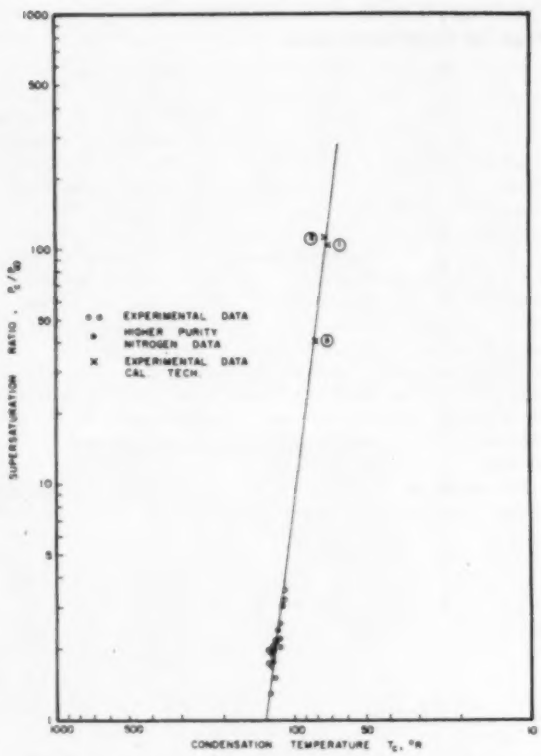

Fig. 8 Supersaturation ratio versus condensation temperature

found assuming that the measured stagnation pressure at that station was the isentropic stagnation pressure at that point. When both the isentropic and measured static pressures were plotted against length along the nozzle, it appears that the two curves separate at the point where condensation begins. Fig. 5, which is also for run 100-5, is a typical curve.

The third method involved the calculation of temperature throughout the expansion by a method developed by Nagamatsu and Willmarth [4]. In this method the temperature is calculated from the continuity, momentum, energy, and state equations. The calculated temperature is plotted against the measured static pressure and the onset of condensation is the point where the calculated temperatures depart from those for an isentropic expansion. Fig. 6 shows this plot for run 100-5.

The onset of condensation as determined by each of these methods was in essential agreement. As a check to make sure that the departure from isentropic expansion was caused by condensation and not by flow breakdown or separation, several runs at elevated stagnation temperatures for given reservoir pressures were made. These results indicated the flow to be essentially isentropic throughout the nozzle and therefore the departures were considered to be caused by condensation.

Discussion of Results

The results of this investigation are shown in Figs. 7, 8, and 9. In Fig. 7 the calculated temperature at the point of condensation T_c (as determined from a plot such as Fig. 6) is plotted against the condensation pressure p_c. The vapor pressure curve for nitrogen is shown on this same plot. Three experimental points which are determined from the experimental work of P. D. Arthur and H. T. Nagamatsu [5] (with bottled nitrogen gas at room temperature) are also shown on this plot, and a limit line of supersaturation has been drawn. The trend of curvature of the limit line is such that it appears as though at critical conditions supersaturation ceases to exist. This is predicted by the well-known von Helmholtz equation,

$$\ln p/p_\infty = \frac{2\sigma}{\rho r R T},$$

for at critical conditions where the surface tension vanishes the equation gives $p/p_\infty = 1$. In the equation p denotes the pressure in equilibrium with the droplet of radius r at absolute temperature T, p_∞ is the saturation vapor pressure in equilibrium with a liquid surface of infinite radius at T, σ is the surface tension for a flat surface (an assumption in error for drops the size encountered in condensation), ρ is the density of the liquid phase, and R is the gas constant.

This limit of supersaturation curve can be used to predict the onset of condensation as well as the number of degrees of supersaturation for given initial stagnation conditions. An isentropic expansion from some initial stagnation condition will intersect the limit line curve and this intersection indicates the temperature and pressure at which condensation should be expected. Since the flow up to the onset of condensation was shown experimentally to be essentially isentropic, the properties at the onset of condensation as well as the position in the nozzle at which condensation begins can then be determined. This is useful in that it enables one to determine the maximum Mach number that can be attained without condensation for given initial stagnation conditions. The number of degrees of supersaturation can also be found from this plot by measurement on the temperature scale of the horizontal distance from the intersection of the isentrope with the limit line to the saturation curve.

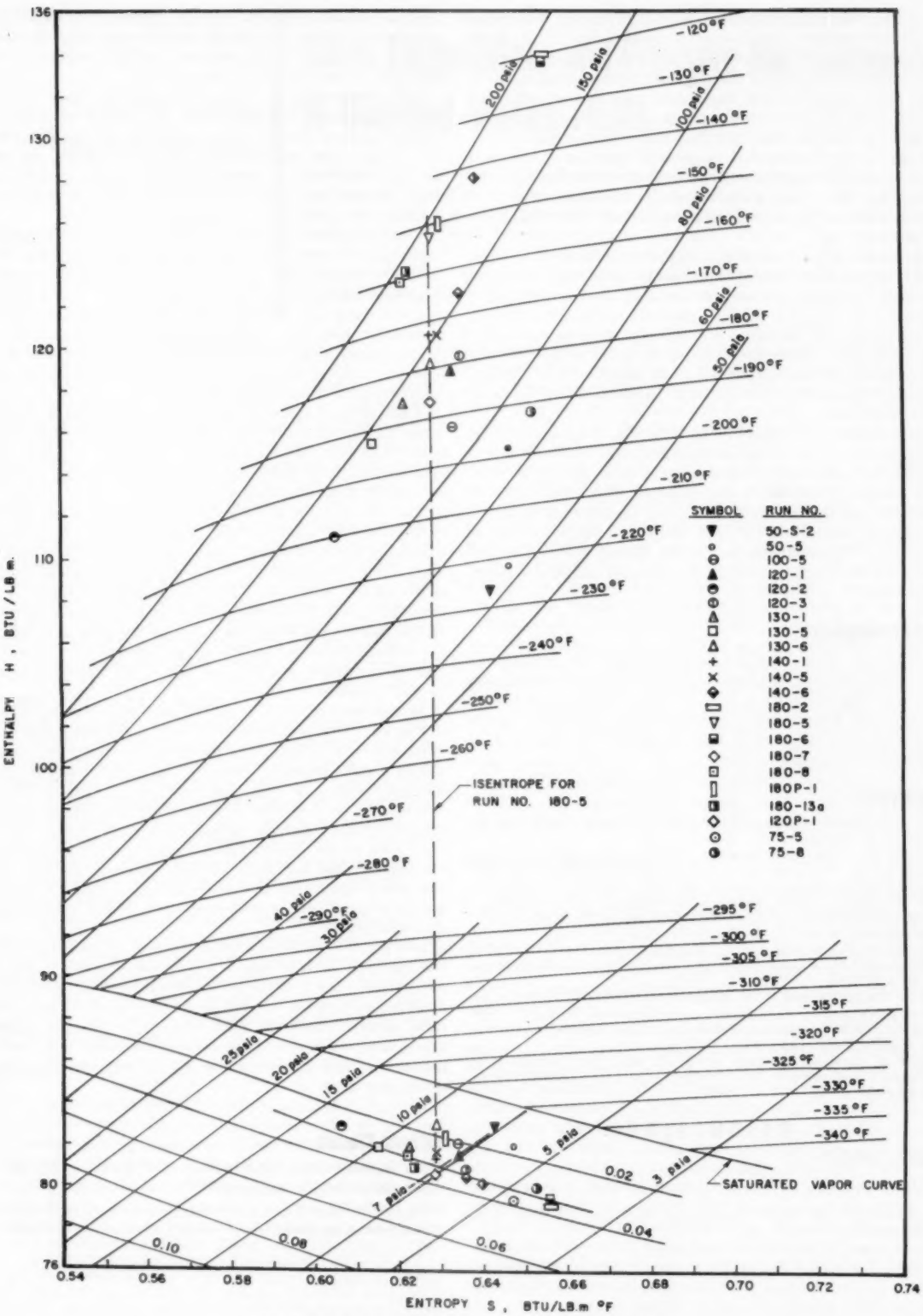

Fig. 9 Mollier diagram with limit line of supersaturation

In Fig. 8 the supersaturation ratio p_c/p_∞ (where p_c is the measured static pressure at the onset of condensation and p_∞ is the saturation pressure for the calculated condensation temperature T_c) is plotted on a log-log chart against the calculated condensation temperature T_c. The three points from the work of Arthur and Nagamatsu [5] referred to previously are also shown on this plot. It is evident from Fig. 8 that the supersaturation ratio increases as the condensation temperature decreases. That is to say, for a given amount of superheat, the lower the initial pressure the greater the amount of supersaturation which can exist.

Fig. 9 shows the limit line of supersaturation on a Mollier diagram.

It should be mentioned that the results from the work of Arthur and Nagamatsu [5] referred to previously are for much lower condensation pressures and temperatures than those test results reported here. In fact, the solid phase of nitrogen is ordinarily observed at their conditions and, therefore, references [4 and 5] may be tests in which solidification of the vapor occurs. The line representing the supersaturation could possibly have a discontinuity in slope in the vicinity of the line separating the liquid and solid phase.

In realization of the fact that both the rate of expansion as well as the purity of the nitrogen could conceivably produce different results the authors contemplate pursuing this aspect of the problem further. Additional experimental work with different divergent nozzle angles and variations of impurities in the flow is planned so as to observe the effect, if any, that this would have on the limit of supersaturation and to also observe whether the limit of supersaturation as reported here is the only limit line of supersaturation.

Acknowledgments

This work was carried out under a grant from the National Science Foundation, and the authors gratefully acknowledge this support. The assistance of Prof. J. A. Clark and other personnel of the Heat Transfer and Thermodynamics Laboratory of the Department of Mechanical Engineering at the University of Michigan is also acknowledged.

References

1 J. I. Yellot, "Supersaturated Steam." TRANS. ASME, vol. 56, 1934, pp. 411–430.

2 H. T. Nagamatsu, "Results of Recent Hypersonic Flow Research in the Army Ordnance—C. I. T. Hypersonic Wind Tunnel," Physical Society Meeting, Urbana, Ill., May, 1950.

3 R. Buhler, "Recent Results of the Condensation Investigation," Army Ordnance, C. I. T. Hypersonic Wind Tunnel Memoranda, July, 1950–August, 1950.

4 H. T. Nagamatsu and W. W. Willmarth, "Condensation of Nitrogen in a Hypersonic Nozzle," *Journal of Applied Physics*, vol. 23, 1952, p. 1089.

5 P. D. Arthur and H. T. Nagamatsu, "Effects of Impurities on the Supersaturation of Nitrogen in a Hypersonic Nozzle," Heat Transfer and Fluid Mechanics Institute, University of California, Los Angeles, Calif., June, 1952.

6 I. D. Faro, T. R. Small, and F. K. Hill, "Supersaturation of Nitrogen in a Hypersonic Wind Tunnel," *Journal of Applied Physics*, vol. 23, 1952, p. 40.

DISCUSSION

John I. Yellott[2]

The authors have done a very commendable job in locating the limit of supersaturation during rapid expansion for a gas which is extremely important but which presents many experimental difficulties due to the low temperature and high pressure at which the experiments had to be conducted.

The authors have determined the point of condensation by measuring impact pressures along the axis of the nozzle and comparing these with the calculated pressures which would obtain if isentropic expansion continued throughout the entire length of the nozzle. Good agreement was obtained by using three different methods to determine the point where the actual expansion departed from the isentropic.

When the writer undertook in 1933 to determine the condensation point of flowing steam, he followed suggestions made by the late Aurel Stodola who had observed the condensation point by allowing steam to expand through glass nozzles. Using this technique, it was found that the sudden formation of extremely small droplets enabled the condensation point to be seen clearly and photographed without difficulty. A static pressure search tube was then used to determine the actual pressures at the point where condensation was observed to occur.

A plot of static pressure against axial position along the nozzle showed a characteristic "bump" at the exact point where condensation was seen. In his discussion of the writer's first paper, reference [1], J. H. Keenan showed that this bump was a necessary result of the condensation process.

There is a considerable body of literature on the subject of the condensation of flowing steam. The writer and C. K. Holland found that the condensation limit was markedly affected by the time-rate of the expansion. A nozzle was built in which the angle of divergence between the sides could be varied continuously and, with this nozzle, it was learned that there were a number of different modes of condensation. J. T. Rettaliata, working with the original apparatus at The Johns Hopkins University, found that the roughness of the nozzle had a very important part to play in condensation.

More recently, Prof. Watson Smith of the University of Florida, during the course of his graduate research at Purdue University, made a theoretical analysis of the condensation process for steam during a rapid expansion using the latest developments in nucleation theory. He found that there was a marked difference between the point at which condensation should occur in a flow process, such an expansion through a nozzle, and in a nonflow process, such as the Wilson Cloud Chamber. Strictly speaking, the term "Wilson line" should be used to refer to nonflow expansion, and another term, such as "Stodola line," might well be used for the locus of condensation conditions during flow through a divergent nozzle.

In a private communication to the writer, one of the authors has expressed the hope that he will be able to continue the work on nitrogen, using both the static pressure traverse and the direct observation methods. It will be interesting to see how closely these methods check the work reported in the present paper. Direct observation should also enable an estimate to be made of the size of the droplets which are formed and the rate at which they grow.

[2] President, John Yellott Engineering Associates, Phoenix, Ariz. Mem. ASME.

Authors' Closure

The authors would like to extend their thanks to Mr. John I. Yellott for his helpful comments. This investigation is currently being continued and it is planned to make use of both the static pressure traverse as well as the direct observation methods.

Some Temperature and Pressure Measurements in Confined Vortex Fields

JOSEPH M. SAVINO
ROBERT G. RAGSDALE
Lewis Research Center,
NASA, Cleveland, Ohio

Studies were conducted on vortex flow generated within two right circular cylinders by injecting air through longitudinal vanes forming the chamber. The length to diameter ratios were 0.107 and 0.50. Experimental end wall static pressure distributions, some total pressures, and total temperature data are presented. The most significant finding was the large radial variations in the total temperature; this is related to the Ranque-Hilsch effect. Also discussed is the relationship between the static wall pressures and the effective velocities in the vortex.

Introduction

MANY STUDIES have been conducted on the behavior of vortex flow confined within a circular cylinder, references [1 through 9][1] to mention a few. Of these the Ranque-Hilsch tube (both the uniflow and counterflow type) has attracted the most recent attention. The uniflow type tube consists of a cylinder open at one end and closed at the other. Compressed air is injected tangentially at the circumference adjacent to the closed end. The unique feature of this device is that the air mass in the central core has a lower total temperature than that of the inlet air while the air in the remaining annular region has a higher total temperature. The counterflow type Ranque-Hilsch tube is a uniflow tube which has a small hole in the center of the closed end for removing the cold air in the core. Thus the outlet air is split into a hot stream and a cold stream. This process is commonly referred to as the Ranque-Hilsch effect, the total-temperature separation, or the energy separation, and has been studied in some detail in references [4 through 9].

Hartnett and Eckert [4], and Lay [5, part 1] measured radial distributions of the velocity vectors, total temperature, and total and static pressures at several axial positions downstream from the closed end in a uniflow tube. Pengelley [8] provided some velocity data and only a qualitative picture of the flow and temperature conditions in the region in contact with the closed end. Lay [5, part 2] and Deissler and Perlmutter [6 and 7] studied the Ranque-Hilsch effect analytically. The analysis in reference [7] agrees well with the data of Hartnett and Eckert and with the gross results of Hilsch [9].

Presented here are some preliminary results from experimental studies of vortex flow inside two right circular cylinders using air as the fluid. These measurements though incomplete reveal something of the actual flow conditions in a vortex. In addition, these data may provide further insight into the Ranque-Hilsch effect, although the study of this phenomenon was not the prime aim of the vortex investigation.

Apparatus

Figs. 1 and 2 show the two vortex chambers used in the present experimental program. Guide vanes of each vortex were spaced equally around the circumference of a circle, forming the surface of a cylindrical chamber, and imparting a swirl to the air as it passed inward from the inlet chamber. The air within the cylinder discharged through an exhaust hole in one end. Vortex 1 operated under positive gage pressure and exhausted into the room; whereas, vortex 2 operated at essentially atmospheric pressure in the inlet chamber and discharged into a vacuum exhaust system. In vortex 1 the flow was essentially incompressible except in the region approximately defined by the nozzle circle (dotted region in Fig. 1). At the circle the Mach number was approximately 0.3 to 0.5. The flow within vortex 2 was in the compressible regime with Mach numbers up to 0.5 at the vane tips. The delivery air temperature was 70 to 80 F in all tests and weight rates of flow were measured by an upstream orifice plate.

Also shown in Figs. 1 and 2 are the regions where the total-pressure and the total-temperature measurements were made in each vortex. Static wall pressures were measured on each end wall of vortex 1 and on the closed end of vortex 2. Total pressures were measured at two radii in vortex 2 only, with 0.030-in. OD pitot tubes. The temperature probes were $^1/_{16}$-in. diameter sheathed thermocouples with bare junctions whose positions were known to within $\pm^1/_{32}$ in. The temperature readings were not corrected for conduction or radiation losses. A single temperature probe was used in vortex 1 to survey the region within the discharge opening (Fig. 1). In vortex 2 the temperature probes were inserted through the closed end wall into the testing region shown in Fig. 2. At various radial positions, the probes were inserted one at a time to minimize the drag effect on the flow field.

Results and Discussion

The total-temperature, static, and total-pressure measurements obtained from the two vortex chambers are presented in Figs. 3 through 7. The most significant finding, discussed later in more detail, was the sizable radial variation of the total temperature T within each vortex cylinder. Also discussed is a qualitative relationship between the static and total-pressure data and the velocities in vortex flow.

The total-temperature data measured within the exhaust hole region of vortex 1 are presented in Fig. 3. These data are typical of similar measurements made at different flow rates W. The reference temperature T_0 is the total temperature of the inlet air measured in the inlet calming chamber. The parameter Z/L is the dimensionless axial position measured from the inside plane of the closed end where L is the distance between the inside planes of the cylinder ends. The region under investigation, shown by dotted lines in Fig. 1, was a cylinder the diameter of the discharge hole with ends bounded by the discharge tube (Z/L = 1.8) and the closed end wall (Z/L = 0). The solid curves of Fig. 3 show that for small Z/L the total temperature is almost wholly dependent on the radius and very little on the axial position except for a small area around the center. The lowest total temperature T_{min} always occurred at the center of the closed end wall and there T_{min} is 32 F less than T_0. The maximum total temperature

[1] Numbers in brackets designate References at end of paper.

Contributed by the Heat Transfer Division and presented at the Summer Annual Meeting, Dallas, Texas, June 5–9, 1960, of THE AMERICAN SOCIETY OF MECHANICAL ENGINEERS.

NOTE: Statements and opinions advanced in papers are to be understood as individual expressions of their authors and not those of the Society. Manuscript received at ASME Headquarters, August 31, 1959. Paper No. 60—SA-4.

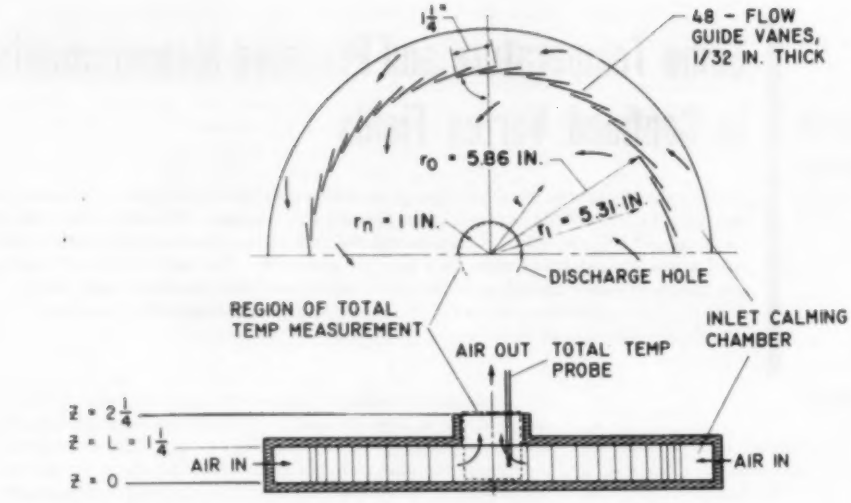

Fig. 1 Vortex chamber 1

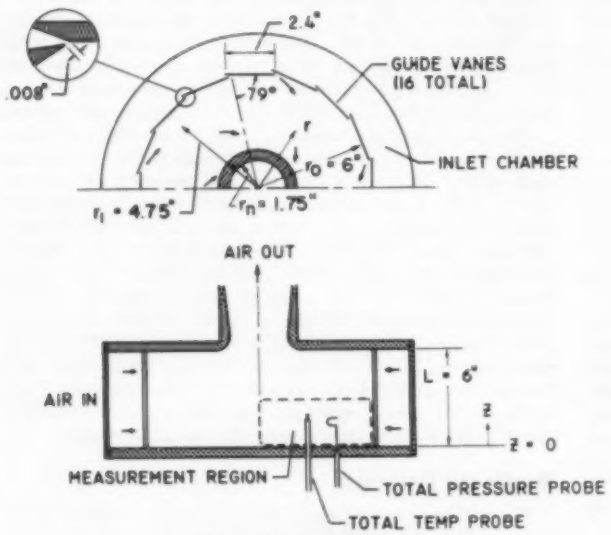

Fig. 2 Vortex chamber 2

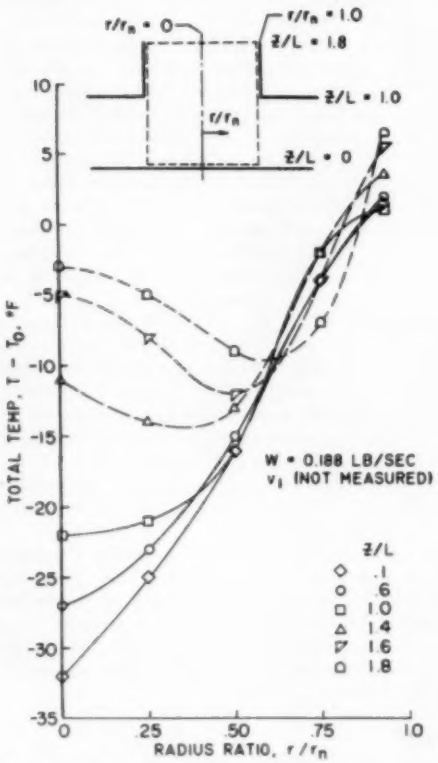

Fig. 3 Total temperatures in exhaust region of vortex 1

was measured near the exhaust radius r_n, and T_{max} did not exceed T_0 by more than 4 F. Also, the static closed end wall pressure drops to a very low value compared to the atmospheric pressure existing just outside the exhaust hole (Fig. 6).

The remaining portion of the region under study in vortex 1 is the cylinder formed by the exhaust tube. In the central core of this region, the total temperature shows a sizable dependence on the axial position as well as on the radius (dashed curves in Fig. 3). This result was probably due to the mixing which occurred between the outgoing vortex air and the room air which was drawn into the vortex "eye" just outside the discharge. The total temperature in the annulus outside the core varied sharply with radius and moderately with the axial position. The most interesting observation to be made here is that the T_{max} of the air adjacent to the hole surface increased as it moved out from within the vortex. Whether this increase in T_{max} can be wholly attributed to frictional dissipation is not known.

The real significance of the results obtained from vortex 1 is best appreciated when viewed in terms of the Ranque-Hilsch tube. The present apparatus can be viewed as a modified uniflow Ranque-Hilsch tube where the vortex chamber is the air inlet and the cylindrical discharge hole is a much shortened tube. As in the usual form of this device, there exists the outer region of high total temperature and a core of very low total temperature. Thus it appears from these results that the Ranque-Hilsch effect occurs in the flow entrance region adjacent to the closed end for which no measurements are available. This agrees with the observation made by Pengelley [8].

The radial total-temperature distributions measured inside vortex 2 are shown in Fig. 4 for a plane positioned $Z/L = 1/3$ from

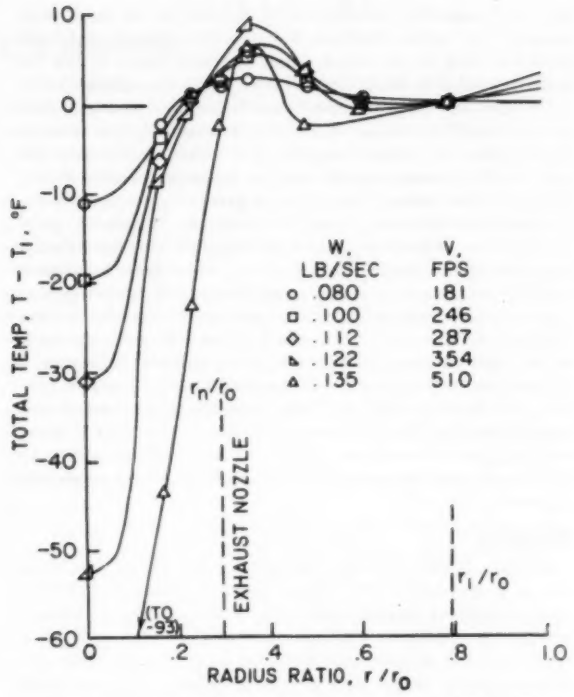

Fig. 4 Radial total temperatures in vortex 2 at Z/L = 1/3

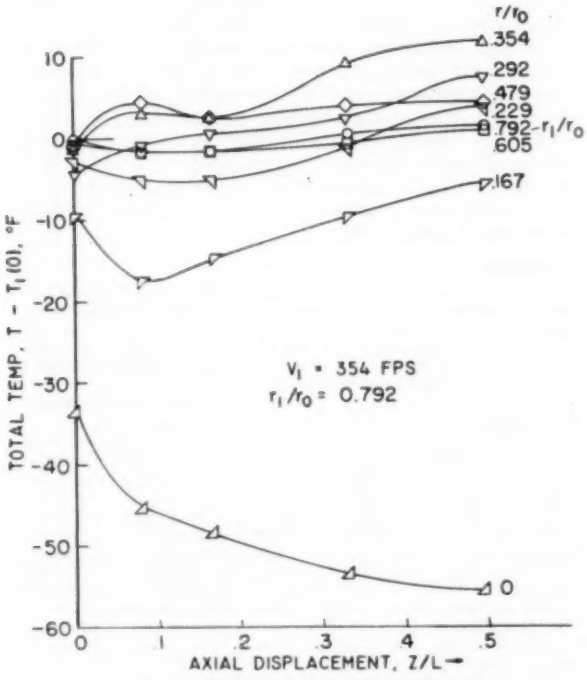

Fig. 5 Axial total temperatures in vortex 2

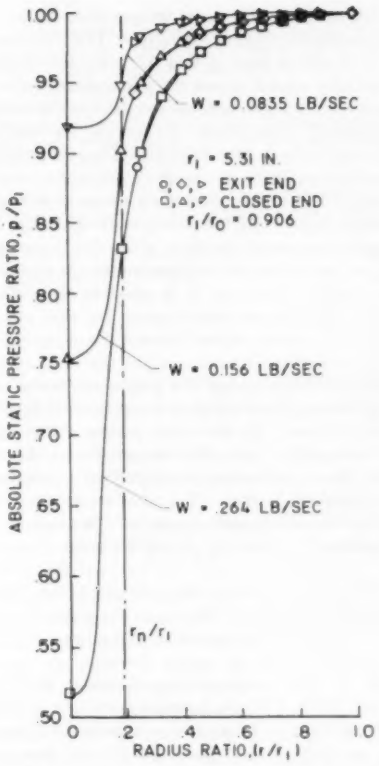

Fig. 6 Static pressures at closed end exhaust and walls of vortex 1

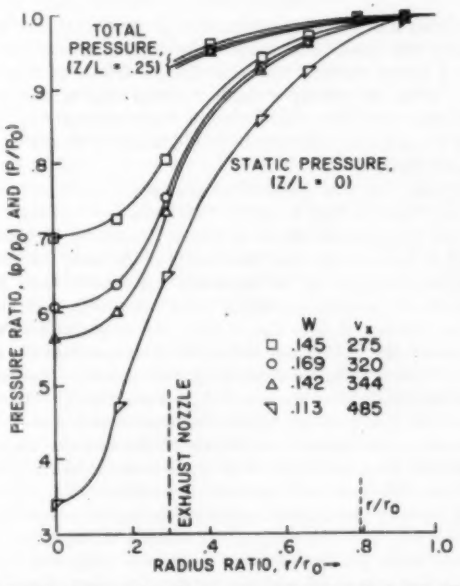

Fig. 7 Static and total pressures at closed end of vortex 2

the closed end surface. The total temperature T_1, as measured at an outermost measuring station $r_1/r_0 = 0.792$, was used as the reference. The weight rate of flow W, with the corresponding tangential velocity v_1 at r_1/r_0 are the parameters in the figure.

The curves exhibit some general trends and also an apparent exception to one of these trends. In general, the total temperature T of the air decreases gradually with decreasing radius before rising somewhat rapidly to a maximum just before reaching the discharge hole. The temperature then drops very sharply to a minimum at the center. All the curves show that T_{min} drops and T_{max} rises as the tangential velocity v_1 of the fluid increases, except for the T_{max} of the curve for the maximum tangential velocity ($v_1 = 510$ ft/sec). However, it is possible that this T_{max} is actually higher than for the other curves, but that (*a*) the maximum occurs in the narrow region between the measured temperatures at $r/r_0 = 0.48$ and 0.355, or (*b*) the drag effect of the thermocouple probe diminished the true temperature of the undisturbed vortex enough to result in an apparent exception to the general trend indicated by the other curves. A third possible factor is a "screaming" noise that occurred near the maximum velocity with an accompanying 10 to 20 F total-temperature increase throughout the vortex. The total-temperature gradients increase as the vortex strength increases. The largest measured difference between T_{max} and T_{min} is 102 F for the $v_1 = 510$-ft-per-sec-curve.

The axial variation of total temperature at various radii in vortex 2 is shown in Fig. 5. The results indicate that the axial dependence of total temperature is slight, and that the predominant variation is in the radial direction, as was found in vortex 1 (Fig. 3). The reference temperature $T_1(0)$ is that at the wall at the radius r_1 and is for a tangential velocity $v_1 = 354$ ft per sec. Again, the measured axial temperature variations are influenced by the drag effect of the probe and the deviation of the indicated temperatures from those of the undisturbed vortex increases with depth of insertion. It is felt, however, that these data are substantially correct, and represent total-temperature variations in vortex flow.

The conclusion to be drawn from the measurements obtained from vortex 2 is that the separation of an air stream into regions of higher and lower total temperature can be achieved inside a confined vortex without the usual Ranque-Hilsch tube arrangement. Thus the results of both vortexes suggest that energy separation results from, and occurs in, the initial region of vortex flow and is either (*a*) unaffected, or (*b*) diminished by any confined axial flow channels.

The static end wall pressure measurements made in vortex 1 and 2 are shown in Figs. 6 and 7. Total pressure P was measured in vortex 2 and is also shown in Fig. 7. In vortex 1 it was impossible to measure the wall pressure near the vane tips because of the manner in which the apparatus was constructed. Hence the outermost pressure tap radius r_1 and pressure p_1 were used as reference values. In both Figs. 6 and 7 the weight rate of flow W is the parameter. In both chambers the static gradient at a given radius increases with increasing tangential velocity; the same is true for the total-pressure ratios P/P_1 in vortex 2. The difference between the total pressure and the static pressure is seen in Fig. 7 to increase as the radius decreases, indicating that the tangential air velocity rises as it moves in toward the exhaust. Fig. 6 shows that the static wall pressure distributions of the two end walls of vortex 1 are identical except for the region enclosed by the exhaust hole. Also, the static pressure at the center of the closed end drops very low and decreases with increasing swirl. These results are in agreement with similar data of others [1 and 2].

A simplified analysis was made to obtain a relationship between the measured static-pressure distribution and the velocities inside the vortex. It was assumed that the centrifugal force was balanced only by the pressure force, that is, the flow was inviscid. Also, the tangential velocities were assumed to be large compared to the radial velocities, and that the cylinder end walls exerted no drag on the vortex. Only the outer region of flow between the exhaust nozzle and the inlet vanes was subject to detailed analysis. To match the measured pressure variation with an analytically determined curve, the air would have to increase its tangential and radial velocities as it moves inward from the vanes to the exhaust similarly to a free vortex as observed above. The agreement between the analytical pressure curve and the experimental curve was very good for vortex 1 and reasonably good for vortex 2. A brief analysis of the region within the exhaust radius shows that the tangential velocity would have to increase with the radius somewhat as in wheel-type fluid motion to produce a radial pressure variation qualitatively similar to the measured distribution. While the analyses just given permit a relation between some average effective tangential velocity and the pressure, they do not reveal the details of the true flow pattern. The presence of the end walls where the velocity and, consequently, the centrifugal forces are zero will have a marked effect on the shape of the velocity profiles. A more refined analysis or experiment would be rather complex and beyond the scope and purpose of this paper.

Conclusion

The data presented herein represent an incremental part of an over-all study of vortex-type flow. They are intended to provide some preliminary experimental results and some positive though restricted conclusions. Within a compressible vortex confined in a right circular cylinder both moderate increases and sizable decreases in total temperature can be obtained. The maximum total temperature occurs in the vicinity of the exhaust hole radius and the minimum at the center line. These results show that the total-temperature separation can be produced within a vortex generator without the aid of axial tubes as used in the conventional uniflow or counterflow Ranque-Hilsch tube.

The static wall pressure measurements indicate that the effective tangential velocity increases as the air moves in from the cylinder circumference toward the exhaust hole and then sharply changes to a flow similar to wheel-type motion within the exhaust hole circle. No conclusions can be drawn about the mechanism causing the energy separation because the flow pattern is complex and many factors such as velocity profiles and vortex geometry remain to be investigated in addition to the relatively simple measurements presented here.

References

1 R. H. Wilson, "The Effect of Viscosity Upon the Pressure Distribution for Swirling Flow Through a Right Circular Cylinder," Rep. 1598, Oak Ridge Nat. Lab., 1953.

2 H. H. Kearsey and N. S. Hibbert, "The Separation of Gases From Liquids by Means of Vortical Flow in a Cylindrical Vessel," CE/R 2628, British AERE, 1958.

3 H. A. Einstein and H. Li, "Steady Vortex in a Real Fluid," Heat Transfer and Fluid Mechanical Inst., 1951, pp. 33–43.

4 J. P. Hartnett and E. R. G. Eckert, "Experimental Study of the Velocity and Temperature Distribution in a High-Velocity Vortex-Type Flow," TRANS. ASME, vol. 79, 1957, pp. 751–758.

5 J. E. Lay, "An Experimental and Analytical Study of Vortex-Flow Temperature Separation by Superposition of Spiral and Axial Flows, Parts 1 and 2," JOURNAL OF HEAT TRANSFER, TRANS. ASME, Series C, vol. 81, 1959; Part 1: pp. 202–212; part 2: pp. 213–222.

6 R. G. Deissler and M. Perlmutter, "An Analysis of the Energy Separation in Laminar and Turbulent Compressible Vortex Flows," Heat Transfer and Fluid Mechanics Inst., 1958, p. 40.

7 R. G. Deissler and M. Perlmutter, "Analysis of the Flow and Energy Separation in a Turbulent Vortex," *International Journal of Heat and Mass Transfer* (accepted for publication).

8 C. D. Pengelley, "Thermal Phenomena in a Vortex," Symposium on the Vortex Tubé as a True Free Air Thermometer, Armour Research Foundation, Chicago, Ill., May 25, 1955.

9 R. Hilsch, "The Use of the Expansion of Gases in a Centrifugal Field as a Cooling Process," *Review of Scientific Instruments*, vol. 18, 1947.

DISCUSSION

E. M. Knoernschild[2]

This paper is a valuable contribution to the flow behavior in vortex chambers. The authors present test results of the pressure and temperature distributions in a vortex chamber and analyze them in the light of the Ranque-Hilsch effect.

The test data emphasize, again, the importance of the ratio mass flux to viscosity for any practical utilization as a cooling device. As already pointed out by Deissler and Perlmutter [10],[3] and before that by the interesting study of Einstein and Li [11], the performance of a vortex tube depends to a large extent on the possibility of the flow to discharge axially. In this case the radial mass flux can be made small compared to the axial flux and hence viscous forces in the flow have time to decelerate the peripheral flow pattern so that finally solid body rotation may evolve. If the flow cannot axially discharge and the ratio mass flow to viscosity becomes large, the action of viscosity on the flow is reduced. This interaction between the inertia forces which are represented by the mass flow and the viscous forces leads to the Reynolds number concept as pointed out in Deissler and Perlmutter [10].

It has to be kept in mind that the foregoing described flow pattern is an equilibrium pattern which develops with time from a free vortex pattern and it is exactly this change of the velocity pattern from one relating to the free vortex to the solid body type which gives rise to energy transfer which shows up in total temperature changes. This is clearly pointed out in the discusser's paper [13]. Hence it is to be expected that a large change of temperature should show only in those regions in which an axial variation of the mass flow can be established, that is in the exit duct region. For instance, Fig. 4 of the discussed paper shows practically no temperature drop in the flow region where the mass flow cannot change, followed by a considerable temperature variation in the exhaust region. This is also shown in Fig. 5 where practically no temperature variation occurs until the radius ratio approaches 0.23. At smaller values of this radius ratio, that is within the diameter of the exit nozzle, considerable changes of the temperature were measured. Considering the basic concept of the analysis of reference [14], which maintains that viscosity is the main influence on the energy transfer, it does not seem too practical to assume that the flow is inviscid, as the authors in their centrifugal force balance do. One should be aware of the fact that whenever a wheel-type rotation is noticed, this rotation comes about by the influence of viscous forces, otherwise the free vortex flow would be dominant.

A valuable contribution to the energy transfer problem is the work by Schiebeler [12], which is not too well known in this country and which presents the axial and peripheral velocity distribution and corresponding pressure distribution in a pipe for various inlet whirl angles.

It is worth mentioning that a valuable contribution to the three-dimensional flow in a vortex, which sheds some light on the axial flow distribution, is given by Sullivan [14].

It is interesting to speculate whether an energy transfer effect may also take place in a flow around a corner or around an air foil. Here the radial flux is zero and in spite of the shortness of the circular flow path the effect of viscosity should result in a transition from potential flow to solid body flow, at least in the layers close to the surface, which means a centrifugation of energy away from the air foil surface. This effect may actually be a contributing factor to the flow separation after curved walls.

[2] The Garrett Corporation, Los Angeles, Calif.

[3] Numbers in brackets from [10–14] designate References at end of this discussion.

References

10 R. G. Deissler and M. Perlmutter, "An Analysis of the Energy Separation in Laminar and Turbulent Compressible Vortex Flows," Heat Transfer and Fluid Mechanics Inst, 1958, p. 40.

11 H. A. Einstein and H. Li, "Steady Vortex in a Real Fluid," Heat Transfer and Fluid Mechanics Inst, 1951, pp. 33–43.

12 W. Schiebeler, "Luftstromungen mit Drall im Kreisrohr hinter radialem Leitapparat," Max Planck Institut für Stromungsforschung, Nr. 12, Gottingen, Germany, 1955.

13 Rudolph Kassner and Eugen M. Knoernschild, "Friction Laws and Energy Transfer in Circular Flow," Report No. F-TR-2198–ND Wright-Patterson Air Force Base, Dayton, Ohio, March, 1948.

14 Roger D. Sullivan, "A Two-Cell Vortex Solution of the Navier-Stokes Equations," *Journal of the Aero/Space Sciences*, vol. 26, no. 11, November, 1959.

J. E. Lay[4]

The authors have presented a simple but ingenious way of generating a vortex flow within two cylinders by means of injection of air through guide vanes. It is certainly logical to view the apparatus as a modified uniflow Ranque-Hilsch tube, but the drastic shortening of the tube may not give results which are representative of the Ranque-Hilsch effect. In view of the fact that various investigators have reported an optimum length of between 6 to 9 diameters, it may be of interest to inquire if the authors plan to conduct tests involving a greater range of Z/L values other than those reported in the present paper. In fact, a very feasible but worth-while extension of the present set of measurements would be to simply extend the length of the discharge tube and see what happens.

Of the several results presented, the stagnation temperature plot of Fig. 3 is the most interesting. It has the same general character as some earlier results discussed by the authors under references [4 and 5]. There is, however, one item that needs elaboration: The abscissa in Fig. 3 is the radius ratio. This being the case, it has been found [4 and 5] that accurate measurements corresponding to a radius ratio of zero are very difficult if not impossible to obtain. It would be of interest to learn from the authors if the data corresponding to a radius ratio of zero are extrapolated data points or data actually obtained from experiment. Speaking of radius ratio, it is not entirely clear as to the difference between the ratios r/r_a, r/r_0, r/r_1, and r_1/r_0 used by the authors in their various plots. An explanation and perhaps an elaboration seems to be in order. As for the velocity distribution, the authors state that the effective tangential velocity increases as the air moves in from the cylinder circumference toward the exhaust hole and then sharply changes to a wheel type of motion. While this seems to be the case in some earlier works, there is very little evidence in the present report to support this contention. The velocity distribution has not been plotted, so it is a bit intriguing as to how this conclusion was arrived at. Certainly it would have to be based on more than just static wall pressure measurements.

Another item needing clarification is the injection of air. In their figures, the authors show the air as already being present in the calming chamber. It is, however, not shown how this air was previously fed into the apparatus. Also, it would be desirable to give the absolute pressure in the calming section since this pressure would most probably correspond to the inlet pressure in a regular Ranque-Hilsch tube. Finally, it may be asked of the authors that if the present apparatus is to be considered as a uniflow Ranque-Hilsch tube, what smallest value can the ratio of cylinder length to cylinder diameter be in order to still maintain this point of view?

The measurements presented here are of great interest because

[4] Professor, Mechanical Engineering Department, Michigan State University, East Lansing, Mich. Assoc. Mem. ASME.

they show that a stagnation temperature separation seems to occur each time a vortex flow is generated even without the aid of axial tubes. Clarification of some of the above questions will do much to add to the usefulness of the paper.

M. L. Rosenzweig[5]

Since confined vortex flows are of considerable technological interest and since experimental results in this field are extremely meager, the present study should yield some interesting and useful data. Unfortunately, the results reported in the present paper are not only incomplete, as suggested by the authors, but also insufficient even to justify some of their own conclusions. For instance, Fig. 3 indicates an increase in total temperature, as measured along the axis of the vortex, with increasing Z/L, while for vortex 2, Fig. 5 shows just the opposite trend, although the curves are not carried beyond $Z/L = 0.5$. Furthermore, if one considers the temperature profiles of Fig. 3, it appears that one is led to a conclusion in variance with that stated in the paper; namely, that the presence of an axial flow tube *does* aid in the energy separation if the cold gas is extracted at $Z/L = 0$ while the hot gas is removed in an annulus at the end of the axial flow tube. In order to do this, however, some obstruction must be placed in the flow at the outflow end of the tube, such as a conical valve as used in the Eckert and Hartnett experiments. Such modifications would invariably alter the flow pattern within the vortex and could conceivably lead one back to the authors' original conclusion.

Important questions, such as the axial variation of the flow variables and the effects of exit geometry and end wall boundary layers on the vortex proper, are still largely unanswered. It is hoped that the continuation of the authors' experimental research program may help to shed some light on this very complex subject.

Authors' Closure

We thank Doctors E. M. Knoernschild, J. E. Lay, and M. L. Rosenzweig for their stimulating discussions. Again it is stressed that these experiments were aside from the main objectives of our vortex studies. We were prompted to make these measurements because (1) the need existed; (2) the apparatus required very few modifications; and (3) the measurements could be made without seriously interrupting our main program. While it is true that the scope and precision of this work was limited, we believe that the data will contribute to furthering the understanding of vortex motion.

First, the intended general conclusions will be elaborated upon. As was stated, it was observed that a total temperature separation similar to that which occurs in a Ranque-Hilsch tube can be produced within a vortex generator without the use of tubes to contain the region of axial flow. It is of course recognized that the air undergoes a transition from radial to axial flow within a vortex generator, as indeed it must do eventually. We are in accord with Dr. Knoernschild's remarks concerning the cause of the total temperature separation. In the region where the flow direction changes from radial to axial, there is a transition of the tangential velocity from that of a free to a forced vortex. It is this change in the tangential velocity which contributes to the energy separation. Since this general flow pattern exists within a vortex generator, the presence of a cylinder to extend the flow in the axial direction is not needed to achieve a separation.

Second, we want to comment further on the inviscid analysis. A number of investigators have used the inviscid model in an attempt to understand the nature of confined vortex flows using only static wall pressure measurements. We clearly stated that the simple inviscid analysis did not describe the actual flow situations inside the vortex chambers. Rather, the analysis was intended to illustrate in an approximate way what the data in Fig. 7 shows; namely, that the average tangential velocity of the air (neglecting wall boundary-layer effects and other variation in the profile between the end walls) increased as it moved radially inward. From physical argument the tangential velocity at the center line must be zero; hence, there must be a transition region between the center line and the exhaust hole radius near which the tangential velocity reaches a maximum. Within this transition region there exists a core around the center line which possesses a solid-body type of rotational motion. Hartnett and Eckert [4] observed this as did Lay [5]. The static wall pressure distributions near the axis (radius ratio range 0 to 0.2) shown in Figs. 6 and 7 can only be explained by the presence of a core region having a solid-body type of rotational motion. The exact details of the flow are undoubtedly complex and difficult to measure.

We regret the possible confusion in the Nomenclature. Originally this paper was submitted as a Brief Note, which accounts for the form. It certainly would have been clearer with a table of symbols. This following definitions will help the reader:

r_n = nozzle radius, r = radial co-ordinate, r_0 = vane circle radius.

In reply to Professor Lay's questions, we would like to point out that the center line total temperatures were measured as indicated in Figs. 1 and 2. Also, by using the method shown, the center line temperatures were the easiest to measure because of zero tangential velocity and the small axial velocity. How short a Ranque-Hilsch tube has to be before it ceases to be one is somewhat arbitrary. The inlet chamber of each vortex was supplied by pipe lines leading from the source.

Dr. Rosenzweig raised a very pertinent question for which we, unfortunately, cannot give a satisfactory explanation, except to say that the exit geometries undoubtedly play an important role. The extent to which they influence the total temperature in the central core can only be determined by more experimentation. Certainly the flow at the exit of vortex 1 is influenced differently because of the mixing with the room air than the flow at the exit of vortex 2, where the air is discharged into a cylinder leading to a vacuum exhaust system. The conduction and radiation losses from the probe tip at the low center line temperatures may have been different in each apparatus. Perhaps, some secondary flow condition such as boundary layer on the solid end wall may have influenced the conditions to produce the opposing axial variation of the total temperature along the center line. All these remarks are just another way of saying that a great deal of experimentation is needed to more fully explain turbulent vortex motion.

As to further work, we might add that we hope to continue our present studies. Some of the results measured to date may become available in the literature in the not-too-distant future.

[5] Space Technology Laboratories, Inc., Los Angeles, Calif.

FREDERICK L. TEST
Associate Professor of Mechanical Engineering, University of Rhode Island, Kingston, R. I. Assoc. Mem. ASME

The Influence of Bypass Channels on the Laminar Flow Heat-Transfer and Fluid Friction Characteristics of Shell and Tube Heat Exchangers

This paper discusses the effect of tube bundle to shell clearance, mean oil temperature, mean water temperature, and oil flow rate on the shell-side heat-transfer film coefficients and pressure losses for laminar flow in unbaffled and cross-baffled heat exchangers. The results for cross-baffled heat exchangers can be correlated by considering the flow to be a combination of flows parallel to the tubes and across the tubes.

Introduction

THE MATERIAL presented in this paper represents a continuation of the work discussed by the author[1] in a previous paper. The earlier research was limited, to some extent, by experimental techniques which have since been improved. The new data extend further into the laminar region and also include information on the experimental units for isothermal and heating runs in addition to the usual cooling runs.

It was felt that the data could best be correlated when the flow was considered a combination of flow across the tubes and parallel to the tubes. In order to investigate this conclusion, runs were made with an unbaffled heat exchanger in addition to the usual cross-baffled units. There has been considerable information published by a group at the University of Delaware[2] on the characteristics of the crossflow path. The general method of correlation by means of effective area and effective Reynolds number was presented by Tinker[3] in a series of papers in 1951. The effective area approach was used in correlating the data in this paper but the method of determining the effective area was not the same as that discussed by other authors or used previously by this author. The technique of calculating effective area presented in this paper is felt to correlate the laminar flow data better than the calculation techniques previously used.

[1] F. L. Test, "A Study of Heat Transfer and Pressure Drop Under Conditions of Laminar Flow in the Shell Side of Cross-Baffled Heat Exchangers," TRANS. ASME, vol. 80, 1958, pp. 593–600.

Contributed by the Heat Transfer Division and presented at the Summer Annual Meeting, Dallas, Texas, June 5–9, 1960, of THE AMERICAN SOCIETY OF MECHANICAL ENGINEERS.

NOTE: Statements and opinions advanced in papers are to be understood as individual expressions of their authors and not those of the Society. Manuscript received at ASME Headquarters, August 3, 1959. Paper No. 60—SA-7.

[2] O. P. Bergelin, A. P. Colburn, and H. L. Hull, "Heat Transfer and Pressure Drop During Viscous Flow Across Unbaffled Banks," University of Delaware, Engineering Experiment Station, Bulletin No. 2, 1950.

O. P. Bergelin, G. A. Brown, and S. C. Doberstein, "Heat Transfer and Fluid Friction During Flow Across Banks of Tubes—IV," TRANS. ASME, vol. 74, 1952, pp. 953–960.

O. P. Bergelin, G. A. Brown, and A. P. Colburn, "Heat Transfer and Fluid Friction During Flow Across Banks of Tubes—V," TRANS. ASME, vol. 76, 1954, pp. 841–850.

O. P. Bergelin, K. J. Bell, and M. D. Leighton, "Heat Transfer and Fluid Friction During Flow Across Banks of Tubes—VII, Fluid By-Passing Between Tube Bundle and Shell," AIChE Paper presented at 2nd National Heat Transfer Conference, August, 1958.

[3] Townsend Tinker, "Shell Side Characteristics of Shell and Tube Heat Exchangers," Proceedings of the General Discussion on Heat Transfer, The Institution of Mechanical Engineers, London, England, 1951, pp. 89–116.

Nomenclature

A_c = tube bundle crossflow area within limits of tube bundle, $S \times D_s$

A_{eff} = effective tube-bundle crossflow area

A_{effL} = effective tube-bundle area for flow parallel to tubes

A_{LBP} = bypass area between tube-bundle and shell for flow parallel to tubes

A_{Lt} = free area within tube-bundle for flow parallel to tubes

C_{p_0} = specific heat of oil at mean oil temperature

C_{p_s} = specific heat of oil at tube surface temperature

D_b = mean diameter of entire tube-bundle

D_c = D_b − (number of tubes in average row)D_t

D_{Lt} = volumetric hydraulic diameter for flow parallel to tubes

D_s = inside shell diameter

D_t = outside diameter of tubes

D_w = volumetric hydraulic diameter for crossflow between baffle windows

$$\frac{4 \times \text{free volume}}{\text{surface area of tubes}}$$

D_1 = tube bundle diameter between baffle windows

f' = crossflow friction factor

g_c = conversion factor in Newton's law of motion, $32.2 \frac{\text{lb}_M}{\text{lb}_F} \cdot \frac{\text{ft}}{\text{sec}^2}$

G_{eff} = effective crossflow mass velocity, W_0/A_{eff}

h_c = portion of oil film coefficient due to heat transferred during crossflow component of flow

h_0 = film coefficient on oil side

J = corrected crossflow heat-transfer factor

J' = over-all heat-transfer factor for cross-baffled units

J_s = heat-transfer factor for unbaffled units based on oil properties at tube surface temperature

k_0 = thermal conductivity of oil at mean oil temperature

(Continued on next page)

The use of Reynolds number, at present, is not too useful a criterion to designate the region of laminar flow in the shell side of a heat exchanger due to different ways in which Reynolds numbers might be calculated. The data presented in this paper were considered to be in the laminar region because the pressure loss was a linear function of the weight rate of flow.

Equipment and Procedure

The experimental apparatus is shown in Figs. 1 and 2. The baffled heat exchangers were of shell and tube construction using half-moon baffles. The baffle cut was 33 per cent of the shell cross section, and the baffle spacings were 2, 4, and 6 in. with entrance and exit regions of 4, 4, and 6 in., respectively. The cross section of the baffled units is shown in Fig. 1. The cross section of the unbaffled unit was the same except that the shell ID was 5.01 in. rather than the $4^7/_8$ in. used for the baffled units. The tube OD was $^3/_8$ in. and all exchangers had a length of 24 in.

The oil flow was governed by a bypass arrangement and the flow was measured with a rotameter. The oil temperature was measured by thermocouples mounted in the tanks shown at the top of Fig. 2. Mixing baffles were installed in each tank and the pipe leading to each tank had additional mixing baffles installed. An electric mixer was also installed in the outlet tank as this was the one with the severest stratification problem. The heat-transfer calculations were corrected for the energy transfers due to the mixing baffles and the electric mixer.

The oil temperature entering the test unit was usually regulated by governing the flow of steam to an oil heater. Water, to cool the oil, could be supplied to the oil heater if the test unit was to operate as a heater. The cooling-water temperature was regulated by controlling the steam supply to a shell and tube water heater. It was possible to vary the cooling-water temperature from 50 to 165 F and the entering oil temperature from 100 to 190 F. The range of oil flows was 7 to 200 lb/min. Variations of water flow did not appear to affect the heat-transfer rate or pressure loss; therefore, in all runs the water rate was held at about 300 lb per min.

All runs were performed with the SAE 60 oil using the four-inch and unbaffled units. Some of the data for the four-inch and all of the data for the two-inch and six-inch units was taken from the previous paper by the author.[1] At a temperature of 100 F the viscosity is 1720 SSU and at 210 F it is 125 SSU for the SAE 60 oil.

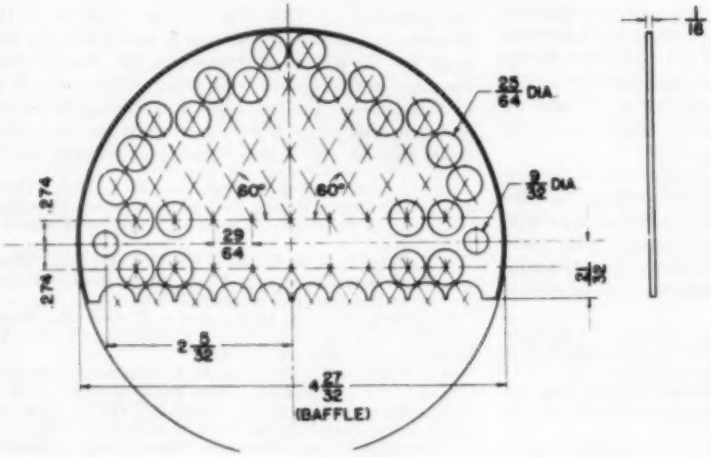

Fig. 1 Exchanger cross section

Nomenclature

k_s = thermal conductivity of oil at tube surface temperature
L = tube length
L' = term proportional to total length of shell side flow path and related to outside surface area of tubes
L_c = the crossflow component of assumed flow path length
L_p = length of bypass channel for crossflow between baffle windows
N_r = number of tube rows traversed between centers of gravity of adjacent baffle windows times number of crossflow passes, 64, 40, and 28 for 2, 4, and 6-in. units, respectively
N_t = number of tubes in heat exchanger
ΔP_{BC} = pressure loss in crossflow bypass channel
ΔP_{BP} = pressure loss in bypass channel for flow parallel to tubes
ΔP_C = pressure loss for crossflow within the tube bundle
ΔP_L = pressure loss for flow parallel to the tube within the tube-bundle
ΔP_T = experimentally determined pressure drop across entire exchanger
$\Delta P_T'$ = calculated pressure drop across entire exchanger
R_{ett} = Reynolds number for crossflow in tube bundle based on effective crossflow area
R_{ett_s} = Reynolds number for flow parallel to tubes based on effective area parallel to tubes
S = baffle spacing
T_{OM} = mean oil temperature
T_{WM} = mean water temperature
W_{BP} = weight rate of oil flow in bypass channel parallel to tubes
W_c = weight rate of oil flow in crossflow path within tube-bundle
W_o = total weight rate of oil flow
W_p = weight rate of oil flow in crossflow bypass channel
W_t = weight rate of oil flow within tube-bundle parallel to the tubes
Z = viscosity ratio, μ_o/μ_s
γ_o = specific weight of oil at mean oil temperature
μ_o = viscosity of oil at mean oil temperature
μ_s = viscosity of oil at tube surface temperature

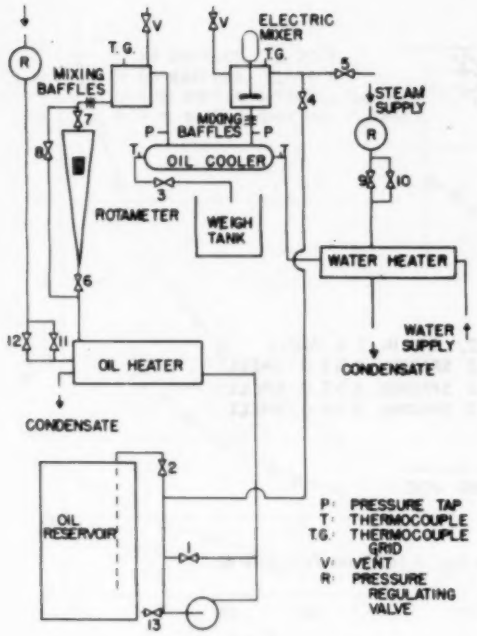

Fig. 2 Schematic arrangement of equipment

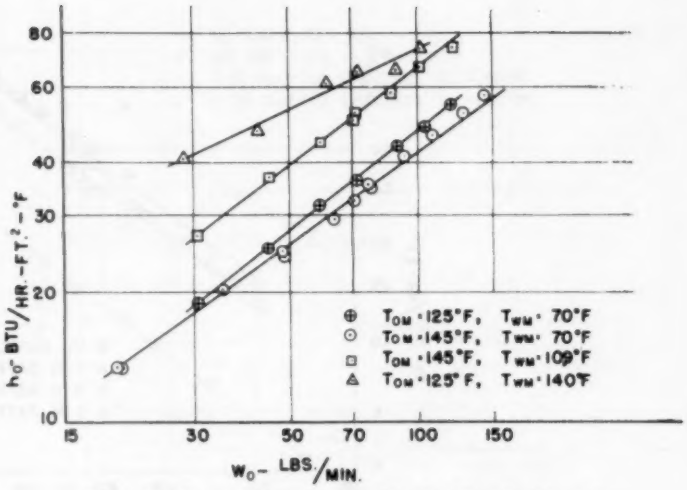

Fig. 3 Oil film coefficient versus weight of oil flow for 4-in. unit

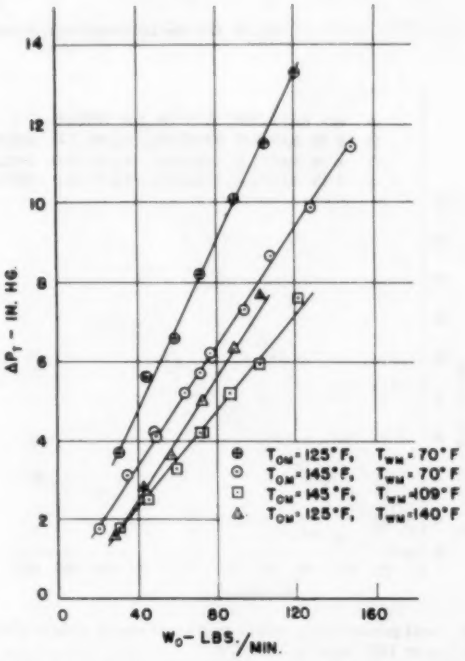

Fig. 4 Total pressure drop across exchanger versus weight of oil flow for 4-in. unit

Discussion of Results

Fig. 3 represents variable oil flow rate runs for the four-inch unit under different mean oil and water temperatures. The plot is on logarithmic co-ordinates so all lines are of the form h_o = const $(W_o)^{exp}$. The exponent would be about 0.75 for all runs except the one with T_{OM} = 125 F and T_{WM} = 140 F. This is the only run in which the oil is heated rather than cooled. A large portion of the deviation in slope might possibly be attributed to the difficulty of obtaining satisfactory data with a viscous oil when the arithmetic mean temperature difference is only 15 F.

The two lower lines of Fig. 3, at T_{WM} = 70 F, show that a decrease in oil temperature improves the oil film coefficient slightly. The principal variable with mean oil temperature is the oil viscosity. McAdams[4] and Jakob[5] give film coefficient relations for laminar flow in tubes or over flat plates which are independent of oil viscosity. However, the oil viscosity is a factor in heat exchangers due to the choice of alternate flow paths. At low tube wall temperatures the flow through the tube bundle will almost stagnate and most of the oil will flow in the bypass passage between the tube bundle and wall. As the mean oil temperature drops, increasing the oil viscosity, the resistance of the bypass passage increases thus decreasing the flow in the bypass and increasing the flow in the main bundle. This will cause a greater per cent of the total oil flow to contact the heat-transfer surface and thus cause an increase in the oil film coefficient.

An increase in water temperature increases the oil film coefficient a very significant amount. This results from a decrease in viscosity at the tube surface and thus less resistance to flow through the tube bundle. Both the effects of varying T_{WM} and T_{OM} will be discussed further during the discussion of Figs. 7, 8, 9, and 10.

Fig. 4 plots pressure loss results for the same data used in Fig. 3. In all runs, the pressure loss is a linear function of W_o, thus indicating laminar flow. The pressure loss decreases with an increase in T_{WM} or T_{OM} due to the effect of oil viscosity on flow path resistance.

Figs. 5 and 6 indicate the effect of oil flow rate on h_o and ΔP_T for various baffle arrangements. The significantly lower values for the unbaffled unit are due to the larger bypass area between the bundle and shell, rather than to the lack of baffles. The data for the 2, 4, and 6-in. units were taken from the earlier paper by the author.[1] It might be noted that at most weight flows, the film coefficient of the 4-in. unit can be improved by either adding or removing baffles. The pressure drop plot shows that there is

[4] W. H. McAdams, "Heat Transmission," McGraw-Hill Book Company, Inc., New York, N. Y., third edition, 1954, pp. 229–232.
[5] M. Jakob, "Heat Transfer," vol. I, John Wiley & Sons, Inc., New York, N. Y., 1949, pp. 451–473.

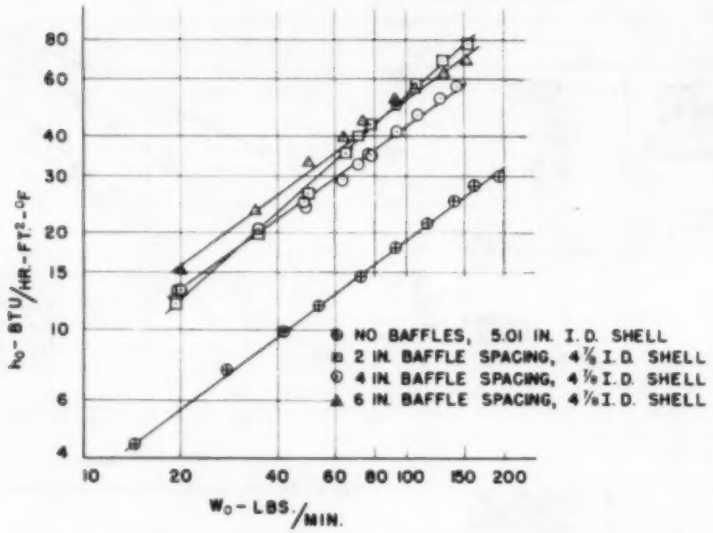
NO BAFFLES, 5.01 IN. I.D. SHELL
2 IN. BAFFLE SPACING, 4⅞ I.D. SHELL
4 IN. BAFFLE SPACING, 4⅞ I.D. SHELL
6 IN. BAFFLE SPACING, 4⅞ I.D. SHELL
h_o - BTU/HR-FT²-°F
W_o - LBS/MIN.

Fig. 5 Oil film coefficient versus weight of oil flow when T_{OM} = 145 F and T_{WM} = 70 F

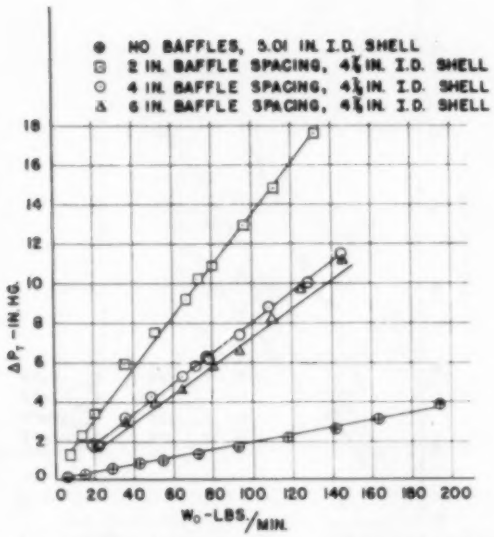
NO BAFFLES, 5.01 IN. I.D. SHELL
2 IN. BAFFLE SPACING, 4⅞ IN. I.D. SHELL
4 IN. BAFFLE SPACING, 4⅞ IN. I.D. SHELL
6 IN. BAFFLE SPACING, 4⅞ IN. I.D. SHELL
ΔP_T - IN. HG.
W_o - LBS/MIN.

Fig. 6 Total pressure drop across exchanger versus weight of oil flow when T_{OM} = 145 F and T_{WM} = 70 F

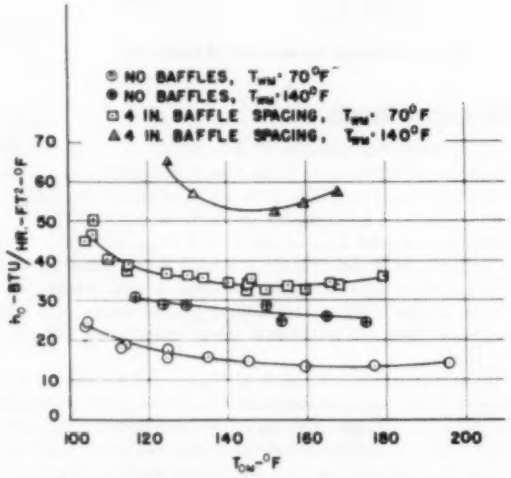

Fig. 7 Oil film coefficient versus mean oil temperature when W_0 = 72.5 lb/min

very little difference in flow resistance between the 4 and 6-in. units, but the 2-in. unit has a large increase in pressure loss.

Fig. 7 shows the variation of oil film coefficient with mean oil temperature at various water temperatures and baffle arrangements. The runs at T_{WM} = 140 F have oil heating at low T_{OM} and oil cooling at high T_{OM}. At high oil temperatures, the variation of T_{OM}, and thus oil viscosity, has very little effect on the value of h_o. At low oil temperatures, the oil film coefficient increases with decreasing oil temperature. The reason for this behavior was given in the discussion of Fig. 3. The trend, at low oil temperature, appears more pronounced in the 4-in. unit than in the unbaffled unit. This can be attributed as much to the different bypass areas as it can to the baffle arrangement. The 4-inch unit at T_{WM} = 140 F shows an increase in h_o with T_{OM} at high oil temperatures. This can be attributed to a tendency for the flow to become turbulent at high values of oil and tube surface temperatures.

Fig. 8 gives the pressure loss results for the same data used in Fig. 7. It might be mentioned again, that the low values of ΔP_T for the unit without baffles is due to the larger bypass channel in the unbaffled unit, rather than to the lack of baffles. This will be explained more fully when the pressure loss correlations are discussed. Under all conditions shown in this plot, the pressure loss increases with a decrease in T_{OM} due to the resulting viscosity increase. In the runs at T_{WM} = 140 F, there is no change in the general trend of the curves as the runs pass from oil heating through isothermal to cooling.

Fig. 9 shows the variation of oil film coefficient with the mean water temperature. The only characteristic on the oil side that can be affected by the mean water temperature is the oil viscosity at the tube surface. All runs pass from oil cooling through isothermal to oil heating. These results show the importance of oil viscosity at the tube surface in the determination

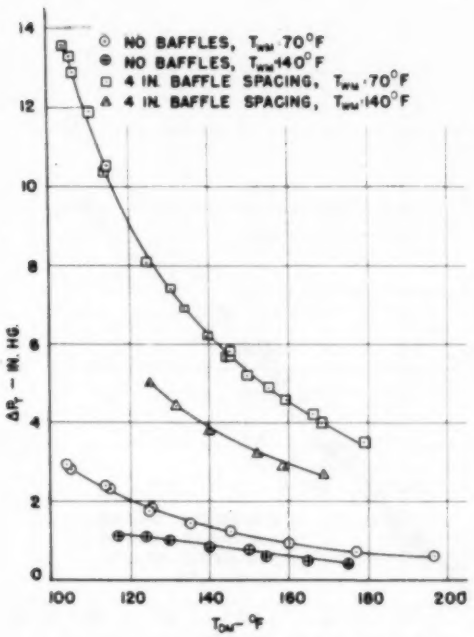

Fig. 8 Total pressure drop across exchanger versus mean oil temperature when W_0 = 72.5 lb/min

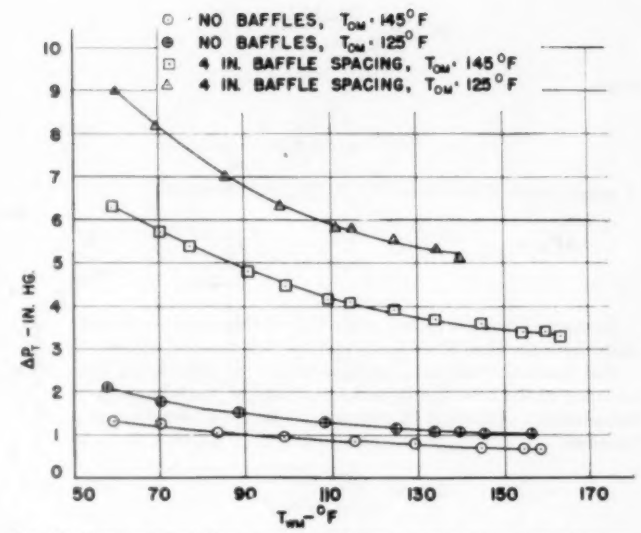

Fig. 10 Total pressure drop across exchanger versus mean water temperature when W_0 = 72.5 lb/min

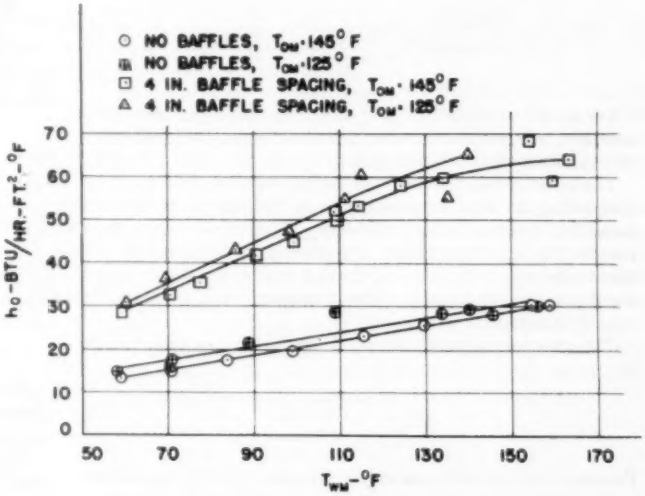

Fig. 9 Oil film coefficient versus mean water temperature when W_0 = 72.5 lb/min

of h_0. As the water temperature increases, the oil viscosity at the tube surface will decrease, thus lowering the resistance to flow through the tube bundle. This decreased resistance is shown in Fig. 10. The lower tube bundle resistance permits a larger per cent of the oil flow to pass through the tube bundle, increasing the value of the heat-transfer coefficient. The values of h_0 appear to level off at high T_{WM}, but it is difficult to draw a rigid conclusion because the heat-transfer data are not too precise in this region. This region is near the isothermal condition and the heat-transfer rate is small thus magnifying the result of any error in temperature readings.

Pressure-Drop Correlation

Previous research by the author[1] indicated that the pressure drop across a cross-baffled heat exchanger could be considered as the sum of pressure drops for flow across the tubes and flow parallel to the tubes. In the present paper, a pressure loss equation for flow parallel to the tubes was obtained by an analysis of the results for an unbaffled exchanger.

The pressure loss for flow parallel to the tubes was calculated by considering the total flow to be the sum of the flows in the bypass passage and tube bundle passage and that the pressure loss in the two passages were equal.

$$W_0 = W_1 + W_{BP} \tag{1}$$

$$\Delta P_{BP} = \Delta P_L \tag{2}$$

These equations were first applied to the isothermal data as the viscosity variation would not be a factor. The equations for ΔP_{BP} and ΔP_L are obtained from McAdams.[6] The flow in the bypass channel was considered to be similar to the flow between two parallel plates.

$$\Delta P_{BP} = \frac{12\mu_0 W_{BP} L}{g_c \gamma_0 A_{LBP} \left(\frac{D_s - D_B}{2}\right)^2} \tag{3}$$

[6] W. H. McAdams, "Heat Transmission," McGraw-Hill Book Company, Inc., New York, N. Y., third edition, 1954, pp. 148–149.

$$\Delta P_L = \frac{32\mu_t W_t L}{g_c \gamma_t A_{Lt} (D_{Lt})^2} \tag{4}$$

where

$$D_{Lt} = \frac{4A_{Lt}L}{\pi D_t N_t L} \tag{5}$$

A combination of Equations (1), (2), (3), and (4) yields:

$$\Delta P_L = \frac{32\mu_0 W_0 L}{g_c \gamma_0 A_{Lt} (D_{Lt})^2} \cdot \frac{1}{1 + \frac{8}{3}\frac{A_{LBP}}{A_{Lt}}\left(\frac{D_s - D_B}{2D_{Lt}}\right)^2} \tag{6}$$

Isothermal runs calculated on the basis of this equation did not differ by more than 8 per cent from the experimental values.

The nonisothermal runs were correlated by considering the viscosity in the tube bundle to be evaluated at the tube surface temperature. Equation (3) remains the same but Equation (4) becomes:

$$\Delta P_L = \frac{32\mu_s W_t L}{g_c \gamma_0 A_{Lt} (D_{Lt})^2} \tag{7}$$

The equation for pressure loss in a nonisothermal unbaffled unit becomes:

$$\Delta P_L = \frac{32\mu_s W_0 L}{g_c \gamma_0 A_{Lt} (D_{Lt})^2} \cdot \frac{1}{1 + \frac{8}{3}\frac{\mu_s}{\mu_0}\frac{A_{LBP}}{A_{Lt}}\left(\frac{D_s - D_B}{2D_{Lt}}\right)^2} \tag{8}$$

For an unbaffled unit $\Delta P_L = \Delta P_T'$, the calculated total pressure drop across the exchanger, and the calculations by equation (8) are indicated as "+" in Fig. 11.

The pressure loss for the cross-baffled units was calculated by considering the total pressure loss to be the sum of the pressure losses for crossflow and parallel-flow. Tinker[3] discusses many possible bypass channels for cross-baffled exchangers, but the channel between the tube bundle and shell is the one of major significance for exchangers of the dimensions used to obtain the data in this paper.

The pressure drop for isothermal crossflow in the tube bundle is:

$$\Delta P_c = \frac{2f' N_r (G_{eff})^2}{g_c \gamma_0} \tag{9}$$

Previous work at the University of Delaware[2] and by the author[1] indicate that the equation for f' when laminar flow is present is:

$$f' = \frac{50}{R_{eff}} \tag{10}$$

where

$$R_{eff} = \frac{D_{Ve} G_{eff}}{\mu_0} = \frac{D_{Ve} W_0}{A_{eff}\mu_0} = \frac{D_{Ve} W_C}{A_C \mu_0} \tag{11}$$

A combination of Equations (9), (10), and (11) gives:

$$\Delta P_C = \frac{100 N_r \mu_0 W_c}{D_{Ve} S D_C g_C \gamma_0} \tag{12}$$

If the flow in the crossflow bypass passage is analogous to the flow between two plates the pressure loss is:

$$\Delta P_{BC} = \frac{12\mu_0 L_p W_P}{\left(\frac{D_s - D_t}{2}\right)^3 S g_c \gamma_0} \tag{13}$$

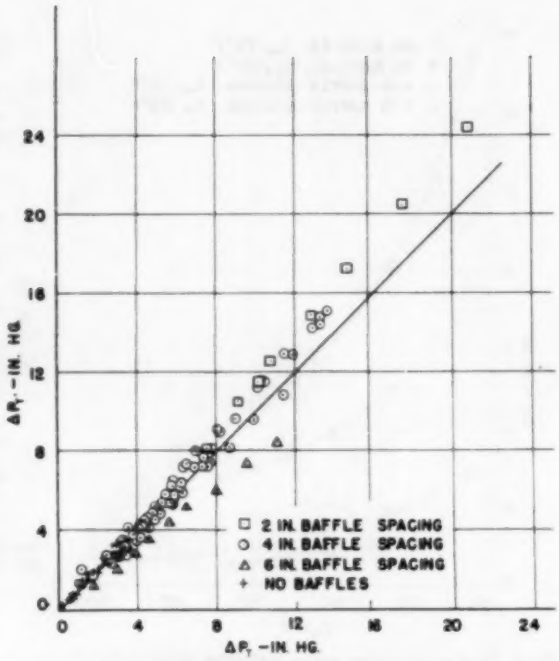

Fig. 11 Calculated total pressure drop versus experimental total pressure drop across exchanger

Since:

$$W_0 = W_p + W_C \tag{14}$$

A combination of Equations (12), (13), and (14) results in:

$$\Delta P_C = \frac{100 N_r \mu_0 W_0}{D_{Ve} S D_C g_c \gamma_0} \cdot \frac{1}{1 + \frac{100}{12} \cdot N_r \frac{\left(\frac{D_s - D_t}{2}\right)^3}{D_{Ve} \cdot D_C \cdot L_P}} \tag{15}$$

The sum of Equations (6) and (15) are used to calculate the pressure loss for isothermal cross-baffled units and the calculated values are within 8 per cent of the experimental values.

For nonisothermal runs the best correlation is obtained when Equation (12) is changed to:

$$\Delta P_C = \frac{100 N_r \mu_0 W_C}{D_{Ve} S D_C g_c \gamma_0 (Z)^{0.14}} \tag{16}$$

This results in Equation (15) taking the form

$$\Delta P_C = \frac{100 N_r \mu_0 W_0}{D_{Ve} S D_C g_C \gamma_0 (Z)^{0.14}} \cdot \frac{1}{1 + \frac{100}{12} \cdot N_r \frac{\left(\frac{D_s - D_t}{2}\right)^3}{D_{Ve} D_C L_p (Z)^{0.14}}} \tag{17}$$

The total pressure drop for a cross-baffled exchanger is the sum of Equations (8) and (17). The calculated and experimental values are compared in Fig. 11. If the calculations and data were exact, all of the points would fall on a line drawn at a forty-five degree angle. The points for the 6-in. unit depart from the line by 20 per cent of the correct value. The reason for this can be traced to Fig. 6, which indicates little difference between the experimental values for the 4 and 6-in. units. The calculated values show some difference due to the N_r term. In general, none

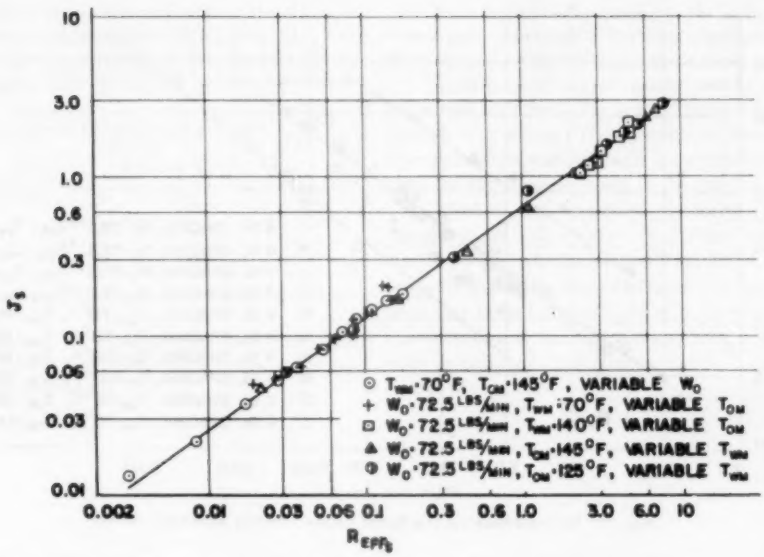

Fig. 12 Heat-transfer factor versus effective Reynolds number at tube surface for exchanger without baffles

of the calculated values differ by more than 20 per cent from the experimental values. The 20 per cent variation is due more to the limitations of the mathematical correlations than to the experimental data.

Heat-Transfer Correlation

A correlation of the data[7] was first attempted for the unbaffled unit as it was felt that this might give a basis for correlating the data of the baffled units. The data correlated quite satisfactorily when the heat-transfer factor (J_s) was plotted as a function of effective Reynolds number (R_{effs}). Both J_s and R_{effs} are evaluated for oil properties at the tube surface for flow parallel to the tubes.

$$J_s = \frac{h_o D_{Lt}}{k_s} \cdot \left(\frac{100}{\frac{C_{PS}\mu_S}{k_s}} \right)^{0.6} \cdot (Z)^{0.4} \tag{18}$$

$$R_{effs} = \frac{D_{Lt} W_o}{A_{effL} \mu_s} \tag{19}$$

where

$$A_{effL} = \frac{A_{Lt} W_o}{W_t} \tag{20}$$

The method of obtaining the flow rates was explained under the discussion of the pressure drop correlation.

The evaluation of properties at the tube surface temperature follows the pattern of the pressure drop correlation for unbaffled units. It might be noted that the Z-term is in the numerator rather than in its usual position in the denominator. This results from evaluating the Prandtl number at the tube surface temperature rather than at the mean oil temperature.

Values of J_s are plotted as a function of R_{effs} on logarithmic coordinates in Fig. 12. The data fall quite close to a straight line with a slope of 0.71. The resulting equation is:

$$h_o = 0.64 \frac{k_s}{D_{Lt}} (R_{effs})^{0.71} \left(\frac{C_{Ps}\mu_s}{100 k_s} \right)^{0.6} \frac{1}{(Z)^{0.4}} \tag{21}$$

Combining the viscosities from the Prandtl number R_{effs} and the Z-term gives $(\mu_s)^{0.29}/(\mu_o)^{0.4}$, which shows the effect of viscosity on the oil film coefficient. This of course does not include the possible large significance of viscosity in determining the value of A_{effL}.

If the values of h_o for unbaffled units had been calculated by Equation (21), but using the shell dimensions of the baffled units, a plot of these points in Fig. 5 would be a straight line lying within the grouping for the 2, 4, and 6-in. units. This supports the earlier statement that the drop in h_o for the unbaffled units is due to a larger bypass passage rather than a lack of baffles.

The heat-transfer data for the cross-baffled units were correlated on the basis of an effective Reynolds number for crossflow. For nonisothermal conditions, Equation (11) becomes:

$$R_{eff} = \frac{D_{VC} W_o}{\mu_o S D_e \left[1 + \frac{100}{12} \cdot \frac{N_r \left(\frac{D_s - D_t}{2} \right)^3}{D_{VC} D_C L_p (Z)^{0.14}} \right]} \tag{22}$$

The heat-transfer factor J' for the cross-baffled units was then plotted as a function of R_{eff} in Fig. 13.

The equation for J' is:

$$J' = \frac{h_o D_{Ve}}{k_o} \left(\frac{100}{\frac{C_{PO}\mu_o}{k_o}} \right)^{1/3} \left(\frac{1}{Z} \right)^{0.27} \tag{23}$$

It should be noted that for crossflow the oil properties are evaluated at the mean oil temperature rather than at the tube surface temperature as in Equation (18). The oil viscosity at the tube surface enters Equation (23) as a result of the Z-term but the effect is diminished due to the exponent in the Z-term.

The plotted points of the 4-in. unit show a scatter of about ±20 per cent in Fig. 13. Most of the points with the greatest

[7] Detailed experimental data may be obtained from the author.

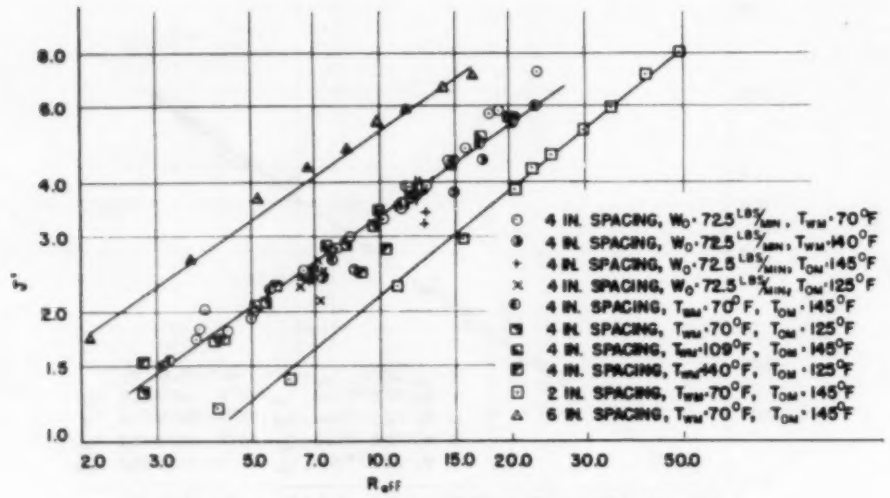
8.0
6.0
4.0
3.0
2.0
1.5
1.0
2.0
3.0
5.0
7.0
10.0
15.0
20.0
30.0
50.0
R_{eff}
4 IN. SPACING, W_O · 72.5 LBS/MIN, T_{WM} · 70°F
4 IN. SPACING, W_O · 72.5 LBS/MIN, T_{WM} · 140°F
4 IN. SPACING, W_O · 72.5 LBS/MIN, T_{OM} · 145°F
4 IN. SPACING, W_O · 72.5 LBS/MIN, T_{OM} · 125°F
4 IN. SPACING, T_{WM} · 70°F, T_{OM} · 145°F
4 IN. SPACING, T_{WM} · 70°F, T_{OM} · 125°F
4 IN. SPACING, T_{WM} · 109°F, T_{OM} · 145°F
4 IN. SPACING, T_{WM} · 140°F, T_{OM} · 125°F
2 IN. SPACING, T_{WM} · 70°F, T_{OM} · 145°F
6 IN. SPACING, T_{WM} · 70°F, T_{OM} · 145°F

Fig. 13 Over-all heat-transfer factor versus effective Reynolds number

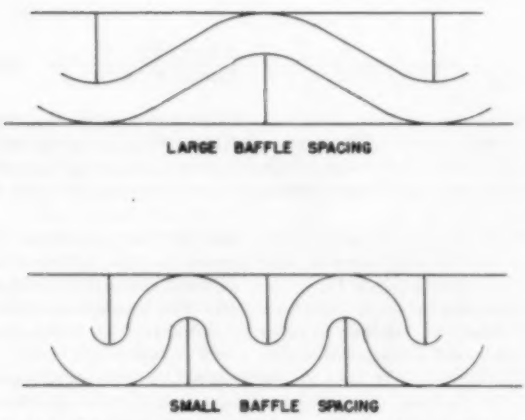

Fig. 14 Schematic representation of assumed change of flow pattern with change of baffle spacing

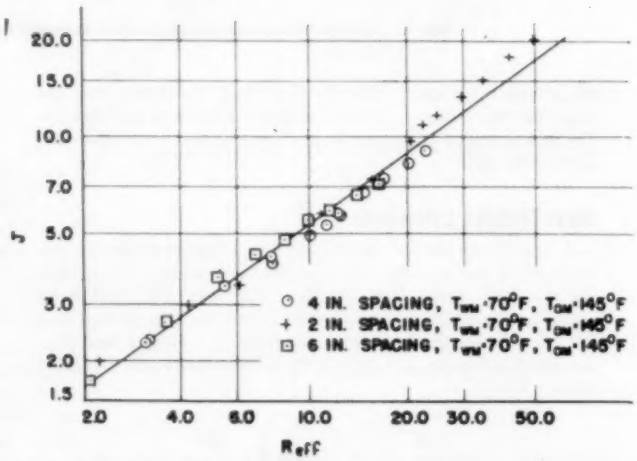

Fig. 15 Corrected crossflow heat-transfer factor versus effective Reynolds number

error are those for which there might be some inaccuracy in the data due to a small mean temperature difference or difficulty in maintaining constant mean water temperature at high values of T_{WM}. The data for the 2 and 6-in. units give different lines from the 4-in. data. The lines all have a slope of about 0.70 showing that they are all the same function of Reynolds number except for a constant.

The different plot for different baffle arrangements was once thought to be due to incorrect determination of flow rates in the bypass passages. The reasonably successful pressure drop correlation seems to discount this explanation. The difficulty perhaps s due to correlating an oil film coefficient that results from a sum of heat transfer for flow parallel to the tubes and flow across the tubes with a Reynolds number for flow across the tubes.

The sketches shown in Fig. 14 are an assumption as to how the flow pattern might change as the number of baffles is changed. The assumption in the sketch is that the area of the flow path normal to the direction of flow remains essentially constant but that the length of the flow path changes. The change in length of flow path is due to the change in crossflow length rather than parallel-flow length. This length would be proportional to the amount of heat transferred and thus the oil film coefficient for the crossflow portion. This would lead to an equation of the form:

$$h_o = h_o \frac{L_c}{L'} \tag{24}$$

The value of L_c is 12, 18, and 30 in. for the 6, 4, and 2-in. units, respectively. Since L' is a constant related to the outside surface area of the tubes, it was assigned a value of 12 for convenience. This then permits the calculation of h_o and the corrected crossflow heat-transfer factor J

where

$$J = J' \frac{L_c}{L'} \tag{25}$$

giving:

$$\left.\begin{aligned} \text{2-in. unit } J &= 2.5J' \\ \text{4-in. unit } J &= 1.5J' \\ \text{6-in. unit } J &= 1.0J' \end{aligned}\right\} \tag{26}$$

The values of J for the variable flow rate runs at the different baffle spacings are plotted as a function of R_{eff} in Fig. 15. The results fall within ±15 per cent of a straight line drawn through the points. The line has a slope of 0.72 on logarithmic co-ordinates.

The resulting equation for the cross-baffled units is:

$$h_0 = 1.03 \frac{L'}{L_c} \frac{k_0}{D_{Te}} (R_{eff})^{0.72} \left(\frac{C_{po}\mu_0}{100k_0} \right)^{1/3} (Z)^{0.37} \qquad (27)$$

Conclusions

1 The flow passage between the tube bundle and shell is very important when considering heat exchanger operating characteristics.

2 It is possible to increase the oil film coefficient by lowering the oil temperature or raising the cooling water temperature due to the effect on flow path resistances.

3 Variation of baffle spacing is not as important as variation of flow path clearances in the determination of shell side film coefficients under conditions of laminar flow.

4 Equations (8) and (17) can be used to calculate the pressure losses and Equations (21) and (27) give a fair correlation of the heat-transfer results. The extension of these relations to different tube geometries would depend upon obtaining satisfactory equations for the pressure losses in the particular flow passages.

5 Most of the experimental results presented in Figs. 3 through 10 are within ±5 per cent of the correct values as demonstrated by the lack of departure from the plotted lines and the reproducibility of the runs at particular points. In a few cases the error may be as high as 20 per cent for runs near the isothermal condition due to the effect of imposing a possible experimental error in temperature recording of 0.5 F on an oil temperature change of only 5 F.

An Analytical Study of Laminar Film Condensation: Part 1—Flat Plates

MICHAEL MING CHEN

Department of Mechanical Engineering, Massachusetts Institute of Technology, Cambridge, Mass.

The boundary-layer equations of momentum and energy are written in a modified integral form and solved for the case of laminar film condensation along a vertical flat plate. The analysis differs from previous works by employing the more realistic boundary condition of stationary vapor at large distances instead of zero velocity gradient at the interface. Solutions for both the liquid film and vapor boundary layer are given for the case $\mu_v\rho_v \ll \mu\rho$. Velocity and temperature profiles are obtained using perturbation method and the modified integral boundary-layer equations. The results show a significant negative velocity gradient at the interface as a result of vapor drag except for small values of $k\Delta t/\mu\lambda$. Theoretical heat-transfer coefficients are computed and found to be lower than previous theories, especially for low Prandtl numbers. Comparison with experimental heat-transfer data is given. The heat-transfer results are also presented in the form of an approximate formula for ease of application.

Introduction

Filmwise condensation along flat plates and round tubes was first formulated by Nusselt [1].[1] By equating the forces of gravity and viscosity, and assuming linear temperature profiles he obtained expressions which showed good qualitative agreement with experimental observations for normal engineering fluids. However, observed heat-transfer rates often varied between 80 to 170 per cent of Nusselt's predicted values for normal fluids [2], and some liquid-metal data [3] were as low as 10–20 per cent of theoretical values. These facts pointed to the need of a more exact analytical description of the process, so that theoretical expressions could be used more safely in computations. Bromley [4] considered the effect of heat capacity and obtained correction factors in terms of $c_p\Delta t/\lambda$. Rohsenow [5] solved the actual temperature profile and gave heat-transfer results applicable for large Prandtl numbers. Sparrow and Gregg [6, 7] used similarity transformations to solve the boundary-layer equations for the film; thus their analysis included the effect of momentum change hitherto neglected. The effect was shown to reduce the condensation heat-transfer rate of liquid metals, although insufficient to account for the extremely low experimental results. However, they assumed zero velocity gradient at the interface, thus neglecting the drag due to initially stationary vapor, an effect of the same order of magnitude as the acceleration terms inside the condensate film.

This paper presents a solution of the condensation problem, including the effect of the drag due to an initially stationary body of vapor. The method of solution is as follows: The momentum and energy equations are written in the integral form using boundary-layer assumptions. These are supplemented by an internal momentum balance for the solution of velocity profiles and an internal energy balance for the solution of temperature profiles. Perturbation methods are employed to solve these equations. The computed velocity profiles show a negative gradient at the interface, as expected, and the heat-transfer results for low Prandtl numbers are significantly lower than previous theories neglecting the vapor drag.

[1] Numbers in brackets designate References at end of paper.

Contributed by the Heat Transfer Division of The American Society of Mechanical Engineers and presented at the ASME-AIChE Heat Transfer Conference, Buffalo, N. Y., August 15–17, 1960. Manuscript received at ASME Headquarters, June 10, 1960. Paper No. 60—HT-37.

Boundary-Layer Equations

The physical model used here is shown in Fig. 1, where a cold vertical plate at uniform wall temperature t_w is placed inside a body of pure saturated vapor at a higher temperature t_i. The

Nomenclature

$A = \left.\dfrac{\partial u^+}{\partial y^+}\right]_{y^+=0}$ (dimensionless)

a = heat-transfer area

$B = \left.\dfrac{\partial r^+}{\partial y^+}\right]_{y^+=0}$ (dimensionless)

$C = \int_0^1 u^{+2}\,dy^+$ (dimensionless)

c = specific heat of constant pressure

$D = 1 - \int_0^1 u^+t^+dy^+$ (dimensionless)

$G = u_\infty y_i\left(\dfrac{g(\rho-\rho_v)k^3\Delta t^3 l^3}{\mu\rho^3\lambda^3}\right)^{-1/4}$ (dimensionless)

g = gravitational constant

h = heat-transfer coefficient

K_{ij} = see equations (19) and (20)

k = thermal conductivity

l = total length of flat plate

$\mathfrak{N}_l = \left(\dfrac{g\rho(\rho-\rho_v)l^3\lambda}{\mu k\Delta t}\right)^{1/4}$ (dimensionless)

$\mathrm{Nu}_l = h_m l/k$ (dimensionless)

$\mathrm{Pr} = c\mu/k$ (dimensionless)

q = heat-transfer rate

t = temperature

$t^+ = (t-t_w)/\Delta t = (t-t_w)/(t_i-t_w)$ (dimensionless)

$\Delta t = t_i - t_w$ (dimensionless)

u = velocity of liquid in x-direction

$u_\infty = \dfrac{1}{y_i}\int_0^{y_i} u\,dy$

u_v = velocity of vapor in x-direction

$u^+ = u/u_\infty$ (dimensionless)

x = co-ordinates measuring distance from leading edge along cooled wall

$Y = y_i\left(\dfrac{g\rho(\rho-\rho_v)\lambda}{k\,\Delta t l\mu}\right)^{1/4}$ (dimensionless)

(Continued on next page)

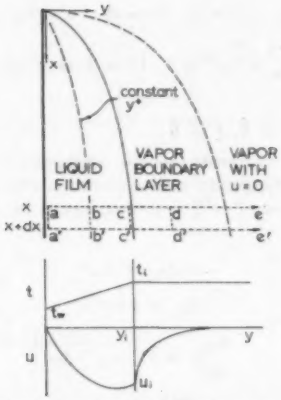

Fig. 1 Physical model used in condensation analysis

condensate film formed on the surface is accelerated downward by gravity and retarded by the wall shear stress. The vapor is assumed to have no initial velocity in the x-direction. As it moves toward the wall, it is gradually accelerated by the falling condensate film through shear stresses. This acceleration constitutes an additional drag on the condensate film, as can be seen from the shape of the velocity profiles in Fig. 1. All properties of both the liquid and the vapor will be considered constant.

Boundary assumptions apply near the leading edge. The integral momentum equation can be derived by considering the momentum balance for the control volume $aa'c'c$:

$$\mu \frac{\partial u}{\partial y}\bigg]_{y=0} + \frac{d}{dx}\int_0^{y_i} \rho u^2 dy - u_i \frac{d}{dx}\int_0^{y_i} \rho u\, dy - \mu \frac{\partial u}{\partial y}\bigg]_{y_i} = y_i g(\rho - \rho_v) \quad (1)$$

where the first term represents the contribution of wall shear stress, the second term the net momentum increase in the film, the third term is the momentum of the entering vapor, and the fourth term is the interface shear stress. The force of gravity is shown at the right-hand side.

Neglecting shear work, the energy equation is

$$k \frac{\partial t}{\partial y}\bigg]_{y=0} + k \frac{\partial t}{\partial y}\bigg]_{y_i} = c \frac{d}{dx}\int_0^{y_i} \rho(t - t_i) u\, dy \quad (2)$$

The coupling of the two equations is provided by the energy balance at the liquid-vapor interface:

$$k \frac{\partial t}{\partial y} = \lambda \frac{d}{dx}\int_0^{y_i} \rho u\, dy \quad \text{at} \quad y = y_i \quad (3)$$

These equations govern the growth of the film layer, but yield no information on the velocity and temperature profiles. To obtain equations for the profiles, one can split the condensate film into two sublayers along $y = y^+ y_i$, $0 \le y^+ \le 1$, and write the momentum and energy equations for either of the two sublayers. Those for the outer sublayer are found by considering the control volume $bb'c'c$:

$$\mu \frac{\partial u}{\partial y}\bigg]_{y^+ y_i} + u_{y^+ y_i} \frac{d}{dx}\int_0^{y^+ y_i} \rho u\, dy + \frac{d}{dx}\int_{y^+ y_i}^{1} \rho u^2 dy - \frac{u_i d}{dx}\int_0^{y_i} u\, dy - \mu \frac{\partial u}{\partial y}\bigg]_{y_i} = (y_i - y^+ y_i)(\rho - \rho_v) g \quad (4)$$

$$-k \frac{\partial t}{\partial y_{y^+ y}} + k \frac{\partial t}{\partial y}\bigg]_{y_i} = c t_{y^+ y_i} \frac{d}{dx}\int_0^{y^+ y_i} \rho u\, dy - c t_i \frac{d}{dx}\int_0^{y_i} \rho u\, dy + \frac{d}{dx}\int_{y^+ y_i}^{y_i} \rho u\, c\, t\, dy \quad (5)$$

Note that equations (1) and (2) are special cases of equations (4) and (5), which must be satisfied by the velocity and temperature profiles for any positive value of y^+ less than unity. In addition, the following conditions must be satisfied by u, y_i, and t:

$$\left.\begin{aligned} u &= 0 \\ y_i &= 0 \end{aligned}\right\} \quad \text{at} \quad x = 0 \quad (6)$$

$$\left.\begin{aligned} u &= 0 \\ t &= t_w = \text{const} \end{aligned}\right\} \quad \text{at} \quad y = 0 \quad (7)$$

$$t = t_i = \text{const at } y = y_i \quad (8)$$

The condition for the velocity profile at the interface must come from the solution of the vapor boundary layer. An order-of-magnitude estimation of the latter indicates that the shear stress at the interface is approximately equal to the momentum of the entering vapor; i.e.,

$$\left| u_i \frac{d}{dx}\int_0^{y_i} \rho u\, dy + \frac{\partial u}{\partial y}\bigg]_{y_i} \right| \approx \frac{\rho_v \mu_v}{\rho \mu} \left| \frac{\partial u}{\partial y}\bigg]_{y=0} \right| \quad (9)$$

A proof of equation (9) and a solution of the vapor boundary layer are given in the Appendix. The ratio $\mu_v \rho_v / \mu \rho$ are of the order of $10^{-3} - 10^{-5}$ for most practical problems (water: 10^{-4}; mercury: 10^{-5}, at normal pressures); therefore the sum of the two interface terms are insignificant compared to the wall shear-stress term, and can be neglected from the momentum equations without resulting in serious error. This simplification corresponds to the case $\mu_v \rho_v / \mu \rho = 0$, and will be adopted in this research. The re-

Nomenclature

y = co-ordinate measuring distance normal to plate
y_i = liquid-film thickness
y^+ = y/y_i (dimensionless)
μ = viscosity
ρ = density
ρ_v = density of vapor
λ = latent heat of vaporization
ζ = $c\,\Delta t/\lambda$, heat-capacity parameter (dimensionless)
ξ = $k\Delta t/\mu\lambda$, acceleration effect parameter (dimensionless)

Subscripts

00 = pertaining to the case $\zeta = \xi = 0$; i.e., neglecting heat capacity and acceleration effects
0 = pertaining to the case $\zeta = 0$
1 = see equation (25)
a = pertaining to the average value over $0 \le y^+ \le 1$
i = pertaining to liquid side of liquid-vapor interface
ij = index denoting order of perturbation; see equations (18) through (21)
m = pertaining to over-all mean value for whole plate $0 \le X \le 1$
v = pertaining to vapor
w = pertaining to wall
$y^+ y_i$ = pertaining to dividing line of two sublayers, Fig. 1

Superscript

$+$ = pertaining to dimensionless velocity and temperature profiles, see u^+, t^+, y^+

sults are expected to be applicable to actual fluids with an error of the order of $\mu_v\rho_v/\mu\rho$, which is small indeed.

It should be pointed out here that either of the two terms at the left-hand side of equation (9), taken individually, is of the order of the condensate acceleration terms and should not be neglected individually when the latter is considered. In fact, it can be shown that the error caused by neglecting either of the two is of the order of $k\Delta t/\mu\lambda$ which can be quite large for fluids of low Prandtl numbers. When both terms are neglected together, the individual effects still exist, although they are considered to cancel each other.

Equations in Dimensionless Form

The solution of the integral boundary-layer equations usually involves assuming appropriate velocity and temperature profiles in dimensionless form. Since we intend to use the actually solved profiles, which are not yet known at the moment, we shall tentatively denote the dimensionless properties of the profiles by the letters A, B, C, D, as given in the Nomenclature, so that the equations can be put in a more convenient form. For example,

$$D = 1 - \int_0^1 u^+t^+dy^+$$

therefore denoting a "temperature defect" of the condensate film.

With these, as well as the dimensionless variables X, Y, G as given in the Nomenclature, and utilizing the simplification afforded by equation (9), one can combine equations (1), (2), and (3) into the following two equations:

$$(A + \xi[2CYG' - CGY' + YGC'])G = Y^3 \tag{10a}$$

$$B = YG' + \zeta(DYG' + YGD') \tag{10b}$$

The symbol $'$ is used to denote differentiation with respect to X, the dimensionless x-co-ordinate. Physically, G can be considered to represent the condensate flow rate and Y the condensate film thickness. Both are to be solved in terms of X.

Note that the terms representing heat capacity and acceleration effects now contain either ζ or ξ. These are therefore readily identified as heat-capacity and acceleration parameters, respectively.

One can combine equations (1) and (4) to eliminate the gravity term. The result in dimensionless form is

$$\frac{\partial u^+}{\partial y^+} + \xi\left\{u^+GY\frac{d}{dX}\int_0^{y^+}u^+dy^+ + GY\frac{d}{dX}\int_{y^+}^1 u^{+2}dy^+ + \left(u^+\int_0^{y^+}u^+dy^+\right)YG' + \left(\int_{y^+}^1 u^{+2}dy\right)2YG' - \left(\int_{y^+}^1 u^{+2}dy^+\right)GY'\right\} = (1-y^+)(A + \xi YGC' + 2\xi CYG' - \xi CGY') \tag{11a}$$

Similarly, the interface conduction term is eliminated between equations (2) and (5):

$$\frac{\partial t^+}{\partial y^+} = (B - \zeta YGD' - \zeta DYG')\left\{1 + \zeta\left[1 - t^+\int_0^{y^+}u^+dy^+ - \int_{y^+}^1 u^+t^+dy^+\right]\right\} - \zeta\left\{GYT^+\frac{d}{dX}\int_0^{y^+}u^+dy^+ + GY\frac{d}{dX}\int_{y^+}^1 u^+t^+dy^+\right\} \tag{11b}$$

Equations (11a) and (11b) will be used to solved for u^+ and t^+, the dimensionless velocity and temperature profiles.

G, Y, u^+, t^+, must also satisfy the following conditions:

$$G = 0, \quad Y = 0 \text{ at } X = 0 \tag{12}$$

$$\left.\begin{aligned} u^+ = 0, \quad t^+ = 0 \text{ at } y = 0 \\ \int_0^1 u^+dy^+ = 1; \ t^+ = 1 \text{ at } y^+ = 1 \end{aligned}\right\} \tag{13}$$

Solutions for $\zeta = 0$, $\xi = 0$

$\zeta = 0$, $\xi = 0$ represents the case considered by Nusselt [1] ignoring both heat-capacity and acceleration effects. If subscript 00 is used to denote $\zeta = \xi = 0$, then equations (10) and (11) reduce to

$$A_{00}G_{00} = Y_{00}^3 \tag{14a}$$

$$B_{00} = Y_{00}G'_{00} \tag{14b}$$

$$\left.\begin{aligned} \frac{\partial u_{00}{}^+}{\partial y^+} = (1 - y^+)A_{00} \\ \frac{\partial t^+{}_{00}}{\partial y^+} = B_{00} \end{aligned}\right\} \tag{15}$$

Equations (12) and (13) are applicable as boundary conditions. From equation (15) we obtain

$$\left.\begin{aligned} u_{00}{}^+ = 3\left(y^+ - \frac{1}{2}y^{+2}\right); \ A_{00} = 3 \\ t_{00}{}^+ = y_{00}{}^+; \ B_{00} = 1 \end{aligned}\right\} \tag{16}$$

The profiles are exactly those used by Nusselt. Since they are independent of X, equations (14a) and (14b) can be combined to give a first-order equation with one single unknown. With $G_{00}(0) = 0$, the solution is

$$\left.\begin{aligned} G_{00} = \frac{1}{3}4^{3/4}X^{3/4} \\ Y_{00} = (4X)^{1/4} \end{aligned}\right\} \tag{17}$$

Perturbation Procedure

For $\zeta \neq 0$, $\xi \neq 0$, a perturbation procedure is used to solve equations (10) and (11). All unknown quantities are expressed in double power series in terms of ζ and ξ:

$$\begin{aligned} G(X) &= G_{00}(X) + \zeta G_{10}(X) + \xi G_{01}(X) + \zeta^2 G_{20}(X) \\ &\quad + \xi^2 G_{02}(X) + \zeta\xi G_{11}(X) + \dots \\ Y(X) &= Y_{00}(X) + \dots \\ u^+(X, y^+) &= u_{00}{}^+(X, y^+) + \dots \\ A(X) &= A_{00}(X) + \dots \end{aligned} \tag{18}$$

Upon substitution into equations (10) and (11), all terms with equal powers of ζ and ξ are combined to form a set of new equations. In particular, those not containing either ζ or ξ (i.e., those containing $\zeta^0\xi^0$) combine to form equations (14) and (15), permitting solutions of G_{00}, Y_{00}, $u_{00}{}^+$, and $t_{00}{}^+$, given in equations (16) and (17).

In general, equations obtained from the coefficients of higher powers of ζ and ξ will all be in this form:

$$\begin{aligned} K_{ij}^{(1)}A_{ij} + K_{ij}^{(2)}G_{ij} &= K_{ij}^{(3)}Y_{ij} + K_{ij}^{(4)} \\ B_{ij} &= K_{ij}^{(5)}G_{ij} - K_{ij}^{(6)}Y_{ij} + K_{ij}^{(7)} \end{aligned} \tag{19}$$

$$\begin{aligned} \frac{\partial u_{ij}{}^+}{\partial y^+} &= (1 - y^+)A_{ij} + K_{ij}^{(8)} \\ \frac{\partial t_{ij}{}^+}{\partial y^+} &= B_{ij} + K_{ij}^{(9)} \end{aligned} \tag{20}$$

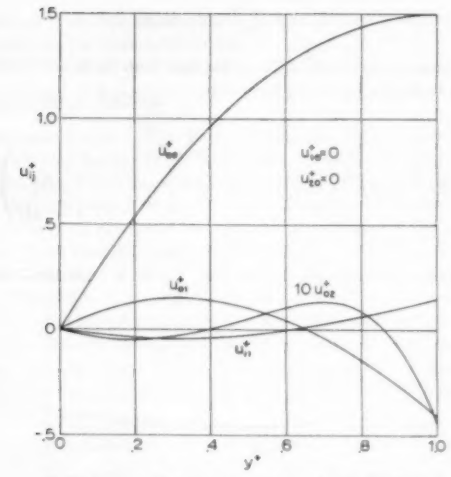

Fig. 2 Some of the perturbation velocity profiles

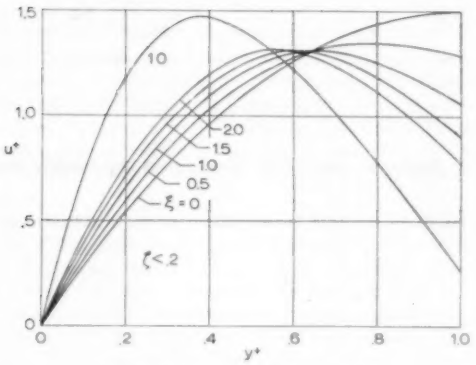

Fig. 3 Velocity profiles for $\zeta < 0.2$

$K_{ij}^{(1)} \ldots K_{ij}^{(9)}$ are functions containing only unknowns of order less than ij; i.e., containing only quantities with index mn, where $m + n < i + j$.

The boundary conditions, equations (12) and (13), give rise to

$$\left.\begin{aligned} &G_{ij} = Y_{ij} = 0 \quad \text{at} \quad X = 0 \\ &u_{ij}^+ = t_{ij}^+ = 0 \quad \text{at} \quad y^+ = 0 \\ &\int_0^1 u_{ij}^+ dy^+ = 0;\ t_{ij}^+ = 0 \quad \text{at} \quad y^+ = 1 \end{aligned}\right\} \quad \text{for} \quad i + j \neq 0 \qquad (21)$$

Equations (19) and (20) are all linear and are easily soluble, provided the coefficients $K_{ij}^{(1)} \ldots K_{ij}^{(9)}$ are known. Indeed they are known functions if one proceeds from the lowest order upward, solving all equations with $i + j = n$ before advancing to $i + j = n + 1$. For example, $K_{10}^{(1)} \ldots K_{10}^{(9)}$ contain only G_{00}, Y_{00}, $u_{00}^+ \ldots$ etc., already given in equations (16) and (17). With these, u_{10}^+, t_{10}^+, A_{10}, and B_{10} can be easily solved from equation (20). The two equations of (19) can then be combined to obtain G_{10} and Y_{10}. A similar method can be used to solve for G_{01}, Y_{01}, u_{01}^+, and t_{01}^+. Armed with these, one can proceed to solve for all sets of equations with $i + j = 2$.

The procedure converges rapidly for moderate values of ζ and ξ. As an illustration of the method, some of the perturbation velocity profiles, u_{ij}^+, are shown in Fig. 2. Using equation (18), the actual velocity profiles are computed and shown in Fig. 3 as a function of ξ. Since the deviation of the velocity profile from a parabola is caused by acceleration terms in the equations of motion, it can be anticipated that all $u_{10}^+ = 0$ for any $i > 0$. Therefore the profiles are only slightly dependent on ζ.

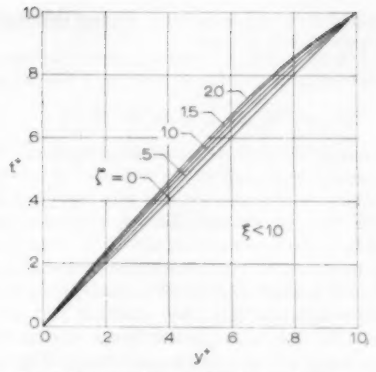

Fig. 4 Temperature profiles for $\xi < 1.0$

In a similar manner, the temperature profile is computed and plotted in Fig. 4 as a function of ζ. Since $t_{0j}^+ = 0$ for $i > 0$, the profiles are not greatly dependent on ξ.

Similarity

While the perturbation procedure outlined in the foregoing is only practical for moderate values of ζ and ξ, it can be used as an induction procedure to establish some conclusions which are generally true, even for large values of ζ and ξ. Among these, the most important ones are

$$G_{ij} \propto (\ ) \propto X^{3/4} \qquad (22a)$$

$$Y_{ij} \propto Y_{00} \propto X^{1/4} \qquad (22b)$$

$$\frac{\partial u_{ij}^+}{\partial X} = 0;\ C' = 0 \qquad (22c)$$

$$\frac{\partial t_{ij}^+}{\partial X} = 0;\ D' = 0 \qquad (22d)$$

An outline of the induction proof for these results is included in the Appendix.

Thus we have established that similar velocity and temperature profiles exist for the condensate film. Equations (10a) and (10b) can now be combined to give an ordinary differential equation:

$$\left(A + {}^5/_3 \frac{CB\xi}{(1 + D\zeta)}\right) GG'^3 = \frac{B^3}{(1 + D\zeta)^3} \qquad (23)$$

which has a solution in close form for $G(0) = 0$

$$G = ({}^4/_3)^{3/4} \left(\frac{B}{1 + D\zeta}\right)^{3/4} \left(A + \frac{5CB\xi}{3(1 + D\zeta)}\right)^{-1/4} X^{3/4} \qquad (24)$$

Solutions for $\zeta \ll 1$, $\xi \gg 1$

The perturbation procedure just outlined yielded accurate heat-transfer results for $\zeta \leq 2$, $\xi \leq 5$ with a series computed to order $i + j = 2$. For larger values of ζ and ξ the procedure converges very slowly. With liquid metals, it is possible to reach a value of 10 for ξ when $\zeta \ll 1$. A solution with these conditions can best be obtained with the following numerical procedure:

For $\zeta \ll 1$, it is possible to write

$$\begin{aligned} u^+(y^+, \zeta, \xi) &= u_0^+(y^+, \xi) + \zeta u_1^+(y^+, \xi) \\ t^+(y^+, \zeta, \xi) &= t_0^+(y^+, \xi) + \zeta t_1^+(y^+, \xi) \end{aligned} \qquad (25)$$

Comparison with equations (18) and the fact that $u_{i0}^+ = t_{i_i}^+ = 0$ for $i > 0$ immediately shows:

$$u_i^+(y^+, \xi) = 0$$
$$t_0^+(y^+, \xi) = t_{00}^+(y) = y^+ \tag{26}$$

u_0^+ for any given ξ can be solved from equation (11*a*) with an iteration procedure similar to the one used in reference [5]. A reasonable trial u_0^+ is assumed and substituted in the integrals of equation (11*a*) from which $\partial u_0^+/\partial y^+$ is computed and then integrated to give a new function u_0^+. The integration can best be done numerically, and with intelligent choices of trial functions yields accurate profiles quickly. The profile for $\xi = 10$ is shown in Fig 3 for comparison with lower values of ξ.

Using u_0^+, t_i^+ can be computed from equation (11*b*) directly without resorting to trial-and-error solutions. The general shape of t^+, from equation (25), is basically similar to those for $\xi = 0$, which is shown in Fig. 4.

Heat-Transfer Results

The heat-transfer rate into the wall is conveniently expressed in terms of h

$$h = \frac{1}{\Delta t}\frac{q}{a} = \frac{k}{\Delta t}\frac{\partial t}{\partial y}\bigg]_{y=0} = B\frac{k}{y_i} \tag{27}$$

From equation (10*b*) and the definition of G and Y we have

$$\frac{hl}{k} = \frac{B}{Y}\mathfrak{N}_l = (1 + D\zeta)G'\mathfrak{N}_l \tag{28}$$

Therefore the average Nusselt number between $x = 0$ and $x = 1$ is given by the expression

$$\mathrm{Nu}_l = \frac{h_m l}{k} = (1 + D\zeta)G\mathfrak{N}_l = (^4/_3 B)^{3/4}\left(\frac{1 + D\zeta}{A + {}^5/_3\dfrac{CB\xi}{1 + D\zeta}}\right)^{1/4} \tag{29}$$

For $\zeta = 0$ and $\xi = 0$, equation (29) reduces to the simple result of Nusselt:

$$\mathrm{Nu}_{l,\infty} = {}^1/_3\, 4^{3/4}\mathfrak{N}_l = 0.943\mathfrak{N}_l \tag{30}$$

In order to evaluate the effects of acceleration and heat capacity, it is convenient to examine the ratio of the actual Nusselt number versus the Nusselt number computed from the simple theory given by equation (30)

$$\frac{\mathrm{Nu}_l}{\mathrm{Nu}_{l,\infty}} = \frac{h_m}{h_{m,\infty}} = \left(\frac{B}{B_\infty}\right)^{3/4}\left(\frac{A_\infty}{A}\right)^{1/4}\left(\frac{1 + D\zeta}{1 + {}^5/_3\dfrac{CB}{A}\dfrac{\xi}{1 + D\zeta}}\right)^{1/4} \tag{31}$$

where the values of A, B, C, D are to be computed from the actual velocity and temperature profiles which have been solved already. Equation (31) is plotted in Figs. 5 and 6. Fig. 5 shows $\mathrm{Nu}_l/\mathrm{Nu}_{l,\infty}$ versus ζ, the heat-capacity parameter. In practice, large values of ζ are only reached for fluids of large Prandtl numbers, for which cases the effect of ξ is seen to increase the heat-transfer rate to a value somewhat higher than that predicted by Nusselt's theory.

The effects of ξ, the momentum parameter, is best indicated in Fig. 6. It is seen that the inclusion of the momentum term greatly reduces the heat-transfer rate for liquid metals. A comparison of these results with other investigations will be given in a later section.

Another quantity which is of interest to designers of condensing equipment is the condensation rate:

$$\Gamma = \rho\int_0^{y_i} u\,dy = \rho u_a y_i \tag{32}$$

A dimensionless condensation rate can then be defined and computed from the following equation:

$$\frac{\dfrac{\Gamma\lambda}{k\Delta t}}{0.943\mathfrak{N}_l} = \frac{\Gamma}{\Gamma_\infty} = \left[\frac{B}{B_\infty(1 + D\zeta)}\right]^{3/4}\left(\frac{A}{A + {}^5/_3\dfrac{CB\xi}{1 + D\zeta}}\right)^{1/4} \tag{33}$$

This relationship is plotted in Fig. 7. It is seen that the con-

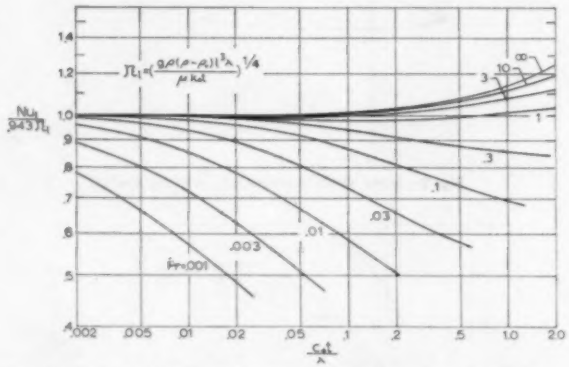

Fig. 5 Theoretical heat-transfer results versus heat-capacity parameter

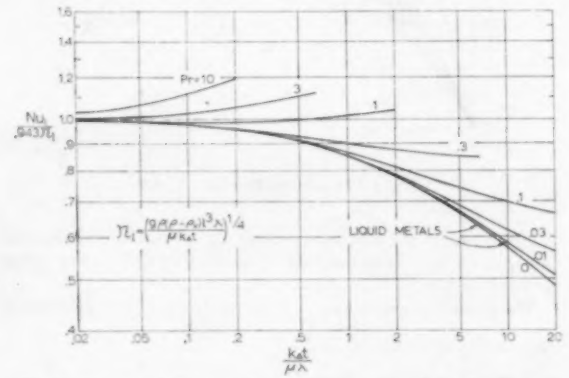

Fig. 6 Theoretical heat-transfer results versus acceleration parameter

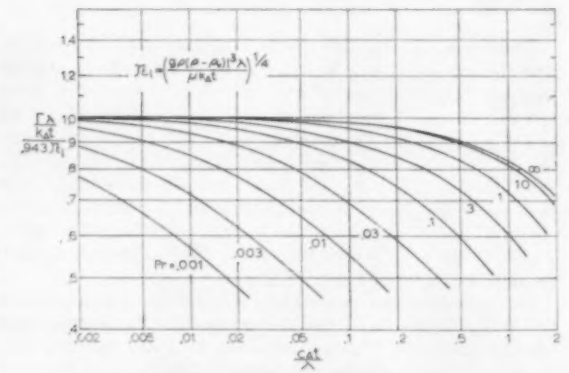

Fig. 7 Theoretical condensation rates

densation rate is actually reduced by heat-capacity effects, in contrast to the heat-transfer rate.

Discussion of Results

Common Liquids. The Prandtl numbers for steam and other common engineering fluids lie between 1 and 10, and ζ generally is less than 1. For these conditions Figs. 5 and 6 predict higher heat-transfer rate than Nusselt's theory, although the improvement is not as large as predicted by Sparrow and Gregg [6, 7], especially at the lower Prandtl numbers. For example, at Pr = 1, Fig. 6 predicts an increase of only 1 per cent for $\zeta = 1$, while references [6 and 7] predict an increase of 10 per cent. The difference is obviously due to vapor drag, which was neglected in references [6 and 7]. For Pr > 10, the present theory is in good agreement with both references [6 and 7] and the theory of Rohsenow [5], indicating that zero shear stress can be neglected for large Prandtl numbers.

A number of experimental investigations have been reported in the literature. Some of these were summarized by McAdams [2]. The observed heat-transfer rate varied from 70 to 107 per cent of Nusselt's theory. The scatter of the data is in general too large for a successful correlation of the present theory, which shows an improvement of less than 15 per cent over Nusselt's result.

Part of the cause of the experimental scatter is probably due to the existence of vapor velocity, although many investigators have eliminated it by introducing the vapor from a perpendicular direction. Some investigators may also have used the condensate flow rate as a measure of heat transfer without a correction for the heat-capacity effect, which may cause an error as high as 20 per cent.

Liquid Metals. The heat-transfer results for Pr $\leq$ 0.03 are plotted in Fig. 8, together with the theory of Sparrow and Gregg [6, 7] who neglected vapor drag. It is seen that the present theory predicts much lower heat-transfer results, indicating the importance of the vapor drag for low Prandtl numbers. Misra and Bonilla [3] reported experimental results for mercury and sodium with values of ξ as large as 9. These data are shown in Fig. 8 to be even lower than the present theory.

The low observed heat-transfer rate may have been caused by an upward vapor velocity, since in Misra's experiments the vapor was introduced from below. It was reported that at certain conditions the vapor velocity was so large that the condensate film was blown off completely. There was also evidence of droplets traveling upward. It seems that the need still exists for more experimental results to test the soundness of the theoretical model.

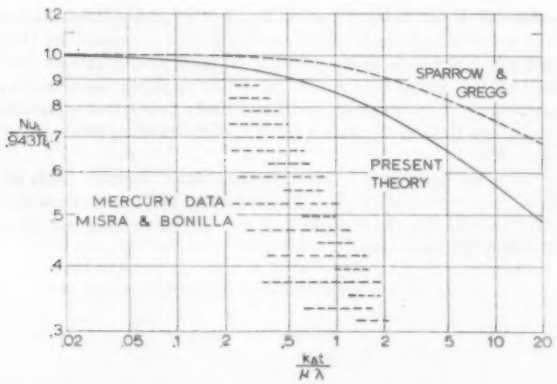

Fig. 8 Comparison with data and other theories for liquid metals

Approximate Formulas

The theoretical results presented in Figs. 5, 6, and 7 can be approximated within 1 per cent by the following relations

$$\frac{h_m}{h_{m,\infty}} = \left(\frac{1 + 0.68\zeta + 0.02\zeta\xi}{1 + 0.85\xi - 0.15\zeta\xi}\right)^{1/4} \tag{34}$$

$$\frac{\Gamma}{\Gamma_\infty} = \frac{h_m}{h_{m,\infty}} \frac{1}{(1 + 0.375\zeta + 0.020\zeta\xi - 0.0005\zeta\xi^2)} \tag{35}$$

Where $h_{m,\infty}$ and Γ_∞ represent the values for $\zeta = 0$, $\xi = 0$, respectively. Both can be computed from Nusselt's simple theory or equations (30) and (33). The ranges of applicability for equations (34) and (35) are $\zeta \leq 2$, $\xi \leq 20$, for liquids with Pr larger than 1 or less than 0.05.

Conclusions

The condition that the x-component of the velocity vanishes outside the boundary layer is met in carefully conducted experimental investigations, for which the vapor is often introduced horizontally to eliminate vertical motion. It is also satisfied approximately in condensing apparatuses when the vapor pressure is high. For these cases, the profiles obtained in this paper showed that it is not realistic to assume a vanishing velocity gradient at the interface when inertia effects are significant, as was done in previous works on the subject. Considering interface shear stress, the present analysis predicted reduced heat-transfer coefficients, particularly for fluids with low Prandtl numbers. The theoretical results, presented graphically and in the form of approximate formulas, should be convenient for use by engineers.

While effects such as vapor velocity and the presence of noncondensable gases may play important roles in the condensation process, the simple model chosen here seemed to be the only physically realistic one which yields to a boundary-layer analysis with similar profiles. It is hoped that the solution presented here may provide a clearer understanding of the process so that some of the other effects can be better defined, both experimentally and analytically.

References

1 W. Nusselt, "Die Oberflachen Kondensation des Wasserdamfes," *Zeitschrift des Vereines Deutscher Ingenieure*, vol. 60, 1916, pp. 541–569.

2 W. H. McAdams, "Heat Transmission," third edition, McGraw-Hill Book Company, Inc., New York, N. Y., 1954.

3 B. Misra and C. F. Bonilla, "Heat Transfer in the Condensation of Metal Vapors," *Chemical Engineering Progress*, Symposium Series No. 18, vol. 52, 1956, pp. 7–21.

4 L. A. Bromley, "Effect of Heat Capacity of Condensate," *Industrial and Engineering Chemistry*, vol. 44, 1952, p. 2966.

5 W. M. Rohsenow, "Heat Transfer and Temperature Distribution in Laminar Film Condensation," TRANS. ASME, vol. 78, 1956, pp. 1645–1648.

6 E. M. Sparrow and J. L. Gregg, "A Boundary-Layer Treatment of Laminar Film Condensation," JOURNAL OF HEAT TRANSFER, TRANS. ASME, Series C, vol. 81, 1959, pp. 13–18.

7 E. M. Sparrow and J. L. Gregg, "Laminar Condensation Heat Transfer on a Horizontal Cylinder," JOURNAL OF HEAT TRANSFER, TRANS. ASME, Series C, vol. 81, 1959, pp. 291–296.

APPENDIX 1

Velocity Profile for Vapor

For the vapor boundary layer, $y^+ > 1$. Referring to Fig. 1, the force balance for the element $dd'e'e$, is

$$\mu_v \frac{\partial u_v}{\partial y} + u_v \left[\frac{d}{dx} \int_0^{y_i} u \, dy + \rho_v \frac{d}{dx} \int_{y_i}^{y^+ y_i} u_v dy \right] + \frac{d}{dx} \int_{y^+ y_i}^{\infty} \rho_v u_v^2 dy = 0 \quad (36)$$

In dimensionless variables, equation (36) becomes

$$\frac{\mu_v}{\mu} \frac{\partial u_y{}^+}{\partial y^+} + \xi \left\{ u_v{}^+ YG' \left(1 + \frac{\rho_v}{\rho} \int_1^{y^+} u_v{}^+ dy \right) + \frac{\rho_v}{\rho} (2YG' - GY') \int_{y^+}^{\infty} u_v{}^{+2} dy^+ = 0 \quad (37)$$

The boundary condition is

$$u_v{}^+ = u_i{}^+ \quad (38)$$

Since $\rho_v \ll \rho$, no serious error will result if all terms containing ρ_v/ρ are neglected:

$$\frac{\mu_v}{\mu} \frac{\partial u_v{}^+}{\partial y^+} = -\xi YG' \, u_v{}^+ \quad (39)$$

Equation (22*c*) shows that YG' is a constant; therefore equation (39) has the following solution:

$$u_v{}^+ = u_i{}^+ e^{(1-y^+)\xi YG'(\mu/\mu_v)} \quad (40)$$

This is only an approximate solution. In order to solve the complete equation (37) without neglecting ρ_v/ρ, a perturbation procedure similar to the one used in the main body of this paper can be employed with ρ_v/ρ as the perturbation parameter. The result is expected to differ only slightly from equation (40), due to the low values of ρ_v/ρ usually encountered.

We will now use equation (40) to estimate the magnitude of the two interface terms. Consider the control volume *cc'e'e* for force balance:

$$\mu \left. \frac{\partial u}{\partial y} \right]_{y_i} + u_i \rho \frac{d}{dx} \int_1^{y_i} u \, dy_v = -\rho_v \frac{d}{dx} \int_{y_i}^{\infty} u_v{}^2 dy \quad (41)$$

In dimensionless parameters, this is

$$\left. \frac{\partial u^+}{\partial y^+} \right]_1 + \xi u^+ YG = -\xi \frac{\rho_v}{\rho} (2G'Y - GY') \int_1^{\infty} u_v{}^{+2} dy^+ \quad (42)$$

Using the result of equation (40), we have

$$\left. \frac{\partial u^+}{\partial y^+} \right]_1 + \xi u^+ YG' = -u_i{}^{+2} \frac{2G'Y - GY'}{2G'Y} \frac{\mu_v \rho_v}{\mu \rho} \quad (43)$$

Therefore

$$\frac{\mu \left. \frac{\partial u}{\partial y} \right]_{y_i} + u_i \rho \frac{d}{dx} \int_0^{y_i} u \, dy^-}{\left. \frac{\partial u}{\partial y} \right]_0} = \frac{\left. \frac{\partial u^+}{\partial y^+} \right]_1 + u^+ YG'}{A} = -\frac{u_i{}^{+2}}{A} \frac{2GY' - G'Y}{2G'Y} \frac{\mu_v \rho_v}{\mu \rho} \approx -\frac{\mu_v \rho_v}{\mu \rho}; \frac{\mu_v \rho_v}{\mu \rho} \ll 1. \quad (44)$$

The ratio $\mu_v \rho_v / \mu_\rho$ only depends on the physical properties of the fluids. μ_v/μ is the order of 10^{-1} to 10^{-2}, whereas ρ_v/ρ is of the order of 10^{-2} for large hydrocarbon molecules, and 10^{-3} for water and liquid metals. Thus the effect of the two interface terms taken together can clearly be neglected from the momentum equation without causing significant error.

It should be pointed out that if warranted, the effect of these terms can easily be considered by a perturbation procedure as used in this paper. The first perturbation would undoubtedly lead to a correction factor of the form $[1 + K(\mu_v \rho_v / \mu \rho)] - 1/4$ where K is a constant of the order of unity.

It is not difficult to see from the dimensionless form of equation (44) that the ratio

$$\left. \frac{\partial u}{\partial y} \right]_{y_i} \Big/ \left. \frac{\partial u}{\partial y} \right]_0$$

is of the order

$$\xi \text{ or } \frac{k\Delta t}{\mu \lambda}$$

the momentum parameter. For Misra's [3] experiments, this quantity reached a value of the order 10.

APPENDIX 2

Outline of Induction Proof of Equation (22)

In order to prove that a statement is generally true by the induction method, one must show that (*a*) it is true for case No. 1; (*b*) if it is true for case No. n, it must also be true for case No. $n + 1$.

That equation (22) is true for $ij = 00$ is clear from equations (16) and (17).

We will next assume that equation (22) is true for all $i \leq m$, $j \leq n$. Using these relationships, equations (19) and (20) can be shown to be in the following form, for the order m, $n + 1$:

$$K_{m(n+1)}{}^{(a)} X^{3/4} A_{m(n+1)} + K_{m(n+1)}{}^{(b)} G_{m(n+1)} = K_{m(n+1)}{}^{(c)} X^{1/2} Y_{m(n+1)} + K_{m(n+1)}{}^{(d)} X^{3/2} \quad (45a)$$

$$B_{m(n+1)} = K_{m(n+1)}{}^{(e)} X^{-3/4} G_{m(n+1)}{}^{3/4} + K_{m(n+1)}{}^{(f)} X^{-1/4} Y_{m(n+1)} + K_{m(n+1)}{}^{(g)} \quad (45b)$$

$$\frac{\partial u_{m(n+1)}}{\partial y^+} + = (1 - y^+) A_{m(n+1)} + K_{m(n+1)}{}^{(h)} \quad (45c)$$

$$\frac{\partial t_{m(n+1)}{}^+}{\partial y^+} = B_{m(n+1)} + K_{m(n+1)}{}^{(i)} \quad (45d)$$

where all K are independent of X. It is not difficult to see that the velocity and temperature profiles solved for equations (45*c*) and (45*d*) would be independent of X, satisfying equations (22*b*) and (22*c*). Using constant A and B and applying the boundary conditions of equation (21), one can easily prove that equations (22*a*) and (22*b*) are satisfied by the solutions of equations (45*a*) and (45*b*).

Thus we have shown that equations (22*a*) through (22*d*) are true for the order m, $n + 1$. In similar manner, we can show that they are valid for the order $m + 1$, n. Therefore equations (22*a*) through (22*c*) are valid.

An Analytical Study of Laminar Film Condensation: Part 2—Single and Multiple Horizontal Tubes

MICHAEL MING CHEN
Department of Mechanical Engineering, Massachusetts Institute of Technology, Cambridge, Mass.

The boundary-layer equations for laminar film condensation are solved for (a) a single horizontal tube, and (b) a vertical bank of horizontal tubes. For the single-tube case, the inertia effects are included and the vapor is assumed to be stationary outside the vapor boundary layer. Velocity and temperature profiles are obtained for the case $\mu_v\rho_v/\mu\rho \ll 1$ *and similarity is found to exist exactly near the top stagnation point, and approximately for the most part of the tube. Heat-transfer results computed with these similar profiles are presented and discussed. For the multiple-tube case, the analysis includes the effect of condensation between tubes, which is shown to be partly responsible for the high observed heat-transfer rate for vertical tube banks. The inertia effects are neglected due to the insufficiency of boundary-layer theory in this case. Heat-transfer coefficients are presented and compared with experiments. The theoretical results for both cases are also presented in approximate formulas for ease of application.*

Introduction

In this paper the treatment used in Part 1 [1][1] for flat plates will be extended to the cases of single horizontal tubes and vertical banks of horizontal tubes. Both cases were first treated by Nusselt [2], who neglected heat-capacity and inertia effects. Sparrow and Gregg [3] presented a boundary-layer analysis for the single-tube case, using the similarity transformation proposed by Hermann [4], and assuming vanishing velocity gradient at the liquid-vapor interface. That such a boundary condition was not realistic has already been discussed [1]. The analysis presented here will employ the condition that vapor velocity will be negligible outside the boundary layer, and the condition that $\mu_v\rho_v \ll \mu\rho$. The reader is referred to [1] for detailed discussions of these assumptions.

For the multiple-tube case, there has been no improvement over Nusselt's theory, although experimental results [5, 6] have generally shown much higher heat-transfer rates for the lower tubes than predicted by Nusselt. The phenomenon has been attributed to splashing and nonuniform spilling, both of which are difficult to predict. While these effects are undoubtedly important, it is proposed that two other effects, the condensation and momentum gain between tubes, may also contribute to increased heat transfer. Both effects will be examined, but only the condensate between tubes can be treated in the framework of boundary-layer theory.

Since much of the analysis is analogous to the flat-plate case considered in reference [1], some of the results which permit direct comparison will be stated without derivation.

Boundary-Layer Equations

The physical model used in the analysis is shown in Fig. 1. The tubes, at constant wall temperature are situated in a body of pure vapor at saturation temperature. The x-component of the vapor velocity will be assumed to vanish outside the boundary layer. Both the vapor boundary layer and the liquid film will be

[1] Numbers in brackets designate References at end of paper.

Contributed by the Heat Transfer Division of The American Society of Mechanical Engineers and presented at the ASME-AIChE Heat Transfer Conference, Buffalo, N. Y., August 15–17, 1960. Manuscript received at ASME Headquarters, June 10, 1960. Paper No. 60—HT-38.

Nomenclature

$A = \left.\dfrac{\partial u^+}{\partial y^+}\right]_{y^+=0}$ (dimensionless)

a = heat-transfer area

$B = \left.\dfrac{\partial t^+}{\partial y^+}\right]_{y^+=0}$ (dimensionless)

$C = \int_0^1 u^+ dy^+$ (dimensionless)

c = specific heat of constant pressure

$D = 1 - \int_0^1 u^+ t^+ dy^+$ (dimensionless)

d = diameter of horizontal cylinder

$G = u_a y_i \left(\dfrac{g(\rho - \rho_v)k^3\Delta t^3 r^3}{\mu\rho^3\lambda^3}\right)^{-1/4}$

g = gravitational constant

h = local heat-transfer coefficient

$h_m^{(n)}$ = mean heat-transfer coefficient for n-horizontal tubes in a vertical row

k = thermal conductivity

$\mathfrak{N}_r = \left(\dfrac{g\rho(\rho - \rho_v)r^3\lambda}{\mu n_r \Delta t}\right)^{1/4}$ (dimensionless)

$\mathfrak{N}_d = \left(\dfrac{g\rho(\rho - \rho_v)d^3\lambda}{\mu k_d \Delta t}\right)^{1/4}$ (dimensionless)

$\mathrm{Nu}_d = h_m d/k$ (dimensionless)

$\mathrm{Nu}_r = h_m r/k$ (dimensionless)

$\mathrm{Pr} = c\mu/k$ (dimensionless)

q = heat-transfer rate

r = radius of cylinder

t = temperature

$t^+ = (t - t_w)_{\Delta t} = (t - t_w)/(t_i - t_w)$ (dimensionless)

$\Delta t = t_i - t_w$

u = velocity of liquid in x-direction

$u_a = \dfrac{1}{y_i}\int_0^{y_i} u dy$

u_v = velocity of vapor in x-direction

$u^+ = u/u_a$ (dimensionless)

$X = x/r$ (dimensionless)

(Continued on next page)

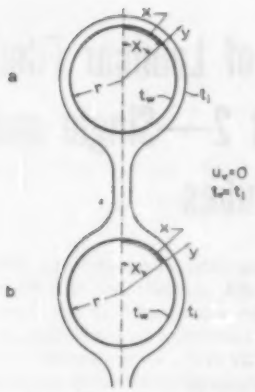

Fig. 1 Physical model used in horizontal tube analysis
(a) Single horizontal tube or top tube in a vertical bank
(b) Single or lower tubes in a vertical bank

considered to be thin compared to the radius of the tube. All properties will be considered constant.

Utilizing the simplification afforded by the stationary vapor and negligible $\mu_v\rho_v/\mu\rho$ assumptions, and following the formulation used in reference [1], the mass, momentum, and energy-conservation laws are incorporated in the following boundary-layer equations in the modified integral form:

$$\mu \frac{\partial u}{\partial y}\bigg]_w + \frac{d}{dx}\int_0^{y_i} \rho u^2\, dy = y_i g(\rho - \rho_v)\sin(x/r) \quad (1)$$

$$-k\frac{\partial t}{\partial y}\bigg]_w + k\frac{\partial t}{\partial y}\bigg]_i = -ct_i\frac{d}{dx}\int_0^{y_i}\rho u\, dy + \frac{d}{dx}\int_0^{y_i}\rho uct dy \quad (2)$$

$$\mu\frac{\partial u}{\partial y}\bigg]_{y^+y_i} + u_{y^+y_i}\frac{d}{dx}\int_0^{y_i y^+}\rho u\, dy + \frac{d}{dx}\int_{y^+y_i}^{y_i}\rho u^2\, dy = (y_i - y^+y_i)(\rho - \rho_v)g\sin(x/r) \quad (3)$$

$$-k\frac{\partial t}{\partial y}\bigg]_{y^+y_i} + k\frac{\partial t}{\partial y}\bigg]_i = ct_{y^+y_i}\frac{d}{dx}\int_0^{y^+y_i}\rho u\, dy - ct_i\frac{d}{dx}\int_0^{y_i}\rho u\, dy + \frac{d}{dx}\int_{y^+y_i}^{y_i}\rho uct dy \quad (4)$$

The coupling between the momentum equations (1) and (3) and the energy equations (2) and (4) is provided by the energy balance at the interface:

$$k\frac{\partial t}{\partial y} = \lambda\frac{d}{dx}\int_0^{y_i}\rho u\, dy \quad \text{at} \quad y = y_i \quad (5)$$

Introducing dimensionless quantities A, B, C, D, and X, Y, G (see Nomenclature) and using equation (5), equations (1) through (4) are put in the form used in Part 1:

$$(A + \xi[2CYG' - CGY' + YGC'])G = Y^3\sin X \quad (6a)$$

$$B = YG' + \zeta(DYG' + YGD') \quad (6b)$$

$$\frac{\partial u^+}{\partial y^+} + \xi\left\{u^+GY\frac{d}{dX}\int_0^{y^+}u^+dy^+ + GY\frac{d}{dX}\int_{y^+}^1 u^{+2}dy^+ + YG'u^+\int_0^{y^+}u^+dy^+ + 2YG'\int_{y^+}^1 u^{+2}dy^+ - GY'\int_{y^+}^1 u^{+2}dy^+\right\} = (1-y^+)(A + \xi YGC' + 2\xi CYG' - \xi CGY') \quad (7a)$$

$$\frac{\partial t^+}{\partial y^+} = (B - \zeta YGD' - \partial DYG')\left\{1 + \left[1 - t^+\int_0^{y^+}u^+dy^+ - \int_{y^+}^1 u^+t^+dy^+\right]\right\} - \zeta\left\{GY^+\frac{d}{dX}\int_0^{y^+}u^+dy^+ + GY\frac{d}{dX}\int_{y^+}^1 u^+t^+dy^+\right\} \quad (7b)$$

The physical meanings of the variables are as follows: X is the angle from the top stagnation point, and G and Y are the condensate-film flow rate and thickness, respectively. G' also represents the heat-transfer coefficient. A, B, C, D are properties of the profiles $u^+(y^+)$ and $t^+(y^+)$, which are to be solved from equations (7a) and (7b).

The velocity and temperature profiles also should satisfy these conditions:

$$u^+ = 0, \quad t^+ = 0 \quad \text{at} \quad y^+ = 0 \quad (8a)$$

$$\int_0^1 u^+dy^+ = 1, \quad t^+ = 1 \quad \text{at} \quad y^+ = 1 \quad (8b)$$

The boundary condition for equations (6a) and (6b) depend on whether the first or a lower tube in a row is considered. They will be stated in each specific case. Referring to the derivation of Part 1, reference [1], the equations governing heat-transfer rates will be

$$\frac{hr}{k} = (1 + D\zeta)G'\mathfrak{N}, \quad (9)$$

For the single tube:

Nomenclature

x = co-ordinates measuring the distance from leading edge along cooled wall

$Y = y_i\left(\frac{\rho g(\rho - \rho_v)}{k_\Delta t r\mu}\right)^{1/4}$ (dimensionless)

y = co-ordinate measuring distance normal to wall

y_i = liquid film thickness

$\zeta = c_\Delta t/\lambda$, heat capacity parameter (dimensionless)

λ = latent heat of vaporization

μ = viscosity

μ_v = viscosity of vapor

$\xi = k\Delta t/\mu\lambda$, acceleration effect parameter (dimensionless)

ρ = density

ρ_v = density of vapor

Subscripts

00 = pertaining to the case $\zeta = \xi = 0$; i.e., neglecting heat-capacity and acceleration effects; see also ij

01 = see ij

10 = see ij

a = pertaining to the average value over $0 \le y^+ \le 1$

i = pertaining to liquid side of liquid-vapor interface

ij = index denoting order of perturbation; e.g., $u^+ = u_{00}{}^+ + \zeta u_{10}{}^+ + \xi u_{01}{}^+ + \zeta^2 u_{20}{}^+ + \ldots$; see reference [1][1] for detailed discussion

m = pertaining to over-all mean value

v = pertaining to vapor

w = pertaining to tube wall

Superscripts

(n) = pertaining to a vertical bank of n horizontal tubes

$+$ = pertaining to dimensionless velocity and temperature profiles; see u^+, t^+, y^+

$$\mathrm{Nu}_r = \frac{h_m r}{k} = (1 + D\zeta)\mathfrak{N}_r \frac{1}{\pi}\int_0^\pi G'dX = \frac{\mathfrak{N}_r}{\pi}(1 + D\zeta)G(\pi)$$

$$\mathrm{Nu}_d = \frac{h_m d}{k} = \frac{2^{1/4}}{\pi}\mathfrak{N}_d(1 + D\zeta)G(\pi) \tag{10}$$

For the top n-tubes in a row:

$$\mathrm{Nu}_r^{(n)} = \frac{h_m^{(n)} r}{k} = \frac{\mathfrak{N}_r}{n\pi}(1 + D\zeta)G^{(n)}(\pi)$$

$$\mathrm{Nu}_d^{(n)} = \frac{h_m^{(n)} d}{k} = 2^{1/4}\frac{\mathfrak{N}_d}{n\pi}(1 + D\zeta)G^{(n)}(\pi) \tag{11}$$

Single Horizontal Tube

For the single horizontal tube the flow rate vanishes at the top stagnation point:

$$G(0) = 0 \tag{12}$$

Solution for $\zeta = \xi = 0$. For $\zeta = \xi = 0$, equations (6a), (6b), (7a), and (7b) reduce to

$$A_{00}G_{00} = Y_{00}^3 \sin X \tag{13a}$$

$$B_{00} = Y_{00}G_{00}' \tag{13b}$$

$$\frac{\partial u_{00}^+}{\partial y^+} = (1 - y^+)A_{00} \tag{14a}$$

$$\frac{\partial t_{00}^+}{\partial y^+} = B_{00} \tag{14b}$$

whose solutions are

$$u_{00}^+ = 3(y^+ - {}^1/_2 y^{+2});\ A_{00} = 3$$
$$t_{00}^+ = y_{00}^+;\ B_{00} = 1 \tag{15}$$

$$G_{00} = ({}^4/_3)^{3/4}\left(\frac{B_{00}^3}{A_{00}}\right)^{1/4}\left[\int_0^X \sin^{1/3} X dX\right]^{3/4} \tag{16}$$

$$Y_{00} = \frac{B_{00}}{G_{00}'}$$

Values of the integral have been computed and tabulated by M. Abramowitz [8], in particular

$$\sin^{1/3} X dX = 2.587$$

Therefore from equation (10)

$$\mathrm{Nu}_{d,00} = 0.7283\mathfrak{N}_d \tag{17}$$

In order to show the variation of the heat-transfer rate, the functions G_{00}, G_{00}', and Y_{00} are plotted in Fig. 2. It is seen that the film thickness reaches ∞ at $X = \pi$, in agreement with physical reality. Therefore the lowest portion of the tube contributes very little to total heat transfer of the entire cylinder.

Boundary-Layer Similarity for $\zeta \neq 0$, $\xi \neq 0$. For $\zeta \neq 0$, $\xi \neq 0$, the perturbation procedure as outlined in reference [1] can be used to solve for G_{10}, u_{10}^+, t_{10}^+; G_{01}, u_{01}^+, t_{01}^+ . . . etc. Equation (7a) shows that the products $Y_{00}G_{00}'$ and $G_{00}Y_{00}'$ appear in the solution of u_{01}'. Although $Y_{00}G_{00}' = B_{00} = 1$, $G_{00}Y_{00}'$ is not a constant, as is shown in Fig. 2. Therefore the profile $u_{01}'(y^+)$ is not independent of X. Further perturbations will show that u_{11}^+, t_{11}^+, and all higher-order perturbations will be dependent on X. This indicates that true boundary-layer similarity cannot exist for the entire tube. However, Fig. 2 shows that the slope of $G_{00}Y_{00}'$ vanishes at $X = 0$, indicating that near $X = 0$, u_{01}^+ is not x-dependent. Indeed, with the use of the induction method, as was used in the Appendix of reference [1], it is possible to show that all $G_{ij}Y_{ij}'$, $G_{ij}'Y_{ij}$, have zero slopes at $X = 0$, and all u_{ij}^+, t_{ij}^+ are independent of X near $X = 0$. Thus u^+, t^+ are also independent of X for $X = 0$, and similarity of profiles exists near the top stagnation point. This fact is analogous to the boundary layer around a cylinder in cross flow, where similarity also exists near the stagnation point.

Hermann [4], studying the analogous problem of natural convection around horizontal cylinders, concluded that approximate boundary-layer similarity exists only near $X = \pi/2$. His results and similarity transformations were later used by Sparrow and Gregg [3] in a study on condensation around tubes. A close examination of Hermann's paper showed that he used an incorrect equation and a procedure incapable of reaching unique conclusions. Thus it appeared that his conclusion on where does similarity exist was incorrect. A discussion of Hermann's similarity transformation is given in the Appendix. It should be pointed out that the accuracy of the solutions in both references was not significantly affected by this fact.

In order to show the change of velocity profiles with position, those for $\xi = 1$, $\zeta = 0$ are computed and shown in Fig. 3. Numerical methods similar to those used in reference [1], for large ξ are used since the perturbation procedure converges very slowly at large values of X. It is seen from Fig. 3 that the profiles are

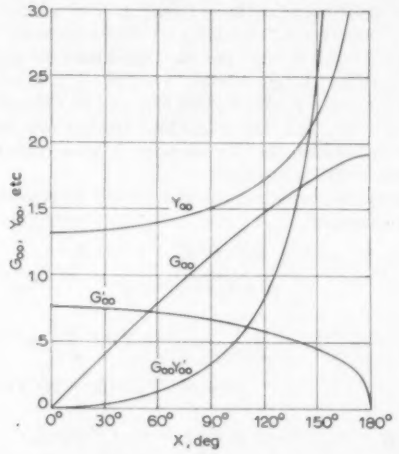

Fig. 2 Variation of dimensionless flow rate G_{00}, film coefficient G_{00}', and film thickness Y_{00} with angular position

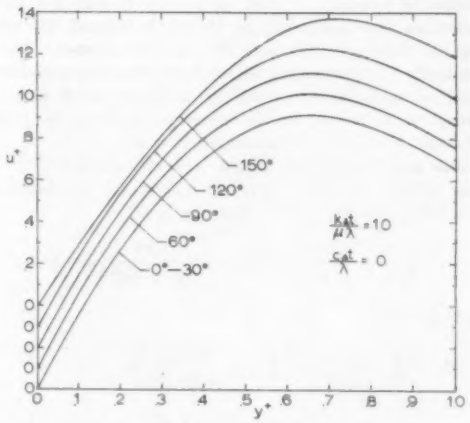

Fig. 3 Velocity profiles for $\xi = 1$

quite similar for $X < 150°$. Those for $X < 90°$ are hardly distinguishable from each other.

Simplifying Assumptions. For the computation of heat-transfer rate, significant simplifications can be obtained if the velocity profile is assumed to remain the same as at the stagnation point, near which similarity has already been shown to exist. Fig. 3 indicates that the deviation from this assumption is small for the top portion of the tube and becomes large only when $X \approx \pi$. Since the heat-transfer rate is only affected by $A^{1/4}$ and $C^{1/4}$, and the contribution of the bottom portion is small, the assumption is not expected to introduce serious error in the calculation of average heat-transfer coefficient of the whole tube. It is further justified by the fact that at $X \approx \pi$, the boundary-layer equations are no longer valid, and the profiles computed may have little physical meaning.

In effect, the use of the stagnation-point velocity profile is equivalent to eliminating GY' from equation (7*a*), since $GY' = 0$ for $X = 0$. Due to the similarity of equations (6*a*) and (7*a*), one also expects no serious error if GY' is eliminated from equation (6*a*). The presence of GY' in equation (6*a*) not only complicates its solution, but also causes the calculated film thickness to be finite at $X = \pi$, instead of the infinite film expected by physical reasoning. Therefore the complete equation (6*a*) may predict an unrealistically high heat-transfer rate, as a result of the inadequacy of the boundary-layer theory at $X \approx \pi$. A numerical solution of equation (6*a*) retaining GY'-term indicated that even at $\xi = \infty$ the result is only 4 per cent higher than the approximate solution equation (21) given later. For finite ξ, as in actual problems, the difference is considerably less, and no difference should exist for $\xi = 0$. Since the actual heat-transfer rate may be expected to lie between the two solutions, it is concluded that the elimination of GY' is justifiable.

To summarize, equations (6) and (7) will be replaced by the following equations:

$$(A + 2\xi CYG')G = Y^2 \sin X \tag{18a}$$

$$B = (1 + D\zeta)YG' \tag{18b}$$

$$\frac{\partial u^+}{\partial y^+} + \xi \left\{ YG'u^+ \int_0^{y^+} u^+ dy^+ + 2YG' \int_{y^+}^1 u^{+2}\, dy^+ \right. = \left. (1 - y^+)(A + 2\xi CYG') \right\} \tag{19a}$$

$$\frac{\partial t^+}{\partial y^+} = (B - D\zeta YG') \left\{ 1 + \zeta \left[1 - t^+ \int_0^{y^+} u^+ dy^+ - \int_{y^+}^1 u^+ t^+ dy^+ \right] \right\} \tag{19b}$$

It should be pointed out that equivalent though not identical assumptions were also made by Hermann [4] and Sparrow and Gregg [3], although they were not explicitly stated. The form of similarity transformation used in both references automatically implied approximations equivalent to those stated here. The difference lies in the fact that in references [3 and 4] the profile at $\pi/2$ is used instead of the profile at $X = 0$.

Solution and Heat-Transfer Results. Since equation (19) yields similar profiles, equations (18*a*) and (18*b*) can be combined to form a first-order differential equation in G:

$$\left(A + \frac{2CB\xi}{1 + D\zeta}\right) GG'^3 = \frac{B^3}{(1 + D\zeta)^3} \sin X \tag{20}$$

With $G(0) = 0$:

$$G = (3/4)^{3/4} \left(\frac{B}{1 + D\zeta}\right)^{3/4} \left(A + \frac{2CB\xi}{1 + D\zeta}\right)^{-1/4} \left[\int_0^X \sin^{1/3} X dX\right]^{3/4} \tag{21}$$

Compared with equations (10), (16), (17), one obtains

$$\frac{\mathrm{Nu}}{\mathrm{Nu}_{d,\infty}} = \frac{\mathrm{Nu}_d}{0.728\mathfrak{N}_d} = \left(\frac{B}{B_\infty}\right)^{3/4} \left(\frac{A_\infty}{A}\right)^{1/4} \left(\frac{1 + D\zeta}{1 + \dfrac{2CB\xi}{A(1 + D\zeta)}}\right)^{1/4} \tag{22}$$

$$\frac{\Gamma\lambda}{k\Delta t} = 2.196\mathfrak{N}_d \left(\frac{B}{B_\infty(1 + D\zeta)}\right)^{3/4} \left(\frac{A_\infty}{A + \dfrac{2CB\xi}{1 + D\zeta}}\right)^{1/4} \tag{23}$$

The velocity and temperature profiles are solved from equations (19*a*) and (19*b*). Perturbation procedure is used for moderate values of ζ and ξ, and a numerical method is used for $\xi \gg 1$, $\zeta \gg 1$. Both methods have been explained in Part 1 [1]. The computed velocity profiles are slightly different from the flat-plate case, as shown in Fig. 4. The temperature profiles are essentially the same as the flat-plate case, reference [1].

Heat-transfer results are shown in Fig. 5 together with the theoretical results of Sparrow and Gregg [3], and the results for flat plate obtained in reference [1]. It is seen that the inertia forces have a larger effect on the heat transfer of round tubes than flat plates. This fact is as expected, since with round tubes the inertia effects are stronger for the top half of the tube, which has a large contribution to the average heat-transfer coefficient. However, it is also possible that the approximations employed in obtaining equations (18*a*) and (18*b*) may have exaggerated this effect. The fact that the heat-transfer results are substantially the same as the flat-plate case, despite the exaggeration, is as-

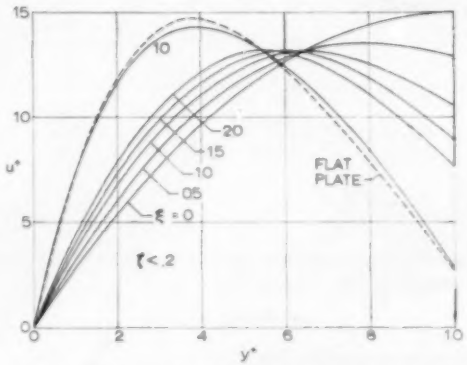

Fig. 4 Velocity profiles for top stagnation point, $X = 0$

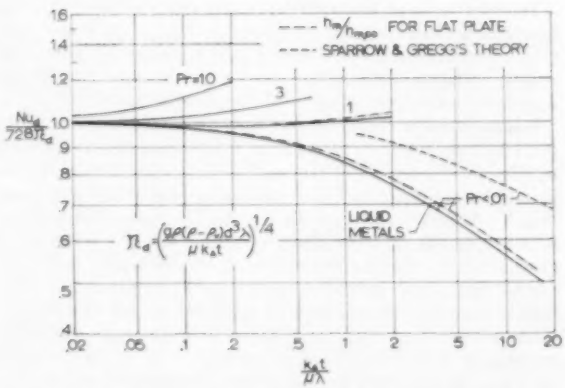

Fig. 5 Heat-transfer results for single horizontal tubes

suring. It clearly shows that an exact solution of the bondary-layer equations is not necessary.

Vertical Banks of Horizontal Tubes

The first tube in a vertical bank of horizontal tubes can be considered as a single tube, and the heat-transfer results already obtained can be used without modification. For the second and lower tubes, boundary condition at $X = 0$ should account for the condensate film falling from previous tubes. Neglecting the unpredictable effects of splashing and ripples, the boundary condition is largely influenced by the following effects:

1 The momentum gain between tubes.
2 The condensation between tubes.

The momentum gained as a result of the vertical drop between tubes contributes to make a thinner film at the lower tube. Since the momentum is in a direction perpendicular to the tube wall at the top of the tube, the effect cannot be treated by the boundary-layer theory. It is reasonable to expect that the effect on heat transfer is of the magnitude of ξ, the momentum parameter. Therefore the effect cannot be justifiably neglected if the other momentum effects are included. Accordingly, we shall restrict our interest to the case $\xi = 0$. This is not a serious restriction, since for most fluids $\Pr > 3$, and $\xi < 0.1$. The result will not apply to liquid metals, except at low temperature differences that $\xi \leq 0(.1)$.

The average temperature of the condensate leaving the first tube is somewhat lower than the saturation temperature of the vapor. During the fall to the next tube, more condensation will take place on the falling film. Due to the thinness of the falling condensate film, it is reasonable to assume that the "temperature defect," equal to $D_\Delta t$, would be completely used up for the additional condensation. Thus an approximate boundary condition for G would be

$$G^{(n+1)}(0) = (1 + D\zeta)G^{(n)}(\pi) \tag{24}$$

The superscript (n) indicates that it is for the nth tube. This condition implies that the film is at t_i at $X = 0$, but since $Y = \infty$ at $X = 0$, one can expect the thermal boundary layer to be well developed before the film becomes thin enough to contribute significantly to over-all heat-transfer rate. Thus the departure from the similar temperature profile should not introduce serious errors.

Solution and Heat-Transfer Results. Equation (20) can be used if ξ is set equal to zero. With equation (24) the solution for the second tube is

$$G^{(2)}\pi = [(1 + D\zeta)^{4/3} + 1]^{3/4}G^{(1)}(\pi) \tag{25}$$

The average heat-transfer rate for the two tubes can be expressed in terms of the first tube:

$$\frac{h_m^{(2)}}{h_m^{(1)}} = \frac{[(1 + D\zeta)^{4/3} + 1]^{3/4}}{2} \tag{26}$$

Solution for the third tube can be obtained in a similar manner. In general, the heat-transfer rate for the top n-tubes is

$$\frac{h_m^{(n)}}{h_m^{(1)}} = \frac{1}{n}\left[\sum_{i=0}^{n-1}(1 + D\zeta)^{4n/3}\right]^{3/4} \tag{27a}$$

From $\zeta = 0$, this reduces to the Nusselt's theory:

$$\frac{h_{m,\infty}^{(n)}}{h_{m,\infty}^{(1)}} = n^{-1/4} \tag{27b}$$

Equation (22) may also be used to obtain the following relation

$$\frac{h_m^{(n)}}{h_{m,\infty}^{(1)}}\, n^{1/3} = n^{-3/4}\left[\sum_{i=0}^{n-1}(1 + D\zeta)^{4n/3}\right]\left(\frac{B}{B_\infty}\right)^{3/4}(1 + D\zeta)^{1/4} \tag{28}$$

Equation (28) represents the departure from Nusselt's theory. It is plotted in Fig. 6.

Discussion of Results

For Single Tubes. If $\mathrm{Nu}_d/0.728\mathfrak{R}_d$ and $\mathrm{Nu}_s/0.948\mathfrak{R}_s$ are viewed as the correction factors to be applied to the simple theory, neglecting heat-capacity and acceleration effects, the results for round tubes are identical to those for a flat plate for $\xi < 0.5$. For $\xi > 0.5$, the round-tube results are only slightly lower than flat-plate results, but the difference is insignificant in view of the scatter of experimental data [9, 10]. Therefore the discussion given in reference [1] is applicable here without modification.

For Vertical Tube Banks. Data for vertical banks of horizontal tubes have been reported by Young and Wohlenberg [5], Katz [6], and Short and Brown [7]. The heat-transfer results for lower tubes have been found to be consistently higher than Nusselt's theory which is identical to the present theory for $\zeta = \xi = 0$. The discrepancy has generally been considered to be caused by splashing and ripples, although no quantitative estimate of the effects has been made. The present theory predicts a higher heat-transfer rate as a result of condensation between tubes. The theory and data are compared in Fig. 7. It is seen that considerable scatter exists among the data, and the lower limit of the data follows the trend of the theoretical curve closely. This seems to be sufficient proof that the effect of condensation between tubes

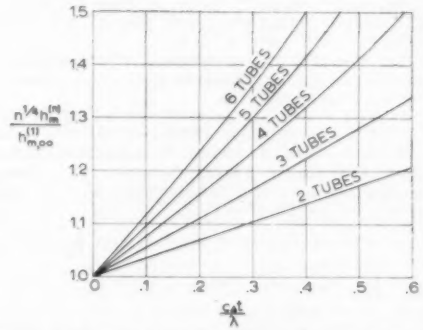

Fig. 6 Average heat-transfer coefficient for a vertical bank of n horizontal tubes

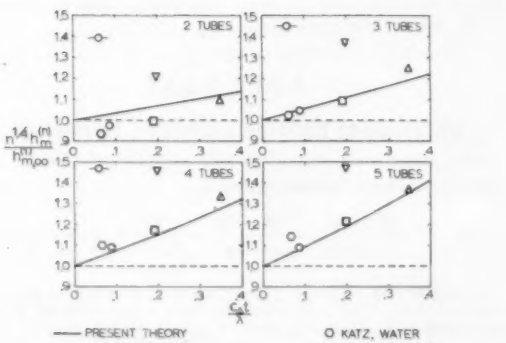

Fig. 7 Comparison of multiple-tube theory with experimental data

can be accounted for by the present approximate theory. Higher heat-transfer rates than theory for some of the data can be attributed to splashing, intermittent dripping, and local dripping, which were probably absent for the tests which agreed with theoretical predictions. Since these phenomena are neither consistent nor predictable, it is felt that their contributions should be neglected when designing new condensing equipment. Accordingly, Fig. 6 is suggested to be used in preference to empirical relations which do not account for the variation of ζ.

Approximate Formulas

The theoretical results obtained in this paper can be approximated to within 1 per cent by the following formula:

$$\frac{h_m^{(n)}}{h_{m,\infty}^{(1)}}\, n^{1/4} = [1 + 0.2\zeta(n-1)] \left(\frac{1 + 0.68\zeta + 0.02\zeta\xi}{1 + 0.95\xi - 0.15\zeta\xi}\right)^{1/4} \tag{29}$$

The ranges of applicability of equation (29) are: $\Pr \leq 0.05$ or $\Pr \geq 1$; $\zeta \leq 2$; $\xi \leq 20$ for single tube, $\xi \leq 0.1$ for multiple tubes; and $\zeta(n-1) \leq 2.0$. For multiple-tube calculations, one may also expect reasonable results if ξ is neglected from equation (29) for $\xi < 0.3$.

References

1 M. M. Chen, "An Analytical Study of Laminar Film Condensation: 1—Flat Plates," published in this issue, pp. 48-54.

2 W. Nusselt, "Die Oberflachen Kondensation des Wasserdampfes," *Zeitschrift des Vereines Deutscher Ingenieure*, vol. 60, 1916, pp. 541–569.

3 E. M. Sparrow and J. L. Gregg, "Laminar Condensation Heat Transfer on a Horizontal Cylinder," JOURNAL OF HEAT TRANSFER, TRANS. ASME, Series C, vol. 81, 1959, pp. 291–296.

4 R. Hermann, "Heat Transfer by Free Convection From Horizontal Cylinders in Diatomic Gases" (transl.), NACA TM 1366, 1954.

5 F. L. Young and W. J. Wohlenberg, "Condensation of Saturated Freon—12 Vapor on a Bank of Horizontal Tubes," TRANS. ASME, vol. 64, 1942, pp. 787–794.

6 D. L. Katz and J. M. Geist, "Condensation on Six-Finned Tubes in a Vertical Row," TRANS. ASME, vol. 70, 1948, pp. 907–914.

7 B. E. Short and H. E. Brown, "Condensation of Vapors on Vertical Banks of Horizontal Tubes," *Proceedings of the General Discussions on Heat Transfer*, 1951, The Institution of Mechanical Engineers, London; and ASME, New York, N. Y., pp. 27–31.

8 M. Abramowitz, "Tables of the Functions $\int_0^\phi \sin^{1/2} x\, dx$ and $^4/_3 \sin^{-4/3} x \int_0^\phi \sin^{1/2} x\, dx$," *Journal of Research*, National Bureau of Standards, vol. 47, 1951, pp. 288–290.

9 W. H. McAdams, "Heat Transmission," third edition, McGraw-Hill Book Company, Inc., New York, N. Y., 1954, pp. 339–342.

10 B. Misra and C. F. Bonilla, "Heat Transfer in the Condensation of Metal Vapors," *Chemical Engineering Progress*, Symposium Series, vol. 52, 1956, pp. 7–21.

APPENDIX

Discussion on Hermann's Similarity Transformation

For natural convection around a horizontal cylinder, the following dimensionless equations apply:[2]

$$\frac{\partial\psi}{\partial y}\frac{\partial^2\psi}{\partial x \partial y} - \frac{\partial\psi}{\partial x}\frac{\partial^2\psi}{\partial y^2} = \frac{\partial^3\psi}{\partial y^3} + \tau \sin x \tag{30a}$$

$$\frac{\partial\psi}{\partial x}\frac{\partial\tau}{\partial x} - \frac{\partial\psi}{\partial x}\frac{\partial\tau}{\partial y} = \frac{1}{\Pr}\frac{\partial^2\tau}{\partial y^2} \tag{30b}$$

where ψ is the stream function and τ the temperature. Introducing f, g, and q

$$\begin{aligned} \tau(x, y) &= t(q) \\ \psi(x, y) &= p(q)f(x) \\ q &= y\varphi(x) \end{aligned} \tag{31}$$

Equations (30*a*) and (30*b*) then become

$$\begin{aligned} p'^2(f^2gg' + ff'g^2) - pp''ff'g^2 &= p'''fg^3 + t \sin x \\ \frac{1}{\Pr}gt'' + f'pt' &= 0 \end{aligned} \tag{32}$$

In order that equation (32) may be ordinary differential equations in terms of q, it is necessary that two functions be found so that the ratios a, b_1, c, d, in the following equations can be constants:

$$a = f'/g \tag{33a}$$

$$b_1 = (ff'g^2 + f^2gg')/\sin x \tag{33b}$$

$$c = ff'g^2/\sin x \tag{33c}$$

$$d = fg^3/\sin x \tag{33d}$$

Three of these equations are independent, and can be satisfied only approximately at best. True similarity of the profiles exists only where the following relations are satisfied:

$$\frac{da}{dx} = \frac{db_1}{dx} = \frac{dc}{dx} = \frac{dd}{dx} \tag{34}$$

Since equations (33) cannot be satisfied exactly, a new set of equations formed by combinations of equations (33) may yield different solutions. Hermann [4] eliminated $ff'g^2$ from equations (33) and obtained the following:

$$\begin{aligned} a &= f'/g \\ b &= f^2gg'/\sin x \\ c &= ff'g^2/\sin x \\ d &= fg^3/\sin x \end{aligned} \tag{35}$$

Matching the constants at $x = \pi/2$, he solved these approximately and then concluded that since the equations are satisfied exactly near $x = \pi/2$, similarity of profiles existed only near this point. It is not difficult to see that one can reach entirely different conclusions by following the same argument, but using different variations of equations (33) and a different point to determine the constants.

A direct substitution of Hermann's functions showed that equation (34) was not satisfied near $x = \pi/2$: $db_1/dx = -1.724$, at $x = \pi/2$. Compared with the magnitude of b_1 which is equal to 2, this represents a significant variation. Therefore the profiles are obviously not similar near $x = \pi/2$.

On the other hand, if one puts $f = k_1G_{00}$, $g = k_2G_{00}' = k_2/Y_{00}$, where k_1, k_2 are constants and $G_{00}Y_{00}$ are the functions given in equation (16), then equations (33) and (34) are satisfied exactly at $x = 0$, and approximately in the vicinity of $x = 0$. Therefore truly similar velocity and temperature profiles exist at $x = 0$ for natural-convection boundary layer, analogous to the condensation problem. This conclusion also restores the unity between the natural-convection boundary layer and the crossflow boundary layer around a cylinder, which has long been shown to have a similar profile at the stagnation point.

[2] Notations of reference [4] are retained as much as possible for easy reference. To avoid confusion with other symbols, these are not listed in the Nomenclature. Symbols not immediately obvious are explained in the text.

Transient Natural Convection From Vertical Elements

B. GEBHART
Associate Professor of Mechanical Engineering, Department of Thermal Engineering, Cornell University, Ithaca, N. Y.
Assoc. Mem. ASME

The transient natural-convection process is analyzed using an integral method of analysis. Differential equations are derived which relate average surface temperature and time for either heating or cooling for vertical elements having arbitrary thermal capacity. The equations are applicable to laminar flow for all fluids. The coefficients are Prandtl number dependent and are estimated for Prandtl numbers in the range 0.01 to 1000. A solution of the equations is presented for the extreme case of a vertical plate of negligible thermal capacity subjected to a step in flux at its surface. Fluids having Prandtl numbers of 0.01, 0.1, 0.72, 1.0, 5, 10, 100, and 1000 are considered. The results, in terms of generalized variables, are practically independent of Prandtl number. Simple one-dimensional transient behavior is followed for approximately 20 per cent of the transient with a subsequent quick approach to the asymptotic value. The results show no substantial overshoot of the average surface temperature. It is doubted that significant temperature overshoot actually occurs for vertical surfaces even for a step in flux.

Introduction

This paper considers the transient natural-convection process which occurs when a vertical element, immersed in an extensive fluid bath initially at rest, is subjected to an energy-dissipation (or absorption) process internal to the element material. Such processes occur in many types of equipment. It is one of the simplest types of transient natural-convection process and is one of the first to be studied.

Certain of the basic features of the exchange process between the element and the fluid are clear. With energy dissipation in the element the distributed source in the solid material results in an increase in the temperature of the element. Heat flows by conduction to the element surface. At short times this simple conduction process extends out into the quiescent fluid as well and may be considered one-dimensional. The temperature field established in the fluid gives rise to buoyancy forces. The fluid accelerates. Eventually a balance is achieved between buoyancy, convection of momentum, and viscous forces. In addition, the conduction of heat to the surface comes into balance with the convection of heat away. The temperature of the solid-fluid interface increases with time to an asymptotic value and steady state has been established.

Several investigators have considered this type of transient natural convection. In 1951 Sugawara and Michiyoshi [1][1] presented a numerical solution of simplified equations of motion for a vertical plate whose surface is subjected to a step in temperature. Dimensionless temperature and velocity distributions were given for two times for a fluid having a Prandtl number of 1.0.

In 1956 Ostroumov [2] reported the results of an investigation of the hydrodynamic and temperature fields around a 0.004-in-diam horizontal wire subjected to a sudden direct current. Temperature overshoot was observed in water and in alcohol. Relatively few data or analysis of heat-transfer behavior are presented and no attempt is made to present dimensionless correlations of heat-transfer data.

Siegel [3] in 1958 presented an approximate analysis of transient natural convection on a vertical plate for the cases of a step in temperature and a step in flux at the element-fluid interface. The von Karman-Pohlhausen type of integral equations were used. The velocity and temperature distributions employed were those suggested by Eckert [4]. Using these approximations, estimates were obtained for the time, after starting, that the one-dimensional conduction regime persisted, the time to steady state, and the surface coefficient for the one-dimensional regime. These results suggest the overshoot observed by Ostroumov with horizontal wires. Because of the complexity of the differential equations, no general solution was obtained by Siegel. These equations are of hyperbolic partial differential form with time and vertical location as independent variables.

Goldstein [9] presents the results of an interferometric study

Contributed by the Heat Transfer Division of The American Society of Mechanical Engineers and presented at the ASME-AIChE Heat Transfer Conference, Buffalo, N. Y., August 15–17, 1960. Manuscript received at ASME Headquarters, June 2, 1960. Paper No. 60—HT-33.

[1] Numbers in brackets designate References at end of paper.

Nomenclature

a_1, a_2, a_3, a_4, a_5 = constants
c = fluid specific heat
c^* = thermal capacity of element per unit surface area
g = local gravitational acceleration
h = local surface coefficient
q^* = instantaneous energy generation rate per unit element surface area
u = velocity component in vertical direction
u_g = a velocity, proportional to that achieved in steady state
u_m = instantaneous local velocity maximum
x = vertical distance from lower edge of element for heating and from upper edge of element for cooling
y = distance out, normal to surface
A, B, C, E = constants relating to generalized velocity and temperature distributions
F = ratio of thicknesses of velocity and temperature layers
H = constant related to buoyancy, equation (22)

(Continued on next page)

of the transient temperature distributions in air and in water surrounding a vertical flat plate subjected to a step in energy input. The plate thermal capacity was relatively high compared to air and relatively low compared to water. Although plate temperatures were not measured, they were inferred from the interferograms. There was apparently no surface temperature overshoot. However, there was a boundary-layer thickness overshoot of relatively short duration.

This paper presents a method of analysis which leads to ordinary differential equations relating the instantaneous average heat-transfer characteristics to a generalized time. The analysis applies to both generation and absorption at time-dependent rates for elements having arbitrary internal thermal capacity. The method of analysis assumes that the velocity and temperature distribution have "similarity" through time and therefore applies to processes in which the fluid flow remains of the laminar, boundary-layer type.

The differential equations derived apply to all vertical elements for which it is sufficiently accurate to consider the local temperature and velocity distributions to be a function only of vertical location and time. This is strictly true for vertical plates and cylinders. The coefficients in the differential equations depend only upon element geometry, element-storage characteristics, and fluid Prandtl number. A solution of these equations is presented for a step in flux for a vertical plate of zero thermal capacity for fluid Prandtl numbers of 0.01, 0.1, 0.72, 1.0, 5, 10, 100, and 1000.

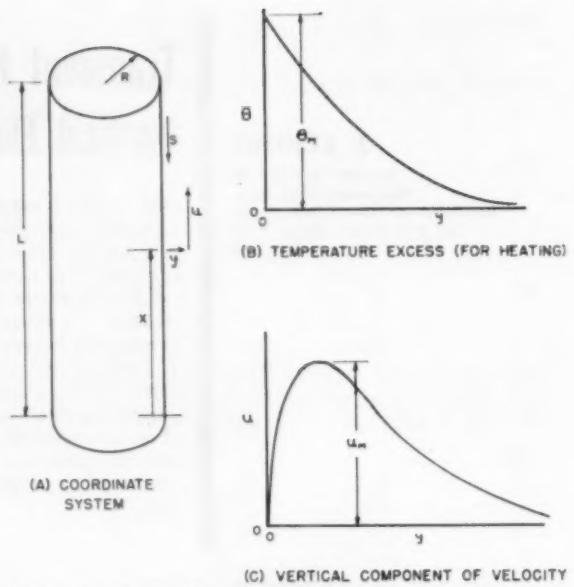

Fig. 1 Co-ordinate system and distributions of temperature and velocity

General Analysis

A majority of the transient natural-convection processes which are encountered in practice are more closely approximated by assigning either an energy-generation rate in the solid element (or a heat flux at the element surface) than by assigning a surface-temperature condition. The later condition, e.g., a step in the surface temperature, can only be approximated roughly, even in experimental apparatus. Therefore the case considered here is the one in which an element, immersed in an infinite bath of fluid at rest, is suddenly subjected to an internal-energy dissipation (or absorption) rate q'' energy units per unit of time per unit of element surface. In general, this dissipation rate may be a function of time and is assumed to approach an asymptotic value q_∞''. The thermal capacity of the element is taken as c'', energy units per unit temperature change per unit of element surface. The assumption is made that the thermal diffusivity of the element material is much greater than that of the fluid. In this circumstance the element material may be considered at a uniform temperature at any height at any instant of time.

Fig. 1 shows an element of height L and radius R immersed in an infinite fluid bath initially at rest at temperature t_r. At any time τ after the beginning of the process and at any vertical location x, the temperature and x-direction velocity-component distributions in the surrounding fluid are of the general form shown.

Considering a time τ, when the internal-energy generation rate is q'', three balances are written; namely, an energy balance for the element, an energy balance for the fluid, and a force-momentum balance for the fluid.

Nomenclature

J = constant related to acceleration, equation (23)
K = constant related to convection of momentum, equation (24)
L = height of element
M = derivative of generalized temperature distribution
N = derivative of generalized velocity distribution
N_{Gr} = conventional Grashof number, based upon L and average temperature excess at infinite time, absolute value
N_{Gr}^* = modified Grashof number, based upon L and surface flux at infinite time, absolute value
N_{Nu} = Nusselt number based upon L and average surface coefficient
N_{Pr} = Prandtl number
Q = constant related to element storage capacity, equation (21)
R = radius of curvature of element surface
S = shear stress, force per unit area
T = $\tau'/\bar{\Delta}^2_{\theta,\infty}$, generalized time
U = u/u_m
V = Prandtl number function, relating generalizing velocity to N_{Gr}^*
X = x/L
Y = $\Delta_\theta/\Delta_{\theta,\infty}$
α = thermal diffusivity of fluid
β = coefficient of thermal expansion of fluid
δ_θ = local thickness dimension of thermal layer
δ_u = local thickness dimension of velocity layer
Δ_θ = δ_θ/L
Δ_u = δ_u/L
η_θ = y/δ_θ
η_u = y/δ_u
θ = local temperature excess $(t - t_r)$
θ_m = instantaneous local temperature maximum (or minimum)
μ = fluid absolute viscosity
ρ = density of fluid
τ = time
τ' = $\alpha\tau/L^2$
ν = fluid kinematic viscosity
ϕ = θ/θ_m, temperature excess ratio
χ = u_m/u_θ
Ψ = $\theta_m/\bar{\theta}_{m,\infty}$

Subscripts

∞ = at infinite time
L = at extreme edge of element
0 = at solid-fluid interface
τ = at time τ

The energy balance for the element includes the generation rate, the rate of change of stored energy, and the rate of energy conduction at the solid-fluid interface

$$2\pi RLq'' - c'' \int_0^L 2\pi R \frac{\partial \theta_m}{\partial \tau} dx + k \int_0^L 2\pi R \left(\frac{\partial \theta}{\partial y}\right)_{y=0} dx = 0 \tag{1}$$

or

$$Lq'' - c'' \int_0^L \frac{\partial \theta_m}{\partial \tau} dx + k \int_0^L \left(\frac{\partial \theta}{\partial y}\right)_{y=0} dx = 0$$

The energy balance for the fluid includes the heat-conduction rate at the solid-fluid interface, the rate of change of stored energy in the fluid immediately adjacent to the surface, and the rate of energy convection away due to flow (at the upper edge when q'' is positive)

$$-k \int_0^L 2\pi R \left(\frac{\partial \theta}{\partial y}\right)_{y=0} dx - \frac{d}{d\tau} \int_0^L \left[\int_0^\infty \rho c\theta \, 2\pi(R+y) dy\right] dx - \int_0^\infty \rho c u_L \theta_L 2\pi(R+y) dy = 0 \tag{2}$$

or

$$k \int_0^L \left(\frac{\partial \theta}{\partial y}\right)_{y=0} dx + \frac{d}{d\tau} \int_0^L \int_0^\infty \rho c\theta \left(1 + \frac{y}{R}\right) dy \, dx + \int_0^\infty \rho c u_L \theta_L \left(1 + \frac{y}{R}\right) dy = 0$$

The force-momentum balance for the fluid includes the buoyant force, the shear stress at the surface, the rate of change of momentum in the fluid immediately adjacent to the surface, and the rate of momentum convection away due to flow (also at the upper edge when q'' is positive). These forces are

$$F_B = \pm \int_0^L \left[\int_0^\infty \frac{\rho g \beta \theta}{g_0} 2\pi(R+y) \, dy\right] dx = \pm 2\pi R \int_0^L \left[\int_0^\infty \frac{\rho g \beta \theta}{g_0} \left(1 + \frac{y}{R}\right) dy\right] dx$$

$$F_s = \int_0^L S_0 2\pi R \, dx = 2\pi R \frac{\mu}{g_0} \int_0^L \left(\frac{\partial u}{\partial y}\right)_{y=0} dx$$

$$F_m = 2\pi R \frac{d}{d\tau} \int_0^L \left[\int_0^\infty \frac{u\rho}{g_0} \left(1 + \frac{y}{R}\right) dy\right] dx$$

$$F_s = 2\pi R \int_0^\infty \frac{u_L^2 \rho}{g_0} \left(1 + \frac{y}{R}\right) dy$$

The complete force balance is therefore

$$\pm \int_0^L \int_0^\infty \rho \frac{g\beta\theta}{g_0} \left(1 + \frac{y}{R}\right) dy \, dx - \int_0^L \frac{\mu}{g_0} \left(\frac{\partial u}{\partial y}\right)_{y=0} dx - \frac{d}{d\tau} \int_0^L \int_0^\infty \frac{u\rho}{g_0} \left(1 + \frac{y}{R}\right) dy \, dx - \int_0^\infty \frac{u_L^2 \rho}{g_0} \left(1 + \frac{y}{R}\right) dy = 0 \tag{3}$$

The double sign before the first term of equation (3) allows for both heating and cooling. If q'' is positive the plus sign applies, if negative the minus sign. For heating, x is measured from the lower edge and, for cooling, from the upper edge of the element. Equations (1), (2), and (3) are general and apply in any circumstance. However, they are not useful in this form because the distributions of temperature, velocity, and properties are not known as functions of x, y, and τ.

The equations may be simplified and generalized. The temperature and velocity distributions may each be written in terms of effective local boundary-layer thicknesses δ_θ and δ_u. These two functions, in general, may depend upon both time and vertical location. In this analysis, the fluid properties are considered constant except for the density variation which produces buoyancy forces. The variables x, δ_θ, and δ_u are generalized by dividing by L. τ is reduced by multiplying by α/L^2. The local instantaneous maximum velocity u_m is generalized by dividing it by u_g, which is proportional to the maximum velocity achieved in steady state. The instantaneous local maximum temperature excess is generalized in a similar fashion. The various substitutions are summarized as follows:

$$\theta/\theta_m = \phi = \phi(y/\delta_\theta) = \phi(\eta_\theta) \tag{4}$$

$$u/u_m = U = U(y/\delta_u) = U(\eta_u) \tag{5}$$

$$X = x/L, \quad \tau' = \alpha\tau/L^2, \quad \Delta_\theta = \delta_\theta/L, \quad \Delta_u = \delta_u/L$$

$$\chi = u_m/u_g \tag{6}$$

From similarity[2] conditions, the generalizing velocity u_g is taken as

$$\frac{u_g L}{\nu} = V \left[\frac{g\beta L^4 q_\infty''}{\nu^2 k}\right]^{2/5} = V(N_{Gr}^*)^{2/5},$$

where $V = V(N_{Pr})$.

$$\psi = \theta_m/\bar{\theta}_{m,\infty} \tag{7}$$

$$Y = \Delta_\theta/\bar{\Delta}_{\theta,\infty} \tag{8}$$

where

$$\bar{\theta}_{m,\infty} = \int_0^1 \theta_{m,\infty} dX \quad \text{and} \quad \bar{\Delta}_{\theta,\infty} = \int_0^1 \Delta_{\theta,\infty} dX$$

Since, for negligible conduction internal to the element in the x-direction,

$$q_\infty'' = -k \left(\frac{\partial \theta}{\partial y}\right)_{0,\infty} = k \frac{\theta_{m,\infty}}{\delta_{\theta,\infty}} \left(-\frac{\partial \phi}{\partial \eta_\theta}\right)_{0,\infty}$$

$$\Delta_{\theta,\infty} = \frac{\delta_{\theta,\infty}}{L} = \frac{k\theta_{m,\infty}}{q_\infty'' L} \left(-\frac{\partial \phi}{\partial \eta_\theta}\right)_{0,\infty} \tag{9}$$

$$\bar{\Delta}_{\theta,\infty} = \int_0^1 \Delta_{\theta,\infty} dX = \frac{k}{q_\infty'' L} \int_0^1 \theta_{m,\infty} \left(-\frac{\partial \phi}{\partial \eta_\theta}\right)_{0,\infty} dX = \frac{k}{q_\infty'' L} \int_0^1 \theta_{m,\infty} M_{0,\infty} \, dX$$

where

$$M_{\eta,\tau} = \left(-\frac{\partial \phi}{\partial \eta_\theta}\right)_{\eta,\tau}$$

$$N_{\eta,\tau} = \left(\frac{\partial U}{\partial \eta_u}\right)_{\eta,\tau}$$

If $M_{0,\infty}$ were independent of X, i.e., if $\bar{M}_{0,\infty} = M_{0,\infty} = M_0$, then:

$$\bar{\Delta}_{\theta,\infty} = \frac{k}{q_\infty'' L} \bar{\theta}_{m,\infty} M_0 \tag{9a}$$

[2] See Appendix 2.

The time variable is further modified and F is introduced as the ratio of the thicknesses of the velocity and temperature layers:

$$T = \frac{\tau'}{\bar{\Delta}^2_{\theta,\infty}} = \frac{\alpha\tau}{L^2\bar{\Delta}^2_{\theta,\infty}} = \frac{\alpha\tau}{\delta^2_{\theta,\infty}}$$

$$F = \Delta_u/\Delta_\theta$$

Equations (1), (2), and (3) are then rewritten as integrals from $X = 0$ to $X = 1$ and over the effective thicknesses of the boundary layers as

$$\left(\frac{q^*}{q^*_\infty}\right) M_{\theta,\infty} - \frac{c^*}{\rho c L\bar{\Delta}_{\theta,\infty}} \int_0^1 \frac{\partial\psi}{\partial T}\, dX - \int_0^1 \frac{\psi}{Y} M_{\theta,\tau}\, dX = 0 \tag{10}$$

$$\int_0^1 \frac{\psi}{Y} M_{\theta,\tau}\, dX - \frac{d}{dT}\int_0^1 \psi Y \left[\int_0^1 \phi\left(1+\frac{y}{R}\right) d\eta_\theta\right] dX - \bar{\Delta}^2_{\theta,\infty} N_{Pr} V (N_{Gr}^*)^{2/5} (Y_L \chi_L \psi_L) \int_0^1 U_L \phi_L \left(1+\frac{y}{R}\right) d\eta_\theta = 0 \tag{11}$$

$$\frac{(\eta_{Gr}^*)^{2/5}}{V}\frac{\bar{\Delta}^2_{\theta,\infty}}{M_{\theta,\infty}} \int_0^1 \psi Y \left[\int_0^1 \phi\left(1+\frac{y}{R}\right) d\eta_\theta\right] dX - \int_0^1 \frac{\chi}{FY} N_{\theta,\tau}\, dX - \frac{1}{N_{Pr}}\frac{d}{dT}\int_0^1 \chi F Y \left[\int_0^1 U\left(1+\frac{y}{R}\right) d\eta_u\right] dX - \bar{\Delta}_{\theta,\infty} V (N_{Gr}^*)^{2/5} F (Y^3{}_L \chi_L) \int_0^1 U_L{}^3 \left(1+\frac{y}{R}\right) d\eta_u = 0 \tag{12}$$

These three equations relate the velocity, temperature, and thermal-layer thickness variables (χ, ψ, and Y) to the generalized time variable T. The principal obstacle to the use of the equations in this form is that insufficient information is available for the general evaluation of the various integrals. These integrals are at least weak functions of time, and the velocity and temperature distributions are unknown. Further, the averaging of unknown distributions and derivatives over the height of the element produces an additional, distinct difficulty.

The difficulty regarding the velocity and temperature distributions disappears if one may consider that the functions in equations (4) and (5) are, for any given fluid and geometry, independent of time. This amounts to the assumption that the temperature and velocity distributions each retain their form through space and time. This proposition is examined in Appendix 1. The result of this consideration is that, for any given fluid Prandtl number and geometry, i.e., R/L, each integral over the distribution is assumed independent of position and time for the laminar boundary-layer type of flow. The relation between the accuracy of this approximation and the way in which q^* changes with time is not known. There is some evidence, Goldstein [9], that such a similarity does not persist for a relatively short intermediate period of the process which results for conditions which approximate a step in flux. However, the step in flux is an extreme and unrealistic case in any practical sense. It is virtually impossible to achieve even in experimental apparatus. For variations of q^*, which are continuous and monotomic, the approximation is evidently much better since in the limit, a quasistatic process, the approximation disappears.

If the values of the integrals of the distributions are denoted by constants, as shown later, equations (10), (11), and (12) become (13), (14), and (15). Similarly, F, which is the ratio of the thicknesses of the velocity and temperature layers, is assumed to depend only upon the fluid Prandtl number and geometry:

$$A = \int_0^1 \phi\left(1+\frac{y}{R}\right) d\eta_\theta, \quad B = \int_0^1 U\left(1+\frac{y}{R}\right) d\eta_u$$

$$C = \int_0^1 U^2\left(1+\frac{y}{R}\right) d\eta_\infty, \quad E = \int_0^1 U_\theta \phi\left(1+\frac{y}{R}\right) d\eta_\theta$$

where

$$U_\theta = U(\eta_\theta/F)$$

$$M_{\theta,\infty} = \bar{M}_{\theta,\infty} = M_{\theta,\tau} = M_\theta$$

$$N_{\theta,\tau} = N_\theta$$

$$\left(\frac{q^*}{q^*_\infty}\right) M_\theta - \frac{c^*}{\rho c L\bar{\Delta}_{\theta,\infty}} \frac{d}{dT}\int_0^1 \psi dX - M_\theta \int_0^1 \frac{\psi}{Y}\, dX = 0 \tag{13}$$

$$M_\theta \int_0^1 \frac{\psi}{Y}\, dX - A\frac{d}{dT}\int_0^1 \psi Y\, dX - \bar{\Delta}^2_{\theta,\infty} N_{Pr} V (N_{Gr}^*)^{2/5} E (Y_L \chi_L \psi_L) = 0 \tag{14}$$

$$\frac{(N_{Gr}^*)^{2/5}}{V} A \frac{\bar{\Delta}^2_{\theta,\infty}}{M_\theta}\int_0^1 \psi Y\, dX - \frac{N_\theta}{F}\int_0^1 \frac{\chi}{Y}\, dX - \frac{BF}{N_{Pr}}\frac{d}{dT}\int_0^1 \chi Y\, dX - \bar{\Delta}^2_{\theta,\infty} V (N_{Gr}^*)^{2/5} C F (Y_L X^2_L) = 0 \tag{15}$$

The integrals remaining in the equations average the dependent variables ψ, Y, and χ (and combinations thereof) over the height of the element. Since at short times the process is one-dimensional, ψ, Y, and χ are uniform over the whole element surface and all integrals may be replaced by average values. However, after flow becomes appreciable, distributions of ψ, Y, and χ arise. These distributions are unknown in the intermediate part of the transient phase of the process. However, they are known from similarity and boundary-layer theory for steady state. These two extremes, short time and steady state, are employed to estimate the relation between the integrals which average combinations of ψ, Y, and χ and the same combinations of the averages of ψ, Y, and χ.

The integrals (and other combinations) are:

(1) $\int_0^1 \psi\, dX = \bar{\psi}$

(2) $\int_0^1 \frac{\psi}{Y}\, dX = \frac{\bar{\psi}}{\bar{Y}}$

(3) $\int_0^1 \psi Y\, dX = a_1 \bar{\psi}\bar{Y}$

(4) $Y_L \chi_L \psi_L = a_7 \bar{Y}\tilde{\chi}\bar{\psi}$

(5) $\int_0^1 \frac{\chi}{Y}\, dX = a_2 \frac{\tilde{\chi}}{\bar{Y}}$

(6) $\int_0^1 \chi Y\, dX = a_4 \tilde{\chi}\bar{Y}$

(7) $Y_L \chi_L{}^2 = a_5 \bar{Y}\tilde{\chi}^2$

The first integral is invariably the average of ψ. From equations (7), (8), and (9), the ψ and Y-distributions are seen to be identical in steady state as well as at short times. Therefore the average of the ratio is equal to the ratio of the averages.

The values of a_1, a_2, a_3, a_4, and a_5 are established in Appendix 2 for flat plates from the analysis of Sparrow and Gregg [5]. These results are extended to apply to vertical cylinders on the basis of measurements and an integral-method analysis presented by Hama and Recesso [6] and Hama and Christiaens [7]. A set of average values of a_1, a_2, a_3, a_4, and a_5 is suggested for the whole transient process. With these changes the equations become

$$\left(\frac{q''}{q_\infty''}\right) - \frac{c''}{\rho c L M_0 \bar{\Delta}_{\theta,\infty}} \frac{d\bar{\psi}}{dT} - \frac{\bar{\psi}}{\bar{Y}} = 0 \tag{16}$$

$$\frac{\bar{\psi}}{\bar{Y}} - \frac{a_1 A}{M_0} \frac{d}{dT}(\bar{\psi}\bar{Y}) - \bar{\Delta}^2_{\theta,\infty} \frac{N_{Pr} V (N_{Gr}^*)^{2/5}}{M_0} a_2 E (\bar{Y}\bar{\chi})\bar{\psi} = 0 \tag{17}$$

$$\frac{(N_{Gr}^*)^{2/5}}{V} \frac{a_1 A \bar{\Delta}^2_{\theta,\infty}}{M_0} (\bar{\psi}\bar{Y}) - \frac{a_3 N_0}{F} \frac{\bar{\chi}}{\bar{Y}} - \frac{a_4 B F}{N_{Pr}} \frac{d}{dT}(\bar{\chi}\bar{Y}) - V\bar{\Delta}^2_{\theta,\infty}(N_{Gr}^*)^{2/5} a_5 C F (\bar{Y}\bar{\chi}^2) = 0 \tag{18}$$

The velocity variable $\bar{\chi}$ is eliminated between (17) and (18). The remaining two equations involve only $\bar{\psi}$ and $\bar{Y}$:

$$\frac{\bar{\psi}}{\bar{Y}} = \left(\frac{q''}{q_\infty''}\right) - Q \frac{d\bar{\psi}}{dT} \tag{19}$$

$$H\bar{\Delta}^5_{\theta,\infty}\bar{\psi}^2\bar{Y}^2 - \left\{\left[\frac{\bar{\psi}}{\bar{Y}} - \frac{a_1 A}{M_0}\frac{d}{dT}(\bar{\psi}\bar{Y})\right] + J\bar{\psi}\bar{Y}^2 \frac{d}{dT}\frac{1}{\bar{\psi}}\left[\frac{\bar{\psi}}{\bar{Y}} - \frac{a_1 A}{M_0}\frac{d}{dT}(\bar{\psi}\bar{Y})\right] + K\frac{\bar{Y}}{\bar{\psi}}\left[\frac{\bar{\psi}}{\bar{Y}} - \frac{a_1 A}{M_0}\frac{d}{dT}(\bar{\psi}\bar{Y})\right]^2\right\} = 0 \tag{20}$$

The coefficients are defined as follows:

$$Q = \frac{c''}{\rho c L M_0 \bar{\Delta}_{\theta,\infty}} \tag{21}$$

$$H = \frac{a_1 a_2 E A F N_{Gr}^* N_{Pr}}{a_3 N_0 M_0^2} \tag{22}$$

$$J = \frac{a_4 B F^2}{a_3 N_0 N_{Pr}} \tag{23}$$

$$K = \frac{a_5 C M_0 F^2}{a_3 a_2 E N_0 N_{Pr}} \tag{24}$$

Equations (19) and (20) may be solved to yield the steady-state heat-transfer behavior and this result is compared with boundary-layer solutions for a vertical plate in the next section. At this point the steady-state result is used merely to eliminate $H\bar{\Delta}^5_{\theta,\infty}$ from the equations.

At large values of T, steady state is approached if q'' approaches a constant value. Therefore, from equation (19)

$$\frac{d\bar{\psi}}{dT} = 0 \quad \text{and} \quad \frac{\bar{\psi}}{\bar{Y}} = 1$$

Then, since $\bar{\psi}$ approaches 1.0, equation (20) becomes

$$H\bar{\Delta}^5_{\theta,\infty} - (1 + K) = 0 \tag{25}$$

From equation (22), H is based upon the modified Grashof number calculated from the asymptotic value of q''; i.e., q_∞''.

The final equations for either heating or cooling, with the general boundary conditions, are

$$\frac{\bar{\psi}}{\bar{Y}} = \left(\frac{q''}{q_\infty''}\right) - Q \frac{d\bar{\psi}}{dT} \tag{19}$$

$$(1+K)\bar{\psi}^2\bar{Y}^2 - \left\{\left[\frac{\bar{\psi}}{\bar{Y}} - \frac{a_1 A}{M_0}\frac{d}{dT}(\bar{\psi}\bar{Y})\right] + J\bar{\psi}\bar{Y}^2 \frac{d}{dT}\frac{1}{\bar{\psi}}\left[\frac{\bar{\psi}}{\bar{Y}} - \frac{a_1 A}{M_0}\frac{d}{dT}(\bar{\psi}\bar{Y})\right] + K\frac{\bar{Y}}{\bar{\psi}}\left[\frac{\bar{\psi}}{\bar{Y}} - \frac{a_1 A}{M_0}\frac{d}{dT}(\bar{\psi}\bar{Y})\right]^2\right\} = 0 \tag{26}$$

at $T = 0$: $\bar{Y} = 0$ and $\left[\frac{\bar{\psi}}{\bar{Y}} - \frac{a_1 A}{M_0}\frac{d}{dT}(\bar{\psi}\bar{Y})\right] = 0$

The meaning of $\bar{\psi}$ and T is as follows:

$$\bar{\psi} = \frac{\bar{\theta}_{m,\tau}}{\bar{\theta}_{m,\infty}} = \frac{N_{Nu,\infty}}{N_{Nu,\tau}}$$

$$T = \frac{\alpha\tau}{L^2\bar{\Delta}^2_{\theta,\infty}} = \frac{\alpha\tau}{L^2}\left[\frac{H}{(1+K)}\right]^{2/5} = \frac{\alpha\tau}{L^2}\left[\frac{a_1 a_2 E A F}{a_3 N_0 M_0}\frac{N_{Pr}}{(1+K)} N_{Gr}\right]^{1/2}$$

The foregoing equations specify the relations between $\bar{\psi}$ and $\bar{Y}$ and the time variable T. The problem has been generalized except for the fluid Prandtl number and the R/L effects. The characteristics of a particular problem are the heater-etorage characteristic Q, and the nature of the flux time dependence q''/q_∞''; that is, the functional relation between the temperature variable $\bar{\psi}$ and time T depends only upon Prandtl number, R/L effects, Q and q''/q_∞'' and does not depend upon the Grashof number, and so on.

The assumptions, approximations, and conditions, upon which these results depend, are summarized as follows:

(*a*) The thermal diffusivity of the element material is large compared to that of the fluid.

(*b*) Vertical heat conduction in the element is assumed negligible.

(*c*) The velocity and temperature distributions retain their form in time and space.

(*d*) The ratio of the thicknesses of the velocity and temperature layers depends only upon the Prandtl number.

(*e*) Average distribution parameters a_1, a_2, a_3, a_4, and a_5 are employed.

(*f*) The generation rate q'' continuously and monotonically approaches a constant value at large time.

Steady-State Solution

The steady-state solution of the general transient equations, equation (25), is compared with two solutions of the boundary-layer equations for the vertical flat plate. The two solutions are the uniform temperature case by Ostrach [8] and the uniform flux case by Sparrow and Gregg [5].

Equation (25) is written in conventional form using relations (9*a*), (22), and (24):

$$H\bar{\Delta}^5_{\theta,\infty} = (1 + K) \tag{25}$$

$$\bar{\Delta}_{\theta,\infty} = \frac{k\bar{\theta}_{m,\infty}}{q_\infty'' L} M_0 = \frac{k}{\bar{h}_\infty L} M_0 = \frac{M_0}{N_{Nu,\infty}}$$

$$H = \frac{a_1 a_2 E A F}{a_3 N_0 M_0^2} N_{Gr}^* N_{Pr} = \frac{a_1 a_2 E A F}{a_3 N_0 M_0^2} N_{Gr} N_{Nu,\infty} N_{Pr}$$

$$\frac{N_{Nu,\infty}}{(N_{Gr})^{1/5}} = \left[\frac{a_1 a_2 E A F M_0^2}{a_3 N_0}\frac{N_{Pr}}{(1+K)}\right]^{1/5} \tag{27}$$

This expression may be written in the following form:

$$\frac{N_{Nu,\infty}}{(N_{Gr})^{1/5}} = P(N_{Pr}) \tag{28}$$

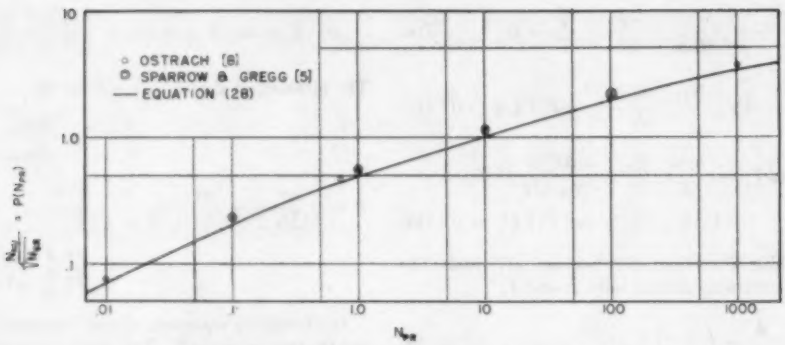

Fig. 2 Comparison of steady-state solutions for a vertical plate

This relation, employing the constants determined in Appendixes 1 and 2, is compared with the results in [5] and [8], in Table 1, and in Fig. 2. The values of $P(N_{Pr})$ are within 9 per cent of those in [8] and the trend is the same. The difference is in part due to the averaging of constants a_3 and a_4 over the whole process. If the values of a_3 and a_4 for steady state are used, the results are essentially identical to those of [8].

Table 1 Comparison of steady-state solutions

	$P(N_{Pr})$		
N_{Pr}	Eq. (28)	Ostrach [8]	Sparrow and Gregg [5]
0.01	0.0715	0.0765	
0.1			0.237
0.72	0.444	0.476	
1.0	0.505	0.535	0.573
10	1.016	1.10	1.17
100	2.01	2.07	2.18
1000	3.42	3.74	

Application to Case of a Step in Flux

The general differential equations derived in the foregoing have been solved numerically for a special case. The case chosen is that of a vertical flat plate of negligible internal capacity (immersed in an infinite fluid at rest) which is suddenly subjected to a thereafter uniform generation rate q'''.

Since $Q = 0$, $\bar{\Psi} = \bar{\Psi}$. From equation (26) the rearranged equation and boundary conditions are

$$J\bar{\Psi}^3 \frac{d}{dT}\left[1 - \frac{a_1 A}{M_0}\frac{d}{dT}(\bar{\Psi}^3)\right] + \left(1 - \frac{JM_0}{2a_1 A}\right)\left[1 - \frac{a_1 A}{M_0}\frac{d}{dT}(\bar{\Psi}^3)\right] + \left(K + \frac{JM_0}{2a_1 A}\right)\left[1 - \frac{a_1 A}{M_0}\frac{d}{dT}(\bar{\Psi}^3)\right]^2 = (1+K)\bar{\Psi}^4 \quad (29)$$

at

$$T = 0\text{: } \bar{\Psi} = 0 \text{ and } \left[1 - \frac{a_1 A}{M_0}\frac{d}{dT}(\bar{\Psi}^3)\right] = 0$$

Equation (29) is converted to a more convenient form for integration by a change of variable:

$$Z = \frac{a_1 A}{M_0}\bar{\Psi}^3 \quad (30)$$

$$W = [1 - Z'] \quad (31)$$

$$ZW' + \left(\frac{a_1 A}{M_0 J} - \frac{1}{2}\right)W + \left(\frac{a_1 AK}{M_0 J} + \frac{1}{2}\right)W^2 = \frac{(1+K)}{J}\left(\frac{M_0}{a_1 A}\right)^{3/2} Z^{3/2} \quad (32)$$

at

$$T = 0\text{: } Z = 0 \text{ and } W = 0 \quad (33)$$

The numerical values suggested in Appendixes 1 and 2 (for the case of a step in flux) yield the coefficients for equation (32) in Table 2.

The role of the fluid Prandtl number is clearly indicated in Table 2. It affects the values of the coefficients in the differential equation.

The relations given in the foregoing for the convection transient contain the solution for the infinite slab subjected to a sudden uniform flux on its exposed face. Equation (31)—or the second boundary condition for equation (29)—yields

$$Z = T \quad (34)$$

This result may be rearranged:

$$\bar{\Psi} = \left(\frac{M_0 T}{a_1 A}\right)^{1/3}$$

$$\bar{\theta}_{w,\tau} = \frac{q'''}{k}\left(\frac{a\tau}{a_1 A M_0}\right)^{1/3} \quad (35)$$

The conduction solution, obtained from the Fourier equation,[3] is

$$\theta_{w,\tau} = \frac{q'''}{k}\left(\frac{4}{\pi}a\tau\right)^{1/2} \quad (36)$$

Employing the average value of $1/a_1 A M_0$, the temperatures given by (35) and (36) differ by 15 per cent.

Since the solution of equations (31) and (32) is not known, the integration was carried out numerically on a high-speed computing machine using a Runge-Kutta procedure. Certain features of the calculation are discussed in Appendix 3. The results for Prandtl numbers of 0.01, 0.1, 0.72, 1, 5, 10, 100, and 1000, in terms of $\bar{\Psi}$, are tabulated in Appendix 3 and plotted in Fig. 3. The one-dimensional transient relation, equation (34), is included for comparison.

The principal features of these results are the small Prandtl number effect in these co-ordinates, i.e., $\bar{\Psi}$ versus T; the close adherence to the trend which characterizes a one-dimensional

[3] See, e.g., p. 258, "Heat Transfer," vol. 1, M. Jakob, John Wiley & Sons, Inc., New York, N. Y.

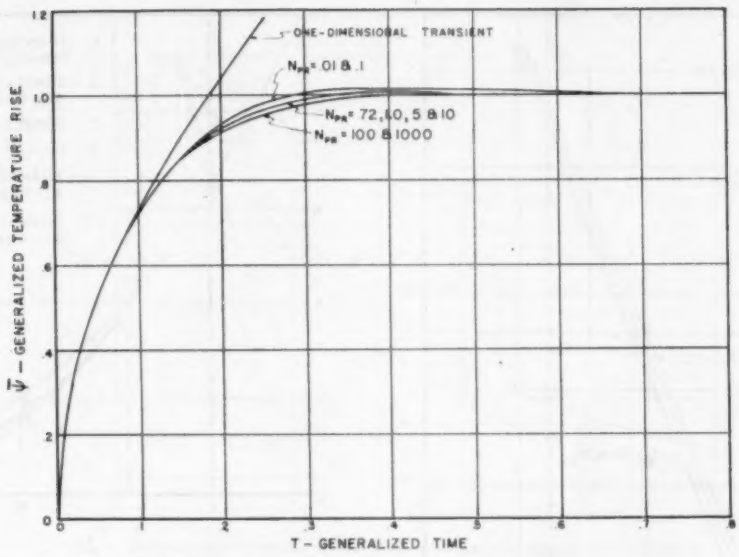

Fig. 3 Temperature-time relation (for a step in flux)

Table 2

N_{Pr}	J	K	$\left(\frac{a_1 A}{M_0}\right)^a$	$\frac{(1+K)}{J}\cdot\left(\frac{M_0}{a_1 A}\right)^{2/3}$	$\left(\frac{a_1 A}{M_0 J} - 1/2\right)$	$\left(\frac{a_1 A K}{M_0 J} + 1/2\right)$
0.01	0.763	5.712	0.179	109.66	−0.2562	1.8924
0.1[b]	0.260	1.800	0.186	134.25	0.2154	1.7877
0.72	0.0965	0.626	0.194	210.05	1.4275	1.7066
1.0	0.0817	0.512	0.192	230.71	1.7767	1.6656
5[b]	0.0360	0.220	0.189	422.46	4.6667	1.6367
10	0.0253	0.152	0.184	567.63	6.8518	1.6175
100	0.00740	0.0394	0.188	1751.0	24.635	1.4903
1000	0.00345	0.0152	0.185	3668.3	53.415	1.3195

[a] An average value of 0.186 was used in the calculations.
[b] The constants for the cases of Prandtl numbers of 0.1 and 5.0 were determined by interpolation.

conduction transient over an appreciable portion of the range; and the rapid approach to the asymptote. If an average curve were drawn in Fig. 3, all results for the convection transients would lie within 1.5 per cent of this curve. In Fig. 4 the short-time results are plotted as the per cent difference between the trend of the one-dimensional transient and the computed convection behavior; i.e., $(T - Z)/T$. The higher Prandtl number fluids diverge most rapidly from the one-dimensional transient which gives less than a 1 per cent error in $\bar{\psi}$ for $T < 0.065$. The "overshoot" in the convection results is extremely small and limited to $N_{Pr} < 5.0$. In a practical sense this overshoot is negligible and, if one denotes by steady state an approach to within 1 per cent of steady-state temperature, the time interval of the transient depends upon Prandtl number as shown in Table 3.

Table 3

Prandtl number	Time interval for the transient
0.01	0.269
0.1	0.270
0.72	0.296
1	0.303
5	0.339
10	0.345
100	0.362
1000	0.365

Conclusions

It is expected that the general equations, (19) and (26), are an accurate description of natural-convection transients for vertical elements with time-dependent internal-energy generation. The important dependent variable is an instantaneous temperature-rise quantity which depends only upon a generalized time. There are only two parameters, the fluid Prandtl number and an element storage-capacity quantity.

The solution of the equations for a limiting case, a vertical plate of zero thermal capacity subjected to a step in flux, shows that the results for all Prandtl numbers correspond within 2.4 per cent. This difference is negligible from any practical point of view and average results are within 1.2 per cent of all values.

The absence of significant overshoot in these results is surprising in view of the data of Ostroumov [2] for a horizontal wire in water and in alcohol. However, when one considers the relative ineffectiveness of the buoyancy forces on the bottom of a horizontal cylinder, the different behavior is more plausible. Although Siegel [3] did not obtain a solution in the analysis for a vertical surface, those results suggest overshoot also. However, the overshoot may result from the chosen velocity and temperature distributions. The author calculated the transients using these same distributions with the present theory and obtained large overshoot at low Prandtl numbers, where these distributions are highly unrealistic, Figs. 5 and 7.

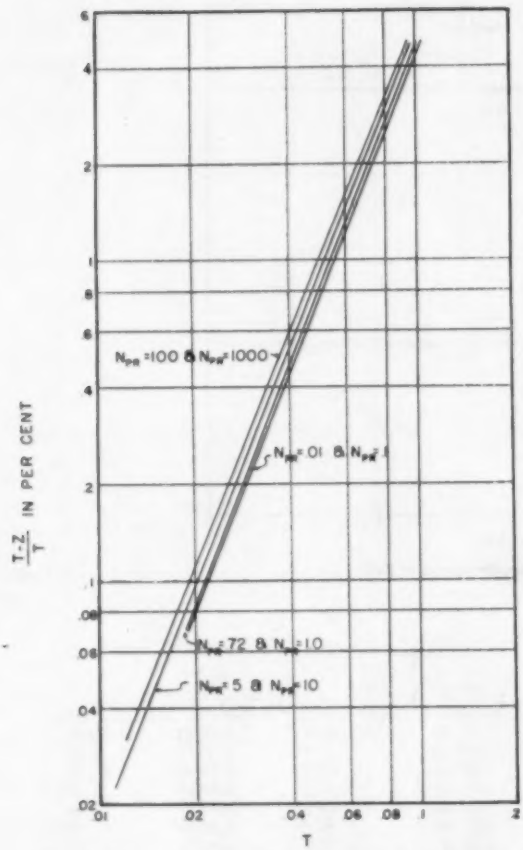

Fig. 4 Temperature-rise characteristics at short times

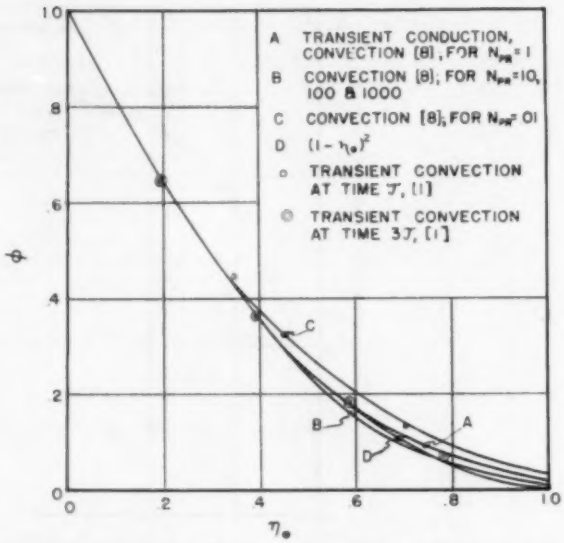
A TRANSIENT CONDUCTION, CONVECTION [8], FOR N_{Pr} = 1
B CONVECTION [8], FOR N_{Pr}=10, 100 & 1000
C CONVECTION [8], FOR N_{Pr}= .01
D $(1-\eta_\theta)^2$
TRANSIENT CONVECTION AT TIME $\mathcal{T}$, [1]
TRANSIENT CONVECTION AT TIME $3\mathcal{T}$, [1]
θ
η_θ

Fig. 5 Transient and steady-state temperature distributions for a vertical plate with uniform temperature

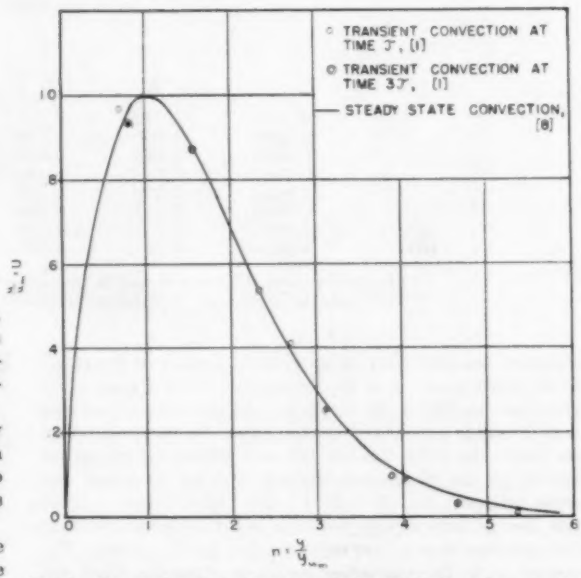

Fig. 6 Transient and steady-state velocity distributions for a vertical plate with uniform temperature, N_{Pr} = 1.0

In experimental studies made by J. Martin and by the author, transient temperatures were measured on vertical plates and on vertical cylinders of low thermal capacity in water. No temperature overshoot has been observed. The measurements of Goldstein indicate no temperature overshoot.

The general equations presented herein, (19) and (26), apply for arbitrary thermal capacity and may be analyzed for such effects. In particular, these equations should be studied to establish the conditions under which a quasi-static analysis is sufficiently accurate.

Further measurements and calculations are now being made with the support of the National Science Foundation. These results will be reported subsequently.

Acknowledgments

The author wishes to express his appreciation to Mrs. Joan Capps who carried out the calculations for the zero-storage case; to Mr. P. Andorn who prepared the figures; and to Mrs. Leora Decker who prepared the manuscript.

During the preparation of this paper a National Science Foundation grant was received. The availability of these funds was helpful in completing this work.

References

1 S. Sugawara and I. Michiyoshi, "Heat Transfer by Natural Convection in the Unsteady State on a Vertical Flat Wall," *Proceedings, First Japan National Congress for Applied Mechanics*, 1951, National Committee for Theoretical and Applied Mechanics Science, Council of Japan, May, 1952, pp. 501–506.

2 G. A. Ostroumov, "Unsteady Thermal Convection About a Horizontal Wire," *Zhurnal tekhnicheskoi fiziki*, vol. 26, 1956, pp. 2720–2730; translated in *Soviet Physics, Technical Physics*, vol. 1, p. 2627.

3 R. Siegel, "Transient Free Convection From a Vertical Flat Plate," TRANS. ASME, vol. 80, 1958, p. 347.

4 E. R. G. Eckert, "Introduction to the Transfer of Heat and Mass," McGraw-Hill Book Company, Inc., New York, N. Y., 1950.

5 E. M. Sparrow and J. L. Gregg, "Laminar Free Convection From a Vertical Plate With Uniform Surface Heat Flux," TRANS. ASME, vol. 78, 1956, p. 435.

6 F. R. Hama and J. V. Recesso, "The Axisymmetric Free-Convection Temperature Field Along a Vertical Thin Cylinder," University of Maryland Technical Note BN-116, January, 1958.

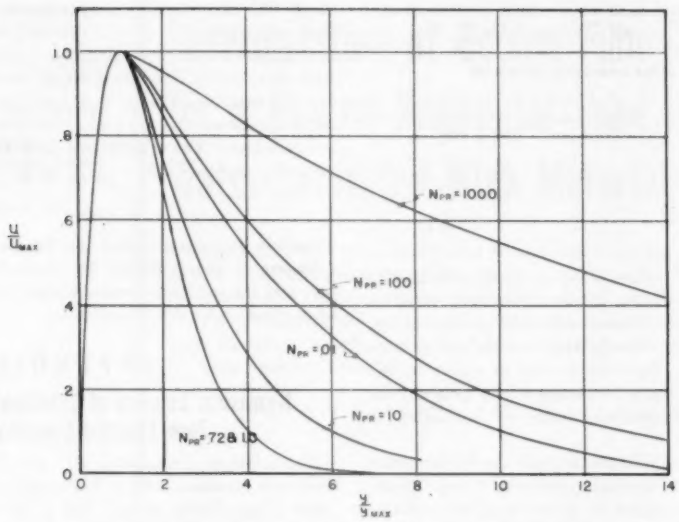

Fig. 7 Velocity distributions, vertical plate with uniform surface temperature, for various Prandtl numbers

Table 4 Constants relating to the velocity and temperature distributions

N_{Pr}	F	A	B	C	E	M_θ	N_θ
0.01	0.95	0.337	0.321	0.199	0.184	1.88	37.8
0.72	1.69	0.348	0.358	0.249	0.226	1.79	14 .7
1	1.90	0.343	0.345	0.246	0.238	1.79	15.3
10	5.27	0.326	0.266	0.170	0.221	1.77	29.2
100	13.6	0.331	0.249	0.156	0.251	1.77	62.6
1000	54.1	0.326	0.269	0.111	0.194	1.76	228

7 F. R. Hama and J. Christiaens, "Experiment on the Axisymmetric Free-Convection Field Along a Vertically Suspended Wire," University of Maryland Technical Note BN-138, May, 1958.

8 S. Ostrach, "An Analysis of Laminar Free-Convection Flow and Heat Transfer About a Flat Plate Parallel to the Direction of the Generating Body Force," NACA Report 1111, 1953.

9 R. J. Goldstein, "Interferometric Study of the Steady-State and Transient Free-Convection Thermal Boundary Layers in Air and in Water About a Uniformly Heated Vertical Flat Plate," PhD thesis, University of Minnesota, 1959.

APPENDIX 1

Velocity and Temperature Distributions in the Fluid

The approximate similarity of the temperature distribution in the fluid, independent of Prandtl number, is evident in Fig. 5. The temperature excess ratio ϕ is plotted versus distance from the solid-fluid interface for the transient one-dimensional conduction solution for a step in temperature,[4] from the numerical results of Sugawara and Michiyoshi [1] for the transient convection process, and from the steady-state convection solution by Ostrach [8] for the isothermal plate. The curves have been related to a comparable scale by choosing distance scales which result in a common intersection at $\phi = 1/2$.

In Fig. 6 velocity distributions are plotted for a Prandtl number of 1.0 from [8] for steady state and from [1] for the transient. The distribution found by Siegel [3] for the velocity distribution arising during the one-dimensional transient phase of the uniform flux case is also in close agreement with the curve in Fig. 6. The assumption of similarity appears reasonable. Fig. 7 shows how the steady-state velocity distribution depends upon the fluid Prandtl number.

Since neither the temperature nor the velocity distribution may be fitted accurately by simple relations, cf. Figs. 5 and 7, the constants A, B, C, and E were determined by graphical integration of the distributions calculated by Ostrach [8]. These distributions apply to a plate having uniform temperature but are the only detailed information available in the literature. The constants are listed in Table 4. The information available at the present time is insufficient to permit an estimation of the conditions under which these constants may be applied to cylindrical elements.

The thickness parameter F is determined as the ratio of the values of y, in [8], where the velocity and temperature distributions are taken as zero for the evaluation of the constants.

APPENDIX 2

Distributions of ψ, Y, and χ in Steady State

As a result of the assumption that the vertical conduction of heat in the element is negligible, the transient process becomes, in steady state, the uniform-flux boundary-condition problem. Since the convection processes considered are restricted to those which result in a laminar boundary-layer type of flow, the ordinary boundary-layer equations apply when a buoyancy term is added to the force balance. A solution for the vertical flat plate with uniform flux has been presented by Sparrow and Gregg [5]. The conditions for a "similar"[5] solution of the flat-plate boundary-layer equations indicate the following proportionalities:

$$\theta_m \propto x^{1/5} \quad \text{and} \quad u_m \propto x^{2/5}$$

Therefore from equations (9), (7), (8), and (6):

$$\psi \propto Y \propto x^{1/5} \quad \text{and} \quad \chi \propto x^{3/5}$$

[4] M. Jakob, "Heat Transfer," vol. 1, John Wiley & Sons, Inc., New York, N.Y. p. 254.

[5] For a discussion of similarity in this sense see, e.g., p. 116, "Boundary Layer Theory," H. Schlichting, Pergamon Press.

The values of a_1, a_2, a_3, a_4, and a_5 in steady state were evaluated from these distributions and are tabulated in Table 5.

Table 5 Values of the averaging constants

Constant	Steady state	One-dimensional transient	Average values for a step in flux
a_1	36/35	1	1
a_2	288/125	1	1.7
a_3	20/21	1	1
a_4	16/15	1	1
a_5	384/125	1	2.0

The proper representative values of a_1, a_2, a_3, a_4, and a_5 for a transient process depend upon the nature of the flux variation with time. For an element of considerable thermal capacity or for a flux which varies relatively slowly with time the steady-state estimates would apply. For the extreme case of a step in flux and zero-element thermal capacity, average values between the steady-state and the one-dimensional transient are listed in Table 5.

The conditions for a similar solution are not known for either the uniform flux or isothermal vertical-cylinder problems. However, some information is available in recent studies by Hama and Recesso [6] and Hama and Christiaens [7] in which an integral method of analysis was applied to the isothermal vertical-cylinder problem. Equations were obtained which are in agreement with experimental measurements on an approximately isothermal cylinder and on an electrically heated wire (perhaps more nearly a uniform flux). Since the uniform temperature and uniform flux distributions are different (an exponent of $^1/_4$ instead of $^1/_5$) the results of Hama, et al., are used only to indicate under what conditions the flat-plate trends may be assumed to apply for cylinders. The calculations show that the surface coefficient is closely proportional to $1/x^{1/4}$, as for the vertical plate, for

$$N_{Gr}(R/L)^4 > 10^3$$

Therefore one assumes that the flat-plate distributions apply to cylinders in approximately the same range in the uniform-flux case and the constants recommended in the foregoing tables may be applied under these conditions.

APPENDIX 3

Numerical Solution of Transient Convection for a Zero Thermal-Capacity Element

The solution of equations (31) and (32) with boundary conditions was obtained with a Burroughs calculator using a fourth-order Runge-Kutta method and a 10^{-6} tolerance. The time interval varied during the calculation because of the accuracy requirement. Every fourth point calculated was printed out. The results, somewhat abridged, are collected in Table 6.

Table 6 Solutions of natural convection transient for zero storage

$N_{Pr} = 0.01$		$N_{Pr} = 0.1$		$N_{Pr} = 0.72$		$N_{Pr} = 1.0$		$N_{Pr} = 5.0$		$N_{Pr} = 10.0$		$N_{Pr} = 100$		$N_{Pr} = 1000$	
T	$\frac{1}{\Psi}$	T	$\frac{1}{\Psi}$	T	$\frac{1}{\Psi}$	T	$\frac{1}{\Psi}$	T	$\frac{1}{\Psi}$	T	$\frac{1}{\Psi}$	T	$\frac{1}{\Psi}$	T	$\frac{1}{\Psi}$
0.02	0.3278	0.02	0.3278	0.02	0.3278	0.02	0.3278	0.004	0.1466	0.004	0.1466	0.021	0.3358	0.020	0.3277
0.04	0.4627	0.04	0.4627	0.04	0.4626	0.04	0.4626	0.008	0.2074	0.008	0.2074	0.025	0.3663	0.024	0.3589
0.06	0.5645	0.06	0.5645	0.06	0.5642	0.06	0.5642	0.011	0.2432	0.011	0.2432	0.029	0.3943	0.029	0.3943
0.08	0.6477	0.08	0.6477	0.08	0.6470	0.08	0.6469	0.013	0.2643	0.013	0.2643	0.033	0.4204	0.033	0.4204
0.10	0.7177	0.10	0.7175	0.10	0.7163	0.10	0.7161	0.015	0.2839	0.015	0.2839	0.037	0.4449	0.037	0.4449
0.14	0.8271	0.12	0.7748	0.12	0.7747	0.12	0.7744	0.019	0.3195	0.017	0.3022	0.044	0.4846	0.043	0.4791
0.18	0.9037	0.14	0.8266	0.14	0.8237	0.14	0.8233	0.023	0.3514	0.019	0.3166	0.052	0.5258	0.049	0.5107
0.22	0.9546	0.16	0.8683	0.16	0.8643	0.16	0.8639	0.027	0.3806	0.022	0.3437	0.056	0.5450	0.053	0.5306
0.26	0.9858	0.18	0.9028	0.18	0.8948	0.18	0.8971	0.031	0.4077	0.026	0.3736	0.060	0.5634	0.057	0.5496
0.30	1.003	0.20	0.9307	0.20	0.9245	0.20	0.9238	0.035	0.4330	0.030	0.4011	0.064	0.5811	0.061	0.5678
0.34	1.0109	0.24	0.9703	0.24	0.9622	0.22	0.9449	0.043	0.4793	0.034	0.4268	0.068	0.5981	0.065	0.5853
0.38	1.0133	0.28	0.9932	0.28	0.9839	0.24	0.9604	0.051	0.5211	0.038	0.4509	0.072	0.6144	0.069	0.6021
0.42	1.0128	0.32	1.0047	0.32	0.9951	0.26	0.9736	0.063	0.5772	0.044	0.4847	0.076	0.6301	0.077	0.6338
0.46	1.0110	0.36	1.0059	0.36	1.0002	0.28	0.9832	0.079	0.6424	0.052	0.5260	0.082	0.6526	0.081	0.6488
0.50	1.0085	0.40	1.0098	0.40	1.0020	0.30	0.9894	0.095	0.6987	0.060	0.5637	0.090	0.6681	0.089	0.6772
0.58	1.0045	0.48	1.0068	0.48	1.0018	0.34	0.9972	0.111	0.7476	0.068	0.5985	0.098	0.7069	0.097	0.7035
0.66	1.0019	0.56	1.0032	0.56	1.0008	0.38	1.0004	0.127	0.7899	0.076	0.6307	0.106	0.7313	0.105	0.7280
0.74	1.0007	0.64	1.0012	0.64	1.0002	0.42	1.0014	0.151	0.8426	0.088	0.6747	0.114	0.7539	0.115	0.7561
0.82	1.0002	0.72	1.0003	0.72	1.0000	0.46	1.0014	0.183	0.8958	0.104	0.7265	0.122	0.7749	0.123	0.7770
0.90	1.0000	0.80	1.0000	0.80	1.0000	0.50	1.0011	0.215	0.9331	0.120	0.7714	0.130	0.7943	0.131	0.7961
1.06	1.0000	0.96	1.0000			0.58	1.0004	0.247	0.9582	0.136	0.8101	0.138	0.8124	0.147	0.8304
						0.66	1.0001	0.279	0.9746	0.152	0.8433	0.146	0.8290	0.163	0.8596
						0.74	1.0000	0.327	0.9884	0.176	0.8840	0.154	0.8444	0.179	0.8842
						0.82	1.0000	0.391	0.9961	0.208	0.9241	0.166	0.8653	0.195	0.9050
								0.455	0.9988	0.240	0.9514	0.182	0.8893	0.211	0.9223
								0.583	0.9999	0.272	0.9694	0.198	0.9094	0.227	0.9366
								0.711	1.0000	0.304	0.9810	0.214	0.9261	0.243	0.9485
								0.903	1.0000	0.352	0.9909	0.230	0.9400	0.259	0.9582
										0.416	0.9967	0.246	0.9514	0.275	0.9656
										0.480	0.9988	0.262	0.9607	0.291	0.9726
										0.608	0.9998	0.278	0.9683	0.307	0.9779
										0.736	1.0000	0.310	0.9795	0.323	0.9822
										0.928	1.0000	0.342	0.9868	0.347	0.9871
												0.374	0.9915	0.379	0.9917
												0.406	0.9946	0.411	0.9946
												0.438	0.9965	0.443	0.9965
												0.502	0.9986	0.475	0.9978
												0.566	0.9994	0.523	0.9989
												0.662	0.9998		

WILLIAM D. ALLINGHAM

JACK A. McENTIRE

Both: Research Engineer, Boeing Airplane Company, Seattle, Wash. Assoc. Mems. ASME

Determination of Boiling Film Coefficient for a Heated Horizontal Tube in Water-Saturated Wick Material

Using an absorbent wick material saturated with a coolant has become attractive from a design standpoint for some missile-cooling applications. However, published data for predicting film coefficients are very limited. In this study, boiling film coefficients for a 1.0-in. OD horizontal copper tube embedded in water-saturated ceramic fiber-wick material were correlated over a heat-flux range from 1000 to 10,000 Btu per hr sq ft by the dimensionless equation

$$\left(\frac{h}{CG'}\right)\left(\frac{C\mu}{K}\right)^{0.8}\left(\frac{\rho_L\sigma}{P^2}\right)^{0.21} = 0.072\left(\frac{D_eG'}{\mu}\right)^{-0.27}$$

where

$$G' = \frac{Q}{A\epsilon\lambda}$$

The presence of wick material next to a heat-transfer surface decreases turbulence in the region near the surface, increases the effective surface area, and provides active sites for bubble formation. This produces a higher film coefficient at low heat flux than occurs with pool boiling. At higher heat flux, the wick-boiling film coefficient was lower than for pool boiling.

Introduction

RECENT DEVELOPMENTS in the art of using coolants for missile-cooling applications have created a need for predicting boiling film coefficients with wick-covered heat-transfer surfaces. Although the subject of nucleate pool boiling is covered extensively by literature, published data on wick-covered surfaces are very limited.

For missile cooling, heat energy may be absorbed by the change of state of the coolant from liquid to vapor. During long space flights the coolant may be condensed in an externally mounted space radiator and returned to the boiler. For space flights of relatively short duration or during flight at high speeds within the atmosphere, radiative cooling is impractical; expendable coolants having a high latent heat of vaporization must be used. Water is very suitable for this purpose because it is nontoxic, readily available, and has a high latent heat of vaporization.

The requirement for keeping liquid in contact with a heated surface during periods of high acceleration or in the absence of a gravitational field has provided the stimulus for two design approaches, each having certain advantages and limitations. Boilers wherein coolant is vaporized in a confined passage by the transfer of heat from the passage walls are often used but usually require means to store, distribute, and control the flow of coolant.

In an alternative method the control and distribution problems are eliminated by embedding the heat-exchange surface in absorbent wick material that has been saturated with a coolant.

Contributed by the Heat Transfer Division of THE AMERICAN SOCIETY OF MECHANICAL ENGINEERS and presented at the ASME-AIChE Heat Transfer Conference, Buffalo, N. Y., August 15–17, 1960. Manuscript received at ASME Headquarters, May 4, 1960. Paper No. 60—HT-11.

Nomenclature

A = area of boiling heat-transfer surface, ft²
C = specific heat of liquid, Btu/lb deg F
D = diameter, ft
D_e = dimension parameter, ft
G = mass velocity of liquid, lb/hr ft²
$G' = \frac{Q}{A\epsilon\lambda}$, lb/hr ft²
$G'' = \frac{Q}{A\epsilon\lambda}\frac{\rho_L}{\rho_v}$, lb/hr ft²
h = boiling film coefficient, Btu/hr ft² deg F
K = thermal conductivity of liquid, Btu/hr ft deg F
L = length, ft
N_P = pressure number, dimensionless
N_{Pr} = Prandtl number, dimensionless
N_R = Reynolds number, dimensionless
N_{St} = Stanton number, dimensionless
P = absolute pressure, lb/ft²
Q = heat flow, Btu/hr
r_h = hydraulic radius, ft
T = temperature, deg F
W = mass flow, lb/hr
ΔT = temperature difference $(T_w - T_b)$, deg F
ϵ = porosity factor $(1 - \rho_{wi}/\rho_f)$, dimensionless
λ = latent heat of vaporization, Btu/lb
μ = viscosity of liquid, lb/hr ft
ρ = density, lb/ft³
σ = surface tension of liquid, lb/ft
ϕ = proportionality constant, dimensionless

Subscripts

b = boiling
e = exit
f = fiber
i = inlet
L = liquid
o = oil
s = surface
v = vapor
w = wall
wi = wick
1 = unit length

This design is particularly attractive for relatively short flight, because it is possible to store all the coolant within the boiler shell, thus contributing to system simplification and weight saving. As an aid in the design and performance evaluation of coolers of this type, an experimental investigation was conducted to study the mechanism of boiling heat transfer from wick-covered surfaces, and to establish means for predicting boiling film coefficients.

Description of Equipment and Test Procedure

Fig. 1 shows a two-pass shell and the tube heat exchanger used to obtain boiling heat-transfer data. Heat was supplied by hot hydraulic oil (MIL-H-5606A) flowing inside a single, horizontal U tube fabricated from 1.0-in. OD (0.083-in. wall) hard-drawn copper tubing. The tube bundle consisted of two straight tubes 65.0 in. long joined at one end by a 3.0-in. center-to-center 180-deg elbow of the same tubing. To minimize heat loss to the surroundings, the heat-exchanger shell (a 5.0-in. ID cylinder, 70 in. long) and the inlet and exit tubing were insulated with Fiberglas blanket insulation. The shell space surrounding the tube bundle was packed with a water-absorbent wick material (Libby-Owens-Ford "Microglass" unbonded "B" fiber) using a packing density of 6.0 lb per cu ft. Steam was removed through a perforated tube installed parallel to the tube bundle.

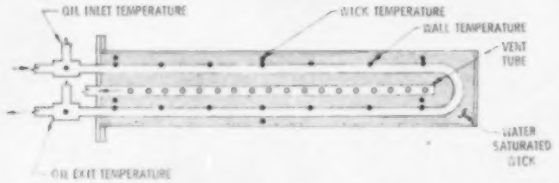

Fig. 1 Experimental boiler used to determine boiling film coefficients with a wick-covered heat-transfer surface

Measurements were taken of the bulk-oil temperature entering and leaving the exchanger using thermocouples installed in mixing sections to obtain an average mixed temperature. Wall temperatures were measured with thermocouples peened to the outer surface of the tube wall at 14 points equally spaced along the tube. Boiling temperature was measured at six equally spaced locations with thermocouples embedded in the wick material about 0.25 in. from the tube wall. All temperature measurements were taken with copper-constantan thermocouples.

A hydraulic test bench consisting of a variable-delivery hydraulic pump, varidrive, reservoir, and necessary controls, was used to circulate heated oil through the U tube. Flow was measured by a turbine-type Fischer and Porter flowmeter, with an electronic frequency counter. Temperatures were recorded continuously with a 48-point Brown recorder. The exhaust duct from the boiler was vented to a vacuum system to maintain a pressure within the boiler corresponding to the selected boiling temperature.

The boiler was flooded with distilled water to saturate the wick and to insure the same degree of wetness at the start of each run. Steady-state temperature, pressure, and flow conditions were obtained as soon as possible to prevent drying of the wick, and the unit was refilled after three experimental points were obtained.

Three boiling temperatures: 120 F, 140 F, and 160 F were selected to evaluate the effect of pressure on the boiling film coefficient. Pressure within the boiler, corresponding to the desired boiling temperature, was adjusted by a valve in the vacuum-exhaust line. Heat flux was varied during successive runs by using three inlet oil temperatures: 200 F, 235 F, and 270 F, in combination with two oil-flow rates: 1.5 and 6.0 gpm.

An effort was made to secure steady-state operation before taking data. Steady-state operation was assumed when the inlet and outlet oil temperatures remained constant for 3 minutes, and temperatures could be recorded twice in sequence without apparent discrepancy between readings. Readings at a given location were separated by a time interval of at least 60 sec.

Analysis

Gilmour [1][1] reports a satisfactory correlation of the nucleate boiling data of a number of investigators with the dimensionless equation

$$\left[\frac{h}{CG}\right]\left[\frac{C\mu}{K}\right]^{0.8}\left[\frac{\rho_L\sigma}{P^2}\right]^{0.425} = 0.001\left[\frac{DG}{\mu}\right]^{-0.3} \quad (1)$$

where

$$G = \frac{W_s\rho_L}{A\rho_v} = \frac{Q\rho_L}{\lambda A\rho_v} \quad (2)$$

Because the physical model presented by a wick-covered surface is decidedly different from that for nucleate pool boiling, the correlation equation for wick-covered surfaces may be expected to be somewhat different. However, it seems reasonable to attempt a correlation for wick-covered surfaces as a function of the same dimensionless groups, i.e., by an equation of the form

$$\left[\frac{h}{CG}\right]^a\left[\frac{C\mu}{K}\right]^b\left[\frac{\rho_L\sigma}{P^2}\right]^c = \phi\left[\frac{DG}{\mu}\right]^d \quad (3)$$

The principal differences between wick and pool boiling are believed to be a function of the mass velocity G and the dimension parameter D_e. To define these differences, a description of a postulated boiling mechanism for wick-covered surfaces is necessary.

An experiment by Comings and Sherwood [2] to demonstrate evaporation in solids offers an explanation of how evaporation occurs at wick-covered surfaces. A glass tube was drawn out to form a tapered capillary several centimeters long, as shown by Fig. 2. This was filled with water and allowed to remain exposed to the atmosphere. It was observed that, as the water evaporated the small meniscus remained stationary at the small end of the tube, while the large meniscus moved progressively from the large toward the small end.

Fig. 3 is a simplified sketch showing how the phenomenon just described may apply to a wick-covered heat-exchange surface. Water evaporates at small menisci formed between randomly

[1] Numbers in brackets designate References at end of paper.

Fig. 2 Evaporation of water from a tapered capillary tube. (Evaporation of liquid causes the meniscus to recede from *A* toward *E*.)

Fig. 3 Enlarged view of wick fibers next to a heated surface. (Water is drawn to the heated surface through tapered capillaries formed by the randomly oriented wick fibers. Steam formed at the heated surface escapes through passages of larger cross section to a region of lower pressure.)

oriented wick fibers near the hot surface. The small curvature of these surface menisci exert sufficient capillary pull to draw liquid through any passages ending in larger menisci. The water vapor generated by the evaporation at the surface is vented to a point of lower pressure, i.e., the vacuum system, through passages of larger cross section where the capillary forces are much smaller.

Flow of liquid in the capillaries is believed to be laminar. This laminar flow phenomenon is in direct contrast with the turbulence resulting from the formation and collapse of vapor bubbles associated with nucleate pool boiling. Gilmour [1] has accounted for the turbulent flow of liquid to fill the void created by vapor bubbles leaving the surface with a density ratio ρ_L/ρ_v in equation (2). The difference in flow near the surface due to the presence of wick fibers should allow elimination of the ratio ρ_L/ρ_v in defining the mass velocity term G for wick boiling. In addition, the presence of fibers near the surface was believed to modify the flow cross section in proportion to a porosity factor ϵ. Therefore the following modified mass velocity term, more suggestive of laminar flow, was used for the data correlation

$$G' = \frac{W_v}{A\epsilon} = \frac{Q}{A\lambda\epsilon} \tag{4}$$

Because only one combination of wick-fiber diameter and packing density was investigated, the significance of the dimension parameter was not demonstrated. However, a consideration of the postulated boiling mechanism suggests that a dimension parameter based on the spacing between fibers is more applicable than a parameter based on some dimension of the heated surface, such as tube diameter. A porosity factor ϵ and dimension parameter D_e, based on an interfiber spacing calculated for the combination of fiber diameter and packing density used in this investigation, are presented in the Appendix.

Assuming the definitions of G' and D_e are valid, correlation of data then consists of determining exponents of the dimensionless groups and the value of ϕ in equation (3). Values of h and Q are obtained from equations (5) and (6), using measured temperatures and flow rates.

$$h = \frac{W_v C_s (T_i - T_s)}{A(T_w - T_b)} \tag{5}$$

$$Q = W_v C_s (T_i - T_s) \tag{6}$$

G' is determined by substituting equation (6) into equation (4). Other parameters needed in the solution of equation (3) are fluid properties, which are available in the literature. All fluid properties used in the correlation are evaluated at boiling temperature.

Results

The method outlined by Gilmour [1] was used to correlate the data. An exponent of unity was chosen for the Stanton number (h/CG') and an exponent of 0.6 for the Prandtl number $(C\mu/K)$. This was considered justified because these exponents are frequently used in heat-transfer correlations involving liquid heating. A plot of the product of these dimensionless groups $(h/CG')(C\mu/K)^{0.6}$ versus Reynolds number (D_eG'/μ) is shown by Fig. 4. The "least squares" line, reference [3], was determined for the plotted data corresponding to each boiling temperature.

Next, the relationship of the pressure number $(\rho_L\sigma/P^2)$ was evaluated by determining the ordinates from each of the three curves of Fig. 4 corresponding to a mean Reynolds number, which was the average of the abscissas of the plotted data. These ordinate values then were plotted versus the reciprocals of pressure numbers calculated for absolute pressures corresponding to the three boiling temperatures (120 F, 140 F, 160 F) represented by the curves. The slope of the plot in Fig. 5 reveals that the reciprocal of the pressure number should have the exponent 0.21.

The dimensionless product, $(h/CG')(C\mu/K)^{0.6}(\rho_L\sigma/P^2)^{0.21}$, then was plotted against Reynolds number as shown in Fig. 6. The slope of the least squares line established an exponent of Reynolds number equal to -0.77. Because the plot is linear, the dimensionless proportionality constant ϕ is equal to the value of $(h/CG')(C\mu/K)^{0.6}(\rho_L\sigma/P^2)^{0.21}$ at $D_eG'/\mu = 1.0$. The value of ϕ was found to be 0.072.

Hence the correlation equation for boiling with the wick-covered heat-exchange surface tested is

$$\left[\frac{h}{CG'}\right]\left[\frac{C\mu}{K}\right]^{0.6}\left[\frac{\rho_L\sigma}{P^2}\right]^{0.21} = 0.072\left[\frac{D_eG'}{\mu}\right]^{-0.77} \tag{7}$$

It is of interest that a correlation for wick boiling also can be obtained by using the density ratio as proposed by Gilmour [1] in determining G, that is

$$G'' = \frac{Q}{A\epsilon\lambda}\frac{\rho_L}{\rho_v} \tag{8}$$

Using this parameter, the data are correlated by the equation

$$\left[\frac{h}{CG''}\right]\left[\frac{C\mu}{K}\right]^{0.6}\left[\frac{\rho_L\sigma}{P^2}\right]^{0.21} = 0.0025\left[\frac{D_eG''}{\mu}\right]^{-0.75} \tag{9}$$

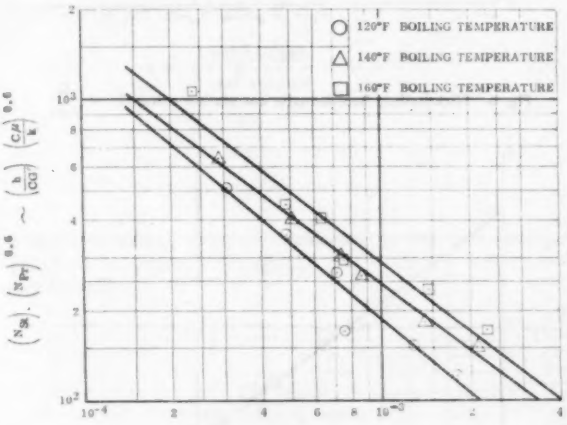

Fig. 4 Plot of $(N_{St})(N_{Pr})^{0.6}$ versus N_R for wick-boiling heat transfer

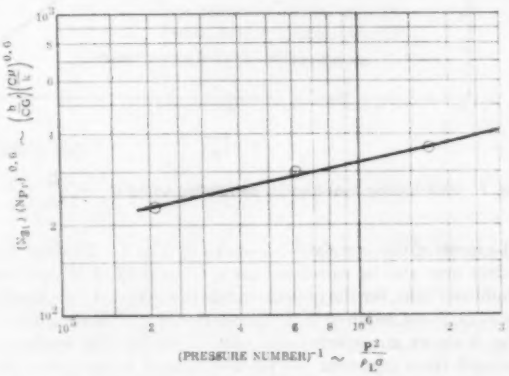

Fig. 5 Cross plot of $(N_{St})(N_{Pr})^{0.6}$ versus $(N_P)^{-1}$ for wick-boiling heat transfer

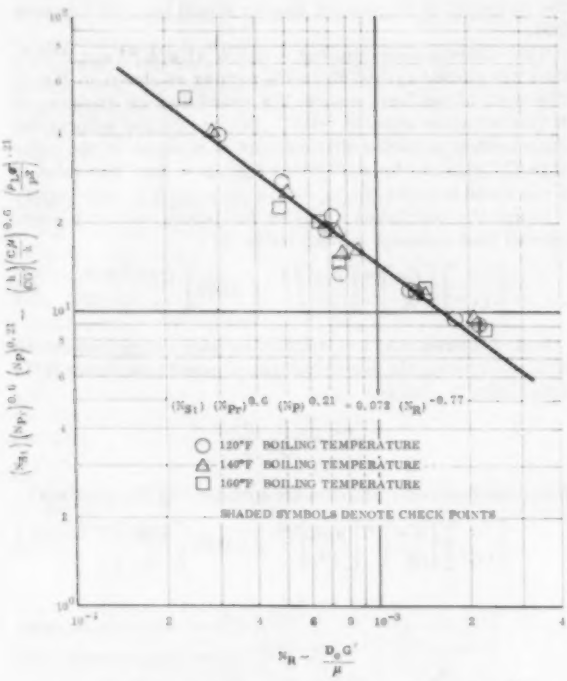

Fig. 6 Wick-boiling heat-transfer correlation using $G' = \frac{Q}{\lambda A_t}$

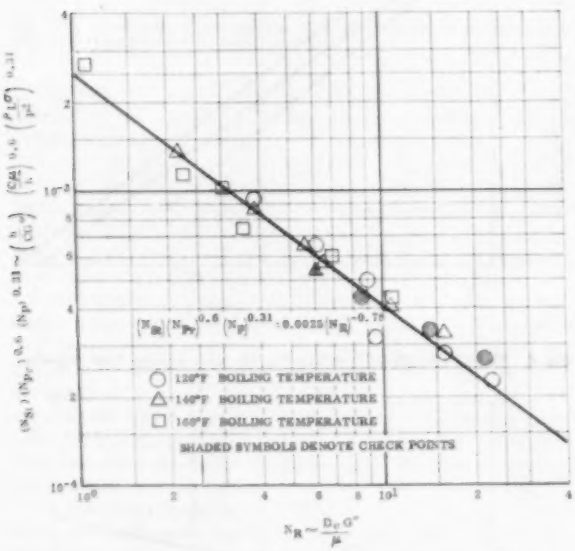

Fig. 7 Wick-boiling heat-transfer correlation using $G'' = \frac{Q}{\lambda A_t}\frac{\rho_L}{\rho_v}$

The result of this correlation is shown by Fig. 7. The fact that the data may also be correlated using G' as defined in equation (4) indicates that, for the pressure range investigated, the density ratio ρ_L/ρ_v is not required in the correlation of wick-boiling data.

Fig. 8 shows an experimental plot of boiling film coefficient calculated from equation (5) plotted against temperature difference ΔT with the analytically derived curves from correlation equation (7) superimposed. The differences between wick and pool boiling can be seen by comparing these curves with the curves for nucleate boiling of Gilmour [1] and Cryder and Finalborgo ([4], p. 309) for a smooth horizontal tube. It can be seen from the slope of the curves that the boiling film coefficient varies directly as $(\Delta T)^{2.3}$ for wick-covered heat-exchange surfaces as compared with $(\Delta T)^{3.3}$ for nucleate pool boiling.

It is of interest that the data of Jakob and Fritz ([4], p. 300) for grooved horizontal plates have a curve of intermediate slope between the curves for pool boiling with smooth tubes and wick boiling. Apparently surface roughness, provided either by grooving the surface or covering it with wick fibers, increases the effective surface area and number of nuclei for bubble formation which would account for the increased boiling film coefficient with wick-covered surfaces at low values of heat flux. At high heat flux, the film coefficient with wick-covered surfaces is lower due to reduction in turbulence and because the flow of vapor away from the surface impedes the capillary flow of fluid to the surface.

Another point of interest is the similarity of the derived equations for nucleate and wick boiling with the equations that correlate turbulent and laminar heating of liquids.

Equation (1) is quite similar in form to the equation ([4], p. 196) for *turbulent* heating of liquids without phase change

$$\left[\frac{h}{CG}\right]\left[\frac{C\mu}{K}\right]^{0.66}\left[\frac{\mu_s}{\mu}\right]^{0.14} = \phi_1\left[\frac{DG}{\mu}\right]^{-0.2} \qquad (10)$$

Also, equation (7), derived in this study for heat exchange from wick-covered surfaces, is quite similar to the equation ([4], p. 196) for *laminar* heating of liquids without phase change

$$\left[\frac{h}{CG}\right]\left[\frac{C\mu}{K}\right]^{0.66}\left[\frac{\mu_s}{\mu}\right]^{0.14} = \phi_2\left[\frac{D}{L}\right]^{0.33}\left[\frac{DG}{\mu}\right]^{-0.66} \qquad (11)$$

This comparison suggests that covering a heat-exchange surface with wick material has the effect of transforming the turbulent heating process associated with nucleate pool boiling into a laminar heating process. This is reasonable, if one considers that the hydraulic radii of the capillary passages between the fibers are extremely small; hence the flow in the capillaries would be expected to be laminar.

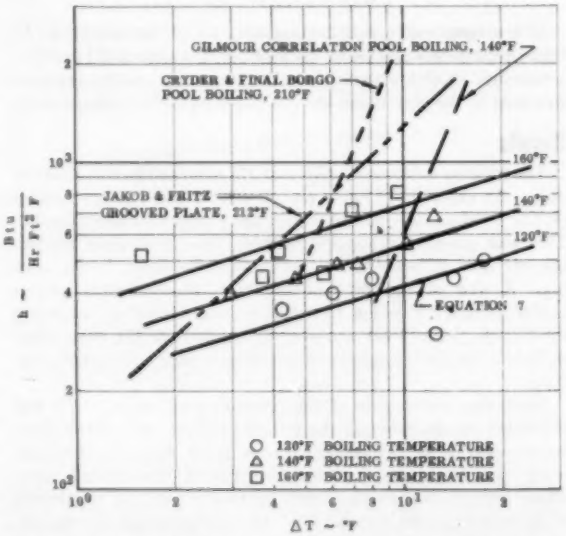

Fig. 8 Comparison of boiling film coefficients for wick boiling and pool boiling

Summary and Conclusions

Wick material adjacent to a heat-transfer surface transforms the turbulent flow process associated with nucleate pool boiling into a laminar flow process. Evidence confirming this was found in the similarity of equation (7) for wick boiling and equation (11) for the laminar heating of liquids without phase change. A similarity was also observed between Gilmour's correlation for nucleate boiling, equation (1), and equation (10) for the turbulent heating of liquids without phase change.

The laminar flow process believed to occur with wick boiling may be due to the small Reynolds number that results from the extremely small hydraulic radii formed by wick fibers next to the heated surface.

At low heat flux, the film coefficient for wick boiling was found to be higher than for pool boiling. This is believed due to the following:

(*a*) Wick fibers increase the effective heat-transfer surface area and provide active sites for bubble formation.

(*b*) The wick fibers greatly increase the ratio of heated surface to liquid volume (this increases the rate of superheat of liquid near the surface, thus aiding the formation of vapor bubbles; with pool boiling at low heat flux, vapor bubbles are not formed rapidly enough to cause much fluid agitation and mixing, hence the film coefficient is lower than with wick boiling).

However, at higher values of heat flux, the film coefficient for wick boiling was lower than for nucleate pool boiling. This may be due to the following:

(*a*) The wick fibers tend to prevent the turbulence and rapid movement of fluid near the surface due to the formation and collapse of vapor bubbles that occurs with nucleate pool boiling.

(*b*) The capillary flow of liquid to the surface is impeded by the counterflow of vapor escaping the surface.

The randomly oriented wick fibers form tapered capillaries having cross sections of various sizes. The flow of liquid to the surface is believed to occur primarily in capillaries of smaller cross section so oriented that their narrow ends terminate at the surface. With evaporation, liquid is drawn toward the small ends of tapered capillaries by the larger surface forces of the more sharply curved menisci. Vapor escapes from the heated surface through passages of larger cross section where the liquid surface forces are much smaller.

The significant dimension parameter for wick boiling is believed to be the width of the capillary passages formed by fibers near the heated surface. The size and orientation of the heated surface would seem to be relatively less important due to the absence of convection currents normally present in pool boiling. Because testing was conducted for only one combination of wick material and metal surface, the effect of changing these parameters was not learned.

APPENDIX

Dimension Parameter, D_e

This derivation includes a sample calculation for the particular combination of wick fiber diameter and packing density used in this study.

Given:

Wick material—unbonded B fiber
Mean fiber diameter, $D_f = 10.4 \times 10^{-6}$ ft (0.00015 in.)
Wick packing density, $\rho_{wi} = 6.0$ lb/ft^3
Glass fiber density, $\rho_f = 162$ lb/ft^3

Fiber volume per unit fiber length

$$V_1 = \frac{\pi}{4} D_f^2 L_1 \tag{12}$$

$$= (0.785)(10.4 \times 10^{-6})^2(1)$$

$$= 8.49 \times 10^{-11} \text{ ft}^3/\text{ft}$$

Fiber weight per unit fiber length

$$W_1 = \rho_f V_1 \tag{13}$$

$$= (162)(8.49 \times 10^{-11})$$

$$= 1.37 \times 10^{-8} \text{ lb/ft}$$

Fiber length per unit volume of wick

$$L_f = \frac{\rho_{wi}}{W_1} \tag{14}$$

$$= \frac{6.0}{1.37 \times 10^{-8}}$$

$$= 4.37 \times 10^8 \text{ ft/ft}^3$$

Fiber surface area per unit volume of wick

$$A_s = \pi D_f L_f \tag{15}$$

$$= (3.14)(10.4 \times 10^{-6})(4.37 \times 10^8)$$

$$= 1.43 \times 10^4 \text{ ft}^2/\text{ft}^3$$

Void volume per unit volume of wick

$$\epsilon = \frac{\text{Void volume}}{\text{Total volume}} = 1 - \frac{\rho_{wi}}{\rho_f} \tag{16}$$

$$= 1 - \frac{6.0}{162}$$

$$= 0.963 \text{ ft}^3/\text{ft}^3$$

Hydraulic Radius. A method analogous to that used for compact heat exchangers (reference [5]) may be used to define a hydraulic radius.

$$r_h = \frac{\epsilon}{A_s} \tag{17}$$

$$= \frac{0.963}{1.43 \times 10^4}$$

$$= 6.73 \times 10^{-5} \text{ ft}$$

Dimension parameter

$$D_e = 4r_h \tag{18}$$

$$= (4)(6.73 \times 10^{-5})$$

$$= 2.69 \times 10^{-4} \text{ ft}$$

References

1 C. H. Gilmour, "Nucleate Boiling—A Correlation," *Chemical Engineering Progress*, vol. 54, no. 10, 1958, pp. 77–79.

2 E. W. Comings and T. K. Sherwood, "The Drying of Solids. VII—Moisture Movement by Capillarity in Drying Granular Materials," *Industrial and Engineering Chemistry*, vol. 26, no. 10, 1934, pp. 1096–1098.

3 W. Volk, "Industrial Statistics," *Chemical Engineering*, vol. 63, 1956, pp. 165–190.

4 W. H. McAdams, "Heat Transmission," McGraw-Hill Book Company, Inc., New York, N. Y., second edition, seventh impression, 1942.

5 W. M. Kays and A. L. London, "Compact Heat Exchangers," National Press, Palo Alto, Calif., 1955, p. 3.

DISCUSSION

J. W. Westwater[2]

Gilmour's equation is a good correlation of data for operating conditions under normal gravity. The correlation contains three dimensionless groups plus a fourth, "pressure group," which is dimensional. Prof. G. M. Dusinberre pointed out, at the Second National Heat Transfer Conference, that this group becomes dimensionless when multiplied by the ratio g/g_c to give $\frac{\rho_L \sigma g}{P^2 g_c}$, where g is acceleration (ft/sec^2) and g_c is the conversion factor $(lb_M)(ft)/(lb_F)$ (sec^2). This ratio is unity for the conditions reported by Allingham and McEntire. It will not be unity for space applications.

Authors' Closure

The authors are indebted to Mr. Gilmour for his pool boiling correlation which suggested a method of correlation for wick boiling. The authors also wish to thank Professor Westwater for his discussion noting Professor Dusinberre's observation that a gravity conversion term should be included in the pressure number to make it dimensionless.

That gravitational force plays an important role in pool boiling heat transfer has been generally recognized and recently demonstrated experimentally. The relative importance of gravitation and surface tension effects appears to be determined by the ratio of liquid volume to wetted surface. Pool boiling occurs normally in containers of appreciable volume with respect to the container surface. In this instance the gravitational force (body force) in the liquid has a major influence on the separation and migration of vapor bubbles from the heated surface. In wick boiling, however, the liquid volumes in the capillary passages formed by the wick fibers are microscopic, and the ratio of surface area to liquid volume, very much greater. Therefore it is the authors' opinion that boiling from wick-covered heated surfaces is influenced primarily by surface tension forces and that the gravitational effect is of minor importance.

The authors agree with Professor Westwater that the validity of the proposed correlation has been demonstrated only for operation at the condition of normal gravity and that further testing is needed to determine the influence of conditions other than normal gravity.

In Fig. 8 of the preprint, the range of the low end of the pool boiling curves was incorrect. A corrected plot appears in this final publication.

---

[2] Professor of Chemical Engineering, University of Illinois, Urbana, Ill.

B. W. SWANSON
E. V. SOMERS
R. R. HEIKES
Mechanics Department, Westinghouse Research Laboratories, Pittsburgh, Pa.

Optimization of a Sandwiched Thermoelectric Device

An analysis is made for optimizing the thermal efficiency of a sandwiched thermoelectric device and is coded for a digital computer. For suitable input data, the computer determines the thermocouple design that approximately maximizes the thermal efficiency of the device. A verification of the analysis indicates that the difference between the approximately optimum efficiency and the optimum efficiency is negligible.

Introduction

Since it is desirable to operate thermoelectric power devices with large temperature drops so that the thermal efficiency is as high as possible, it is necessary to have the thermocouples operate over a large temperature interval. In the present state of material development, no single thermoelectric material is satisfactory for use over the complete temperature range. It is therefore necessary to use different materials in each temperature range. This may be accomplished in two ways: (*a*) The materials may be used in stages such that each stage operates over a fixed temperature interval while being electrically insulated from but thermally in contact with the remaining stages. (*b*) The other method is to form each leg of the couple by joining in series; that is, forming a sandwich structure of the appropriate thermoelectric materials for each range. A typical sandwiched thermoelectric device is shown in Fig. 1. Simplified design equations of a thermocouple of sandwich construction, optimized to approximate the maximum thermal efficiency, were coded for an IBM 704; the equations and an example showing computed results are presented.

Contributed by the Heat Transfer Division of The American Society of Mechanical Engineers and presented at the ASME-AIChE Heat Transfer Conference, Buffalo, N. Y., August 15–17, 1960. Manuscript received at ASME Headquarters, May 19, 1960. Paper No. 60—HT-24.

Statement of Problem

In Fig. 1, n P-type materials $P_1, P_2, \ldots P_n$ are sandwiched to form a positive thermoelectric element P, and n N-type materials are sandwiched to form a negative thermoelectric element N.[1] The hot and cold-junction temperatures are denoted by T_h and T_c, respectively, and the element lengths of each individual sandwich member are denoted by $l_{ij} (i = P, N;\ j = 1, 2 \ldots n)$. Ideally, the interface temperature T_{ij} is the lower temperature limit for material ij and the upper temperature limit for material $ij + 1$. The optimization problem is to maximize the thermal efficiency, subject to specification of the interface temperatures T_{ij}, over-all thermoelectric length L, cross-sectional area A_p, and the temperature-averaged values of material properties α_{ij}, ρ_{ij}, and K_{ij}. Average values of these properties are used since an average parameter approximation has been suitably justified for the case of single P and N-type elements.[2]

Optimization of Efficiency

The reciprocal thermal efficiency is defined as the quotient of the heat rate supplied to the hot junction from the heat source

[1] The number of P and N-type elements need not be equal. They are assumed equal only for convenience in notation.

[2] B. Sherman, R. W. Ure, and R. R. Heikes, "Computation of Efficiency of Thermoelectric Devices," *Journal of Applied Physics*, vol. 31, 1960, p. 1.

Nomenclature

A_i = $i = P, N$ for A_P and A_N; cross-sectional areas of thermoelectric elements
E = circuit voltage produced by cumulative Seebeck effect
ϵ_c = Carnot efficiency, $\epsilon_c = \dfrac{T_h - T_c}{T_h}$
I = current
i = material subscript index
j = position subscript index of segment in thermocouple
K_{ij} = $K_{ij} = \dfrac{\bar{K}_{ij}A_i}{l_{ij}}$, thermal conductance of ij-segment
K_{ij}' = $K_{ij}' = K_{ij}/A_i$, thermal conductance per unit area of ij-segment, equations (7)
L = $L = \sum_{j=1}^{n} l_{pj} = \sum_{j=1}^{n} l_{nj}$, length of thermocouple
l_{ij} = length of ij-segment
M = figure of merit, equation (15)
N_j = negative j-segment (N-type material)
P = external electric power produced by thermocouple
P_j = positive j-element (P-type material)
Q = thermal power added to hot junction from heat source
R = $\begin{cases} R_P + R_N \\ \sum_{i=P,N} \sum_{j=1}^{n} \dfrac{\bar{\rho}_{ij} l_{ij} + r_{cij}}{A_i} \end{cases}$, total resistance internal to thermocouple
R_0 = load resistance external to thermocouple
R_{ij} = $R_{ij} = \dfrac{\bar{\rho}_{ij} l_{ij}}{A_i}$, electrical resistance of ij-segment in thermocouple
R_{ij}' = $R_{ij}' = R_{ij}A_i$, electrical-resistance-area product of ij-segment, equations (7)
r_{cij} = contact-resistance-area product between segment ij and segment $ij + 1$; for $j = 1$; hot-junction resistance-area product is also included
S = convergence index for IBM 704 code
T_h = hot-junction temperature
T_c = cold-junction temperature
T_{ij} = junction temperature between segment ij and segment $ij + 1$; $T_{i0} = T_h$; $T_{in} = T_c$
$\bar{T}_{ij}$ = $\bar{T}_{ij} = \frac{1}{2}(T_{ij-1} + T_{ij})$
ΔT_{ij} = $(T_{ij-1} - T_{ij})$

(Continued on next page)

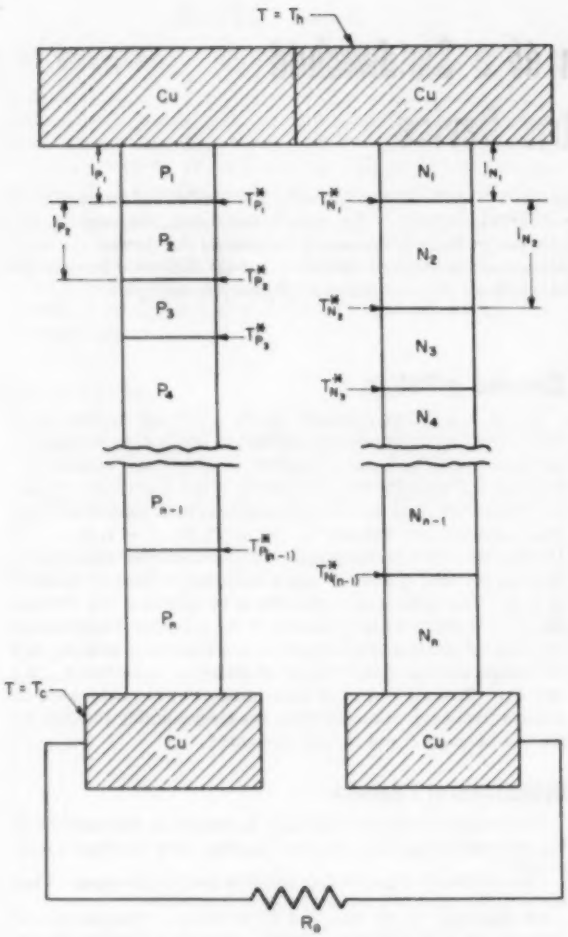

Fig. 1 Sandwiched thermoelectric device

and the electrical power dissipated by the external load.[3] In equation form, the reciprocal efficiency is given by

$$\frac{Q}{P} = \frac{(T_h - T_{P_1})K_{P_1} + (T_h - T_{N_1})K_{N_1} - \frac{I^2}{2}(R_{P_1} + R_{N_1}) + \hat{\pi}I}{I^2 R_0} \tag{1}$$

The terms in the numerator of equation (1) represent the net heat conducted away from the hot junction. It is quickly recognized that the first two terms are simply the normal thermal conductivity process under zero current, while the third term represents that portion of the Joule heat which is returned to the hot junction. The temperatures T_{P_1} and T_{N_1} are the specified interface temperatures between elements P_1 and P_2; and N_1 and N_2, respectively. The terms K_{P_1} and K_{N_1} are the thermal conductances for elements P_1 and N_1; A_P and A_N are the respective cross-sectional areas of the P and N-elements; and l_{P_1} and l_{N_1} are the respective lengths of elements P_1 and N_1. The fourth term in the numerator of equation (1) is the Peltier heat rate absorbed at the hot junction plus the Thomson heat rates generated in elements P_1 and N_1. In equation (1), the current I is given by the equation

$$I = \frac{E}{R + R_0} \tag{2}$$

Here, E is the circuit voltage produced by the cumulative Seebeck effect in the positive and negative elements; the sandwich elements may be compared to batteries connected in series. The voltage E is given by

$$E = \alpha'(T_h - T_c) \tag{3}$$

where the parameter α' is an effective Seebeck coefficient for the sandwiched thermoelement and is made up of temperature-averaged values $\bar{\alpha}_{ij}$ of the individual Seebeck coefficients.

In equation (2), R represents the internal electrical resistance of the sandwich, given by summing the resistances of the individual elements. In the fourth term of equation (1), the coefficient $\hat{\pi}$ is the summing of the Peltier and Thomson effects in the P_1 and N_1-elements, as derived in the Appendix.

[3] A. F. Ioffe, "Semiconductor Thermoelements and Thermoelectric Cooling," Infosearch Limited, London, England, 1957, chapter 2.

Nomenclature

$X = \left(1 + 4M\frac{\hat{\alpha}}{\alpha'}\right)^{1/2}$, equations (18)

y = dimensionless scaling factor, equation (27)

z = dimensionless scaling factor, equation (27)

$\left(\frac{P}{Q}\right)^*$ = optimum value of thermal efficiency

α_{ij} = $\alpha_{ij}(T)$, Seebeck coefficient of ij-segment when at uniform temperature T

$\bar{\alpha}_{ij} = (T_{ij-1} - T_{ij})^{-1}\int_{T_{ij}}^{T_{ij-1}} \alpha_{ij}(T)dT$, average Seebeck coefficient of segment when nonuniform in temperature

$\alpha' = \sum_{i=P,N}\sum_{j=1}^{n} |\bar{\alpha}_{ij}|(T_{ij-1} - T_{ij})/(T_h - T_c)$, effective Seebeck coefficient for sandwiched thermocouple

$\Delta\alpha_{ij}$ = difference in Seebeck coefficients evaluated at the two junction temperatures of the ij-segment

$\hat{\alpha} = |\alpha_{P_1}| + |\alpha_{N_1}| \pm \left|\frac{\Delta\alpha_{P_1}}{2}\right|\frac{T_{P_1}}{T_h} \pm \left|\frac{\Delta\alpha_{N_1}}{2}\right|\frac{T_{N_1}}{T_h}$, effective Seebeck-Thomson coefficient at hot-junction interface; Appendix

$\delta = \frac{R_{P_1} + R_{N_1}}{2R_0}$

κ_{ij} = $\kappa_{ij}(T)$, thermal conductivity of ij-segment when at uniform temperature T

$\bar{\kappa}_{ij} = (T_{ij-1} - T_{ij})^{-1}\int_{T_{ij}}^{T_{ij-1}} \kappa_{ij}(T)dT$, average thermal conductivity of ij-segment when nonuniform in temperature

π_{ij} = Peltier effect at junction between ij and $(ij + 1)$-segments

$\hat{\pi} = \hat{\alpha}T_h$, effective Peltier coefficient at hot-junction interface

ρ_{ij} = $\rho_{ij}(T)$, electrical resistivity of ij-segment when at uniform temperature T

$\bar{\rho}_{ij} = (T_{ij-1} - T_{ij})^{-1}\int_{T_{ij}}^{T_{ij-1}} \rho_{ij}(T)dT$, average electrical resistivity of ij-segment when nonuniform in temperature

θ_P, θ_N = dimensionless temperature, equations (5)

The third term in the numerator of equation (1) is a good approximation to that part of the Joule heat rate generated in elements P_1 and N_1 which returns to the hot junction.

In the denominator, the load power P is represented by I^2R_0, where R_0 is the resistance of the external load. With equation (3) and the definition of $\hat{\alpha}$ substituted into equation (1), the expression for thermal efficiency becomes

$$\frac{Q}{P} = \frac{(T_h - T_{P_1})K_{P_1} + (T_h - T_{N_1})K_{N_1} + \frac{T_h\hat{\alpha}}{R + R_0}E - \frac{E^2(R_{P_1} + R_{N_1})}{2(R + R_0)^2}}{\frac{E^2R_0}{(R + R_0)^2}} \quad (4)$$

With variables θ_P and θ_N defined by the equations

$$\theta_P = \frac{T_h - T_{P_1}}{T_h - T_c}; \quad \theta_N = \frac{T_h - T_{N_1}}{T_h - T_c} \quad (5)$$

and multiplying the numerator and denominator of equation (4) by $(R + R_0)^2$, equation (4) becomes

$$\frac{Q}{P} = \frac{(T_h - T_c)[\theta_P K_{P_1} + \theta_N K_{N_1}](R + R_0)^2 + T_h\hat{\alpha}E(R + R_0) - \frac{E^2}{2}(R_{P_1} + R_{N_1})}{E^2R_0} \quad (6)$$

With the quantities R_P', R_N', K_{P_1}', K_{N_1}', defined by the equations

$$R_P' = R_PA_P; \quad K_{P_1}' = \frac{K_{P_1}}{A_P}$$
$$R_N' = R_NA_N; \quad K_{N_1}' = \frac{K_{N_1}}{A_N} \quad (7)$$

equation (6) becomes

$$\frac{Q}{P} = \frac{(T_h - T_c)[\theta_P K_{P_1}'A_P + \theta_N K_{N_1}'A_N]\left(\frac{R_P'}{A_P} + \frac{R_N'}{A_N}\right)\left(1 + \frac{R_0}{R}\right)\left(1 + \frac{R}{R_0}\right)}{E^2} + \frac{T_h\left(\frac{\hat{\alpha}}{\alpha'}\right)\left(1 + \frac{R}{R_0}\right)}{T_h - T_c} - \frac{(R_{P_1} + R_{N_1})}{2R_0} \quad (8)$$

The general form of equation (8) is

$$\frac{Q}{P} = F\left(\frac{A_N}{A_P}, \frac{R_0}{R}, l_{ij}, \bar{\alpha}_{ij}, \bar{\rho}_{ij}, \bar{\kappa}_{ij}, T_h, T_c, T_{ij}\right) \quad (9)$$

A basic problem associated with the analysis of a sandwiched thermocouple is that an energy-balance boundary condition must be satisfied at each interface between different materials. An inspection of this energy relationship, given in equation (25), reveals that the element lengths are functions of the ratios A_N/A_P and R_0/R; i.e.,

$$l_{ij} = l_{ij}\left(\frac{A_N}{A_P}, \frac{R_0}{R}, \bar{\alpha}_{ij}, \bar{\rho}_{ij}, \bar{\kappa}_{ij}, T_h, T_c, T_{ij}\right) \quad (10)$$

Therefore the partial derivative of Q/P with respect to A_N/A_P is correctly given by

$$\frac{\partial\left(\frac{Q}{P}\right)}{\partial\left(\frac{A_N}{A_P}\right)} = \frac{\partial F}{\partial\left(\frac{A_N}{A_P}\right)} + \sum_i\sum_j \frac{\partial F}{\partial l_{ij}}\frac{\partial l_{ij}}{\partial\left(\frac{A_N}{A_P}\right)} \quad (11)$$

A similar expression exists for the partial derivative of Q/P with respect to R_0/R. The following assumptions are now made:

$$(a) \quad \frac{\partial l_{ij}}{\partial\left(\frac{A_N}{A_P}\right)} = 0$$
$$(b) \quad \frac{\partial l_{ij}}{\partial\left(\frac{R_0}{R}\right)} = 0 \quad (12)$$
$$(c) \quad \frac{R_0}{R} \neq f\left(\frac{A_N}{A_P}\right)$$

An order-of-magnitude analysis of the energy relationship, equation (25), reveals that the element lengths l_{ij} are determined primarily by thermal conduction in the P and N-elements and, therefore, assumptions (a) and (b) are reasonable. The validity of assumption (c), and in fact of all of the assumptions, is established in the section on "Verification of the Analysis."

With the partial derivative of F with respect to A_N/A_P, set equal to zero according to equations (11) and (12), Q/P becomes a minimum for a ratio of the cross sections such that

$$\frac{A_N}{A_P} = \left(\frac{\theta_P K_{P_1}'R_N'}{\theta_N K_{N_1}'R_P'}\right)^{1/2} \quad (13)$$

With equation (13), equation (8) becomes

$$\frac{Q}{P} = \frac{[(\theta_{P_1}R_P'K_{P_1}')^{1/2} + (\theta_N R_N'K_{N_1}')^{1/2}]^2\left(1 + \frac{R_0}{R}\right)\left(1 + \frac{R}{R_0}\right)}{(\alpha')^2(T_h - T_c)} + \frac{T_h\left(\frac{\hat{\alpha}}{\alpha'}\right)\left(1 + \frac{R}{R_0}\right)}{T_h - T_c} - \frac{(R_{P_1} + R_{N_1})}{2R_0} \quad (14)$$

With the figure of merit M defined as

$$M = \frac{(\alpha')^2T_h}{4[(\theta_PR_P'K_{P_1}')^{1/2} + (\theta_NR_N'K_{N_1}')^{1/2}]^2} \quad (15)$$

equation (14) becomes

$$\frac{Q}{P} = \frac{T_h\left(1 + \frac{R_0}{R}\right)\left(1 + \frac{R}{R_0}\right)}{4M(T_h - T_c)} + \frac{T_h\left(\frac{\hat{\alpha}}{\alpha'}\right)\left(1 + \frac{R}{R_0}\right)}{(T_h - T_c)} - \frac{(R_{P_1} + R_{N_1})}{2R_0} \quad (16)$$

With the partial derivative of Q/P with respect to R_0/R set equal to zero, again according to equation (12) the numerator of equation (16) is minimized for the ratio

$$\frac{R_0}{R} = \left(1 + 4M\,\frac{\hat{\alpha}}{\alpha'}\right)^{1/2} \tag{17}$$

Finally, with R_0 and R adjusted to satisfy equation (17), the thermal efficiency is approximately optimized with equation (12) to be

$$\left(\frac{P}{Q}\right)^* = \epsilon_c\,\frac{X-1}{\left(\frac{\hat{\alpha}}{\alpha'}\right)(X+1) - \delta\epsilon_c(X-1)} \tag{18}$$

where

$$X = \left(1 + 4M\,\frac{\hat{\alpha}}{\alpha'}\right)^{1/2}$$

$$\delta = \frac{R_{P_1} + R_{N_1}}{2R_0}$$

$$\epsilon_c = \frac{T_h - T_c}{T_h}$$

Optimum Design Problem

Design Equations. The optimum design problem may now be stated as follows: Given the values of $\bar{\alpha}_{ij}$, $\bar{\rho}_{ij}$, $\bar{\kappa}_{ij}$, r_{cij}, ΔT_{ij}, T_h, T_c, A_P, and L determine the values of A_N, l_{ij}, R, R_0, I, and $(P/Q)^*$.

Solution of this problem requires that the following equations be satisfied:

$$I = \frac{\alpha'(T_h - T_c)}{R + R_0} \tag{19}$$

$$\frac{A_N}{A_P} = \left(\frac{\theta_P K_{P_1}' R_N'}{\theta_N K_{N_1}' R_P'}\right)^{1/2} \tag{20}$$

$$\frac{R_0}{R} = \left(1 + 4M\,\frac{\hat{\alpha}}{\alpha'}\right)^{1/2} \tag{21}$$

$$M = \frac{(\alpha')^2 T_h}{4[(\theta_P K_{P_1}' R_P')^{1/2} + (\theta_N K_{N_1}' R_N')^{1/2}]^2} \tag{22}$$

$$L = \sum_{i=1}^{n} l_{pi} = \sum_{i=1}^{n} l_{ni} \tag{23}$$

$$R = \sum_{i=P,N} \sum_{j=1}^{n} \frac{\bar{\rho}_{ij} l_{ij} + r_{cij}}{A_i} \tag{24}$$

$$\overset{\text{Joule}}{\tfrac{1}{2}\left(\frac{I}{A_i}\right)^2} \bar{\rho}_{ij} l_{ij} + \overset{\text{Joule}}{\tfrac{1}{2}\left(\frac{I}{A_i}\right)^2} \bar{\rho}_{ij+1} l_{ij+1} + \overset{\text{Joule}}{\left(\frac{I}{A_i}\right)^2} r_{cij} \pm \overset{\text{Thomson}}{\left(\frac{I}{A_i}\right)\frac{|\Delta\alpha_{ij}|}{2}}\,\bar{T}_{ij} \tag{25}$$

$$\pm \overset{\text{Thomson}}{\left(\frac{I}{A_i}\right)\frac{|\Delta\alpha_{ij+1}|}{2}}\,\bar{T}_{ij+1} \pm \overset{\text{Peltier}}{\pi_{ij}\left(\frac{I}{A_i}\right)} + \overset{\text{Conduction}}{\frac{\bar{\kappa}_{ij}\Delta T_{ij}}{l_{ij}}} = \overset{\text{Conduction}}{\frac{\bar{\kappa}_{ij+1}\Delta T_{ij+1}}{l_{ij+1}}}$$

$$\left(\frac{P}{Q}\right)^* = \frac{\epsilon_c(X-1)}{\left(\frac{\hat{\alpha}}{\alpha'}\right)(X+1) - \delta\epsilon_c(X-1)} \tag{26}$$

Equation (25) is an energy balance for the interface between elements ij and $ij+1$. It states that the amount of energy flowing to the interface, plus or minus the amounts of energy generated or absorbed at the interface, is equal to the amount of energy flowing from the interface. One half of the Joule effects in elements ij and $ij+1$ is assumed to flow to this interface. One half of the Thomson effects in these elements is assumed to flow to or away from the interface depending on the source or sink nature of these effects. The interface Joule effect due to contact resistance is a source term, and the interface Peltier effect may be a source or sink term. The last two terms in the equation are the conduction terms which give the approximate amounts of heat conducted to and away from the interface.

Numerical Scheme (IBM 704). This design problem may now be solved by the following iteration method which has been coded for an IBM 704:

Step

(*a*) Calculate $\bar{\alpha}_{ij}$, $\bar{\kappa}_{ij}$, $\bar{\rho}_{ij}$ per definitions in Nomenclature.
(*b*) Calculate $\bar{\alpha}'$, α, θ_P, θ_N.
(*c*) Obtain initial estimates of l_i from the equations

$$\frac{\bar{\kappa}_{ij}\Delta T_{ij}}{l_{ij}} = \frac{\bar{\kappa}_{ij+1}\Delta T_{ij+1}}{l_{ij+1}}; \quad L = \sum_{j=1}^{n} l_{ij}.$$

(*d*) Calculate R_P', R_N', K_{P_1}', K_{N_1}'.
(*e*) Calculate A_N/A_P from equation (20) and A_N.
(*f*) Calculate M from equation (22).
(*g*) Calculate R_0/R from equation (21).
(*h*) Calculate R from equation (24).
(*i*) Calculate R_0.
(*j*) Calculate I from equation (19).
(*k*) Calculate a new set of l_{ij} from equation (25):

- (*k*-1) Assume l_{P_1}.
- (*k*-2) Solve for l_{Pj} from equation (25).
- (*k*-3) Check if $\sum_{j=1}^{n} l_{Pj} = L$.
- (*k*-4) Repeat steps (*k*-1) to (*k*-3) until $\sum_{j=1}^{n} l_{Pj} = L$.
- (*k*-5) Repeat steps (*k*-1) to (*k*-3) for l_{nj}.

(*l*) Repeat steps (*d*) through (*k*) until $|I - I_4| < 10^{-S}$ where S is specified convergence index.
(*m*) Compute R_{P_1}, R_{N_1}, and δ.
(*n*) Compute (P/Q) from equation (26) or from equation (1).

Efficiency Independent of Geometry. Suppose that this analysis has been carried out for $L = 1$ cm and $A_P = 1$ cm^2 and let the symbol $\langle\ \rangle$ about a parameter denote its value for this case. Now consider the effect of multiplying each l_{ij} by some factor z and the area A_P by some factor y. First, it is noted that the ratio A_N/A_P and the figure of merit M are not changed since the factor z appears in the denominator of K_{P_1}', K_{N_1}', and in the numerator of R_P' and R_N'. Therefore A_N is multiplied by y and the internal resistance R, with contact resistance disregarded, can be written as

$$R = \left(\frac{z}{y}\right) \sum_{i=P,N} \sum_{j=1}^{n} \frac{\bar{\rho}_{ij} l_{ij}}{A_i} = \left(\frac{z}{y}\right)\langle R\rangle \tag{27}$$

Since the ratio R_0/R is also independent of z and y, R_0 will be multiplied by z/y, and the current I becomes

$$I = \frac{\alpha'(T_h - T_c)}{\left(\frac{z}{y}\right)[\langle R\rangle + R_0)]} = \left(\frac{y}{z}\right)\langle I\rangle \tag{28}$$

Now, for the case of no contact resistance, it is observed that each term of equation (25) will be multiplied by $1/z$, since

$$\frac{I}{A_i} = \frac{y}{z}\frac{\langle I\rangle}{yA_i} = \frac{1}{z}\left\langle \frac{I}{A_i}\right\rangle \tag{29}$$

and all lengths l_{ij} are multiplied by z. Furthermore, equation (26) also holds since all terms, including δ, are not affected by y or z. Therefore equations (19) through (22) also hold for a device with the modified parameters $y\langle A_i\rangle$, $z\langle l_{ij}\rangle$, and $z/y\langle R_0\rangle$. Moreover,

$$\left\langle \frac{l_{ij}}{L}\right\rangle = \frac{zl_{ij}}{zL}$$

$$\left\langle \frac{A_N}{A_P}\right\rangle = \frac{yA_N}{yA_P} \tag{30}$$

$$\left\langle \frac{R_0}{R}\right\rangle = \frac{(z/y)R_0}{(z/y)R}$$

Thus it has been shown that the optimization yields a set of "approximately optimum" ratios A_N/A_P, l_{ij}/L, R_0/R, and that any values of A_P and L can be used to determine them. This means that the approximately optimum efficiency without contact resistance is independent of the specific geometry of the device and is a function only of its material properties, the source and sink temperatures, and the optimum geometrical ratios. For the case when $L = z$ cm and $A_P = y$ cm^2, the load power I^2R_0 becomes

$$I^2R_0 = \left(\frac{y}{z}\right)^2\langle I\rangle^2\left(\frac{z}{y}\right)\langle R_0\rangle = \left(\frac{y}{z}\right)\langle I^2R_0\rangle \tag{31}$$

Thus the load power developed is y/z times the power produced in a device with unit length and area.

Code Description and Numerical Example

An example of a thermoelectric device considered is shown in Fig. 2. The P-type elements are designated as P_1, P_2, P_3, and the N-types as N_1 and N_2. In general, the thermoelectric properties α_{ij}, ρ_{ij}, and κ_{ij} are temperature-dependent. The variation of these properties with temperature is fed into the computer in the form of tabular functions, and the computer averages these properties over their respective temperature ranges, as defined in the Nomenclature. The average values of these properties are given in Table 1. Besides the temperature dependence of these properties, the computer requires the following information:

(*a*) Hot-junction temperature... $T_h = 880$ deg K
(*b*) Cold-junction temperature.. $T_c = 300$ deg K
(*c*) Interface temperatures..... $T_{P_1} = 720$ deg K;
$T_{P_2} = 420$ deg K;
$T_{N_1} = 420$ deg K
(*d*) Over-all length..... $L = 1$ cm
(*e*) Area of P-elements..... $A_P = 1$ cm^2
(*f*) Contact resistances..... $r_{c_{ij}} = 0$
(*g*) Convergence factor..... $S = 2$

With this information, the computer runs through the iteration method described earlier, and solves for the optimum thermal efficiency and the optimum design parameters. The optimum solution for the example is given in Table 2.

Verification of Analysis

The thermal efficiency can be obtained from equation (8) without recourse to the optimizing criteria. If the ratios A_N/A_P and R_0/R are specified, along with the parameters $\bar{\alpha}_{ij}$, $\bar{\rho}_{ij}$, $\bar{\kappa}_{ij}$, T_h, T_c, T_{ij}, A_P, and L, the thermal efficiency of a sandwiched couple can be obtained from equation (8) and equations (19), (23), (24), and (25). Thus it is possible to use the analysis to "optimize" a sandwich thermocouple, go "off-optimum" not using equations (12) with respect to the ratios A_N/A_P and R_0/R, calculate the thermal efficiency, and compare this efficiency with the predicted optimum. Such a subprogram has been built into the code and provides a method for verifying the analysis. The off-optimum

Table 1 Average values of parameters

Location	ρ, ohm-cm	κ, watts/cm deg C	α, volts/deg C	ΔT, deg C
P_1	0.00053	0.04636	0.000154	160
P_2	0.00361	0.01258	0.000226	300
P_3	0.00074	0.01861	0.000159	120
N_1	0.00405	0.01342	0.000231	460
N_2	0.00130	0.01453	0.000212	120

Table 2 Optimum design data for numerical example

l_{P_1}/L	0.551
l_{P_2}/L	0.291
l_{P_3}/L	0.158
l_{N_1}/L	0.772
l_{N_2}/L	0.228
A_N/A_P	1.985
R_0/R	1.376
$(P/Q)^*$	0.1148
R	0.00318 ohm
R_0	0.00438 ohm
I	32.135 amp
P	4.5 watts

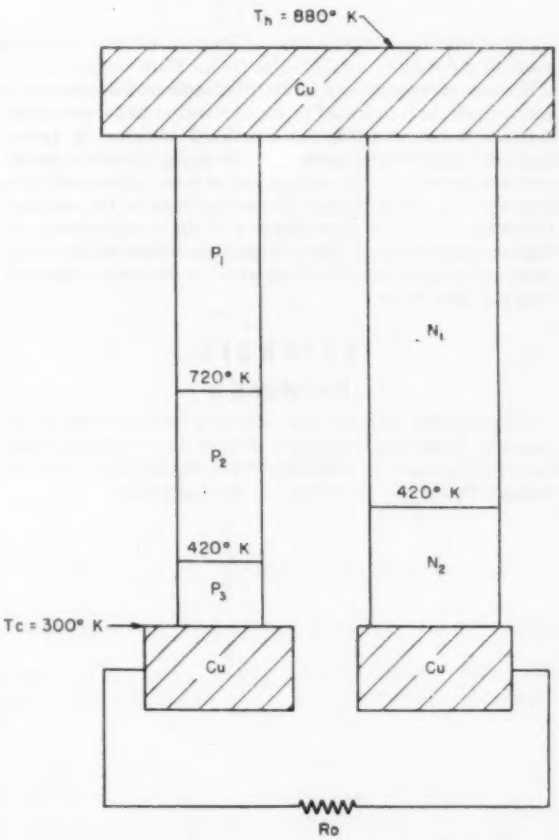

Fig. 2 Sandwiched device for numerical example

Table 3 Off-optimum values of efficiency versus R_0/R for $A_N/A_P = 1.985$

Per cent of optimum R_0/R	P/Q
10	0.04199
70	0.11263
80	0.11422
90	0.11485
95	0.11490
98	0.11485
100 (optimum)	0.11480
102	0.11472
105	0.11457
110	0.11424
120	0.11332
130	0.11213
200	0.10091
300	0.08517

Table 4 Off-optimum values of efficiency versus A_N/A_P for $R_0/R = 1.376$

Per cent of optimum A_N/A_P	P/Q
10	0.04601
70	0.11228
80	0.11384
90	0.11461
95	0.11476
98	0.11480
100 (optimum)	0.11480
102	0.11478
105	0.11473
110	0.11457
120	0.11402
130	0.11325
200	0.10498
300	0.09215

values of efficiency for the numerical example are given in Tables 3 and 4.

Because of assumptions made, the optimization analysis is approximate, as is indicated by the fact that at 95 per cent of the optimum value of R_0/R, the calculated efficiency is greater than the approximately-optimum efficiency. However, an off-optimum analysis of this couple, and of many others that have been studied, indicates that the assumptions in the optimum analysis yield a good approximation to the exact optimum efficiency, and the approximately optimum values of the design parameters A_N/A_P and R_0/R are close to the exact optimizing values of these ratios.

APPENDIX

Derivation of $\hat{\alpha}$

The parameter $\hat{\alpha}$ is an effective Seebeck coefficient for the hot junction. It includes the Seebeck effect at the hot-junction interface plus the source or sink character of the Thomson effects in elements P_1 and N_1. The latter effects are given by

$$\pm \frac{|\Delta\alpha_{P_1}|}{2} \frac{\bar{T}_{P_1}}{T_h} \quad \text{and} \quad \pm \frac{|\Delta\alpha_{N_1}|}{2} \frac{\bar{T}_{N_1}}{T_h}$$

and their derivation follows.

The Thomson effect is given by the term

$$I\mu \frac{dT}{dx}\, dx \quad \text{or} \quad I\mu dT$$

Since the Thomson coefficient varies with temperature, an average value $\bar{\mu}$ is to be used, where

$$\bar{\mu} = \frac{\int_{T_c}^{T_h} T\left(\frac{d\alpha}{dT}\right) dT}{T_h - T_c}$$

If the variation of α with T is assumed to be linear, $d\alpha/dT$ becomes a constant $C = \Delta\alpha/\Delta T$. Then

$$\bar{\mu} = c\frac{\int_{T_c}^{T_h} T dT}{T_h - T_c} = \frac{c\left.\frac{T^2}{2}\right|_{T_c}^{T_h}}{\Delta T}$$

$$\bar{\mu} = c\frac{(T_h^2 - T_c^2)}{T_h - T_c} = c\frac{(T_h + T_c)}{2} = \frac{\Delta\alpha}{\Delta T}\frac{(T_h + T_c)}{2}$$

Since to a good approximation, one half of the Thomson heat affects the hot junction, $\bar{\mu}$ becomes

$$\frac{\bar{\mu}}{2} = \tfrac{1}{2}\frac{\Delta\alpha}{\Delta T}\frac{(T_h + T_c)}{2} = \frac{\Delta\alpha}{\Delta T}\frac{\bar{T}}{2}$$

and

$$(\bar{\mu}/2)\Delta T = (\Delta\alpha/2)\bar{T}$$

The Thomson effects for elements P_1 and N_1 are thus given by

$$\frac{|\Delta\alpha_{P_1}|}{2}\frac{(T_h + T_{P_1})}{2}$$

and

$$\frac{|\Delta\alpha_{N_1}|}{2}\frac{(T_h + T_{N_1})}{2}$$

The term $\hat{\alpha}T_h$ gives the over-all sink effect at the hot junction, where

$$\hat{\alpha}T_h = (|\alpha_{P_1}| + |\alpha_{N_1}|)T_h \pm \frac{|\Delta\alpha_{P_1}|}{2}\bar{T}_{P_1} \pm \frac{|\Delta\alpha_{N_1}|}{2}\bar{T}_{N_1}$$

and thus

$$\hat{\alpha} = |\alpha_{P_1}| + |\alpha_{N_1}| \pm \frac{|\Delta\alpha_{P_1}|}{2}\frac{\bar{T}_{P_1}}{T_h} \pm \frac{|\Delta\alpha_{N_1}|}{2}\frac{\bar{T}_{N_1}}{T_h}$$

THEODORE R. GOODMAN
Principal Engineer,
Allied Research Associates, Inc.
Boston, Mass.

The Heat-Balance Integral—Further Considerations and Refinements

Integral methods have previously been applied to transient heat conduction in a slab with constant thermal properties. In this paper the method is extended so as to include temperature-dependent thermal properties in the analysis. In addition, it is shown how to improve the accuracy of a solution by increasing the order of the polynomial used to represent the temperature profile. For the case of a prescribed step surface temperature in a semi-infinite slab, a quartic profile is shown to give excellent accuracy.

Introduction

THE heat-balance integral mentioned in the title is an integral of the transient heat-conduction equation in a solid and is analogous to the momentum integral in boundary-layer theory. The use of an integral method in transient heat-conduction problems was first presented by Goodman [1].[1] It was further exploited by Reynolds and Dolton [2], Goodman [3], Yang and Szewczyk [4], and Goodman and Shea [5]. The purpose of the present paper is to extend the method by showing how to (*a*) use integral methods when the thermal properties are temperature-dependent, and (*b*) improve the accuracy obtainable from integral methods by increasing the order of the polynomial which describes the temperature profile. In using an integral method there is never a unique procedure to follow, and the ultimate criterion for determining whether or not a particular procedure is successful must involve an assessment of both its accuracy and simplicity. The technique presented here results in a relatively simple analysis; furthermore, the accuracy is certainly acceptable for engineering purposes as will be confirmed by comparing a particular solution obtained using the method with its exact counterpart.

Analysis

The simplest way to present the refinements mentioned in the title is by way of example. For this purpose, consider a semi-infinite slab initially at zero temperature which consists of a material whose thermal properties are temperature-dependent. At the surface, either the heat flux or the temperature is prescribed.

The differential equation for the temperature $u(x, t)$ together with the two sets of boundary conditions are:

$$\rho c \frac{\partial u}{\partial t} = \frac{\partial}{\partial x}\left(k \frac{\partial u}{\partial x}\right), \quad x > 0 \tag{1}$$

$$\left.\begin{aligned} u(x, 0) &= 0, \quad x > 0 \\ u(\infty, t) &= 0, \quad t > 0 \end{aligned}\right\} \tag{2}$$

for prescribed surface temperature:

$$u = u_s, \quad x = 0 \tag{3a}$$

for prescribed surface heat flux:

$$\left(k \frac{\partial u}{\partial x}\right)_s = -H(t), \quad x = 0 \tag{3b}$$

Both k and ρc are assumed to be temperature-dependent. The designations *a* and *b* will continue to refer, respectively, to the case of prescribed surface temperature and prescribed surface heat flux.

At this point, a transformation of the dependent variable is made which is the key to the entire analysis which follows. Let

$$v = \int_0^u \rho c \, du \tag{4}$$

The quantity v is a one-to-one function of the temperature u. In terms of v, Equations (1) to (3) become, respectively,

$$\frac{\partial v}{\partial t} = \frac{\partial}{\partial x}\left[\zeta(v) \frac{\partial v}{\partial x}\right] \tag{5}$$

$$\left.\begin{aligned} v(x, 0) &= 0, \quad x > 0 \\ v(\infty, t) &= 0, \quad t > 0 \end{aligned}\right\} \tag{6}$$

$$v = v_s, \quad x = 0 \tag{7a}$$

$$\left(\frac{\partial v}{\partial x}\right)_s = -H(t)/\zeta_s, \quad x = 0 \tag{7b}$$

In accordance with the method as presented by Goodman [1],

[1] Numbers in brackets designate References at end of paper.

Contributed by the Heat Transfer Division and presented at the Summer Annual Meeting, Dallas, Texas, June 5–9, 1960, of THE AMERICAN SOCIETY OF MECHANICAL ENGINEERS. Manuscript received at ASME Headquarters, January 12, 1960. Paper No. 60—SA-9.

Nomenclature

A = dimensionless parameter involved in quartic profile, see Equation (18)
c = specific heat
H = surface heat flux
k = thermal conductivity
t = time
u = temperature
v = see Equation (4)
x = distance into the solid measured from surface
$y = x\sqrt{\rho c/2}\sqrt{k_0 t}$
α = constant in linear temperature variation of thermal conductivity $\left[k = k_0\left(1 + \alpha \frac{u}{u_s}\right)\right]$
δ = thermal layer at which temperature and heat flux remain unaltered
θ = see Equation (10)
ζ = diffusivity $(k/\rho c)$
ρ = mass density
$(\,)_0$ = initial value
$(\,)_s$ = surface value (at $x = 0$)

define a thermal layer δ at which $v(\delta, t) = 0$, $\frac{\partial v}{\partial x}(\delta, t) = 0$. By differentiating $v(\delta(t), t) = 0$, with respect to t and applying Equation (5) it can readily be shown that $\frac{\partial^2 v}{\partial x^2}(\delta, t) = 0$. This additional derived constraint on the profile may be termed a "smoothing" condition. These three conditions at $x = \delta$ plus Equation (7) at $x = 0$ are sufficient to define a cubic profile which evidently must take the form:

$$v = v_s(1 - x/\delta)^3 \tag{8a}$$

$$v = (H\delta/3\zeta_s)(1 - x/\delta)^3 \tag{8b}$$

Now, integrate Equation (5) from $x = 0$ to $x = \delta$ and apply Equations (8). The resulting heat-balance integrals are:

$$\frac{d\theta}{dt} = 3\zeta_s v_s/\delta \tag{9a}$$

$$\frac{d\theta}{dt} = H(t) \tag{9b}$$

where, in both cases,

$$\theta = \int_0^\delta v\,dx \tag{10}$$

Substitute Equations (8) into Equation (10), and use the results in Equations (9). This yields the following differential equations for δ:

$$\frac{d}{dt}\left(\frac{v_s\delta}{4}\right) = \frac{3\zeta_s v_s}{\delta} \tag{11a}$$

$$\frac{d}{dt}\left(\frac{H\delta^3}{12\zeta_s}\right) = H \tag{11b}$$

Notice that only the thermal properties at the surface enter the problem. The solution of these equations, subject to the initial condition $\delta(0) = 0$, is

$$\delta = \frac{2\sqrt{6}}{v_s}\left[\int_0^t \zeta_s v_s^2 dt\right]^{1/2} \tag{12a}$$

$$\delta = 2\sqrt{3}\left[\frac{\zeta_s}{H}\int_0^t H dt\right]^{1/2} \tag{12b}$$

Equations (4), (8a), and (12a) comprise the solution for prescribed surface temperature in terms of quadratures. For prescribed surface heat flux, on the other hand, the thermal layer δ is not determined from Equation (12b) because the diffusivity at the surface ζ_s is given in terms of the surface temperature which is not yet known. However, v_s may be determined in terms of δ from Equation (8b) by setting $x = 0$. Upon eliminating δ between the resulting equation and Equation (12b) there results the following transcendental equation for v_s:

$$\zeta_s v_s^3 = \frac{4}{3} H \int_0^t H dt \tag{13}$$

Once v_s has been determined as a function of time by solving Equation (13), the complete solution is given by Equations (4), (8a), and (12b).

An Example

Now, suppose the prescribed surface temperature is a step, so that v_s is constant. This problem has been solved exactly by Yang [6] and his results will be used to assess the accuracy of the integral approach. Since ζ_s depends solely on v_s, ζ_s is also constant, and Equation (12a) reduces to

$$\delta = 2\sqrt{6\zeta_s t} \tag{14}$$

Substituting into Equation (8a), there is obtained

$$\frac{v}{v_s} = \left[1 - \frac{x}{2\sqrt{6\zeta_s t}}\right]^3 \tag{15}$$

Suppose now that ρc is constant. By virtue of Equation (4), v is then proportional to u. At the same time, let $k = k_0(1 + \alpha u/u_s)$ describe the temperature variation of the thermal conductivity. It follows that $\zeta_s = k_s(1 + \alpha)/\rho c$. Let $y = x\sqrt{\rho c}/2\sqrt{k_s t}$, and Equation (15) then becomes

$$\frac{u}{u_s} = \left[1 - \frac{y}{\sqrt{6(1 + \alpha)}}\right]^3 \tag{16}$$

The symbols y and α are defined precisely as was done by Yang [6]. This closed form solution is plotted in Fig. 1 and compared with Yang's exact solution. The accuracy is comparable to that obtained by Yang and Szewczyk [4], who also solved the problem using an integral technique; but the differential equation for the time dependence can be solved in closed form in the present instance and is, therefore, much simpler. Also shown in Fig. 1 is a comparison between $-\frac{d}{dy}\left(\frac{u}{u_s}\right)_{y=0}$ as calculated exactly by Yang [6] and as calculated approximately from Equation (16). The heat flux at the surface is directly proportional to this quantity.

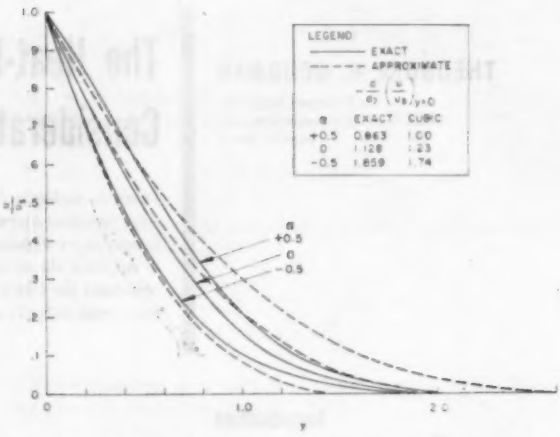

Fig. 1 Comparison of approximate and exact temperature profiles for step surface temperature using cubic profile

Improving the Accuracy

The problem of a prescribed surface temperature step with constant ρc will now be used to illustrate how the accuracy of a solution may be improved by using a higher-order polynomial for the profile. In particular, a quartic will be used. This introduces another constant into the profile, thereby requiring an additional constraint. Instinctively, one would probably derive another smoothing condition at $x = \delta$, and require that $\frac{\partial^2 v}{\partial x^2}(\delta, t) = 0$. However, instinct would be wrong, for this condition actually makes the resulting solution worse than the one obtained from a cubic profile. On the other hand, if the boundary condition at the other end of the interval, Equation (7a), is differentiated with respect to time, and then the time derivative is eliminated by

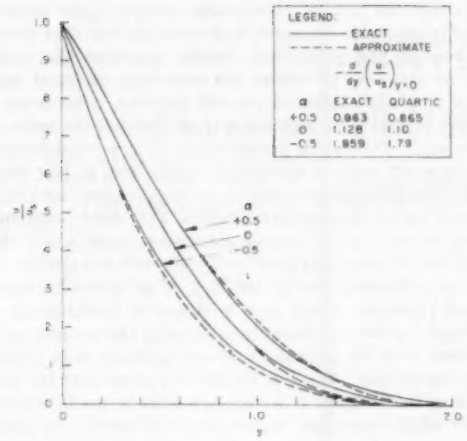

Fig. 2 Comparison of approximate and exact temperature profiles for step surface temperature using quartic profile

using Equation (5), the following alternate condition at $x = 0$ is obtained:

$$\zeta_s \left(\frac{\partial^2 v}{\partial x^2}\right)_s + \left(\frac{\partial v}{\partial x}\right)_s^2 \left(\frac{d\zeta}{dv}\right)_s = 0 \qquad (17)$$

The highest-order derivative involved in this constraint is the second, whereas the third derivative was involved in the unacceptable smoothing condition. It has been found that using Equation (17) will definitely improve the results. This fact is an illustration of the following fundamental rule:

> In selecting a derived constraint at one end of the interval in order to determine an additional constant in the profile, the accuracy will be improved only if preference is given to the one which involves the lower order derivative. If the highest-order derivative involved in both possibilities is the same, then the choice is arbitrary.[1]

A comment must be added, namely, that this rule is to be followed whenever possible. There are cases when it is impossible to follow, and this will become clarified as the example of the prescribed surface temperature step is carried out.

Assume, then, a quartic of the form

$$\frac{v}{v_s} = \frac{u}{u_s} = A(1 - x/\delta)^3 + (1 - A)(1 - x/\delta)^4 \qquad (18)$$

and substitute into Equation (17). This results in a quadratic for A, the pertinent solution to which is

$$A = \frac{3 + 7\alpha - \sqrt{3(3 + 7\alpha)(1 + \alpha)}}{\alpha} \qquad (19)$$

Notice that A vanishes for $\alpha = -3/7$. For A to vanish is equivalent to the condition $\frac{\partial^2 v}{\partial x^2}(\delta, t) = 0$, and this is precisely the smoothing condition that was previously discarded in favor of Equation (17). Thus when $\alpha = -3/7$, Equation (17) and the smoothing condition are both satisfied by the quartic profile.

[1] Although the author originally presented this rule without justification, K. T. Yang [7] pointed out that the rule is probably correct because what we mainly wish to accomplish by approximating the actual profile by an arbitrary assumed one is a good check on the profile values themselves, and that deviations would definitely become increasingly larger if successive derivatives are compared. Thus it is more important to satisfy a condition associated with a lower-order derivative.

It is to be expected, therefore, that the quartic profile will be most accurate for $\alpha = -3/7$ since at that point an additional constraint has automatically been satisfied. Now it is inconceivable that this very pinnacle of accuracy should likewise be the threshold of the mathematical breakdown of the entire solution. But for $-1 < \alpha < -3/7$, A is complex and the resulting solution has no meaning. In order to circumvent this difficulty it is proposed that for α in this range the fundamental rule be discarded, since it is impossible to follow, and the smoothing condition be applied instead. Thus for α in this range A will be taken to be identically zero.

It is conjectured that the simultaneous occurrence of the mathematical breakdown of the solution and the automatic satisfaction of the alternate constraint is not accidental, but that, for any general problem involving an integral method, if the solution breaks down mathematically somewhere it will necessarily be at the point where the alternate constraint is automatically satisfied. The proper way to continue the solution into the forbidden region then, is to retain the alternate constraint and ignore the original constraint, thus, in effect, discarding the fundamental rule. The remainder of the analysis may be carried out in a manner quite similar to that used for the cubic profile. The final result is

$$\frac{u}{u_s} = A\left[1 - y\sqrt{\frac{4 + A}{10(4 - A)(1 + \alpha)}}\right]^3 + (1 - A)\left[1 - y\sqrt{\frac{4 + A}{10(4 - A)(1 + \alpha)}}\right]^4 \qquad (20)$$

where A is given by Equation (19) for $\alpha \geq -3/7$, and $A = 0$, for $-1 < \alpha < -3/7$. This solution is shown in Fig. 2, together with the exact solution of Yang. Also shown is the quantity $-\frac{d}{dy}\left(\frac{u}{u_s}\right)_{y=0}$. These results constitute a considerable improvement over those obtained using a cubic profile as may be confirmed by comparing with Fig. 1.

References

1 T. R. Goodman, "The Heat-Balance Integral and Its Application to Problems Involving a Change of Phase," TRANS. ASME, vol. 80, 1958, pp. 335–342.

2 W. C. Reynolds and T. A. Dolton, "Use of Integral Methods in Transient Heat-Transfer Analysis," ASME Paper No. 58—A-248 (1958).

3 T. R. Goodman, "The Heating of Slabs With Arbitrary Heat Inputs," *Journal of Aero/Space Sciences*, vol. 26, 1959, pp. 187–188.

4 K. T. Yang and A. Szewczyk, "An Approximate Treatment of Unsteady Heat Conduction in Semi-Infinite Solids With Variable Thermal Properties," JOURNAL OF HEAT TRANSFER, TRANS. ASME, Series C, vol. 81, 1959, pp. 251–252.

5 T. R. Goodman and J. J. Shea, "The Melting of Finite Slabs," *Journal of Applied Mechanics*, vol. 27, TRANS. ASME, Series E, vol. 82, 1960, pp. 16–24.

6 K. T. Yang, "Transient Conduction in a Semi-Infinite Solid With Variable Thermal Conductivity," *Journal of Applied Mechanics*, vol. 25, TRANS. ASME, vol. 80, 1958, pp. 146–147.

7 K. T. Yang, personal communication, 1959.

DISCUSSION

K. T. Yang[1]

The author is to be complimented on adding another piece of work to the literature on the application of integral procedures to unsteady heat-conduction problems. His explicit use of the transformation, Equation (4), which reduces the original heat-condition equation to a diffusion equation with concentration-

[1] Associate Professor, Department of Mechanical Engineering, University of Notre Dame, Notre Dame, Ind. Assoc. Mem. ASME.

dependent diffusion coefficient, is extremely valuable since it decreases the mathematical complexity of the problem greatly.

However, it is rather unfortunate that the author demonstrates the increased accuracy of using the Pohlhausen's fourth-degree temperature polynomial on the basis of comparison of results with only one exact solution. Whether or not this conclusion is still valid for arbitrary surface-temperature or surface heat-flux variations has yet to be shown, especially in view of the fact that in laminar boundary-layer theory it is well known that using higher-order profile polynomials in integral procedures does not necessarily improve their accuracy. Furthermore, in a problem where the surface heat flux is prescribed, the alternate condition, which corresponds to Equation (17) and is obtained by evaluating Equation (5) at $x = 0$, complicates the analysis greatly, and simple expressions like Equations (12*b*) and (13) are no longer obtainable. In addition, a limiting condition as $t \to 0$, which is necessary to carry out the solution and similar to that indicated in reference [4] of the paper, has to be established.

There is no doubt in the discusser's mind that the integral procedure represents a potential tool for dealing with general unsteady conduction problems. However, for general problems of variable thermal properties, with and without moving boundaries, of finite plates with different boundary conditions including surface convection and radiation, of composite slabs, with cylindrical or spherical symmetry, or even of two-dimensional and three-dimensional unsteady conduction, many details of the integral procedure have not yet been established; and it is certain that the analyses involved would not be as simple as those already shown in the literature, including those by the author, though the procedure may still enjoy a definite advantage over the purely numerical solutions. Therefore it seems that much more has to be done in order to fully establish this procedure in conduction calculations.

Author's Closure

The history of integral methods is replete with attempts to improve the accuracy of the original Pohlhausen one parameter approach. Among these attempts are the use of higher order polynomials to represent the profile and also a two parameter method together with an additional weighted integral equation. These methods have usually yielded better accuracy; but sometimes, as Professor Yang points out, the accuracy becomes demonstrably worse. Nevertheless, it is certainly desirable to use the least primitive profile available. Even though it can be shown that the accuracy obtainable using a higher order polynomial occasionally decreases, it is certainly true that increasing the order of the polynomial usually improves the accuracy. Since no alternate procedure has ever been proposed together with a proof that the accuracy will improve, it behooves us to try the simplest thing first, namely, to increase the order of the polynomial. If it can be demonstrated by numerical comparison with an exact solution that the accuracy does in fact improve, then we must accept the result as an improvement for this problem and others of a similar nature. This demonstration does not, of course, tell us the circumstances under which the accuracy will improve and those under which it will become worse, and this is entirely due to the lack of an adequate theory of integral methods. Until such a theory is forthcoming, there will remain a certain arbitrariness in using the method, and any argument over the superiority of one approach over another is purely subjective. What is needed is a proof that the integral procedure as we know it is the first step in an iteration procedure which converges to the exact solution. In addition, there is required an estimate of the error introduced by stopping after the nth iteration. But even if these shortcomings were overcome the arbitrariness would still remain because, as in all iteration procedures, there is no rule for making the initial guess, and the initial guess itself characterizes the usual integral method completely. Nevertheless, one would have the assurance that the error could be made as small as desired regardless of the assumption about the profile, merely by carrying out the iteration procedure to a sufficient number of steps. Mathematicians, instead of pursuing this fruitful line of inquiry, have tended to pooh-pooh the method entirely by pointing out that almost any answer can be obtained by choosing a profile which is sufficiently outlandish. This criticism is true, of course, but it avoids the problem instead of solving it. Engineers are wiser, and in their bungling way stick with the method despite lack of rigor. The introduction of integral methods to transient heat conduction problems constitutes not only a practical engineering tool, but also, since the heat conduction equation is just about the simplest conceivable equation for which the integral method can be used, it introduces the prototype equation for integral methods in general. Thus, the heat conduction equation is a logical proving ground for mathematicians to introduce rigor into the integral method. These statements are not meant as a refutation of Professor Yang's last paragraph, but rather as an underscoring of it. Let us hope the mathematicians will heed this clarion call and join us for, surely, they cannot lick us.

Effect of Aspect Ratio and Tube Orientation on Free Convection Heat Transfer to Water and Mercury in Enclosed Circular Tubes[1]

FLOYD W. LARSEN
FluiDyne Engineering Corporation, Minneapolis, Minn. Mem. ASME

JAMES P. HARTNETT
Professor, Mechanical Engineering Department, University of Minnesota, Minneapolis, Minn. Mem. ASME

Free convection heat transfer to water and to mercury in a circular tube closed at the bottom end, open to a cooled reservoir at the top, and heated through the wall with a uniform heat flux, has been investigated with emphasis on the effect of length-to-radius ratio and tube inclination. Dimensionless wall and fluid temperatures are presented for several tube inclinations over a range of imposed dimensionless heat fluxes to a tube of length-to-radius ratio 14.6; these results are compared to earlier measurements in a tube of length-to-radius ratio 21.0.

Over the range of the investigation the flow was apparently in fully mixed turbulent motion, as evidenced by the large fluid temperature fluctuations recorded during the tests. Inclination of the tube was found to result in a considerable decrease in temperature fluctuations and a corresponding increase in heat transfer above that observed with the tube axis vertical.

Introduction

THE STUDY of free convection in enclosed spaces has been prompted by present day interest in the fields of nuclear power and gas turbines. Application in the nuclear reactor might be the emergency removal of heat, in the event of pump breakdown. Also, a knowledge of heat transfer in this geometry is necessary for consideration of transient cooling of large structural parts when analyzing thermal stresses. In addition, the possibility of internal cooling of gas turbine blades has been of considerable interest for quite some time due to the increased efficiency possible if only hotter gases could be used than are presently tolerated by uncooled blades. A convective fluid contained in radial holes in the turbine blades leading to a heat sink in the hub would cool the blades due to the circulation of the fluid brought on by density differences in the fluid under the influence of the centripetal acceleration of the rotating system.

Free convection heat transfer to a variety of fluids in enclosed tubes (commonly called thermosyphon tubes) has been investigated at length by a number of authors. Most of these analytical and experimental investigations pertain to a uniform wall temperature condition. Martin and his co-workers [1, 2][2] have presented results for fluids of widely varying Prandtl numbers (air, water, glycerine), tested in tubes of length-to-radius ratio ranging from 7.5 to 47.5. At moderate values of the Rayleigh number, these results showed reasonable agreement with the approximate analysis of Lighthill [3] for laminar flow which predicted "similarity," "nonsimilarity," and laminar boundary-layer regimes. For high values of the Rayleigh numbers, Martin reported turbulent results which showed that fluids of high Prandtl number yielded dimensionless heat transfer superior to fluids of Prandtl number near unity.

Hartnett and Welsh studied the free convection to water in an enclosed tube with a constant wall heat flux boundary condition [4] and found good agreement with the constant wall temperature results of Martin. This constant heat flux investigation was extended to the use of mercury as a working fluid and included the influence of inclining the tube from the vertical. A significant increase in heat-transfer performance was reported when the tube containing mercury was inclined 30 deg from the vertical [5].

Martin and Cresswell [6] also have recently reported results for water and ethylene glycol in an inclined tube. The performance with water (Prandtl number of 2 to 10) as the convective

[1] Publication from Heat Transfer Laboratory, University of Minnesota.

Contributed by the Heat Transfer Division and presented at the Summer Annual Meeting, Dallas, Texas, June 5–9, 1960, of THE AMERICAN SOCIETY OF MECHANICAL ENGINEERS. Manuscript received at ASME Headquarters, March 3, 1960. Paper No. 60—SA-21.

[2] Numbers in brackets designate References at end of paper.

Nomenclature

$a = \frac{\rho^2 \beta c g}{k\mu}$ = fluid property grouping, $\frac{1}{\text{ft}^3 \text{ deg F}}$

c = specific heat of fluid, Btu/lb deg F

$g = 4.17 \times 10^8 \frac{\text{ft}}{\text{hr}^2}$ = gravitational constant

$h = \frac{q}{t - t^*}$ = heat-transfer coefficient, Btu/hr ft^2 deg F

k = thermal conductivity of fluid, Btu/hr ft deg F

k_w = thermal conductivity of wall

L = tube length, ft

q = heat flux density, Btu/hr ft^2

r = tube radius, ft

Δr_w = wall thickness

t = local wall temperature, deg F

t_f = local fluid temperature

t^* = center-line fluid temperature entering mouth of tube

x = distance from bottom, ft

β = volumetric thermal expansion coefficient of fluid, 1/deg F

θ = tube inclination angle

ρ = density of fluid, lb/ft^3

μ = viscosity of fluid, lb/ft hr

Nu = hr/k = Nusselt number

Pr = $c\mu/k$ = Prandtl number

Ra = $(t - t^*)ar^3 \cos\theta$ = Rayleigh number

RaNu = $a(r^4 q \cos\theta)/k$ = Rayleigh-Nusselt product

fluid was reported to increase with inclination of the tube, while that using the high Prandtl number fluid, ethylene glycol (Pr = 15 to 250), decreased as the tube was inclined.

It was the major goal of the present research to determine in detail the quantitative effect of the angle of inclination and the length-to-radius ratio of the tube on heat transfer for a constant wall heat flux boundary condition and to compare these results for two fluids of widely differing Prandtl number, water and mercury.

Apparatus

The mild steel tube shown in Fig. 1 constructed for the first phase of the free convection program was 21¼ in. long, 2.000 in. ID, and 2.500 in. OD. The tube was machined to tolerances of ±0.002 in. for the diameter dimensions and ±0.005 in. for concentricity of diameters. A reservoir of 6-in. depth and 6-in. diameter was welded to the upper end of the tube and a ⅛-in. thick plug was inserted in the lower end of this tube. This base plug fitted into the bottom of the tube to a distance of ¼ in. thereby making the inside length of the tube 21 in. (from the upper side of the base plug to the bottom level of the reservoir base plate). A heat sink was provided in the reservoir in the form of a helically bent stainless-steel cooling coil. Circulation of cooling water through this tube allowed the control of temperature level at which the system came to steady state.

At twelve axial positions along the tube, longitudinal slots of ⅛-in. width, ⅛-in. depth, and 1-in. length were milled into the outer surface of the tube wall, allowing the installation of thermocouples. As a result, leads from the thermocouples pass away from the junctions through a moderate temperature gradient, thus minimizing conduction errors. Mild steel plugs of identical dimensions were inserted over the thermocouple installations to maintain uniformity of the wall. Nichrome heating wire in fiberglass insulation was then tightly wound about the outside of the tube. Six heater sections covered equal lengths of the 21-in. test section. Four longitudinal segments of molded 85 per cent magnesia insulation, 1-in. thick, were applied over the heaters with the heater and thermocouple leads passing out radially between the segments.

The thermocouple probe utilized to measure fluid temperatures in the tube consisted of three 30-gage iron-constantan steel-sheathed thermocouple leads incased in a 0.215-in. OD stainless-steel tube as shown in Fig. 1. One thermocouple junction of this probe was located at the tube center line while the other two were located at radii of 0.45 and 0.90 in., to allow measurement of the radial temperature distribution. Sealing of the thermocouple junctions and tube was accomplished with porcelain cement. The probe was adjusted axially by moving a cross member along two upright rods located atop the reservoir.

The tube and reservoir were placed in an insulating box filled with rockwool insulation, Fig. 2. Thermocouples were installed in the base plug and a guard heater was positioned beneath the plug. By careful monitoring of the plug temperature distribution, the appropriate guard heater input was maintained to insure an adiabatic boundary condition along the base of the tube.

In the mercury program, the reservoir was sealed to allow evacuation of the space above the mercury surface. After evacuation, the space was filled with helium and maintained at a pressure of about one psig with a permanent connection to a pressure regulator and helium tank to prevent oxidation of the mercury. The small leakage of helium and mercury vapor from the reservoir lid and the teflon sliding probe seal was trapped in a sheet metal housing from which hoses lead to a blower exhausting outside the building. Removal of the reservoir lid after high temperature runs revealed no oxidation of the mercury surface.

Individual power inputs to the heaters were controlled by variable autotransformers. A calibrated wattmeter measured the input power to each heater when plugged into the respective wattmeter connection switch. A calibrated Leeds and Northrop Speedomax Recorder was used to record the thermocouple emfs. Samples of both the wall and probe thermocouples were calibrated for the temperature range anticipated.

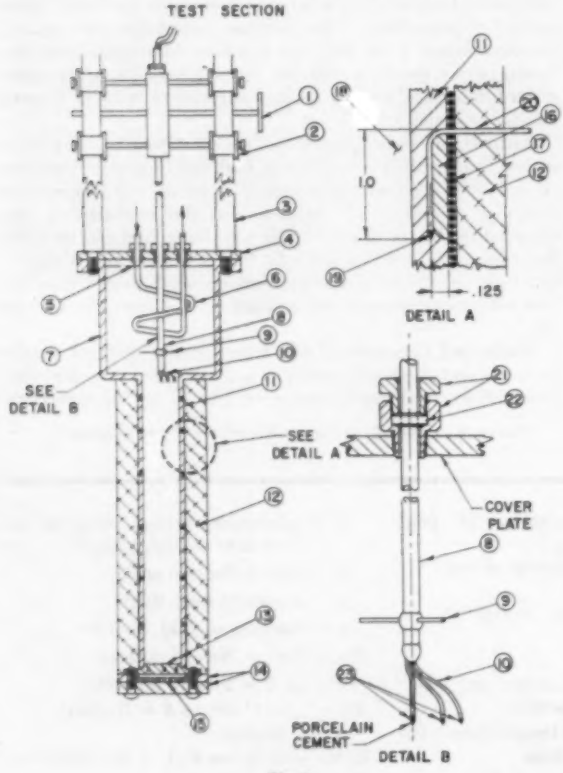

Fig. 1

Number on figure	
1	Probe adjusting wheel
2	Rollers (4)
3	Upright rods
4	Reservoir cover
5	Convective fluid level
6	Cooling coil, approximately 13 feet of ¼-in. stainless steel tubing
7	Reservoir, steel, 6-in. ID by 6 in. deep
8	Probe tube, stainless steel
9	Spacers (3) 120 degrees apart
10	Probe thermocouples (3), steel sheathed iron constantan
11	Tube, steel, 21 or 14.6 in. long
12	Insulation, 85 per cent magnesia, 1-in. thick
13	Bottom plug, steel
14	Guard-heater holder, transite
15	Guard-heater
16	Wall thermocouple plug, steel
17	Wall heaters, 0.040-in. Nichrome wire in fiberglass sleeve
18	Convective fluid
19	Wall thermocouple junction
20	Iron-constantan thermocouple lead in fiberglass insulation
21	Steel fittings
22	Sliding probe seal, teflon
23	Thermocouple junctions, at center line and radii of 0.45 and 0.90 in.

For the runs in the tube of length-to-radius ratio equal to 14.6, the tube was simply shortened and replugged. This, of course, eliminated a few of the lower wall thermocouples and the bottom two heaters. The probe arrangement for the shortened tube was the same as above, but the probe tube diameter was 0.110-in. OD and only a center line thermocouple was used.

Procedure

Before the 2.000-in-diameter tube was installed in the free convection system as described in the Apparatus Section, it was fully instrumented and subjected to a forced convection test using water as the working fluid to validate the test procedure. The results, as reported in Ref. [4], covered a range of Reynolds numbers from 79,000 to 348,000 and agreed within 10 per cent, except for three points (which were within 20 per cent), with the conventional turbulent relationship of Nusselt number as a function of the Reynolds and Prandtl numbers.

After completion of this check-out program and assembly of the test section as shown in Fig. 1, the water tests were initiated. When the water tests in the 21.0-in. test section were completed, the tube was completely drained and cleaned in preparation for the mercury tests.

Throughout the tests in the 21.0-in. and 14.6-in. test sections, uniform wall heat fluxes were supplied by the heaters, and cooling was accomplished by means of a steady flow of water through the cooling coil in the reservoir. After approximately six hours of steady operation, the system was found to be at steady state (actually quasi-steady state, since a true steady state was never attained) allowing readings of the thermocouples to be taken for the run. Because of the fluctuating flow in the tube, steady thermocouple readings were never obtained, and all wall and fluid temperature readings were time-averaged values.

Experimental Results

The product of this paper is mainly the wall and fluid temperatures occurring throughout the test section as a function of the imposed heat input and the entering fluid temperature t^*. (It is assumed that t^* will be known; if this is not the case, Ref. [3] gives a method for estimating it for some geometries.) This relationship has been investigated for both mercury (Pr = 0.014 to 0.024) and water (Pr = 2 to 8) in two tubes of different length-to-radius ratios, with the tube in both the vertical and in inclined positions.

The temperatures will be presented in dimensionless form as Rayleigh numbers[5] defined as:

$$\mathrm{Ra} = (t - t^*)\, a \cos\theta\, r^3$$

The dimensionless heat input is shown as the product of the Rayleigh and Nusselt numbers:

$$\mathrm{RaNu} = \frac{a \cos\theta}{k} r^4 q$$

Fluid properties used to form these parameters were evaluated at the temperature of the fluid entering the tube from the reservoir t^*.

The term, $\cos\theta$, appears in the above groups since an inspection of the governing differential equations reveals that it is the axial *component* of the gravitational acceleration (see Fig. 2) which enters these dimensionless parameters

A. Water

1. Length-to-Radius Ratio of 14.6

a. Local Wall Temperature. Rayleigh numbers were calculated from temperatures indicated by each of two sets of four thermocouples located along the wall of the 14.6-in. test section. One set is located along the upper edge of the test section, the other along the lower edge, Fig. 2. Thermocouple temperatures for typical water and mercury runs are shown in Fig. 3. When

[5] The Rayleigh number will be recognized as the product of the Grashof and Prandtl numbers; the dimensionless temperatures can be represented by either the Rayleigh or the Grashof numbers, the choice being arbitrary.

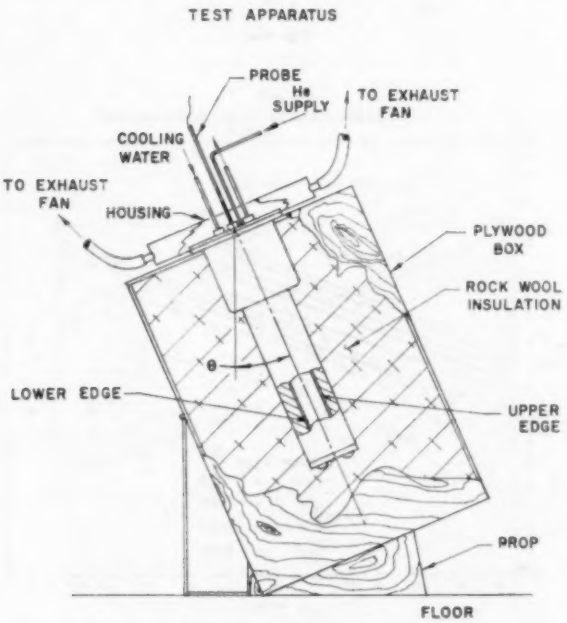

Fig. 2

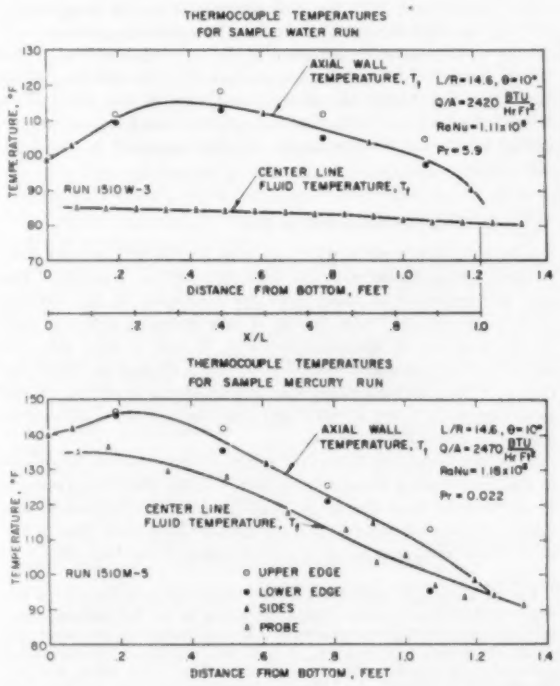

Fig. 3

forming Rayleigh numbers, these temperatures were, of course, first corrected for temperature drop through the wall assuming simple radial heat flow.[4] Rayleigh numbers thus obtained for several of the runs taken with each of the inclinations 0, 5, 10, 20, and 45 degrees are plotted in Figs. 4(*a* and *b*) as a function of the dimensionless heat input RaNu, for four different positions along the tube. Upon examining this presentation, the large initial effect of tilting the apparatus is evident, maximum wall temperature values along the tube for fixed RaNu, in each case being reduced about 30 per cent by inclining only 5 deg.

Also illustrated by these figures is the fact that the temperatures along the upper edge exceed those along the lower edge when the tube is inclined and that the difference increases with increasing inclination over the range of angles studied. This suggests that the upward and downward moving fluid streams are separated, such that the upward moving heated fluid is concentrated along the upper edge allowing the entering cooler stream to flow downward close to the lower edge.

b. Fluid Temperature. Temperatures measured with the thermocouple probe along the center line of the tube are reported for vertical runs in Fig. 5. The $L/r = 21.0$ data also shown in this figure will be discussed in a later section. The dimensionless presentation used here is Ra_f versus RaNu which essentially gives the fluid temperature as a function of the wall heat flux for four separate axial positions. Several points also appear in this figure which represent fluid temperatures in the tube tilted at 30 deg. It is seen that these points lie an order of magnitude below those of the vertical runs. Because of these much smaller temperature differences, of the order of two degrees, scatter becomes too great to allow further meaningful presentation. However, these relatively low fluid temperatures do give further evidence of the increased heat-transfer performance to be obtained by tilting the tube from the vertical position; apparently such tilting results in an increased circulation of the fluid, thereby accounting for a decrease in the fluid temperature when compared at a fixed heat input with the vertical geometry.

As was noticed with the wall temperatures, the temperature field in the fluid is characterized by the generally unstable condition of decreasing temperature in the upward direction. This places the more dense fluid above that of lower density, which thereby brings about the motion occurring in the tube. This motion was not a steady flow but rather a random one as suggested by the time-temperature records measured in the fluid, Ref. [5].

2. Length-to-Radius Ratio of 21.0

The runs taken with water at this length-radius ratio were entirely accomplished with the tube in a vertical position. The wall temperatures of these runs are compared to the vertical tests in the 14.6-in. tube in Fig. 6 (the mercury data are also shown and will be discussed below). It can be seen that the performance is changed considerably by a change in length-to-radius ratio; dimensionless wall temperatures observed in the long tube reach values about 75 per cent higher than in the shorter tube at a given RaNu value.

Fluid temperatures measured in the longer tube are presented in Fig. 5 allowing a direct comparison with the short tube results. It can be seen from this figure that the fluid temperature in this longer test section reaches a much higher value than that in the shorter one when compared at a fixed value of wall heat flux.

[4] It is recognized that there exists temperature gradients in the wall which are not purely radial, particularly for the inclined tube runs. Rigorously this means that the conductance of the tube wall enters into the performance; indeed an additional dimensionless parameter, $k_w \Delta r_w / kr$, characterizes this effect. Its value was approximately constant at 17 for the water and 1.1 for the mercury tests.

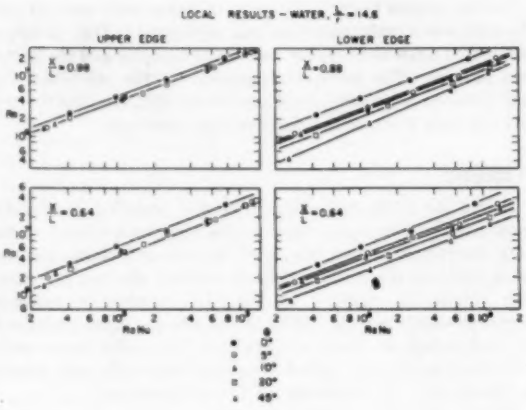

Fig. 4(a)

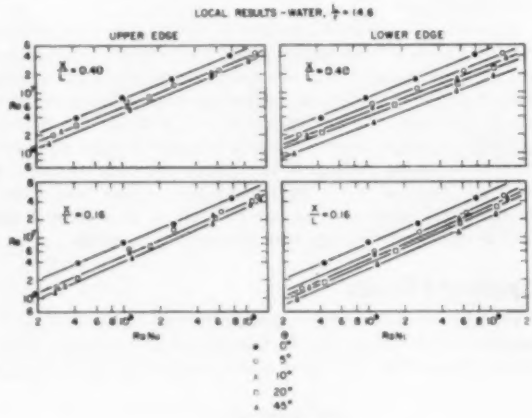

Fig. 4(b)

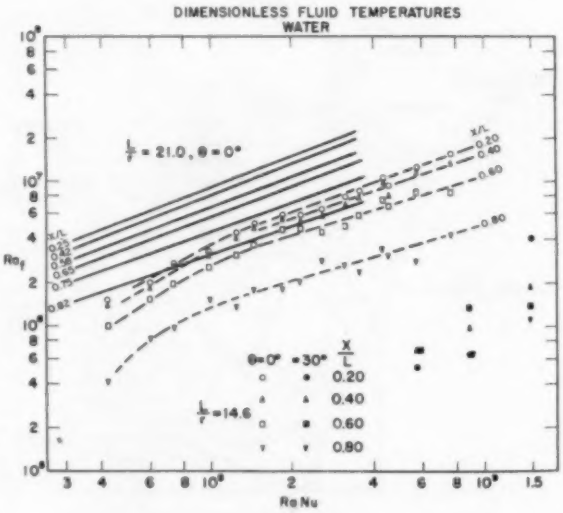

Fig. 5

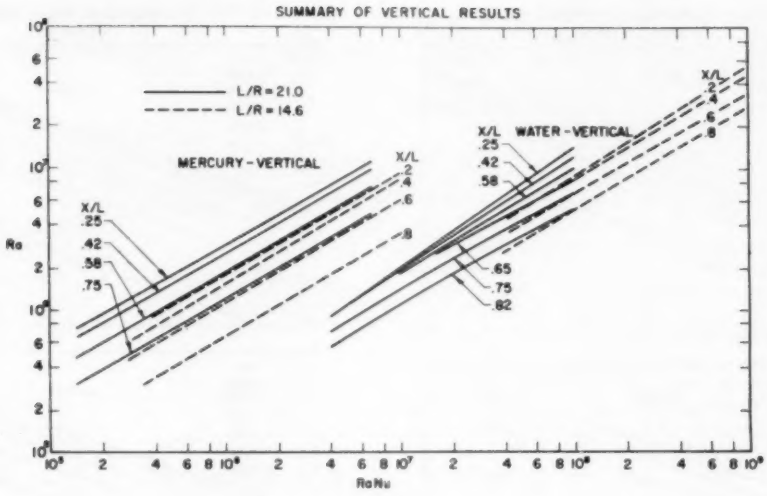

Fig. 6

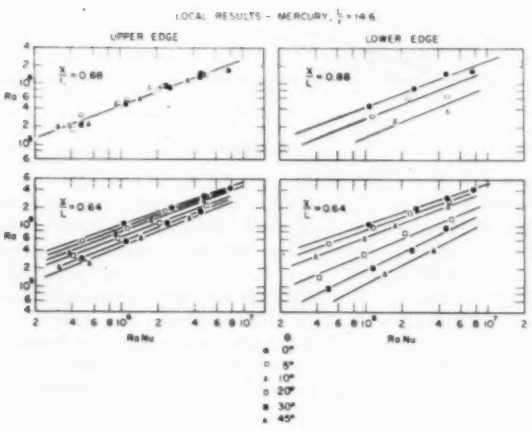

Fig. 7(a)

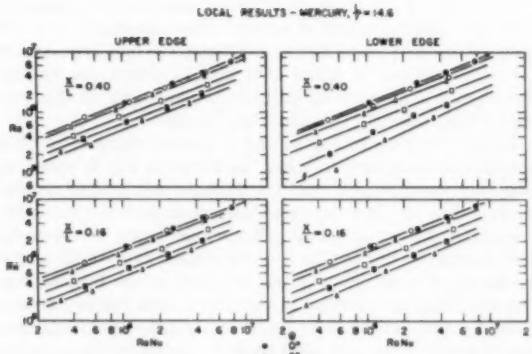

Fig. 7(b)

B. Mercury

1. Length-to-Radius Ratio of 14.6

a. Local Wall Temperature. Inclined tube local results are reported for mercury in the 14.6-in. test section at angles of 0, 5, 10, 20, 30, and 45 deg. The data obtained are plotted in Figs. 7(a and b) in the same fashion as the water tests already described.

As with the water results, a consistent decrease in wall temperatures along both the upper and lower edges accompanies the increasing angles of inclination. In the mercury tests, however, the effect starts more gradually than with water, and the heat-transfer performance increased approximately in a linear fashion with tube inclination throughout the angles tested. This is in contrast to the water results which demonstrated a large increase in heat transfer when the tube was inclined 5 deg from the vertical position; on further tilting, the performance continued to increase but not nearly as rapidly.

It has been noted in the mercury results that dimensionless local wall temperatures along the lower edge go to zero below the reservoir. This fact can be observed in Fig. 3 where a curve passing through points plotted for lower edge thermocouples would go below t^*. This low temperature observed at the lower edge of the tube mouth occurs because the cool fluid enters the tube at a temperature below t^*.

b. Fluid Temperature. Temperatures measured along the center line of the test section for these runs form profiles like the one shown in Fig. 3. From this figure it is evident that a much steeper fluid temperature gradient in the axial direction occurs with mercury than was the case with water. The dimensionless fluid temperatures measured along the tube center line, during runs with the tube vertical and inclined 30 deg, are presented in Fig. 8. The family of curves formed for each of the orientations appears quite similar. The magnitudes of these dimensionless temperatures, however, are seen to decrease by 75 per cent when the tube is tilted from 0 to 30 deg.

2. Length-to-Radius Ratio of 21.0

The data presented for mercury in this tube include runs taken with the tube vertical and inclined 30 deg.

a. Local Wall Temperature. Dimensionless wall temperatures are plotted in Fig. 9. Upon close examination of these curves, one can observe an effect like that of the $L/r = 14.6$ tube; for a given dimensionless heat flux (i.e., RaNu), the dimensionless wall temperature (i.e., Ra) is decreased about 50 per cent when the tube is tilted from 0 to 30 deg.

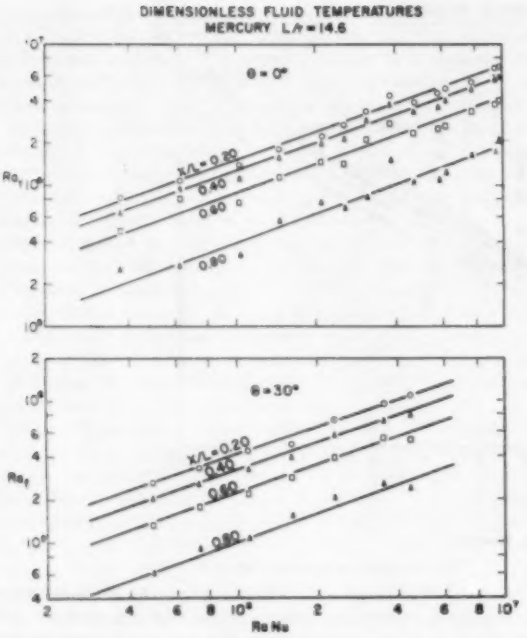

Fig. 8

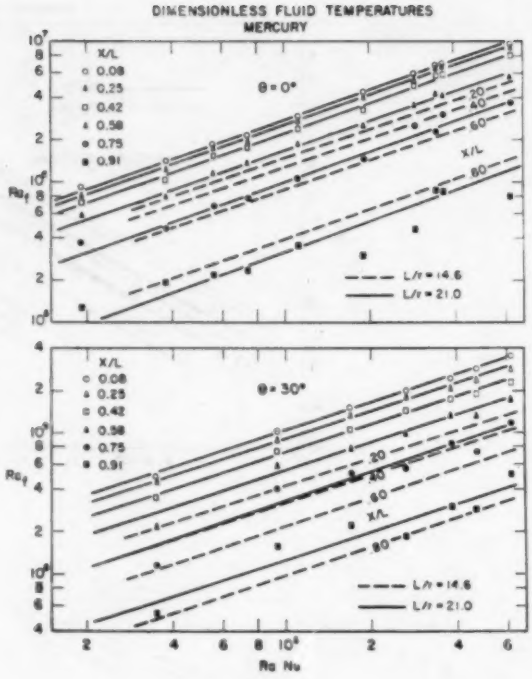

Fig. 10

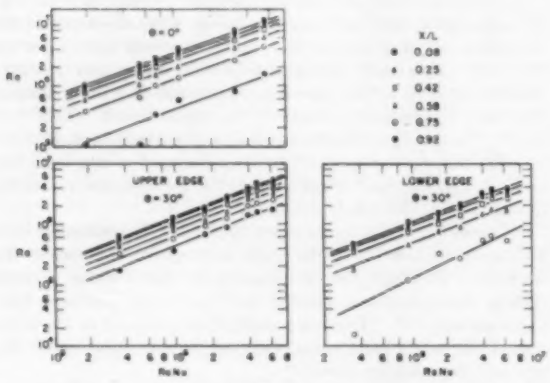

Fig. 9

b. Fluid Temperature. For the 21-in. tube at both angles, dimensionless fluid temperatures are shown in Fig. 10. For comparison, the results for the shorter tube are also included showing dimensionless temperatures, Ra_f, about half those of the $L/r = 21.0$ tube.

The data obtained with the probe, bearing three thermocouples at different radii, in the 21-in. test section inclined 30 deg, provide a qualitative measure of the radial temperature variation. Due to the fluctuations no actual radial profile could be constructed but some information was evident. The temperature close to the lower edge was decidedly lower than that found along the center line, or along the upper edge higher at any given axial position. This was also observed up into the reservoir suggesting that the temperature of the entering fluid was below the t^* value by several degrees.

3. Comparison With Water

A summary of the dimensionless wall temperatures versus the dimensionless heat fluxes for the tube in the vertical position is shown in Fig. 6, which includes both water and mercury results. These curves show that the higher Prandtl number liquid, water, is characterized by higher dimensionless heat transfer than mercury; that is, when compared at a given wall temperature (i.e., Rayleigh number), higher heat fluxes (i.e , RaNu values) are found for water than for mercury.

The behavior of the fluid temperatures in water and mercury differ as has been pointed out in Ref. [5], with the temperature fluctuations being much greater with mercury as the working fluid. Also, the fluid temperature profiles shown in Fig. 3 for mercury and water runs at comparable heat inputs are of different shape. In each case, mercury temperatures were observed to increase toward the bottom, maintaining a value several degrees below that of the wall at each position. In the water, however, the temperature was nearly constant increasing only slightly in the downward direction. For high heat inputs with mercury, in the vertical $L/r = 14.6$ tube, the fluid temperatures t_f reached values of about 200 deg F above the entrance temperature t^*; however, only about one tenth of this value occurred in water at equivalent heat inputs.

Tilting the tube 30 deg caused a marked decrease in center line fluid temperatures in water, as shown in Fig. 5, which was relatively much greater than the decrease observed in mercury, shown in Fig. 8. It is suggested that an improved circulation is responsible for an increased effective flow rate of convective fluid in and out of the tube. An increased flow would account for the lower fluid temperatures observed in the inclined tube. The quantitative difference in this effect, with the two fluids of unlike Prandtl number, is probably due to differing flow patterns. Such a difference in flow patterns may occur since the important parameter RaNu was generally an order of magnitude higher for the water runs than for the mercury. It would be of considerable value to extend the liquid metal investigation to high values of this number to substantiate (or negate) the explanation advanced.

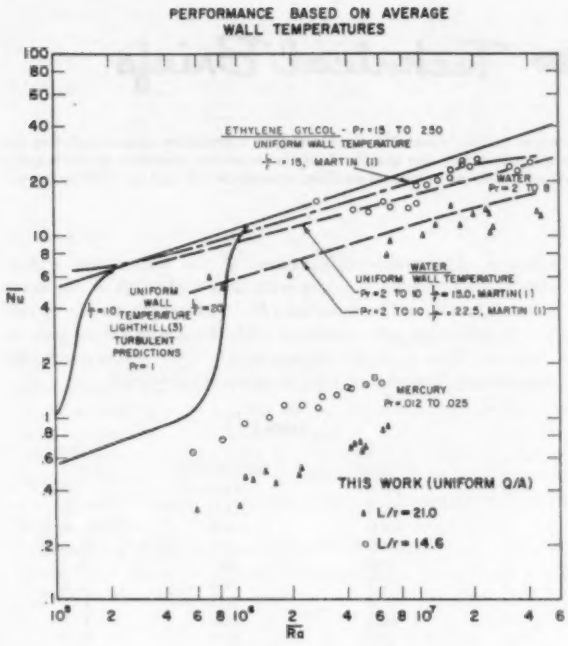

Fig. 11

C. Comparison With Other Investigations

A comparison of the present uniform wall heat flux results with the constant wall temperature predictions and experiments is most readily accomplished by using the co-ordinates generally adopted for the constant wall temperature boundary conditions, namely, $\overline{Nu}$ versus $\overline{Ra}$. Insufficient information makes it impossible to transform the other investigations to the present Ra versus RaNu presentation. To obtain the required mean Nusselt values $\overline{Nu}$ and mean Rayleigh number $\overline{Ra}$ from the present results, the measured wall temperatures were averaged according to the following rule:

$$\bar{t} = \frac{\int_0^L t dx}{L}.$$

The results are shown in Fig. 11. Also shown in this figure are the constant wall temperature predictions of Lighthill for Pr = 1.0 for two length-to-radius ratio tubes. Lighthill predicted a turbulent nonsimilarity regime followed by a turbulent boundary layer regime, having a tenfold increase in heat transfer, as $\overline{Ra}$ is increased past a critical value governed by the length-to-radius ratio. Nusselt numbers predicted by Lighthill lie above those observed experimentally by Martin [1]. Although Lighthill predicts that the heat transfer is independent of L/r in the Rayleigh number range of this investigation, the present data and those reported by Martin give strong evidence that the length-to-radius ratio does have considerable influence on the heat-transfer performance. A decrease in length-to-radius ratio from 22.5 to 15.0 results in approximately 100 per cent increase in the Nusselt numbers. The constant heat flux results of this investigation for water are in good agreement with the constant wall temperature water data of Martin.

Average results for the vertical tube mercury runs are also shown in Fig. 11. The resulting mean Nusselt values for the mercury (Pr = 0.012 to 0.025) are an order of magnitude lower than those for the water (Pr = 2 to 10) when compared at constant Rayleigh number. The effect of tube length-to-radius ratio is seen to be comparable to that found for water, with an increase in heat-transfer performance accompanying a decrease in length-to-radius ratio.

Acknowledgments

The authors desire to express their thanks to the National Science Foundation for its financial aid.

References

1 B. W. Martin, "Free Convection in an Open Thermosyphon With Special Reference to Turbulent Flow," *Proceedings of the Royal Society of London*, vol. 230, series A, 1955, p. 502.

2 B. W. Martin and H. Cohen, "Heat Transfer by Free Convection in an Open Thermosyphon Tube," *British Journal of Applied Physics*, vol. 5, March, 1954, pp. 91–95.

3 M. J. Lighthill, "Theoretical Considerations on Free Convection in Tubes," *Quarterly Journal of Mechanics and Applied Mathematics*, vol. 6, 1953, pp. 392–439.

4 J. P. Hartnett and W. E. Welsh, "Experimental Studies of Free Convection Heat Transfer in a Vertical Tube With Uniform Wall Heat Flux," TRANS. ASME, vol. 79, 1957, p. 1551.

5 J. P. Hartnett, W. E. Welsh, and F. W. Larsen, "Free Convection Heat Transfer to Water and Mercury in an Enclosed Cylindrical Tube," Nuclear Engineering and Science Conference, preprint 27, Session XX, Chicago, March 17–21, 1958.

6 B. W. Martin and D. J. Cresswell, "Influence of Coriolis Forces on Heat Transfer in the Open Thermosyphon," *The Engineer*, December 27, 1957, pp. 926–930.

Journal of HEAT TRANSFER — Technical Briefs

This section consists of contributions of 750 words or less (about 2½ double-spaced typewritten pages, including figures). Technical Briefs will be reviewed and approved by the specific division's reviewing committee prior to publication. After approval such contributions will be published as soon as possible, normally in the next issue of the Journal.

A Note on the "Implicit" Method for Finite-Difference Heat-Transfer Calculations

G. M. DUSINBERRE[1]

THE APPARENT advantage of the implicit method lies in the possibility of using relatively large time intervals. But this may be accompanied by (1) considerable sacrifice in accuracy and (2) no corresponding saving in digital computer time.

Nomenclature

- C = heat capacity of a node
- K = conductance of a heat-flow path
- t = temperature at beginning of a time interval
- t' = temperature at end of a time interval
- $\Delta\tau$ = finite time interval

In the "explicit" application of finite differences to heat-transfer problems, one uses the typical equations

$$K_{in}(t_i - t_n) + K_{jn}(t_j - t_n) \cdots = C_n(t_n' - t_n)/\Delta\tau \quad (1)$$

Thus one calculates each future temperature explicitly as a function of a number of present temperatures. The calculation is stable if, for each node, n:

$$\Delta\tau \leq C_n/\Sigma K_n \quad (2)$$

In the implicit application one writes:

$$K_{in}(t_i' - t_n') + K_{jn}(t_j' - t_n') \cdots = C_n(t_n' - t_n)/\Delta\tau \quad (3)$$

Thus each future temperature is a function of one present temperature and a number of future temperatures. All equations must be solved simultaneously, but the calculations are stable for all values of $\Delta\tau$.

This method was advocated by Liebmann[2] and apparently has attained some popularity.[3] In a practical case, the temperature history may often be adequately described in terms of a $\Delta\tau$ larger than that imposed by equation (2). And, other things equal, the number of calculations for a given period of time will be inversely as $\Delta\tau$.

The important question is whether the "other things" are really equal, first in respect to accuracy and second in respect to total operating time required on a digital computer.

As an example, let us consider the case of a long cylinder initially at 1000 deg with the surface suddenly cooled to 0 deg. This is a one-dimensional case for which there is an analytical solution. Using four subdivisions of the radius the author[4] obtained a numerical solution with $\Delta\tau$ equal to $^4/_5$ of the maximum value allowed by equation (2). The results, for the centerline temperature, are compared with the analytical solution in Table 1. Thus if we are concerned only about errors much over one per cent, this solution may be taken as a standard.

Table 1

$\tau/\Delta\tau$	Explicit	Analytical	Per cent error
0	1000	1000	0
1	1000	1000	0
2	1000	1000	0
3	1000	997	0.3
4	993	987	0.6
5	977	965	1.2
6	944	933	1.1
7	904	893	1.1
8	857	848	0.9
9	808	801	0.7
10	760	754	0.6
11	712	707	0.5
12	665	662	0.3
13	621	618	0.3

Let us note that an explicit solution of a one-dimensional problem with m nodes requires about $3m$ multiplications and m additions per time step. A three-dimensional problem would require about $7m$ multiplications. Thus the number of operations runs as the first power of the number of nodes.

For an implicit solution, in order to make a significant difference in the size of $\Delta\tau$, this was chosen as four times the limiting value from equation (2), or five times the value used in the explicit solution. It may be noted that Liebmann, when he wished to demonstrate *accuracy* for the implicit method, used a $\Delta\tau$ *less* than the limiting value for an explicit solution.

The general disadvantage of the implicit method is that the equations must be solved simultaneously. But in the present one-dimensional case, successive elimination gives a remarkably simple set of equations:

$$t_4' = 0.450\,t_4' + 0.004\,t_0 + 0.036\,t_1 + 0.125\,t_2 + 0.385\,t_3 \quad (4)$$

$$t_3' = 0.487\,t_2' + 0.011\,t_0 + 0.112\,t_1 + 0.390\,t_3 \quad (5)$$

$$t_1' = 0.577\,t_2' + 0.038\,t_0 + 0.385\,t_1 \quad (6)$$

$$t_0' = 0.800\,t_1' + 0.200\,t_0 \quad (7)$$

(The subscript 0 refers to the axis, 4 to the outer surface, etc.)

Thus, only a few more calculations are required to compute five time steps than were required to compute a single time step explicitly!

But is to be noted that the number of calculations now runs as the second power of the number of nodes, so that this advantage will be lost as the number of nodes increases. This number is imposed by other aspects of the problem (for example, by the need to make stress calculations) and will not depend on the method of solution used.

[1] Department of Mechanical Engineering, The Pennsylvania State University, University Park, Pa. Fellow ASME.

[2] G. Liebmann, "A New Electrical Analog Method for the Solution of Transient Heat-Conduction Problems," TRANS. ASME, vol. 78, 1956, p. 655.

[3] D. J. Campbell and D. B. Vollenweider, "Unusual Techniques Employed in Heat Transfer Programs," 1959 Proceedings of the Eastern Joint Computer Conference.

Contributed by the Heat Transfer Division of THE AMERICAN SOCIETY OF MECHANICAL ENGINEERS. Manuscript received at ASME Headquarters, July 26, 1960.

[4] G. M. Dusinberre, "Numerical Analysis of Heat Flow," McGraw-Hill Book Company, Inc., New York, N. Y., 1949.

Table 2

	Point	Explicit	Implicit	Per cent discrepancy
$\tau/\Delta\tau = 5$	0	977	899	− 7.8
	1	963	874	− 8.9
	2	779	781	+ 0.2
	3	442	550	+10.8
$\tau/\Delta\tau = 10$	0	760	743	− 1.7
	1	700	704	+ 0.4
	2	527	579	+ 5.2
	3	273	345	+ 7.2
$\tau/\Delta\tau = 15$	0	539	586	+ 4.7
	1	494	546	+ 5.2
	2	364	428	+ 6.4
	3	185	236	+ 5.1

It is also to be noted that if an iterative method is chosen for the solution of the simultaneous equations, the number of calculations must be multiplied by an uncertain number of iterations (on the order of m), not to mention the computer instructions required for cycling and testing.

It remains to examine the accuracy of the results in our example problem. In Table 2 the two solutions are compared at corresponding times. It is seen that the discrepancies are far from negligible.

Thus the purported advantages of the implicit method may be illusory in respect to computation time and, what is worse, in respect to accuracy.

The Influence of Prandtl Number on the Heat Transfer From Rotating Nonisothermal Disks and Cones

J. P. HARTNETT[1] AND E. C. DELAND[2]

Nomenclature

- A = constant defined in equation (5)
- c_p = specific heat at constant pressure
- F = dimensionless radial velocity defined, equation (3)
- H = dimensionless axial velocity defined, equation (3)
- h_r = local heat-transfer coefficient for rotating disk or cone, $q_r/(T_w - T_\infty)$
- k = thermal conductivity of the fluid
- m = exponent in the assumed power function wall temperature distribution, equation (5)
- Nu_r = local Nusselt number for rotating disk or cone, $(h_r/k)(\nu/\omega \sin\alpha)^{1/2}$
- Pr = Prandtl number of the fluid, $\mu c_p/k$
- q_r = local heat transfer from rotating disk or cone per unit area per unit time
- r = distance from center of disk or cone, Fig. 1
- T = temperature
- u = velocity parallel to the surface of the disk or cone
- w = velocity normal to the surface of the disk or cone
- z = distance normal to surface of the disk or cone
- ω = rotational speed of disk or cone
- μ = dynamic viscosity of the fluid
- ν = kinematic viscosity of the fluid
- ρ = fluid density
- θ = dimensionless temperature, equation (4)
- η = dimensionless distance from disk or cone, equation (2)

[1] Professor of Mechanical Engineering, University of Minnesota, Minneapolis, Minn.; Consultant to The RAND Corporation. Mem. ASME.

[2] The RAND Corporation, 1700 Main Street, Santa Monica, Calif.

Contributed by the Heat Transfer Division of THE AMERICAN SOCIETY OF MECHANICAL ENGINEERS. Manuscript received at ASME Headquarters, July 24, 1960.

Introduction

THE heat-transfer performance of a disk rotating in a quiescent fluid of large extent has been treated in two recent technical notes [1, 2].[3] In reference [1] laminar heat-transfer results are reported for an *isothermal* disk rotating in a fluid of any Prandtl number, thereby lifting the restriction imposed on the earlier work of Millsaps and Pohlhausen [3] who treated only a limited range of the Prandtl modulus. In reference [2], the heat-transfer performance of a *nonisothermal* disk rotating in a fluid with a Prandtl number of 0.72 was given for the case where the disk surface varied as a power function of the radius [i.e., $(T_w - T_\infty) = Ar^m$] for values of m from 0 to 10.

More recently, Tien [4] pointed out that these solutions are immediately applicable to the rotating cone. To obtain the heat-transfer coefficient for the cone it is only necessary to read off the values for the rotating disks from references [1 to 3] and multiply by $(\sin\alpha)^{1/2}$ where α is the half angle of the cone, Fig. 1.

In the present note, additional solutions of the energy equation are reported for the rotating nonisothermal disk or cone with power function surface temperature distribution covering a range of Prandtl number from 0.1 to 100, and values of the exponent m from 0 to 10.

Analysis

The energy equation for the rotating cone or disk takes the following form when the usual boundary-layer approximations are used:

$$\rho c_p u \frac{\partial T}{\partial r} + \rho c_p w \frac{\partial T}{\partial z} = k \frac{\partial^2 T}{\partial z^2} \tag{1}$$

This partial differential equation can be simplified into an ordinary differential equation if the following substitutions are introduced:

$$\eta = z(\omega \sin\alpha/\nu)^{1/2} \tag{2}$$

$$u = (\omega r \sin\alpha)F(\eta);\quad w = (\nu\omega \sin\alpha)^{1/2}H(\eta) \tag{3}$$

[3] Numbers in brackets designate References at end of paper.

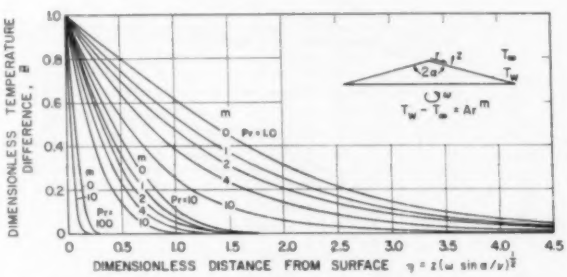

Fig. 1 Boundary-layer temperature profiles on a rotating disk or cone

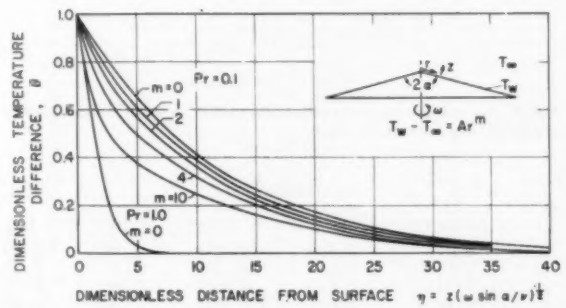

Fig. 2 Boundary-layer temperature profiles on a rotating disk or cone

$$\theta(\eta) = \frac{T - T_\infty}{T_w - T_\infty} \tag{4}$$

The inclusion of the term $(\sin \alpha)$ in equations (2) and (3) brings the transformed momentum equations for the cone into identically the same form as for the disk, allowing a direct use of the functions F and H already available in the literature [5, 6]. Although θ is a function of η only, the wall temperature is allowed to vary in the following manner:

$$T_w - T_\infty = Ar^m \tag{5}$$

The resulting energy equation for the nonisothermal rotating disk or cone becomes:

$$mF\theta + H\frac{d\theta}{d\eta} = \frac{1}{\mathrm{Pr}}\frac{d^2\theta}{d\eta^2} \tag{6}$$

Boundary conditions:

$$\begin{aligned} \theta &= 1 \quad \text{at} \quad \eta = 0 \\ \theta &= 0 \quad \text{at} \quad \eta \to \infty \end{aligned} \tag{7}$$

Solutions of this equation have been accomplished for Prandtl numbers of 0.1, 0.72, 1.0, 10, and 100.

Results

The temperature profiles are shown in Figs. 1 and 2 and reveal the rapid increase of the thermal boundary-layer thickness with decreasing Prandtl number when compared at a fixed value of the temperature distribution exponent m. At constant Prandtl number, increasing the exponent m results in a thinner thermal boundary layer. We would therefore expect an increased heat transfer as we increase either m or the Prandtl number, keeping other conditions fixed. To obtain a quantitative measure of the heat transfer, the local heat-transfer coefficient h_r is introduced:

$$q_r = h_r(T_w - T_\infty) \tag{8}$$

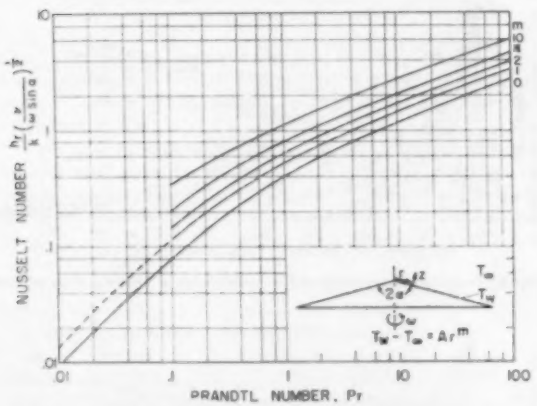

Fig. 3 Nusselt number for nonisothermal disk or cone versus Prandtl number of the surrounding fluid

Table 1

m ↓	Pr → 0.1	0.72	1.0	10	100
0	0.0766	0.330	0.396	1.13	2.69
1	0.110	0.437	0.518	1.41	3.28
2	0.141	0.524	0.616	1.62	3.71
4	0.197	0.661	0.769	1.95	4.46
10	0.330	0.935	1.073	2.60	5.95

where q_r is the heat flow per unit area and is determined from the temperature gradient at the surface; therefore:

$$h_r = -k\left(\frac{\partial T}{\partial z}\right)_{z=0} \Big/ (T_w - T_\infty)$$

$$= -k\left(\frac{\omega \sin\alpha}{\nu}\right)^{1/2}\left(\frac{d\theta}{d\eta}\right)_{\eta=0} \tag{9}$$

These results are most conveniently reported as local Nusselt numbers which are simply the slope of the dimensionless temperature distributions evaluated at the solid surface; that is:

$$\mathrm{Nu}_r = \frac{h_r}{k}\left(\frac{\nu}{\omega \sin\alpha}\right)^{1/2} = -\left(\frac{d\theta}{d\eta}\right)_{\eta=0} \tag{10}$$

These Nusselt values are shown graphically in Fig. 3 and tabulated below in Table 1.

It is clear that substantial changes in the Nusselt number occur when the disk or cone departs appreciably from nonisothermal conditions. In Fig. 3, the result obtained from equation (6) for a Prandtl value of 0.01 is shown for $m = 1$ as a dotted line to indicate an uncertainty in the validity of this solution. This uncertainty arises from the neglect of the radial conduction term which begins to play a significant role at low Prandtl numbers when the surface temperature is variable, particularly for large values of m. If the radial conduction term is retained, it is not possible to obtain an ordinary differential equation for the temperature distribution and the solution is correspondingly more difficult.

References

1 E. M. Sparrow and J. L. Gregg, "Heat Transfer From a Rotating Disk to Fluids of Any Prandtl Number," JOURNAL OF HEAT TRANSFER, TRANS. ASME, Series C, vol. 81, 1959, p. 249.

2 J. P. Hartnett, "Heat Transfer From a Nonisothermal Disk Rotating in Still Air," *Journal of Applied Mechanics*, TRANS. ASME, Series B, vol. 81, 1959, p. 672.

3 Knox Millsaps and K. Pohlhausen, "Heat Transfer by Laminar Flow From a Rotating Plate," *Journal of Aeronautical Sciences*, vol. 19, 1952, p. 120.

4 C. L. Tien, "Heat Transfer by Laminar Flow From a Rotating Cone," JOURNAL OF HEAT TRANSFER, TRANS. ASME, Series C, vol. 82, 1960, p. 252.

5 W. G. Cochran, "The Flow Due to a Rotating Disk," *Proc. Cambridge Phil. Soc.*, vol. 30, 1934, p. 365.

6 Simon Ostrach and P. R. Thornton, "Compressible Laminar Flow and Heat Transfer About a Rotating Isothermal Disk," NACA TN 4320, 1958.

A Fully Integrated Solution of the Problem of Laminar or Turbulent Flow in a Tube With Arbitrary Wall Heat Flux

R. N. NOYES[1]

Introduction

IN REFERENCE [1][2] a closed form solution is presented for the case of fully developed laminar flow in a tube with constant heat flux. The authors of reference [1] show how the constant heat-flux solution may be extended to the case of arbitrary heat-flux variation. In reference [2] a counterpart similar to that derived in reference [1] is given for turbulent flow.

In either of the above two references, the extensions of the constant heat-flux solutions to arbitrary heat-flux variation involve the evaluation of integrals for the particular heat-flux distribution of concern. It is the purpose of this report to derive an

[1] Principal Engineer, General Electric Company, ANP Department, Cincinnati, Ohio. Mem. ASME.

[2] Numbers in brackets designate References at end of paper.

Contributed by the Heat Transfer Division of THE AMERICAN SOCIETY OF MECHANICAL ENGINEERS. Manuscript received at ASME Headquarters, April 27, 1960.

integrated closed form solution for the variation of the heat-transfer coefficient for the case of fully developed laminar flow in a tube with an arbitrary analytical heat-flux distribution along the length of the tube. From reference [2] and the results reported herein, the case of turbulent flow with arbitrary heat flux may also be treated.

Method of Analysis

In reference [1] the variation of wall temperature T_w in laminar flow with axial distance x through a tube with arbitrary heat flux q'' is shown to be given by

$$T_w - T_i = \frac{1}{k}\int_0^x \left[\frac{4}{\mathrm{RePr}} - \sum_{n=1}^{\infty} \frac{C_n \beta_n^2 R_n(1)}{\mathrm{RePr}}\, e^{-\frac{\beta_n^2}{\mathrm{RePr}}\left(\frac{x-\xi}{a}\right)}\right] q''(\xi)\,d\xi \quad (1)$$

where Re and Pr are the Reynolds and Prandtl numbers, a is the tube radius, k is the thermal conductivity, and C_n, β_n, and R_n are constants, eigenvalues, and eigenfunctions, respectively. Equation (1) may be written in the form

$$\theta_w = \frac{2}{\mathrm{Gz}}\int_0^{\bar{x}} \left[4 + \sum_{n=1}^{\infty} \lambda_n e^{-\frac{2}{\mathrm{Gz}}\beta_n^2(\bar{x}-\bar{\xi})}\right] f(\bar{\xi})\,d\bar{\xi} \quad (2)$$

where $\theta_w = k\,(T_w - T_i)/q''_{\mathrm{ave}}\,a$, $\mathrm{Gz} = \mathrm{Re\,Pr}/(L/D)$, $\lambda_n = -C_n\,\beta_n^2\,R_n\,(1)$, $\bar{x} = x/L$, and $f\,(\bar{x})$ is the ratio of local to average heat flux.

From the above definitions the dimensionless bulk temperature is given by

$$\theta_b = \frac{T_b - T_i}{q_{\mathrm{ave}}'' a/k} = \frac{8}{Gz}\int_0^{\bar{x}} f(\bar{\xi})\,d\bar{\xi} \quad (3)$$

Since the Nusselt number Nu is given by

$$\mathrm{Nu} = \frac{h(2a)}{k} = \left(\frac{q''}{T_w - T_b}\right)\left(\frac{2a}{k}\right) = \frac{2f(\bar{x})}{\theta_w - \theta_b} \quad (4)$$

then from equations (2), (3), and (4), it follows that

$$\mathrm{Nu} = \frac{f(\bar{x})}{\frac{1}{\mathrm{Gz}}\int_0^{\bar{x}} \left[\sum_{n=1}^{\infty} \lambda_n e^{-\frac{2}{\mathrm{Gz}}\beta_n^2(\bar{x}-\bar{\xi})}\right] f(\bar{\xi})\,d\bar{\xi}} = \frac{f(\bar{x})}{D(\bar{x})} \quad (5)$$

In order to evaluate the integral in equation (5), the heat-flux distribution in the range $0 \leqslant x \leqslant L$ is assumed to be an analytical normalized function, and hence may be expanded in a Maclaurin series as

$$\frac{q''(\bar{x})}{q_{\mathrm{ave}}''} = f(\bar{x}) = b_0 + b_1\bar{x} + b_2\bar{x}^2 + \ldots + b_m\bar{x}^m = \sum_{j=0}^{m} b_j \bar{x}^j \quad (6)$$

where m may have any value between zero and infinity. When $m = 0$, $b_0 = 1$ which corresponds to the case of constant heat flux.

By substituting into equation (5) the series expansion of $f(\bar{x})$ as given by equation (6), the integral in the denominator term $D(\bar{x})$ may be evaluated term-by-term. The results may be suitably collected so that equation (5) will eventually take the form

$$\mathrm{Nu} = \frac{1}{\frac{11}{48} - \frac{1}{f(\bar{x})}\sum_{n=1}^{\infty}\frac{\lambda n}{2\beta_n^2}\left[b_0 e^{-K_n\bar{x}} + \sum_{j=1}^{m} j b_j F_{j-1}(\bar{x})\right]} \quad (7)$$

where:

$$F_0(\bar{x}) = \frac{1 - e^{-K_n\bar{x}}}{K_n}, \quad K_n = \frac{2\beta_n^2}{\mathrm{Gz}}$$

$$F_j(\bar{x}) = \frac{\bar{x}^j - jF_{j-1}(\bar{x})}{K_n}, \quad \frac{11}{48} = \sum_{n=1}^{\infty}\frac{\lambda_n}{2\beta_n^2}, \text{ (from reference [1])}$$

when $m = 0, f(\bar{x}) = b_0 = 1$, and equation (7) reduces to equation (10) of reference [1]; namely

$$\mathrm{Nu} = \frac{1}{\frac{11}{48} - \sum_{n=1}^{\infty}\frac{\lambda_n}{2\beta_n^2} e^{-K_n\bar{x}}} \quad (8)$$

Discussion of Results

As examples of the results obtained by the use of equation (7), two cases were considered. In case I the following arbitrary variation of heat flux with distance was assumed.

$$\frac{q_{\mathrm{local}}''}{q_{\mathrm{ave}}''} = f(\bar{x}) = 0.885 - 0.127\bar{x} + 2.987\bar{x}^2 - 3.269\bar{x}^3 \quad (9)$$

In Fig. 1 the variation of $f(\bar{x})$ according to equation (9) is shown by the dash line. Using the values of b_0, b_1, b_2, and b_3 from equation (9), equation (7) was evaluated for various values of Graetz number Gz. These results are shown by the family of solid curves in Fig. 1. From Fig. 1, it is seen that as $\mathrm{Gz} \to 0$, $\mathrm{Nu} \to 4.36+ = 48/11$. This becomes apparent when it is realized that as $\mathrm{Gz} \to 0$, $F_j(\bar{x}) \to 0$ and that in equation (7) the exponential term approaches zero. Thus in equation (7) the summation term over n disappears.

In case II, equation (7) was used to compute the Nu variation

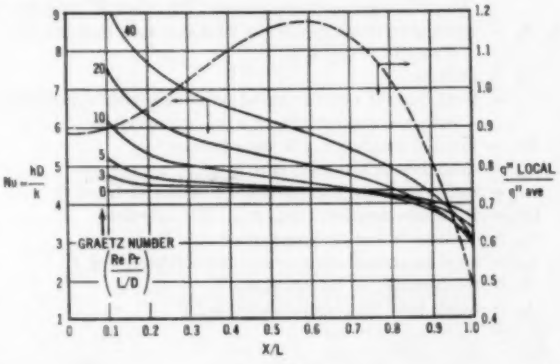

Fig. 1

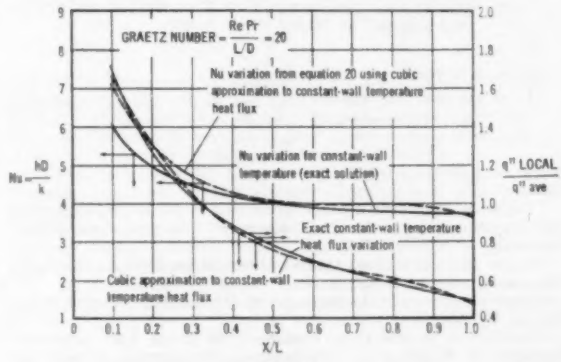
GRAETZ NUMBER = Re Pr / L/D = 20
Nu variation from equation 20 using cubic approximation to constant-wall temperature heat flux
Nu variation for constant-wall temperature (exact solution)
Exact constant-wall temperature heat flux variation
Cubic approximation to constant-wall temperature heat flux
Nu = hD/k
q'' LOCAL / q'' ave
X/L

Fig. 2

with $\bar{x}$ when $f(\bar{x})$ was assumed to be a cubic approximation to the heat-flux variation that would be required in the constant-wall temperature solution. Fig. 2 shows the results of this calculation for a Graetz number of 20. In Fig. 2 there are two sets of curves, each set being composed of a solid curve and a dash curve. One set illustrates Nu variation (ordinate scale on left), and the other set depicts heat-flux variation (ordinate scale on right). The dash lines portray the results of the cubic approximation and the solid lines indicate the exact constant-wall temperature solution. Except at low $\bar{x}$ values, exact and approximate Nu values are in as good agreement as the exact and approximate $f(\bar{x})$ values.

References

1 R. Siegel, E. M. Sparrow, and T. M. Hallman, "Steady Laminar Heat Transfer in a Circular Tube With Prescribed Wall Heat Flux," *Applied Scientific Research*—Applied Mechanics, Heat, Chemical Engineering, Mathematical Methods, section A, vol. 7, no. 5, pp. 386–392.

2 R. Siegel and E. M. Sparrow, "Turbulent Flow in a Circular Tube With Arbitrary Internal Heat Sources and Wall Heat Transfer," JOURNAL OF HEAT TRANSFER, TRANS. ASME, Series C, vol. 81, 1959, p. 280.

The Leveque Solution With a Finite Wall Resistance[1]

EDWARD M. ROSEN[2] AND EDWARD J. SCOTT[3]

Nomenclature

a = inside radius of tube, ft
A_i = inside area of tube, ft²
c_p = heat capacity of fluid, Btu/(lb$_m$)(deg F)
d = outside radius of tube, ft
h_d = local heat-transfer coefficient based on outside wall minus entrance temperature, Btu/(hr)(ft²)(deg F)
k, k_s = thermal conductivity of the fluid and wall, respectively, (Btu/(hr)(ft)(deg F)
n = an index
Nu_d = local Nusselt number based on outside wall minus the entrance temperature, $h_d a/k$, dimensionless
Pr = Prandtl number, $c_p\mu/k$, dimensionless
q_w = heat flow at the wall, Btu/hr
r = radial distance measured from center of tube, ft
Re = Reynolds number, $aU_{avg}\rho/\mu$, dimensionless
t_d = outside tube wall temperature, deg F
t_m = local mean (or mixing-cup) temperature, deg F
t_0 = temperature at entrance, deg F
t_w = inside tube wall temperature, deg F
$T_d = (t_d - t_w)/(t_0 - t_w)$
$T_{mc} = (t_m - t_0)/(t_d - t_0)$
U_{avg} = average fluid velocity in tube, ft/hr
y = distance measured radially from tube wall, ft
z = distance measured downstream from start of heat-transfer section, ft
$Z = z/a$
$Z^* = Z/\pi\,\mathrm{RePr}$
Γ = gamma function
$\eta = \dfrac{\lambda 18^{1/3}\Gamma(4/3)\pi^{1/3}}{2\Gamma(2/3)}$
$\lambda = k_s/k \ln(d/a)$
μ = viscosity, (lb$_M$)(ft)/(hr)
ξ, ξ^* = dummy variables
π = constant 3.14159265
ρ = density lb$_M$/ft³
Σ = summation

[1] Taken in part from a thesis submitted in partial fulfillment of the requirements for the PhD degree in Chemical Engineering, University of Illinois, 1959.

[2] Senior Mathematician, Applied Mathematics Section, Monsanto Chemical Company, St. Louis, Mo.

[3] Associate Professor, Department of Mathematics, University of Illinois, Urbana, Ill.

Contributed by the Heat Transfer Division of THE AMERICAN SOCIETY OF MECHANICAL ENGINEERS. Manuscript received at ASME Headquarters, June 3, 1960.

Introduction

AN ANALYTICAL SOLUTION for the rate of heat transfer between a fluid of constant physical properties flowing in a tube with a fully developed laminar velocity profile and with the wall of the tube held at a constant temperature was presented by Graetz [1][4] in the form of an infinite series. Although Sellars, Tribus, and Klein [5] presented a solution for all the eigenvalues and eigenfunctions necessary for its evaluation, the series converges very slowly near the start of the heat-transfer section. As a result, the Leveque [2] flat plate solution which approximates the exact solution very well in this region has been used.

Schenk and Dumore [4] and Yih and Cermak [7] have extended the Graetz solution to the case in which the outside wall of a tube with a finite wall resistance is held at a constant temperature. The inside wall temperature of the tube then varies with distance downstream. To evaluate the rate of heat transfer near the start of the heat-transfer section in this case it is convenient to extend the Leveque solution.

Analysis

Fig. 1 defines the system. Near the start of the heat-transfer section the tube may be approximated by a flat plate. Tribus and Klein [6][6] have shown that the flux at a distance Z downstream is given by[4]

$$\frac{q_w}{A_i} = \frac{2k}{a\Gamma(4/3)}\sqrt[3]{\frac{\mathrm{RePr}}{18}}\int_0^Z (Z-\xi)^{-1/3}\frac{dt_w}{d\xi}\,d\xi \qquad (1)$$

By an energy balance through the tube wall

$$\frac{q_w}{A_i} = \frac{k_s(t_d - t_w)}{a\ln(d/a)} \qquad (2)$$

Then equating equations (1) and (2) there results

$$\eta(t_d - t_w) = \frac{1}{\Gamma(2/3)}\int_0^{Z^*}(Z^* - \xi^*)^{-1/3}\frac{dt_w}{d\xi^*}\,d\xi^* \qquad (3)$$

This equation may be solved by means of the Laplace trans-

[4] Numbers in brackets designate References at end of paper.

[5] The Leveque expression given in Table 2 of reference [6] should be multiplied by 3.

[6] All symbols are defined in the Nomenclature.

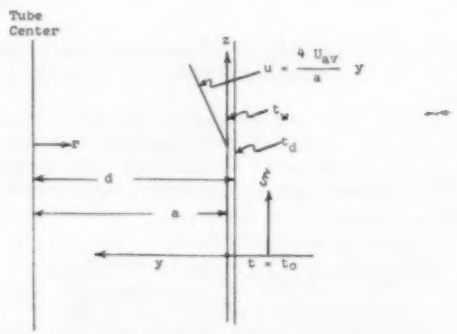

Fig. 1 Definition of co-ordinates and Nomenclature

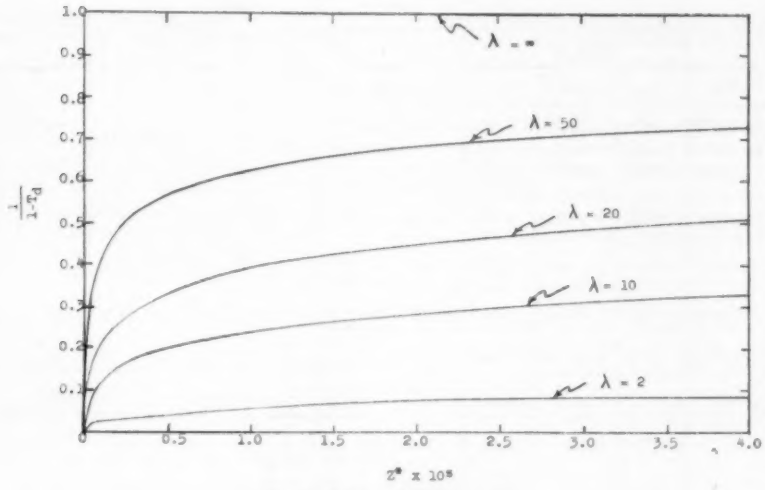

Fig. 2 Tube wall temperature

formation for the variation of t_w with Z^*. Details are given by Rosen [3]. The result is

$$\frac{t_w - t_0}{t_d - t_0} = \frac{1}{1 - T_d} = \sum_{n=1}^{\infty} (-1)^{n+1} \frac{(\eta Z^{*1/3})^n}{\Gamma(1 + n/3)} \quad (4)$$

Substituting equation (4) into equation (1) and integrating term by term the flux becomes

$$\frac{q_w}{A_i} = \frac{k\lambda(t_d - t_0)}{a}\left[1 + \sum_{n=1}^{\infty} (-1)^n \frac{(\eta Z^{*1/3})^n}{\Gamma(1 + n/3)}\right] \quad (5)$$

The local Nusselt number based on $(t_d - t_0)$ follows as

$$\mathrm{Nu}_d = \lambda\left[1 + \sum_{n=1}^{\infty} (-1)^n \frac{(\eta Z^{*1/3})^n}{\Gamma(1 + n/3)}\right] \quad (6)$$

The mean (or mixing-cup) temperature at any point downstream may be obtained using equation (5) in a total energy balance. Thus:

$$T_{mc} = \frac{t_m - t_0}{t_d - t_0} = 2\lambda\pi Z^*\left[1 + \sum_{n=1}^{\infty} (-1)^n \frac{(\eta Z^{*1/3})^n}{\Gamma(2 + n/3)}\right] \quad (7)$$

Heat-Transfer Results

Series (4), (6), and (7) which converge for all values of η and Z^* were evaluated on an IBM 704 digital computer using single precision arithmetic (8 significant digits) until the series changed by no more than 0.00001. For large values of $\eta Z^{*1/3}$, however, the terms become very large and many more digits must be carried to insure the desired accuracy. This fact set the limits on the values of Z^* and λ presented in Table 1 and Figs. 2, 3, and 4. Water (k = 0.355 Btu/hr ft deg F) flowing through a 0.863 in. ID, 0.984 in. OD "Pyrex" glass pipe (k_s = 0.650 Btu/hr ft deg F) at a mean temperature of 70 deg F would have λ = 13.8. The Leveque solution ($\lambda \to \infty$, $t_d \to t_w$) is given for comparison.

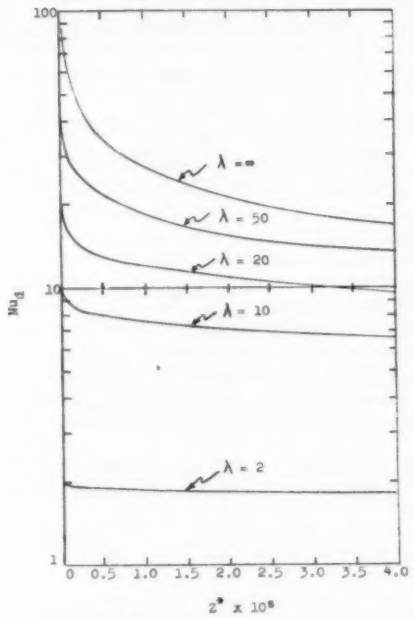

Fig. 3 Local Nusselt number

Acknowledgment

The advice and comments of Prof. T. J. Hanratty are gratefully acknowledged.

References

1 L. Graetz, "Über die Wärmelietungsfähigkeit von Flüssigkeiten," *Annalen der Physik and Chemie*, vol. 25, 1885, p. 337.

2 M. A. Leveque, "Transmission de chaleur par convection," *Annales des Mines*, vol. 13, sec. 12, 1928, pp. 201, 305, 381.

3 E. M. Rosen, "Effect of Heat Transfer on Flow Field at Low Reynolds Numbers in Vertical Tubes," PhD thesis in Chemical Engineering, University of Illinois, Urbana, Ill., 1959.

4 J. Schenk and J. M. Dumore, "Heat Transfer in Laminar Flow Through Cylindrical Tubes," *Applied Science Research*, Sec. A, vol. 4, 1953, p. 39.

5 J. R. Sellars, M. Tribus, and J. S. Klein, "Heat Transfer to Laminar Flow in a Round Tube or Flat Conduit—The Graetz Problem Extended," TRANS. ASME, vol. 78, 1956, p. 441.

6 M. Tribus and J. Klein, "Forced Convection From Nonisothermal Surfaces," Heat Transfer Symposium; Engineering Research Institute, University of Michigan, Ann Arbor, Mich., 1952.

7 C. S. Yih and J. E. Cermak, "Laminar Heat Convection in Pipes and Ducts," Civil Engineering Dept., Colorado A and M College, ONR Contract N9Gnr-82401, NR 063-071/1-19-49, 1951.

Table 1

$z^* \times 10^5$	$\lambda = 2$			$\lambda = 10$			$\lambda = 20$			$\lambda = 50$			$\lambda = \infty$		
	$\frac{1}{1-\pi_d}$	Nu_d	T_{mc}	$\frac{1}{1-\pi_d}$	Nu_d	T_{mc}	$\frac{1}{1-\pi_d}$	Nu_d	T_{mc}	$\frac{1}{1-\pi_d}$	Nu_d	T_{mc}	$\frac{1}{1-\pi_d}$	Nu_d	T_{mc}
0.00	0.00000	2.00000	0.00000	0.00000	10.00000	0.00000	0.00000	20.00000	0.00000	0.00000	50.00000	0.00000	1.0	∞	0.00000
0.02	0.01634	1.96733	0.00000	0.07720	9.22804	0.00001	0.14438	17.11249	0.00002	0.30124	34.93799	0.00005	1.0	99.77866	0.00019
0.04	0.02051	1.95899	0.00000	0.09555	9.04455	0.00002	0.17592	16.48152	0.00004	0.35379	32.31034	0.00009	1.0	79.19437	0.00030
0.06	0.02341	1.95318	0.00001	0.10803	8.91968	0.00003	0.19683	16.06345	0.00006	0.38649	30.67573	0.00013	1.0	69.18265	0.00039
0.08	0.02571	1.94857	0.00001	0.11775	8.82247	0.00005	0.21279	15.74417	0.00008	0.41038	29.48085	0.00017	1.0	62.85661	0.00047
0.10	0.02765	1.94470	0.00001	0.12582	8.74184	0.00006	0.22583	15.48337	0.00010	0.42926	28.53716	0.00020	1.0	58.35091	0.00055
0.20	0.03462	1.93076	0.00002	0.15397	8.46028	0.00011	0.26998	14.60034	0.00020	0.48909	25.54531	0.00037	1.0	46.31315	0.00087
0.40	0.04327	1.91346	0.00005	0.18720	8.12802	0.00021	0.31943	13.61142	0.00037	0.54941	22.52932	0.00067	1.0	36.75877	0.00139
0.60	0.04926	1.90149	0.00007	0.20913	7.90873	0.00032	0.35058	12.98849	0.00054	0.58421	20.78955	0.00094	1.0	32.11174	0.00182
0.80	0.05398	1.89205	0.00010	0.22583	7.74169	0.00041	0.37355	12.52906	0.00070	0.60843	19.57871	0.00120	1.0	29.17546	0.00220
1.00	0.05793	1.88414	0.00012	0.23944	7.60555	0.00051	0.39180	12.16397	0.00086	0.62686	18.65695	0.00144	1.0	27.08409	0.00255
2.00	0.07202	1.85596	0.00024	0.28534	7.14657	0.00097	0.45040	10.99205	0.00158	0.68161	15.91961	0.00251	1.0	21.49666	0.00405
3.00	0.08163	1.83664	0.00035	0.31461	6.85388	0.00141	0.48554	10.28924	0.00225	0.71154	14.42310	0.00346	1.0	18.77906	0.00531
4.00	0.08924	1.82151	0.00047	0.33638	6.63616	0.00184	0.51062	9.78768	0.00288	0.73141	13.42929	0.00434	1.0	17.06191	0.00643

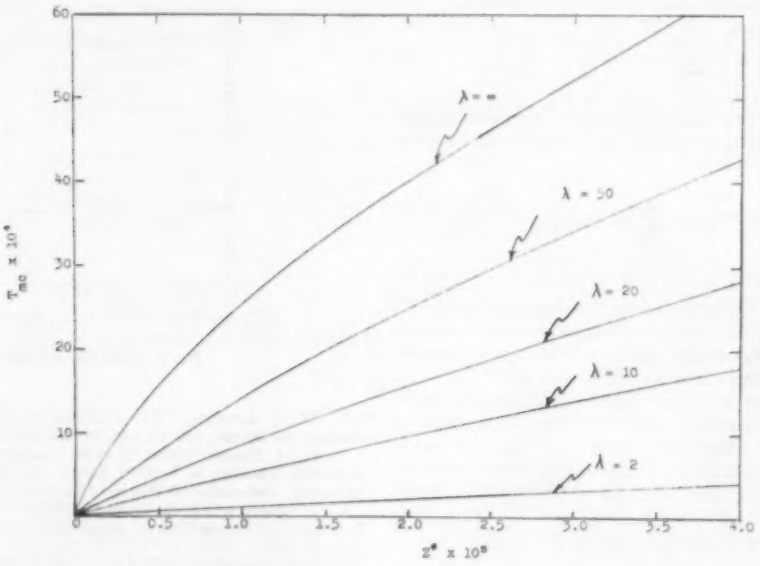

Fig. 4 Mean fluid temperature

Condensation on a Rotating Cone

E. M. SPARROW[1] **and J. P. HARTNETT**[1]

Introduction

IT HAS ALREADY BEEN recognized that the centrifugal forces generated in a rotating system may be utilized to replace the gravity force in a condensation process. Rotating condensation systems appear potentially attractive for space vehicle applications, where the force of gravity is essentially zero. In addition, rotating condensation also seems promising for earth-bound applications where higher condensation rates are desired than are obtainable with gravity.

The problem of laminar film condensation on a cooled rotating disk has already been studied both analytically [1, 2][2] and experimentally [3]. Reasonably good agreement was found between measurement and analysis; but even more important, the experiments demonstrated that the use of centrifugal force fields in condensation is technically feasible.

Another configuration where centrifugal fields may be conveniently generated for use in a condensation process is the rotating cone. In fact, condensation on a rotating cone has already been proposed [4] as part of a system for obtaining drinking water from saline water. It is the purpose of this brief report to make available heat-transfer results for condensation on a rotating cone.

The system considered for study is pictured schematically in Fig. 1. A cooled rotating cone is situated in a large quiescent body of pure vapor at its saturation temperature T_{sat}. The surface temperature of the cone is uniform at a value T_w and $T_w < T_{sat}$. Consideration will be given to the situation where the condensate forms a laminar film over the cone. The co-ordinates for the analysis are shown schematically in the figure: x measures the distance along the cone surface from the apex; y measures the distance normal to the surface; and φ gives the angular position. The opening angle of the cone is 2α. Under the action of the centrifugal field, the condensate is impelled along the disk, in the x-direction.

Analysis

The problem of flow and heat transfer about a rotating cone has been treated in references [5 and 6] for a single phase fluid. It was shown there that for cones which were not too slender, the boundary-layer assumptions reduce the mass, momentum, and energy equations to the following form:

mass:

$$\frac{\partial V_x}{\partial x} + \frac{V_x}{x} + \frac{\partial V_y}{\partial y} = 0 \tag{1}$$

x momentum:

$$V_x \frac{\partial V_x}{\partial x} + V_y \frac{\partial V_x}{\partial y} - \frac{V_\varphi^2}{x} = \nu \frac{\partial^2 V_x}{\partial y^2} \tag{2}$$

φ momentum:

$$V_x \frac{\partial V_\varphi}{\partial x} + V_y \frac{\partial V_\varphi}{\partial y} + \frac{V_x V_\varphi}{x} = \nu \frac{\partial^2 V_\varphi}{\partial y^2} \tag{3}$$

energy:

$$V_x \frac{\partial T}{\partial x} + V_y \frac{\partial T}{\partial y} = \alpha \frac{\partial^2 T}{\partial y^2} \tag{4}$$

These equations are written for axisymmetric conditions, $\partial/\partial\varphi = 0$. The y momentum equation has not been included here since it serves only to determine the pressure distribution, but otherwise does not influence the heat-transfer calculation. To complete the statement of the problem, the boundary conditions which are imposed are:

$$\left.\begin{array}{l} V_x = 0 \\ V_\varphi = x\omega \sin\alpha \\ V_y = 0 \\ T = T_w \end{array}\right\} \quad y = 0 \text{ (cone surface)} \quad \left.\begin{array}{l} V_x = 0 \\ \tau_{yx} = 0 \\ \tau_{y\varphi} = 0 \\ T = T_{sat} \end{array}\right\} \quad y = \delta \text{ (liquid-vapor interface)} \tag{5}$$

where τ_{yx} and $\tau_{y\varphi}$ are shear stresses. The assumption of vanishing interfacial shear is recognized to be an approximation, the effects of which have been surveyed in reference [2]. For Prandtl numbers above unity, the effect of the zero shear assumption leads to only small errors in the heat-transfer results. For liquid metals, the errors are greater and could even reach 25 per cent for thick condensate layers and very low Prandtl numbers. Because a complete set of solutions including interfacial shear are not now available for the low Prandtl number range, we will continue to use the zero shear boundary conditions, remembering that the results thus obtained overestimate liquid metal heat transfer for thick condensate layers.

The problem described by equations (1) through (5) is made tractable by introducing new variables [5, 6] as follows

$$\eta = y\sqrt{\frac{\omega \sin\alpha}{\nu}}, \qquad \theta = \frac{T_{sat} - T}{T_{sat} - T_w} \tag{6a}$$

$$F(\eta) = \frac{V_x}{x\omega \sin\alpha}, \qquad G(\eta) = \frac{V_\varphi}{x\omega \sin\alpha}, \qquad H(\eta) = \frac{V_y}{\sqrt{\omega\nu \sin\alpha}} \tag{6b}$$

This transformation differs from that for the rotating disk (von Karman's) due to the presence of the $\sin\alpha$ factors. When the new variables are substituted into equations (1) to (5), it is found that the governing equations and boundary conditions for F, G, θ, and H are identical to those for the rotating disk as given in reference [1].

To complete the analysis, it only remains to satisfy over-all conservation of energy, which may be expressed as follows:

$$h_{fg}\int_0^\delta \rho 2\pi x \sin\alpha\, V_x dy + \int_0^\delta \rho 2\pi x \sin\alpha\, V_x c_p (T_{sat} - T) dy = k\left(\frac{\partial T}{\partial y}\right)_{y=0} \pi x^2 \sin\alpha \tag{7}$$

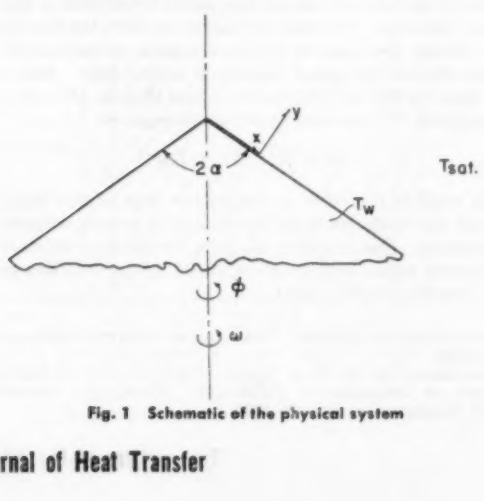

Fig. 1 Schematic of the physical system

[1] Professor of Mechanical Engineering at the University of Minnesota, Minneapolis, Minn. E. M. Sparrow is Assoc. Mem. ASME and J. P. Hartnett is Mem. ASME.

[2] Numbers in brackets designate References at end of paper.

Contributed by the Heat Transfer Division of THE AMERICAN SOCIETY OF MECHANICAL ENGINEERS. Manuscript received at ASME Headquarters, July 11, 1960.

where we have used assumptions consistent with the derivation of equations (1) to (4). The first term on the left is the energy released as latent heat, while the second term accounts for the subcooling of the condensate. The right side represents the heat transferred to the cooling surface. With the new variables of equation (6), the energy balance (7) becomes

$$\frac{c_p\,(T_{sat} - T_w)}{h_{fg}\ \mathrm{Pr}} = \left[\frac{H}{d\theta/d\eta}\right]_{\eta=\eta_\delta} \tag{7a}$$

which corresponds precisely to the over-all energy balance for the rotating disk.

So, even though F, G, H, θ, and η are differently defined for the rotating cone, they have the same set of governing equations. Hence all the solutions obtained in reference [1] for condensation on a rotating disk immediately are at our disposal for the rotating cone.

Results

The local heat transfer to the surface is found by applying Fourier's law: $q = k(\partial T/\partial y)_{y=0}$. Introducing the new variables of equation (6a), the expression for q becomes

$$q = -k(T_{sat} - T_w)\sqrt{\omega \sin \alpha\ /\nu}(d\theta/d\eta)_{\eta=0} \tag{8}$$

where the $(d\theta/d\eta)_{\eta=0}$ is obtained from the solutions as found in reference [1]. Defining a local heat-transfer coefficient as

$$h = \frac{q}{T_{sat} - T_w} \tag{9}$$

the heat-transfer results take the form

$$\frac{h\left[\dfrac{\nu}{\omega \sin \alpha}\right]^{1/2}}{k} = -(d\theta/d\eta)_{\eta=0} \tag{10}$$

Comparing this with the findings for condensation on a rotating disk, it follows that

$$h_{cone}/h_{disk} = (\sin \alpha)^{1/2} \tag{11}$$

So, h for the cone is always less than that for the disk.

By utilizing equation (11), the computation of heat-transfer coefficients for condensation on a rotating cone becomes a relatively simple matter: The h-values for the disk are read from Figs. 2 or 3 of reference [1] and then multiplied by $(\sin \alpha)^{1/2}$. The important practical conclusion to be drawn is that the deviations of h_{cone} from h_{disk} are not large. For example, when $\alpha = 60$ deg, the deviation is only 7 per cent; while for $\alpha = 45$ deg, the deviation is 16 per cent.

The determination of the condensate layer thickness δ is also facilitated by the use of reference [1]. After finding δ_{disk} from Figs. 4 or 5 of the reference, δ_{cone} is computed from

$$\delta_{cone}/\delta_{disk} = (\sin \alpha)^{-1/2} \tag{12}$$

The results for the rotating cone apply over that region of the surface where boundary-layer assumptions are fulfilled. Since condensate films are generally very thin, this is not expected to be a serious limitation. A more important question is the onset of turbulence, the answer to which awaits experimental investigation.

References

1 E. M. Sparrow and J. L. Gregg, "A Theory of Rotating Condensation," Journal of Heat Transfer, Trans. ASME, Series C, vol. 81, 1959, pp. 113–120.

2 E. M. Sparrow and J. L. Gregg, "The Effect of Vapor Drag on Rotating Condensation," Journal of Heat Transfer, Trans. ASME, Series C, vol. 82, 1960, pp. 71–72.

3 S. S. Nandapurkar and K. O. Beatty, Jr., "Condensation on a Horizontal Rotating Disc," Preprint 112, presented at the Third National Heat Transfer Conference, ASME-AIChE, Storrs, Conn., August, 1959.

4 L. A. Bromley, "Prediction of Performance Characteristics of Hickman-Badger Centrifugal Boiler Compression Still," *Industrial and Engineering Chemistry*, vol. 50, 1958, pp. 233–236.

5 C. S. Wu, "The Three Dimensional Incompressible Boundary Layer on a Spinning Cone," *Applied Scientific Research*, section A, vol. 8, 1959, pp. 140–146.

6 C. L. Tien, "Heat Transfer by Laminar Flow From a Rotating Cone," Journal of Heat Transfer, Trans. ASME, Series C, vol. 82, 1960, pp. 252–253.

Refrigerator Heat Leak for Sandwiched Thermoelectric Elements

B. W. SWANSON[1] AND E. V. SOMERS[1]

Nomenclature

- a = radius of thermoelectric column, cm
- A_i = area of insulation cell, cm^2 $A_i = \pi b^2$
- b = outer radius of insulation cell, cm
- J = current, amps
- l = height of insulation cell; distance between hot and cold junction plates, cm
- l^* = dimensionless length of thermoelectric column; $l^* = 1 - z_1/l$
- r = radial co-ordinate, cm
- r^* = dimensionless parameter; $r^* = a/b$
- Q = heat leak into insulation cell, defined by equation (3), watts
- Q_{ci} = insulation heat leak defined by equation (1)
- T_h = temperature of hot-junction plate, deg C
- T_c = temperature of cold-junction plate, deg C
- T_0 = reference temperature, $T_0 = T_h - T_c$
- x = linear co-ordinate for one-dimensional temperature distribution, equation (2), cm
- Z = axial co-ordinate, cm
- β = dimensionless parameter, $\beta = l/b$
- κ = thermal conductivity, watts/cm deg C
- K_i = thermal conductivity of insulation, watts/cm deg C
- ρ = electrical resistivity, ohm-cm
- λ_n = eigenvalues, defined by equation (10)
- z_1 = height of copper peg, cm

Introduction

The design of a thermoelectric refrigerating unit generally separates the hot and cold-junction plates by columns of thermoelectric material. To reduce the cost of the unit, the thermoelectric columns are replaced by much smaller thermoelectric elements attached to almost isothermal copper pegs. Since heat leak from the hot to cold-junction plates through the insulation is important, the one-dimensional design equation

$$Q_{ci} = K_i A_i (T_h - T_c) l^{-1} \tag{1}$$

which neglects the effect of the copper pegs on the heat leak through the insulation must be replaced by a more accurate approximation. Design curves are given for different values of the geometrical parameters associated with a better heat flow model that yield the values of Q/Q_{ci}.

[1] Mechanics Department, Westinghouse Research Laboratories, Pittsburgh, Pa.

Contributed by the Heat Transfer Division of The American Society of Mechanical Engineers. Manuscript received at ASME Headquarters, July 26, 1960.

Definition and Solution of Mathematical Model

Consider the thermoelectric element shown in Fig. 1. With the thermoelectric properties constant, the temperature distribution within the thermoelectric element, surrounded by insulation with the copper peg isothermal at T_c, is given by the approximately one-dimensional solution.

$$T = \left[T_h - \frac{x}{l_1}(T_h - T_c)\right] + \frac{J\rho^2}{2\kappa} x(l_1 - x) \qquad (2)$$

The first term of equation (2), linear in x, is the solution for the case of zero current, while the second term is a parabolic function in x because of the Joulean heat. For this analysis, the Joulean heat is assumed negligible, so that the temperature in the thermoelectric element drops linearly along its length. The hot-junction plate, and cold-junction plate with the copper peg, can be assumed isothermal at the temperatures T_h and T_c, respectively.

These assumptions suggest the following mathematical model. A hollow cylindrical insulation cell is considered, as shown in Fig. 2, with the inner radius of the cell that of the thermoelectric-copper column and the outer radius half the distance between adjacent column centers. The cell height is the distance between the hot and cold plates. The following boundary conditions apply:

(a) The top surface of the cell is isothermal, at temperature T_h.

(b) The bottom surface of the cell is isothermal at temperature T_c.

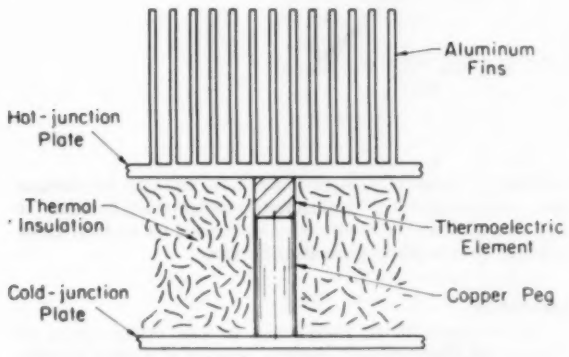

Fig. 1 Thermoelectric element with copper peg

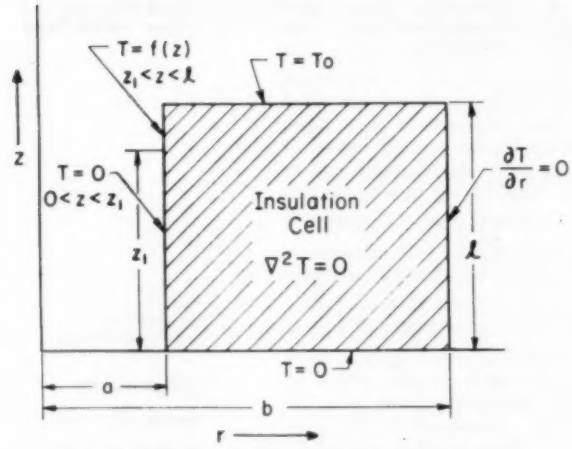

Fig. 2 Temperature problem for insulation cell

(c) An adiabatic condition exists on the outer cylindrical surface.

(d) The inner cylindrical surface is isothermal at temperature T_c along the height of the copper column and is subject to a linear gradient between T_h and T_c along the height of the thermoelectric peg.

The steady-state temperature distribution within the cell can be calculated, and the total insulation heat-leak rate found by integrating the axial derivative of the cell temperature over the upper surface of the cell.

$$Q = -\kappa \int_a^b 2\pi r \left.\frac{\partial T}{\partial z}\right|_{z=l} dr \qquad (3)$$

The variation of the ratio of the heat leak given by this model to the heat leak computed by equation (1), denoted by Q/Q_{ci}, is studied with respect to its geometrical parameters.

The mathematical model for the insulation cell is defined by the following equations:

$$\frac{\partial^2 T(r,z)}{\partial r^2} + \frac{1}{r}\frac{\partial T(r,z)}{\partial r} + \frac{\partial^2 T(r,z)}{\partial z^2} = 0 \qquad \begin{matrix} a < r < b \\ 0 < z < l \end{matrix} \qquad (4)$$

$$T(a,z) = f(z); \quad f(z) = 0, \qquad 0 < z < z_1$$

$$f(z) = \frac{z - z_1}{l - z_1} T_0, \qquad z_1 < z < l \qquad (5)$$

$$\frac{\partial T(b,z)}{\partial r} = 0 \qquad (6)$$

$$T(r,l) = T_0 \qquad (7)$$

$$T(r,0) = 0 \qquad (8)$$

The temperature distribution was determined by standard techniques [2][1] and the result employed in equation (3) yielded the ratio Q/Q_{ci},

$$\frac{Q}{Q_{ci}} = \frac{\pi^2 r^{*2}\beta}{[1 - r^{*2}]} \sum_{n=1}^{\infty} \frac{\lambda_n J_1^2(\lambda_n)[J_0(\lambda_n r^*)Y_1(\lambda_n r^*) - Y_0(\lambda_n r^*)J_1(\lambda_n r^*)]^2 \cosh \lambda_n \beta}{[J_0^2(\lambda_n r^*) - J_1^2(\lambda_n r^*)] \sinh \lambda_n \beta} \qquad (9)$$

$$- \frac{4r^*}{[1 - r^{*2}]} \sum_{n=1}^{\infty} \frac{\left[I_1\left(\frac{n\pi}{\beta}\right) K_1\left(\frac{n\pi r^*}{\beta}\right) - K_1\left(\frac{n\pi}{\beta}\right) I_1\left(\frac{n\pi r^*}{\beta}\right)\right]\left(1 - \frac{\sin n\pi l^*}{n\pi l^*}\right)}{\frac{n\pi}{\beta}\left[I_0\left(\frac{n\pi r^*}{\beta}\right) K_1\left(\frac{n\pi}{\beta}\right) + K_0\left(\frac{n\pi r^*}{\beta}\right) I_1\left(\frac{n\pi}{\beta}\right)\right]} \qquad (10)$$

where

$$J_0\left(\lambda_n \frac{a}{b}\right) Y_1(\lambda_n) - J_1(\lambda_n) Y_0\left(\lambda_n \frac{a}{b}\right) = 0$$

Presentation of Results

The variation of the ratio Q/Q_{ci} with l^* for $r^* = 0.1$, 0.2, and 0.3 and $\beta = 1.0$, 2.0, 3.0, and 4.0 is shown in Figs. 3 through 6. It is observed that for low values of l^*, which are desirable for cost reduction, Q/Q_{ci} of the model can be quite large. Although a more usual geometry for the thermoelectric structure would be

[1] Numbers in brackets designate References at end of paper.

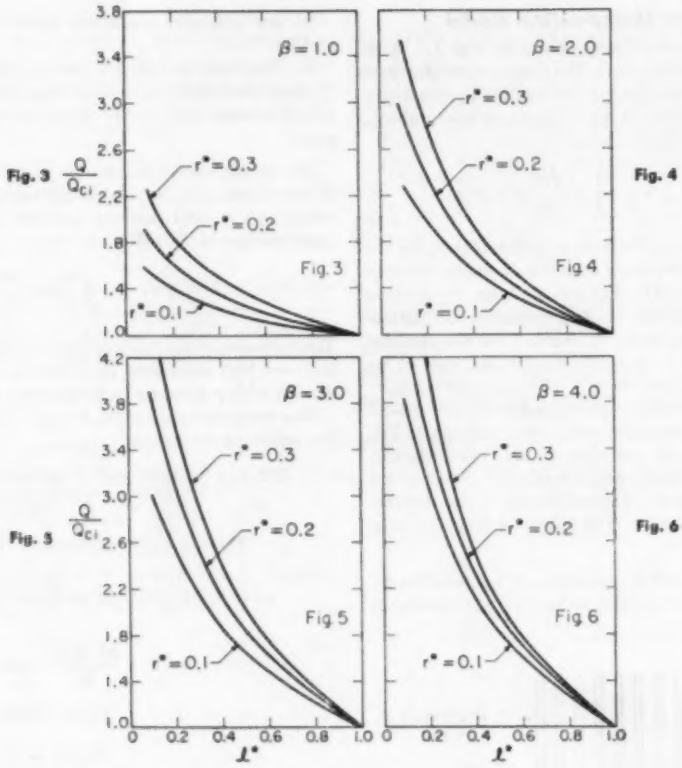

that of circular cylindrical pegs within rectangular cross-sectional, rather than circular cross-sectional cells, the solvable model presented here can be applied to the rectangular-celled geometry on a basis of determining the outer radius b by equating the rectangular cross-sectional area to πb^2; a similar approach has been used for fin efficiencies of square fins on circular tubes [3].

Conclusion

It has been shown that the insulation heat leak for a thermoelectric refrigerator model, using thermoelectric-copper columns, can greatly exceed that leak computed on a simple one-dimensional heat-flow basis. The ratio of these two heat leaks has been evaluated analytically for a reasonable model, and its variation is represented in graphical form suitable for thermal design computations of thermoelectric-refrigerating devices. It is recognized that the results can also be used for thermal losses in thermoelectric power generating devices.

References

1 B. Sherman, R. R. Heikes, and R. Ure, "Computation of Efficiency of Thermoelectric Devices," *Journal of Applied Physics*, 1959.

2 H. S. Carslaw and J. C. Jaeger, "Conduction of Heat in Solids," Oxford University Press, London, England, pp. 172–180.

3 H. Zabronsky, "Temperature Distribution and Efficiency of a Heat Exchanger Using Square Fins on Round Tubes," ASME Paper No. 54—A-12, 1953.

Journal of HEAT TRANSFER

Information for Authors

• Manuscripts should be submitted in final form to the Editor. Each manuscript must be accompanied by a statement that it has not been published elsewhere nor has it been submitted for publication elsewhere. A paper which would occupy more than 8 pages of the Journal may be returned to the author for abridgment.

• The author should state his business connection, the title of his position, and his mailing address. A short abstract (50 to 100 words) should be included on the first page immediately preceding the introductory paragraph of the paper.

Three copies of the manuscript are required. One of these must be a carefully prepared printer's copy, typed in double spacing, on one side of the page only, with wide margins, on $8^1/_2$ by 11-in. opaque white paper. Mimeographed manuscripts, if prepared with exceptional care, can be accepted provided they are completely edited.

• As far as possible, all mathematical expressions should be typewritten. Greek letters and other symbols not available on the typewriter should be carefully inserted in ink. Care should be taken to distinguish between capital and lowercase letter, between zero (0) and the letter (*O*), between the numeral (1) and the letter (*l*), etc. A letter representing a vector cannot be printed with an arrow above or below it. The letter should be underscored with a single wavy line, wherever it appears in the text, to designate boldface type.

• A list of symbols carefully marked for the use of the editor (thus: κ, Greek l.c. kappa), if it has not been included in the body of the paper, should accompany the manuscript on a separate page.

• Before preparing a manuscript the author should study printed articles in the Journal, with special attention to the form and style of mathematical expressions, tables, footnotes, references, and abstract. Numbers that identify mathematical expressions should be enclosed in parentheses. Numbers that identify references at the end of the paper should be enclosed in brackets. Care should be taken to arrange all tables and mathematical expressions in such a way that they will fit into a single column when set in type. Equations that might extend beyond the width of one column (fractions that should not be broken or long expressions enclosed in parentheses) should be rephrased to go on two or more lines within column width. Fractional powers are preferred to root signs and should always be used in more elaborate formulas. The solidus should be used instead of the horizontal line for fractions wherever possible.

• A normal paper should not exceed 8 pages in the Journal. It is about 8000 words or 20 double-spaced typewritten pages exclusive of drawings. A Technical Brief should not exceed 750 words or about one page in the Journal inclusive of drawings.

• Originals and two copies of figures must accompany the manuscript. Line drawings should not be larger than $8^1/_2 \times 11$ in. and should be planned for reduction to column width. Lettering should be large enough to be clearly legible when the illustration is reduced. The originals of line drawings must be in India ink on white or pale blue tracing paper or tracing cloth. Photographs of equipment or test specimens must be glossy prints and should be used sparingly. Captions for figures should be typed double-spaced and included as the last page of the manuscript. The figure number and author's name should be written in the margin or on the back of each illustration.

• Titles of papers should be brief.

• Authors can obtain copies of the ASME Manual MS-4, "An ASME Paper," from the Editor and are urged to do so before drafting their papers in final form.

• Papers published in Journals of the Transactions of the ASME must be presented at a Meeting, either in person or by title.

• An author is entitled to 25 preprints free of charge (in the case of two authors, 15 each; three or more authors, 10 each). Larger quantities of preprints or reprints can be ordered from Editorial Department, The American Society of Mechanical Engineers, 29 West 39th Street, New York 18, N. Y. Quotations will be sent on request.

Please address all communications to:

Editor, ASME,

29 West 39th Street,

New York 18, N. Y.

ASME Publications Committee